UNIVERSITÄT DUISBURG ESSEN

Offen im Denken

NON-COVALENT INTERACTIONS IN NAPHTHALENEDIYL-SUBSTITUTED HEAVY GROUP 15 ELEMENTS

DISSERTATION

ZUR ERLANGUNG DES AKADEMISCHEN TITELS

DOCTOR RERUM NATURALIUM

– DR. RER. NAT. –

VORGELEGT VON

ALEXANDER GEHLHAAR, M. SC.

ANGEFERTIGT IM INSTITUT FÜR ANORGANISCHE CHEMIE DER FAKULTÄT FÜR CHEMIE
DER UNIVERSITÄT DUISBURG-ESSEN

ESSEN **2022**

DOI: 10.17185/duepublico/76953
URN: urn:nbn:de:hbz:465-20221007-115827-9

„No. Try Not. Do… or do not. There is no try.“

Yoda, Jedi Grandmaster

Die vorliegende Arbeit wurde im Zeitraum von September 2018 bis Januar 2022 im Arbeitskreis von Prof. Dr. Stephan Schulz des Instituts für anorganische Chemie der Fakultät Chemie an der Universität Duisburg-Essen angefertigt.

1. Gutachter: Prof. Dr. Stephan Schulz

2. Gutachter: Prof. Dr. Alexander A. Auer

Vorsitz: Jun.-Prof. Dr. Jens Voskuhl

Tag der Abgabe: 26.07.2022

Tag der Verteidigung: 16.09.2022

Danksagung

Im Folgenden möchte ich allen Personen danken, die zum Gelingen dieser Dissertation beigetragen haben.

Zunächst möchte ich mich besonders bei meinem Doktorvater, Prof. Dr. Stephan Schulz, bedanken für die Betreuung dieser Arbeit, für die Chance an diesem herausfordernden Forschungsthema zu arbeiten, für die Freiheiten um eigene Ideen einzubringen, sowie für die exzellente Ausstattung und Arbeitsatmosphäre um diese Arbeiten umzusetzen.

Prof. Dr. Alexander A. Auer danke ich für die Übernahme des Zweitgutachtens und Jun.-Prof. Dr. Jens Voskuhl danke ich für die Übernahme des Prüfungsvorsitz.

Weiterhin möchte ich Prof. Dr. Gebhard Haberhauer, Prof. Dr. Georg Jansen, Prof. Dr. Alexander A. Auer, Dr. Eduardo Schiavo, Felix van der Vight und Nina Semleit für die konstruktive, produktive und erfolgreiche Zusammenarbeit danken.

Dr. Christoph Wölper danke ich für Aufnahme und Verfeinerung von Kirstallstrukturdaten, sowie den zahlreichen fachlichen und persönlichen Gesprächen vor und abseits der Diffraktometer.

Zudem möchte ich Beate Römer für die Aufnahme einiger (ungewöhnlicher) NMR Spektren, die Durchführung diverser Elementaranalysen und Geduld mit einigen Proben danken.

Dr. Thorsten Schaller und Dr. Felix Niemeyer gilt mein Dank für die Aufnahme einiger NMR Spektren. Weiterhin möchte ich Robin Meya und Kerstin Brauner für die Durchführung der Elementaranalysen danken.

Schließlich möchte ich dem gesamten Arbeitskreis Schulz für die angenehme, lustige und zu weilen auch produktive Arbeitsatmosphäre danken. Meinen (ehemaligen) Bürkollegen Dr. Kevin Huse, Dr. Christoph Helling, Yannick Schulte, Micha Weinert danke ich für die vielen (hilfreichen) fachlichen und privaten Gespräche und Diskussionen. Micha Weinert gilt noch ein besonderer Dank für die Durchführung der Cyclovoltammetrie. Dr. Kevin Dzialkowski danke ich für seine Vorarbeiten und Ratschläge zu diesem Themengebiet, sowie die stets lustigen fachlichen, sowie privaten Unterhaltungen und der im allgemeinen angenehme Zeit. Auch Dr. Georg

Bendt möchte ich trotz seiner manchmal chaotischen Organisation danken. Dr. Sarah Salloum gebührt mein Dank für das Korrekturlesen dieser Arbeit.

Einen besonderen Dank möchte ich Dr. Julia Krüger, Dr. Juliane Schoening, Dr. Kevin Kaiser und Anna Bücker nicht nur für das Korrekturlesen meiner Arbeit, sondern auch die Möglichkeit der vielen Bürobesuche und dabei geführten Gespräche, die Spieleabende und allgemein freundschaftliche Beziehung aussprechen.

Abschließend möchte ich meinen Freunden und Familie für die Unterstützung während dieser Arbeit, sowie zuweilen auch nötige Ablenkung von dieser Arbeit danken! Einen besonderen Dank möchte ich abschließend an meine Freundin Nora Rode für ihre Unterstützung und gemeinsamen Zeit richten.

Abstract

In recent years, the importance of non-covalent interactions has steadily grown and the stabilizing effect of *London* dispersion interactions has become widely accepted even in organometallic chemistry. Although hydrogen bonds, ligand-ligand interactions, as well as organic molecules represent major topics in the field of non-covalent interactions, recent studies showed that *London* dispersion also plays a significant role for heavy elements, *e.g.* late group 15 elements like antimony and bismuth. In the early 1900s, *Boris Nikolayevic Menshutkin* reported on the formation of various pnictogen halide complexes by dissolving PnX_3 in aromatic and non-aromatic solvents *via* measurement of thermodynamic data. After several decades the formation of Pn···π complexes was finally proven by single-crystal X-ray diffractometry, however combined theoretical and experimental approaches only recently demonstrated that the nature of Pn···π contacts is typically dominated by *London* dispersion.

This thesis provides further insights into the driving forces and their significance on the formation of bonds and the crystal packing. To initiate inter- and intramolecular Pn···Pn, Pn···π, and π···π contacts, the 1,8-positions of naphthalene, also known as the *peri*-positions, were substituted with pnictogen groups. The intramolecular Pn···Pn contacts were of special interest since the close *peri*-distance evokes a balance of repulsion and attraction. The resulting systems were characterized by standard methods (NMR, IR, elemental analysis, sc-XRD) and further investigated by quantum chemical means.

The synthesis of Bi_2Naph_2, containing a covalent Bi–Bi single bond that is bridged by two naphthalenediyl fragments was specifically targeted since both the arsenic and antimony derivatives were already isolated, whereas the properties of the corresponding bismuth compound were entirely predicted. Bi_2Naph_2 was obtained in very low yields, however the compound exhibited an unusual crystal packing which deviated from previous theoretical predictions including missing π···π contacts among other things. A new polymorph of As_2Naph_2 was also obtained containing different contacts compared to the previous packing. Quantum chemical computations demonstrated that the crystal packing of the Pn_2Naph_2 (Pn = P-Bi) is driven by the maximization of *London* dispersion *via* the formation of specific dimers.

After completing the series of Pn-(II) compounds, the preparation and investigation of Pn-(III) systems were taken into account. Being the most simple aryl group, phenyl was therefore selected as starting point. The bis(diphenylpnicta)naphthalenes 1,8-$(Ph_2Pn)_2$Naph (Pn = Sb, Bi), as well as the acenaphthene derivative 5,6-$(Ph_2Sb)_2$Acenaph (acenaphthene = 1,8-ethylenenaphthalene) were prepared *via* salt-metathesis reactions. In contrast to the Pn-(II) analogues, no inter- or intramolecular Sb···π contacts were observed, but intermolecular Bi···π contacts. Increasing the halide:aryl ratio by utilizing $PhBiCl_2$ led to the formation of $(PhBiNaph)_2$, which resembled the molecular structure and crystal packing of Pn_2Naph_2. The computational studies performed on $(PhBiNaph)_2$ confirmed a *London* dispersion driven nature, as well as the importance of specific dimer interactions for the whole crystal packing, as was previously reported for Pn_2Naph_2.

The aryl size was then increased by using 2,4,6-tri-*iso*-propylphenyl (Trip) as ligand, which led to a decreased intramolecular Pn···Pn distance for antimony, and an elongated distance for bismuth. Interestingly, a lower oxidation potential for the antimony compound 1,8-$(Trip_2Sb)_2$Naph was observed. One-electron oxidation of 1,8-$(Trip_2Sb)_2$Naph using oxidation agents like ferrocenium $[Fc]^+$ or nitrosonium $[NO]^+$ formed the [1-$(Trip_2Sb)$-8-(TripSb)][$BAr^{F\text{-}20}$] ($Ar^{F\text{-}20}$ = $(C_6F_5)_4$) complex *via* elimination of TripH. The complex contains a dative Sb···Sb interaction that was deemed stronger than the covalent bond of the corresponding “regular” distibane $(TripSb)_2$Naph, which was obtained *via* one-electron reduction with KC_8.

Utilizing the even bulkier terphenyl ligand 2,6-$Trip_2$-C_6H_3 (TTP) resulted in a series of single-atom *peri*-bridged naphthalenes TTPPnNaph (Pn = As-Bi) in good yields. These compounds contain unprecedented, strained four-membered rings with highly acute C–Pn–C angles.

In conclusion, this thesis contributes significantly to the understanding of Pn-based interactions by giving different samples of contact formation, thus allowing classification for a broader context. This work also gives further insights into the reactivity of *peri*-substituted group 15 complexes and provides a foundation for future studies on *peri*-substituted Pn-(III) complexes.

Kurzfassung

Die Bedeutung nicht-kovalenter Wechselwirkungen hat in den letzten Jahren stetig zugenommen und auch der stabilisierende Effekt der *London* Dispersion ist unter anderem in der Organometallchemie nun weithin anerkannt. Obwohl ein signifikanter Anteil der Forschung auf Wasserstoffbindungen, Liganden-Liganden-Wechselwirkung bzw. organische Moleküle fokussiert, zeigten weitere Studien, dass *London* Dispersion auch für schwere Elemente, wie die späten Gruppe 15 Elemente Antimon und Bismut, eine wichtige Rolle spielt. Zu Beginn des 20. Jahrhundert schloss *Boris Nikolayevic Menshutkin* durch Messung thermodynamischer Daten auf die Bildung verschiedener Pniktogenhalogenkomplexe mit aromatischen und nicht-aromatischen Molekülen. Der eindeutige Nachweis zur Bildung dieser Komplexe konnte erst einige Jahrzehnte später erbracht werden. Weitere Studien zeigten, dass diese Pn···π Kontakte typischerweise von *London* Dispersion dominiert werden.

Diese Dissertation liefert weitere Erkenntnisse zur Triebkraft der Bildung von inter- und intramolekularen Wechselwirkungen und Kristallpackungen metallorganischer Verbindungen. Dafür wurde die Substitution der 1,8-Positionen von Naphthalin, welche auch als *peri*-Positionen bekannt sind, mit Pniktogenen durchgeführt, um die Bildung inter- und intramolekulare Pn···Pn, Pn···π, and π···π Kontakte zu ermöglichen. Durch den kurzen Abstand zwischen den *peri*-Positionen sind dabei besonders intramolekulare Pn···Pn Kontakte von Interessen, da ein Gleichgewicht zwischen Repulsion und Attraktion zu erwarten ist. Die erhaltenen Systeme wurden mittels Standardmethoden (NMR, IR, Elementaranalyse, sc-XRD) charakterisiert und ihre elektronische Struktur mittels quantenchemischer Methoden untersucht.

Zunächst wurde die Synthese des Bi_2Naph_2 angestrebt. *Schulz et al.* berichteten zuvor von den entsprechenden Antimon- und Arsenderivaten, während die Eigenschaften des Bi_2Naph_2 nur basierend auf quantenchemischen Rechnungen postuliert wurden. Bi_2Naph_2 konnte nun mehr in geringer Ausbeute erhalten werden und bildete eine Anordnung im Kristall, die vom theoretischen Postulat abwich, da unter anderem typische π···π Kontakte nicht beobachtet werden konnten. Zusätzlich wurde ein neues Polymorph des As_2Naph_2 erhalten, welches unterschiedliche intermolekulare Kontakte aufwies. Mit Hilfe quantenchemischer Rechnungen wurde gezeigt, dass die Bildung der unterschiedlichen Packung der Pn_2Naph_2 (Pn = P-Bi) auf die Maximierung von *London* Dispersion zurückgeführt werden kann, wobei einzelne

Dimerwechselwirkungen eine relevante Rolle spielen und dabei die gesamte Packung bestimmen können.

Nachdem die Serie der Pn-(II) Verbindung vervollständigt war, wurde die Synthese vergleichbarer Pn-(III) Verbindung angestrebt. Zunächst wurde der einfachste aromatische Ligand, der Phenylligand gewählt und die Bis(diphenylpnicta)naphthalene 1,8-$(Ph_2Pn)_2$Naph (Pn = Sb, Bi) und das Acenaphthenderivat 5,6-$(Ph_2Sb)_2$Acenaph (Acenaphthen = 1,8-Ethylennaphthalen) mittels Salzmetathese hergestellt. Im Gegensatz zu den Pn-(II) Verbindungen wurden keine Sb$\cdots\pi$ Kontakte in der Kristallpackung des Antimonderivates beobachtet, während entsprechende Bi$\cdots\pi$ Kontakte in der entsprechenden Bismutverbindung auftreten. Durch den Einsatz von $PhBiCl_2$ konnte auch $(PhBiNaph)_2$ erhalten werden, welches in seiner Molekülstruktur und Kristallpackung den Pn_2Naph_2 ähnelte. Quantenchemische Rechnungen konnten in Analogie zu den Pn_2Naph_2 zeigen, dass die intermolekularen Kontakte im $(PhBiNaph)_2$ von *London* Dispersion dominiert werden und spezifische Dimerwechselwirkungen die Packung signifikant beeinflussen.

Durch Verwendung des sterisch anspruchsvolleren 2,4,6-Tri-*iso*-propylphenyl-liganden (Trip) wurden die entsprechenden *peri*-substituierten Verbindungen 1,8-$(Trip_2Pn)_2$Naph hergestellt. Diese zeigten ein unerwartetes Verhalten, denn während im Antimonderivat der intramolekulare Sb$\cdots$Sb Abstand verkleinert wurde, kommt es zu einer Verlängerung des Bi$\cdots$Bi Abstandes im Bismutderivat. Darüber hinaus wurde ein erniedrigtes Oxidationspotential des 1,8-$(Trip_2Sb)_2$Naph festgestellt. Durch eine Ein-Elektronen-Oxidation mit Ferrocenium $[Fc]^+$ oder Nitrosonium $[NO]^+$ konnte der kationische Komplex $[(Trip_2Sb)(TripSb)Naph][BAr^{F\text{-}20}]$ ($Ar^{F\text{-}20} = (C_6F_5)_4$) erhalten werden, welcher über die Elimierung von TripH gebildet wird. Hierbei wird eine dative Sb$\cdots$Sb Wechselwirkung ausgebildet. Quantenchemische Rechnungen ergaben eine höhere Energie und damit stärkere Wechselwirkung für die dative Wechelwirkung im Vergleich zur kovalenten Bindung im „regulären“ Distiban $(TripSb)_2$Naph, welches durch Reduktion des kationischen Komplexes mit KC_8 erhalten wurde.

Eine weitere Erhöhung des sterischen Anspruchs durch Verwendung des Liganden 2,6-$Trip_2$-C_6H_3 (TTP) führte in guten Ausbeuten zur Bildung einer Serie von Naphthalinverbindungen TTPPnNaph (Pn = As-Bi), in denen die *peri*-Positionen durch ein Pniktogenatom verbrückt werden. Diese Verbindungen beinhalten somit gespannte, viergliedrige Ringe mit sehr spitzen C–Pn–C Winkeln.

Zusammenfassend trägt diese Arbeit signifikant zum Verständnis pniktogenbasierter Wechselwirkungen bei. Darüber hinaus wurden weitergehende Erkenntnisse zur Reaktivität *peri*-substituierter Gruppe 15 Komplexe gewonnen.

Table of Contents

List of Abbreviations and Symbols

Acenaph	5,6-acenaphthenediyl, 1,8-ethylenenaphthalene-5,6-diyl, $C_{12}H_{10}$
ADF	Amsterdam density functional
Ar	aryl, specified in text
avg.	average
b.p.	boiling point
BCP	bond critical point
BSSE	basis set superposition error
n-Bu	*n*-butyl, $CH_3(CH_2)_3$
t-Bu	*t*-butyl, $(CH_3)_3C$
CCP	cage critical point
CV	cyclic voltammetry
$\Delta G^{\neq}$	Gibbs free energy change
$\Delta\nu$	chemical shift difference [Hz]
DCM	dichloromethane, CH_2Cl_2
DFT	density functional theory
DMF	dimethylformamide, $HC(O)N(CH_3)_2$
e.g.	*exempli gratia:* for example
E	element, specified in text
Et	ethyl, C_2H_5
et al.	*et alii:* and others
φ	dihedral angle [°]
Fc	ferrocene, $Fe(C_5H_5)_2$
h	Planck constant, $6.626 \cdot 10^{-34}$ J Hz^{-1}
HOMO	highest occupied molecular orbital
HPE	hexaphenylethane, $(C_6H_5)_6C_2$
IQA	Interacting quantum atoms
i.e.	*id est:* that is
IR	infrared
IR abbreviations	m – medium s – strong w – weak
k_B	Boltzmann constant, $1.380 \cdot 10^{-23}$ J K^{-1}
L	ligand, specified in text
LED	local energy decomposition
LD	London dispersion
LDFs	London dispersion forces
LUMO	lowest unoccupied molecular orbital
m.p.	melting point
M	metal; specified in text

MBO	Mayer bond order
Me	methyl, CH_3
Mes	mesityl, 2,4,6-trimethylphenyl, 2,4,6-$(CH_3)_3C_6H_2$
Naph	1,8-naphthalenediyl, $C_{10}H_6$
NBO	natural bond orbital
NCI	non-covalent interaction
NMR	nuclear magnetic resonance
NMR abbreviations	s – singlet s (br) – broad singlet d – doublet dd – doublet of doublets m – multiplet q – quartet sept – septet t – triplet tt – triplet of triplets δ – chemical shift
Ph	phenyl, C_6H_5
Pn	pnictogen atom, specified in text
ppm	parts per million
i-Pr	*iso*-propyl, $(CH_3)_2CH$
QTAIM	quantum theory of atoms in molecules
R	organic group, specified in text
R	universal gas constant, 8.314 J K^{-1} mol^{-1}
r_{vdW}	van der Waals radius [Å]
RCP	ring critical point
RMSD	root-mean-square deviation
sc-XRD	single-crystal X-ray diffraction
T	temperature; tetrel, specified in text
T_c	coalescence temperature
thf	tetrahydrofuran, C_4H_8O
TMEDA	tetramethylethylenediamine, $((CH_3)_2N)_2C_2H_4$
TMS	trimethylsilyl, $(CH_3)_3Si$
TMSn	trimethylstannyl, $(CH_3)_3Sn$
TPM	triphenylmethyl, $(C_6H_5)_3C$
Trip	2,4,6-tri-*iso*-propylphenyl, $((CH_3)_2CH)_3C_6H_2$
TTP	1,3-bis(2,4,6-tri-*iso*-propylphenyl)phenyl, $(((CH_3)_2CH)_3C_6H_2)_2C_6H_3$
UV-vis	ultraviolet-visible
VT-NMR	variable temperature NMR
WBI	Wiberg bond index
X	halide, specified in text
ZPE	zero-point vibrational energy

1. Introduction

Bonding interactions between atoms and molecules can be assigned to one of four general types, *i.e.* covalent, metallic, ionic, or non-covalent. While ionic interactions describe the type of chemical bondings, or better yet, the "electron exchange" in classical salts such as NaCl, bonds of the covalent type are typically found in, *e.g.* C–C and C–H bonds and are instead formed *via* "electron sharing". Metallic bonding, which is commonly found in elemental metals, can be understood as "electron distribution" whereby the formation of an "electron cloud" is the result of the orbital band structure. The fourth type of interaction, the non-covalent interactions (NCIs), is rather abstract in comparison. One of the most prominent examples are the *van der Waals* forces named after *Johannes Diderik van der Waals* (*1837-†1923) which describe three types of dipole interactions. These include the *directed effect* (the interaction of two permanent dipoles), the *inducted effect* (the interaction of a permanent dipole with an induced dipole), and the *dispersion effect* (the interaction of two induced dipoles).[1,2] The *dispersion effect* or the *London dispersion* (LD) named after *Fritz London* (*1900-†1954) has received increasing interest within the last decade. Even though the strength of a single LD interaction is typically rather weak, LD has a significant contribution to the stabilization of molecular and supramolecular structures and should therefore not be neglected.[3,4–6] This was proven by the isolation of sterically heavily crowded ethane derivatives synthesized by *Schreiner et al*. In contrast to their less crowded predecessors, these compounds showed improved thermal stability and formed one of the longest C–C bonds known to date, which was stabilized through multiple H···H contacts.[7,8] In conjunction with these findings, various investigations including theoretical and experimental methods in solution,[9] in the gas-phase,[10–12] and in the solid-state[13–15] were performed, while the re-evaluation of previous studies[4–6] often revealed a stronger LD contribution than initially believed.

2. Non-Covalent Interactions

In the late 1970s, *Kollman* defined non-covalent interactions "[…] *as those in which: (1) electrons stay paired in reactants and products and (2) there is no change in the type of chemical bonding in reactants and products.*"[16] This definition may apply to various types of interactions including hydrogen bonds,[17] charge-transfer complexes,[18] σ/π-hole interactions,[19] π-complexes,[17] and *London* dispersion (LD).[20]

Although LD describes a specific phenomenon, the nature of remaining interactions is often not directly evident whereby electrostatics have frequently been considered as the driving forces behind these interactions.[16,17,21] Nevertheless, the development of new methods such as dispersion corrections for DFT computations[22] or *local energy decomposition analysis* (LED)[23,24] are now offering a more detailed understanding of these interactions, often revealing a more significant if not major contribution from LD.[4–6,25,26,27]

2.1. London Dispersion Forces

When two nonpolar atoms are brought in close proximity, they experience an attractive force before *Pauli* repulsion becomes too strong. This attraction occurs due to electron correlation effects and can be vaguely described as the fluctuation of electron density, which causes a temporal and uneven distribution of charge, thus leading to the formation of a momentarily induced dipole. This induced dipole can interact with the other atom, generating a dipole which results in an attractive force. The dipole in the first atom does not persist and continues to fluctuate. In contrast, the dipole in the second atom will follow these fluctuations causing a correlation between the dipoles and as a result a non-zero attractive force known as *London* dispersion.[2,16,27] A popular estimation of this interaction is the *Lennard-Jones* potential,[17,28] which describes the repulsion and attraction of two approaching particles in qualitative accuracy;

$$E_{\mathrm{LJ}}(\mathrm{r}) = \varepsilon \left[\left(\frac{\mathrm{r}_0}{\mathrm{r}} \right)^{12} - 2 \left(\frac{\mathrm{r}_0}{\mathrm{r}} \right)^{6} \right] \qquad (1)^{[20]}$$

where ε represents the depth of the potential minimum for which r_0 is the necessary distance between the particles. Since ε and r_0 are constants, the overall potential energy $E_{LJ}(r)$ is solely dependent on the distance r. Furthermore, the potential has an attractive and repulsive term whereby the attraction scales with r^{-6}, whereas the repulsion experience a scaling with r^{-12}.[20]

A single LD interaction typically has low energy which can only give a minimal energetic contribution to the overall stabilization of a molecular state. For the noble gases, *London dispersion forces* (LDFs) represent the only occurring interactions causing their relatively low boiling and melting points (Table 1).[16,20]

Table 1. Comparison of boiling (b.p.) and melting points (m.p.) of noble gases and chalcogens of the respective period.[29]

	m.p. [°C]/b.p. [°C]		**m.p. [°C]/b.p. [°C]**
Ne	–248.59/–246.08	F_2	–219.67/–188.12
Ar	–189.35/–185.85	Cl_2	–101.5/–34.04
Kr	–157.38/–153.22	Br_2	–7.2/58.8
Xe	–111.79/–108.12	I_2	113.7/184.4

Although singular LD interactions are relatively weak, these interactions increase with atomic number and thus with the polarizability of the respective atom. However, as larger contact radii increase the distance r between heavy atoms, this causes a loss in LD energy due to its r^{-6} dependency.[30] Nevertheless, LDFs show a greater effect in alkanes; as these compounds are highly unipolar, their main form of intermolecular interactions are dominated by *van der Waal* forces. In contrast to noble gases, these compounds can interact through a higher number of atoms per molecule, and due to the additive nature of LDFs, a larger interaction energy is the result (Table 2).[2,20,31,32]

Table 2. Boiling and melting points of selected alkanes.[29]

	m.p. [°C]/b.p. [°C]		**m.p. [°C]/b.p. [°C]**
CH_4	–182.47/–161.48	*n*-C_6H_{10}	–95.35/68.73
C_2H_6	–182.79/–88.6	*n*-C_7H_{16}	–90.55/98.4
n-C_3H_8	–187.63/–42.1	*n*-C_8H_{18}	–56.82/125.67
n-C_5H_{12}	–129.67/–36.06	*n*-C_9H_{20}	–53.46/150.82

As indicated by the boiling and melting points of alkanes, *London* dispersion forces also grow in proportion to the number of atoms involved, which further demonstrates the additive character of these interactions.[31,32]

2.1.1. London Dispersion in Action

In modern research, the role and relevance of LDFs have been neglected and underestimated for a long time *e.g.* in the stabilization of molecular structures. *Schreiner* and co-workers pointed at this misconception with the aid of hexaphenylethane (HPE, **1**$_2$). While the unsubstituted HPE is not isolable and the corresponding triphenylmethane radical (TPM, **1**$^\bullet$) dimerizes in the quinoid structure **2**, the all-*meta*-*tert*-butyl-substituted HPE (*t*-Bu-**1**$_2$) has been known for decades.[7,33,34] Although a significant electronic influence of the *tert*-butyl groups was firstly dismissed in the early literature,[33] later computations indicated a significant attractive force between these groups, stabilizing ethane *t*-Bu-**1**$_2$.[35] *Schreiner* and co-workers used these insights to design ethane derivatives by employing the diamondoid substituents adamantane (**3**), diamantine (**4**), and triamantane (**5**), which resulted in species that are sterically more crowded and also provide a larger H···H contact surface. While the *tert*-butyl substituted HPE (*t*-Bu-**1**$_2$) is a stable compound, it is thermally labile, however the dimers **3•5**, **4•4**, and **5•5** exhibit high melting points (Scheme 1).[7]

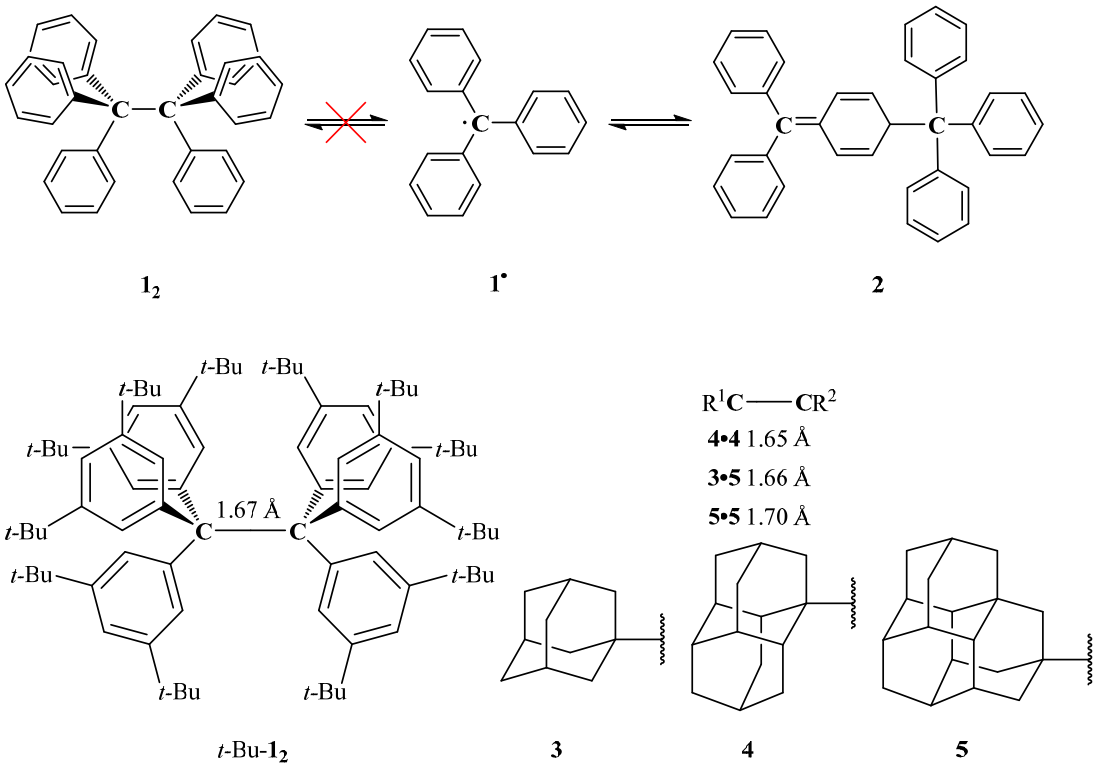

Scheme 1. The dimerization of sterically hindered methyl radicals. Contrary to early beliefs, the triphenylmethyl radical (**1**$^\bullet$) does not dimerize to hexaphenylethane (**1**$_2$), but instead the quinoid structure **2** is formed. However, increasing the steric demand allows the isolation of the all-*meta*-substituted hexaphenylethane derivative *t*-Bu-**1**$_2$ as well as the more stable bisdiamondoids **3**-**5**.[7,33,34]

These results offered a new perspective on molecular chemistry. Not only did they allow the isolation of one of the longest C–C single bonds[8] and shortest H···H contacts[15] reported to date, they have also led to the development of a correction potential function for DFT computations, which lacked the contribution of *London* dispersion,[22,36] as well as a re-evaluation of stabilizing forces in organometallic compounds.[4–6] The stabilizing effect of bulky substituents in organometallic compounds was generally described by kinetic hindrance *via* shielding of the metal centers. While this is still a notable contribution, ligand-ligand interactions have been neglected or were solely viewed as destabilizing due to *Pauli* repulsion.[4–6] However, the re-evaluation of some of these old compounds including *Lapperts'* distannene $Sn_2\{CH(SiMe_3)_2\}_4$ (**6**)[37] or *Powers'* "jack-in-the-box" dipnictanes $Pn_2\{CH(SiMe_3)_2\}_4$ (Pn = P **7**, As **8**)[38] gave important insights with respect to heavy main group chemistry. Taking into account newly developed methods and understanding of LD, DFT computations without dispersion correction suggested that the monomers of the ditetrenes $T_2\{CH(SiMe_3)_2\}_4$ (T = Ge **9**, Sn **6**, Pb **10**) and dipnictanes **7** and **8** should be preferred over their respective dimers, which is in contrast to the experimental observations (Table 3).[39,40]

Table 3. Calculated thermodynamic data for the dissociation of compounds **6-10** into their respective monomers at 25 °C. The energies are given in kcal mol^{-1}.[39,40]

	$T_2\{CH(SiMe_3)_2\}_4 \rightarrow 2\ \ddot{T}\{CH(SiMe_3)_2\}_2$					
	Ge (**9**)		Sn (**6**)		Pb (**10**)	
	B3PW91	B3PW91-D3	B3PW91	B3PW91-D3	B3PW91	B3PW91-D3
ΔE^a	–2.3	28.7	2.1	26.3	–0.6	15.2
ΔH	–2.3	30.1	2.2	27.0	–1.5	15.2
$-T\Delta S$	–15.5	–20.7	–17.0	–19.9	–8.4	–16.9
ΔG	–17.8	9.4	–14.8	7.1	–9.9	–1.4
	$Pn_2\{CH(SiMe_3)_2\}_4 \rightarrow 2\ \dot{P}\ddot{n}\{CH(SiMe_3)_2\}_2$			
	P (**7**)		As (**8**)	
	B3PW91	B3PW91-D3	B3PW91	B3PW91-D3
ΔE^b	–10.3	37.6	–6.5	37.1
ΔH^b	–13.2	32.6	–8.8	34.0
$-T\Delta S^b$	–18.9	–21.7	–20.8	–26.3
ΔG^b	–35.5	10.9	–29.6	7.7

[a]With ZPE and BSSE correction. [b]With BSSE correction.

These examples highlighted the ligand-ligand-based LDF, while subsequent studies manifested the importance of these interactions.[13,15,41,42] However, it is important to note that the difference in energy between a calculation performed with and without the D3 correction does not correspond to the total LD contribution, but can be viewed as an order of magnitude estimation.[41,43]

The ligand-ligand-based *London* dispersion forces represent one aspect of possible interactions. As described before, the energy of LD increases when the interacting atoms grow in atomic number (Table 1). Besides these existing interactions between noble gases, other element-element interactions of considerable strength have also been observed. Another common example are *metallophilic* interactions, which describe strong attractive forces between heavy closed-shell species such as $d^{10}\cdots d^{10}$ interactions in Au(I) compounds,[44,45] and $s^2\cdots s^2$ interactions between Tl(I) or In(I) atoms.[46,47] Previous assumptions underestimated the effects of *London* dispersion and regarded the relativistic effect, *i.e.*, the radial contraction and stabilization of low-lying *s*- and *p*-orbitals due to the acceleration of electrons near the nucleus, as the sole reason for this behavior.[26,48,49] However, later computations indicated that dispersion also plays a leading role in these interactions.[26,27,50,51,52,53] Interestingly, metallophilic interactions have also been observed for the lighter homologs silver[51,54] and copper,[54,55] although the energy of these interactions is typically lower than for the heavier homolog since they can be improved through the relativistic effect, thereby even reaching the strength of weak covalent bonds.[47,50,53,56] These findings are not only limited to homometallic systems, but instead a plethora of heterometallic systems adapting this kind of interaction have been also reported (Figure 1).[50,57,58,59]

In general, *London* dispersion was not only an underestimated force, but an improved understanding of this force allowed the achievement of novel and surprising results.[7,11,35,59] This highlights the necessity for further investigation on LDFs in order to improve our understanding and therefore the ability to control these inter- and intramolecular forces.

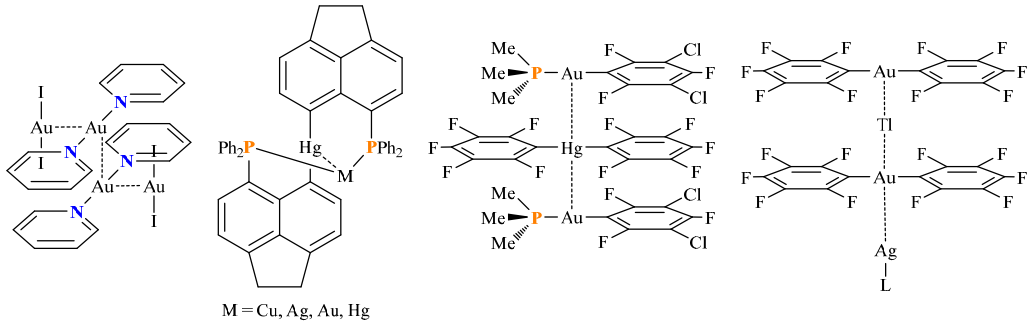

Figure 1. Metallophilic contacts formed by various metals in homo- and heterometallic systems.[44,58,59]

2.2. Pnictogen Bonding

In the 18th century, *Louis-Claude Cadet de Gassicourt* prepared a compound with a strong garlic odor, which was later identified by *Bunsen* as Me_4As_2 (**11**),[60] which represents the first known organometallic compound, while heavier homologs Me_4Sb_2 (**12**) and Me_4Bi_2 (**13**) were synthesized in the 20th century.[61,62] Even though the first reports on the heavy homologs are almost a century old,[61] their structures and closely related derivatives are still subjects to modern research. These compounds, which are liquids at room temperature, undergo a color change upon melting/solidifying, the so called *thermochromic behavior*. Early reports concluded that this effects is caused by the formation and breaking of intermolecular Pn···Pn contacts.[61–73] This hypothesis was further supported by comparable dipnictanes with bulky substituents, which lack any intermolecular Pn···Pn contacts and do not show this behavior.[70,74] More recent studies on Sb_2Et_4 (**14**) demonstrated that warming a solid crystalline sample from –150 °C up to –80 °C also resulted in a color change while retaining the crystallinity of the sample. A subsequent sc-XRD study revealed that the Pn···Pn contacts remained intact in the heated phase, thus excluding the breaking of Pn···Pn contacts as the origin of the thermochromic effect (Figure 2).[75]

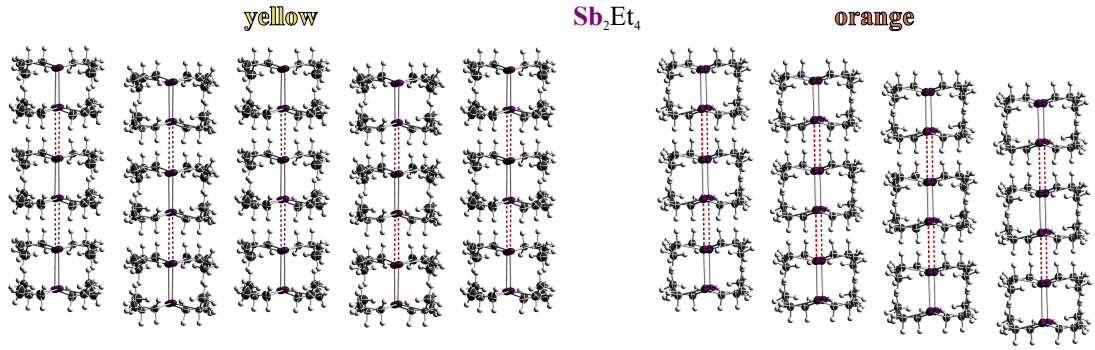

Figure 2. Different solid-state structures of Sb_2Et_4 (**14**). An alternating offset resulting in a zigzag-like arrangement is observed for the yellow phase (left), while a unidirectional offset is observed for the orange phase (right).[75]

Quantum chemical computations on simplified $(Pn_2H_4)_2$ dimers (Pn = As-Bi) suggested that LDFs have a major contribution to the interaction energy, and as a consequence, their dimer formation was compared to metallophilic interactions.[76] In addition to Pn···Pn contacts observed in heavy pnictogens in the formal oxidation state +II,[61–70,72,73,75] examples of intermolecular Pn···Pn contacts are also known for Pn(III) compound, although they rarely represent the main intermolecular interaction[77–80] or are not discussed in detail.[81,82–84] A theoretical investigation regarding the formation of ethane-like $X_3Pn{\cdots}PnX_3$ dimers (Pn = N-Bi, X = F-I) also

found an LD dominated interaction with an energetic minimum for PI_3, while the halogen X showed a significant influence on the strength of the interaction.[79] For the heavier pnictogens antimony and bismuth, such dimers were deemed unstable, although examples of $–X_2Pn\cdots PnX_2–$ interactions were already reported in the literature at the time.[79,82,84,85] Furthermore, when the halogen X was substituted by methylgroups, dimer formation for Me_3Sb (**15**)[77] and Me_3Bi (**16**)[78] was observed, while no dimerization occured for Me_3P (**17**)[86] and Me_3As (**18**)[77] (Figure 3).

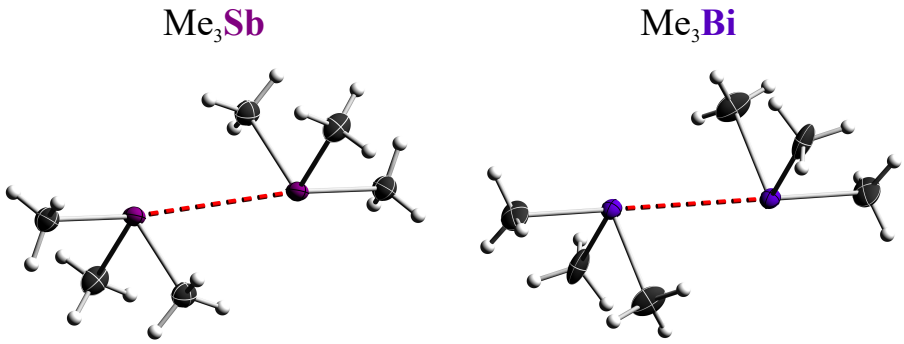

Figure 3. The dimerization of Me_3Pn (Pn = Sb **15**, Bi **16**). The intermolecular Pn···Pn distances of 3.8374(2) Å (**15**)[78] and 3.899(1) Å (**16**)[77] are well below the sum of the respective van der Waals radii.[87]

In addition to the more "weakly" bonded dimers, stronger Pn···Pn contacts forming molecular units have also been observed. An inherent characteristic of trivalent group 15 compounds is their ability to act as *Lewis* acids in addition to the prevalent *Lewis* basic character.[88] As a result, neutral donor-acceptor complexes between two PnR_3 species can be realized, although more complexes with the more *Lewis* basic phosphanes PR_3 are known.[88,89] For the heavier elements, the number of complexes is more limited since the strength of donor-acceptor interactions typically decreases with increasing atomic number. However, such complexes can be stabilized by increasing the *Lewis* acidity of the heavier element. This can be achieved through the formal generation of pnictenium ions R_2Pn^+, where a ligand is removed from a trivalent pnictogen atom. In addition to phosphane stabilized pnictenium ions,[88,90,91] arsane,[92,93] stibane[93,94] and bismuthane[95] stabilized complexes are known (Figure 4).

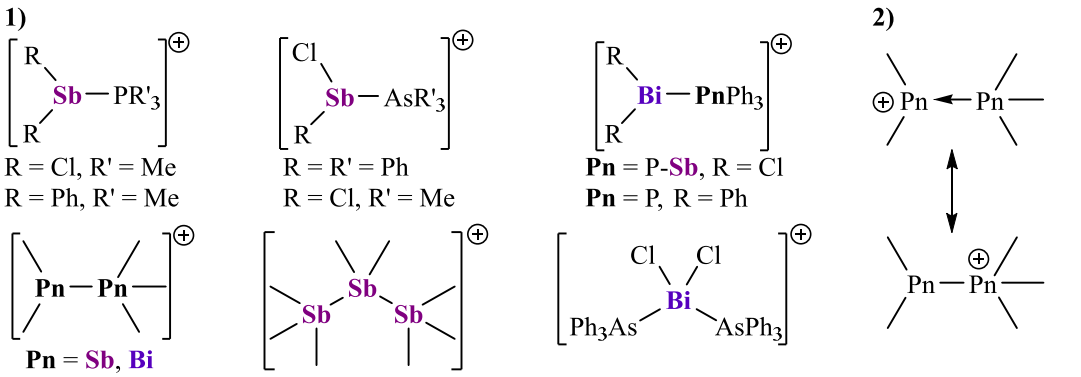

Figure 4. 1) Pnictane-stabilized pnictenium ions $[R_3Pn–PnR_2]^+$ of the heavy group 15 elements. **2)** The bonding situation can be described *via* dative or covalent bonds.

The bonding situation in these cationic complexes can be described by dative or covalent bonds, resulting in different resonance structures (Figure 4.2).[96] Nevertheless, the neutral $R_3Pn–Pn'R_3$ and cationic $[R_3Pn–Pn'R_2]^+$ can be regarded as partial σ-hole or charge-transfer complexes, which belong to the field of non-covalency.[97] Thus, in analogy to, *e.g.* tetrel,[98,99] chalcogen,[12,99,100], and halogen bonds[99,101] they represent examples of pnictogen bonds.[99,102–105] These "element bonds" however do not only include E···E' interactions but instead refer to donor-acceptor interactions between electron-rich and electron-deficient sites of one or more molecules.[19,105] As the electron-deficient site is often represented by an antibonding σ*- or π*-orbital of the respective molecule, they can also be called σ- or π-hole interaction.[19,106,107] While the formation of *Lewis* adducts is typically driven by a significant amount of electrostatic interaction,[103–105,107,108] a growing number of studies indicated that LDFs play an important if not dominant role.[23,102,109,110,111] In addition, the nature of the interaction is significantly influenced by the ligand bonded to the interacting elements.[110–112]

Aside from Pn···Pn interactions, other types of Pn-based interactions are also of major interest. In 1882, colorless crystals from a saturated mixture of $SbCl_3$ and naphthalene or benzene were reported.[113] The resulting complex formed between the arene and $SbCl_3$ is called a *Menshutkin* complex.[114,115] They are named after *Boris N. Menshutkin* who studied eutectic diagrams of antimony trihalides with a large variety of organic compounds.[116] Structural evidence of those complexes was later achieved for different pnictogens with various arenes ArH (Figure 5).[114,115,117,118,119,120]

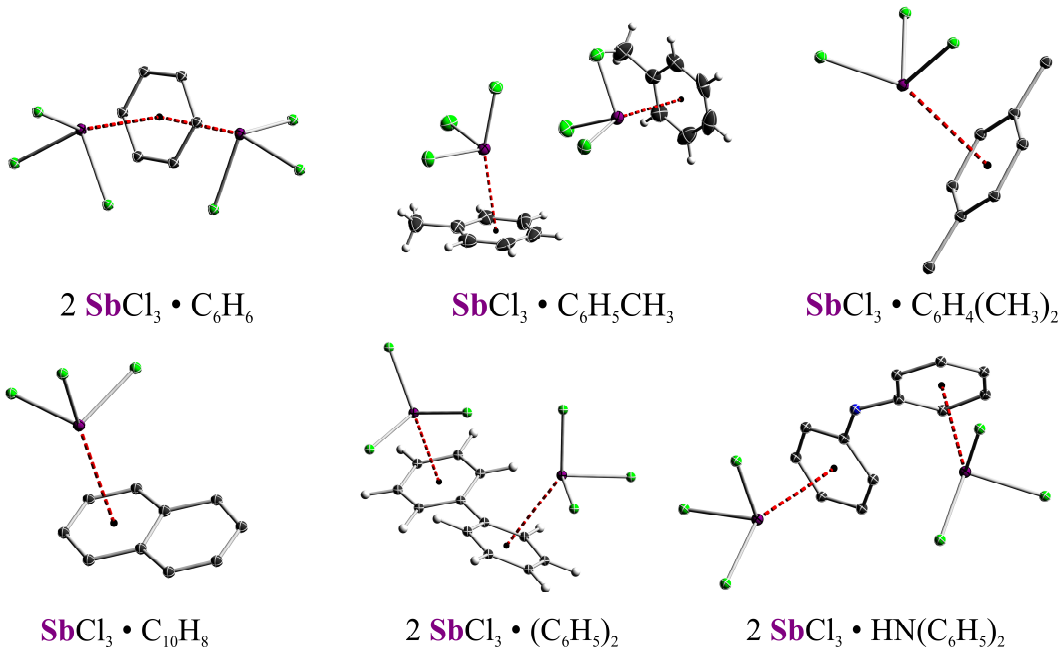

Figure 5. A selection of structural characterized antimony-(III) trichloride *Menshutkin* complexes. Hydrogens are depicted if given in the sc-XRD data.[114,115,117,119,120,121]

The complex formation with arenes is not limited to pnictogen trihalides and was observed with a variety of ligands through inter- and intramolecular contacts.[122,123] Since *Menshutkin*-type complexes are usually formed *via* the interaction of a pnictogen center with an arene, they are typically described as Pn–π complexes. However, early reports described these as charge-transfer-type interactions,[124] while a recent study concluded, that the interaction between the pnictogen center and the arene is more or less independent from the π-system of the arene. In order to demonstrate their hypothesis, the authors compared the interaction of different PnR_3 (Pn = As-Bi, R = Cl, OMe, Cl) with benzene and cyclohexane which resulted in similar interactions, even though the interactions with benzene were of higher energy. They therefore concluded that Pn···π contacts are another form of pnictogen dispersion interactions, which are amplified by a present π-system.[125] This description is in line with the recent developments regarding the interaction of two arenes, where a "special" π···π interaction was also not found.[126] However, experimental evidence of *Menshutkin*-type complexes with saturated cyclic hydrocarbons is still underway. Similar to the Pn···Pn contacts, the strength and nature of those interactions heavily depend on the ligands bound to the pnictogen center and the arene, respectively.[123–125,127]

3. The Naphthalene-Ligand Scaffold

A suitable system for the investigation of close Pn–Pn and Pn–π interactions is the naphthalene scaffold. In naphthalene, the protons in the *peri*-position are separated by roughly 2.5 Å, and are fixed in a structural rigid ligand skeleton (Figure 6).[128]

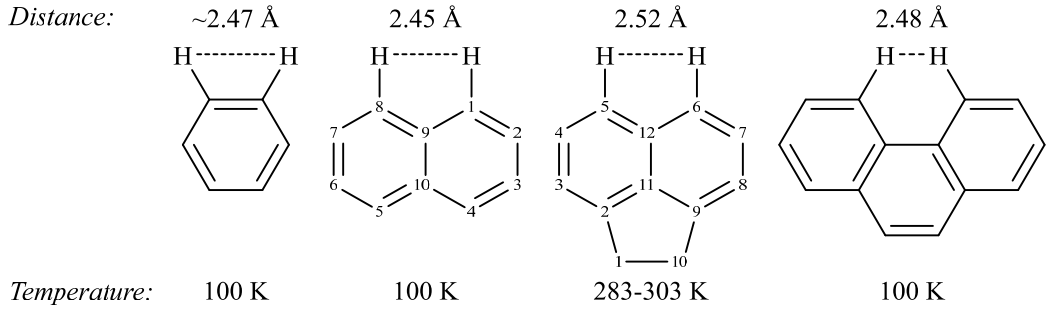

Figure 6. Distances between neighboring protons in different aromatic systems.[128,129] The respective temperature of the sc-XRD measurements are given at the bottom.

Due to the parallel orientation of the protons in naphthalene, substitution with heavier elements and/or sterically more demanding groups will result in an increased steric strain as well as repulsive intramolecular interactions.[130–134] However, this substitution may also enable attractive interactions. 1,8-$(Me_2N)_2$Naph (**19**, Naph = 1,8-naphthalenediyl),[135] also known as proton sponge, is one of the strongest known organic bases for which a pK_a of 12.34 was measured for its conjugated acid.[136] The strong basicity of **19** is attributed to either the relief of steric strain, as a result of protonation and/or an interaction between the nitrogen lone pairs.[137] Its counterpart, the hydride sponge 1,8-$(Me_2B)_2$Naph (**20**), was also investigated, revealing a high capability of removing hydrides *via* the formation of unusual strong complexes.[138]

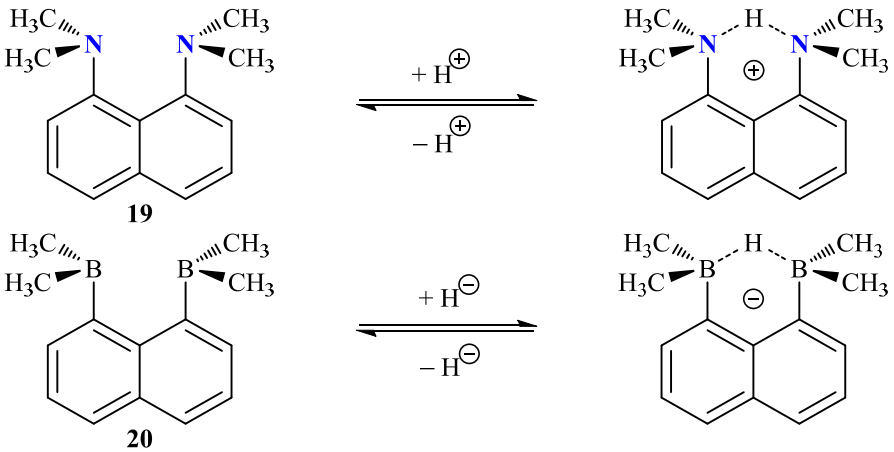

Scheme 2. The proton (**19**) and hydride sponge (**20**) are early examples of strong interactions between groups in close proximity within the naphthalene ligand framework.

However, the close distance between the *peri*-positions can also result in strong steric hindrance. In the case of 1,8-(TMS)$_2$Naph (**21**, TMS = Me$_3$Si), the repulsion leads to a significantly hindered rotation, whereas 1,8-(TMSn)$_2$Naph (**22**, TMSn = Me$_3$Sn) shows no sign of such steric strain.[131] Interestingly, the steric strain was strongest in 1,8-(Me$_3$C)$_2$Naph (**23**) and subsequently decreased with growing atomic number. This trend was associated with the increasing T–C bond lengths (T = C-Sn), which allow easier movement of the methyl groups on the heavier elements (Figure 7).[139]

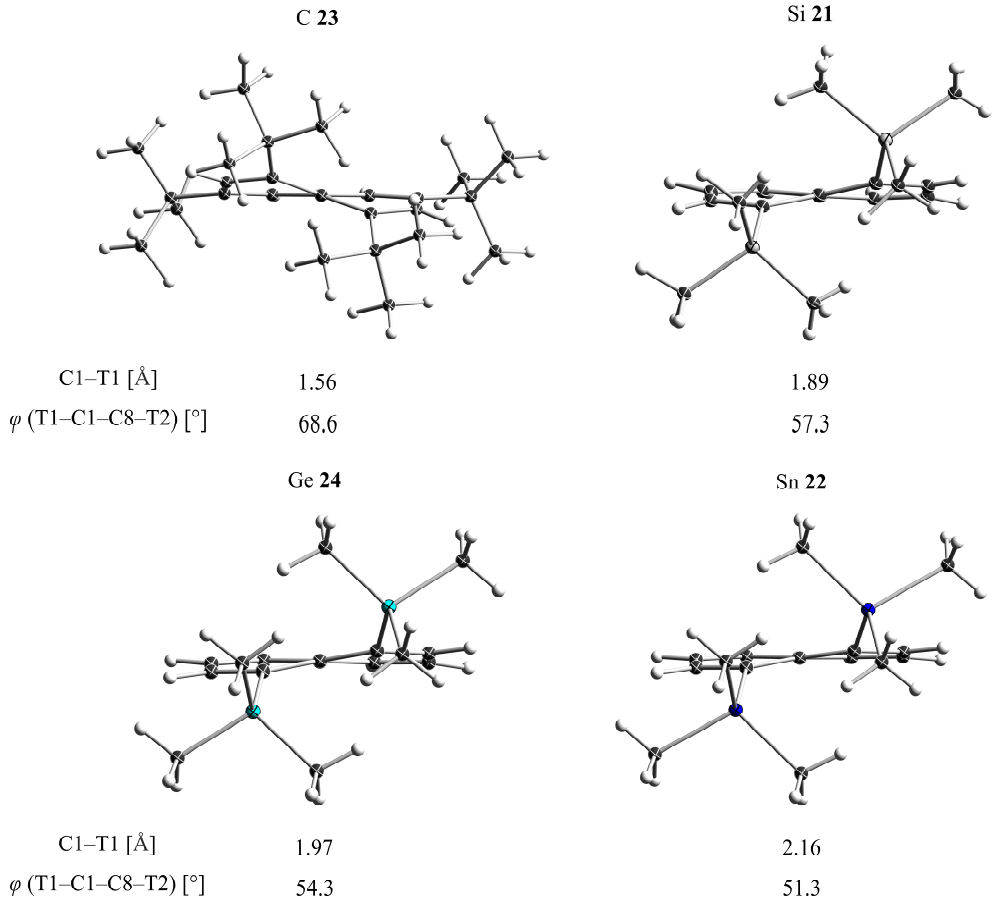

Figure 7. The reduction of steric strain in 1,8-(Me$_3$T)$_2$Naph (T = C **23**, Si **21**, Ge **24**, Sn **22**). As the bond length between the *peri*-carbons and Me$_3$T increases, the dihedral angle φ decreases.

The steric strain in *peri*-substituted naphthalenes is observable *via* different means; in compounds **21-24** two of those effects are observed (Figure 7). On one hand, the *peri*-substituents are deflected significantly out-of-plane, which can be measured with a dihedral angle or torsion angle φ in the chain R1–C1–C8–R2, with R1 and R2 being the substituents in *peri*-position. On the other hand, there is a distortion of the planarity of the naphthalene backbone. The planarity of naphthalene is reflected by a dihedral angle in the chains C1–C9–C10–C5 or C8–C9–C10–C4, respectively. Another possibility to reduce steric strain is an in-plane deflection or a stretching of the bonds (Figure 8).[134]

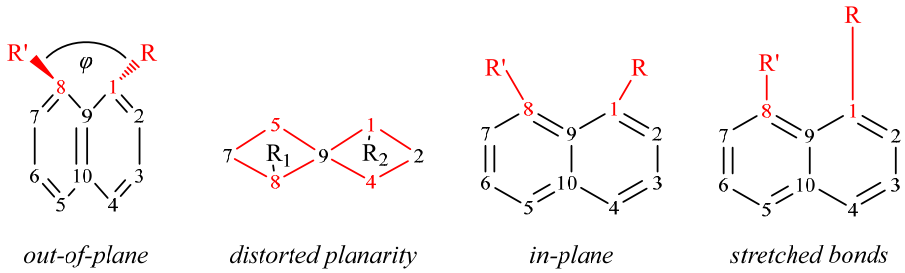

Figure 8. The *peri*-substitution of naphthalene can lead to steric strain that a given system tries to minimize.

The described characteristics of naphthalene are excellent for investigating element-element interactions, especially since a degree of repulsion and attraction can be derived from the molecular structure. In addition, intramolecular interactions between the *peri*-substituted elements can be observed *via* though-space-couplings in NMR spectroscopy, by utilizing suitable nuclei.[140] In consequence, naphthalene and its acenaphthene derivative were established as desirable systems to investigate inter- and intramolecular interactions. They have been specifically employed to study *e.g.* double bonds between heavy elements,[141,142] metallophilic contacts,[49,143] or odd-electron σ-bonds (Figure 9).[144,145]

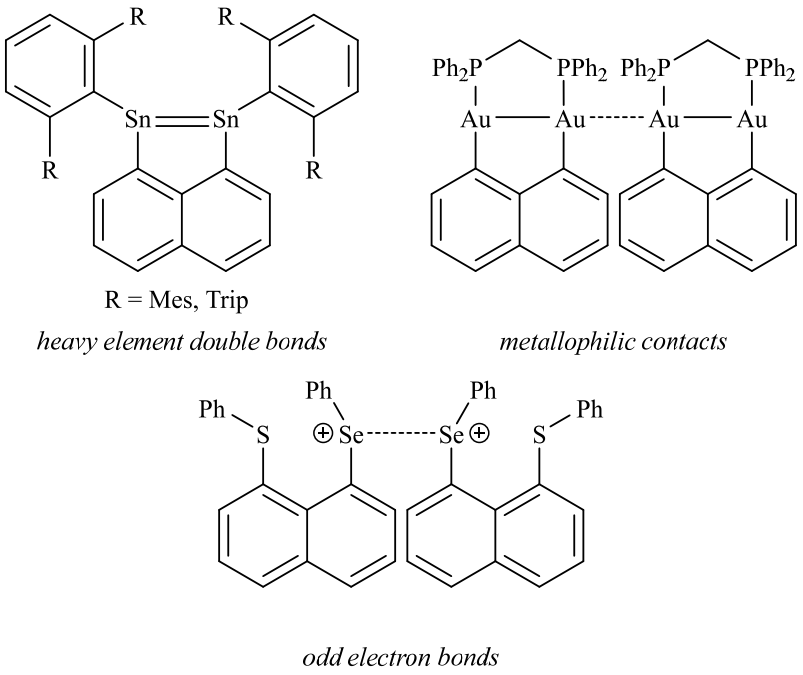

Figure 9. Examples for studied systems involving *peri*-substitution in the naphthalene framework.

3.1. Group 15 *peri*-Substituted Naphthalenediyls

A variety of bis(phosphorous)naphthalenes and -acenaphthenes in the common oxidation state +III are known, which were typically synthesized *via* salt-metathesis reactions between 1,8-Li_2Naph (**25**) and the respective phosphorous halide (Scheme 3).[130,146–149,150,151–154]

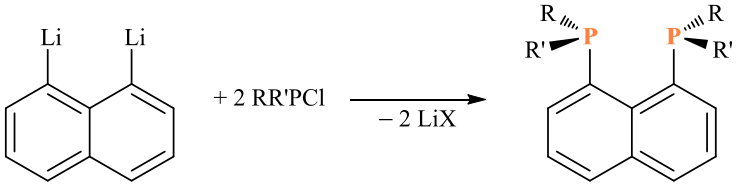

26	**a**	**b**	**c**	**d**	**e**	**f**	**g**
R	Me	*i*-Pr	Cy	Ph	Ph	Me_2N	Et_2N
R'	Me	*i*-Pr	Cy	Ph	*t*-Bu	Me_2N	Et_2N

Scheme 3. Selected examples for the synthesis of 1,8-bis(phospha)naphthalenes **26** *via* salt-metathesis reactions.

However, increasing the size of the ligand by adding sterically more demanding groups like R = R' = *t*-Bu or R = *t*-Bu, R' = C_6F_5 were attributed to the steric demand of the ligands.[147,151] Increasing the halide:phosphorous ratio to phosphorousdihalides RPX_2 in the reaction with **25** gave different products, depending on the ligand R. While employing dichlorophenylphosphine $PhPCl_2$ gave the five-membered ring **27** with a P–P covalent bond, the di(*iso*-propyl)amine derivative *i*-Pr_2NPCl_2 yielded a strained four-membered ring **28** (Scheme 4).[155]

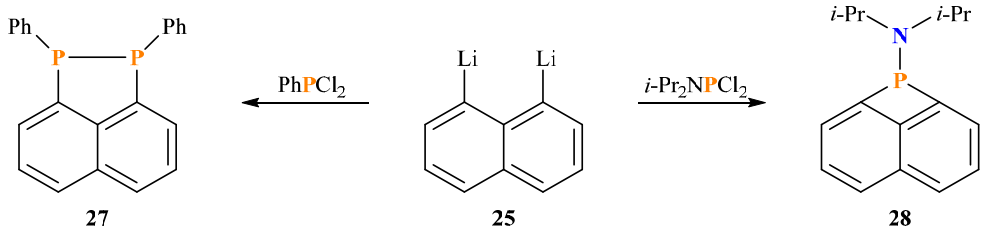

Scheme 4. Different reactivities of phosphorousdihalides towards **25** based on the ligand R were observed.

An alternative route involves the reaction of a monophosphanaphthalene 1-(RPCl)-8-Br-Naph with an alkyl lithium reagent allowing the formation of strained four-membered rings. However, this reaction showed a sensitivity towards the employed lithium reagent which resulted in the formation of cyclic and non-cyclic reaction products.[156] An even higher halogen to phosphorous ratio, *i.e.* PX_3, generally led to unidentifiable product mixtures,[148] while treating **26g** with an excess of HCl resulted

in the desired compound 1,8-($Cl_2P)_2$Naph (**29**),[148,149] which is a suitable synthon for the synthesis of various bis(phospha)naphthalenes such as **30-32** (Scheme 5).[130,149,152]

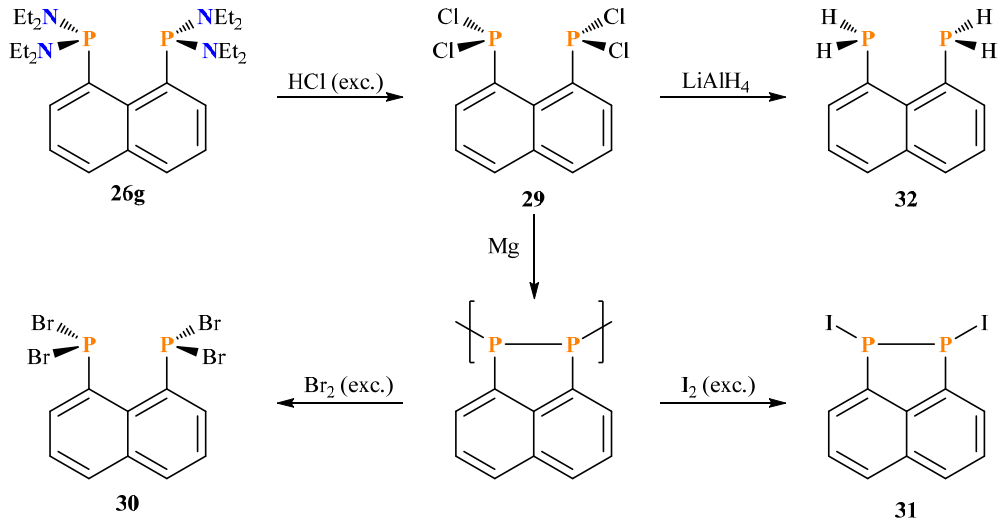

Scheme 5. Chlorophosphine **29** serving as synthon for different phosphines.

In addition, bis(phospha)naphthalenes **26** can act as chelating donors, as was shown by the coordination of transition metals.[133,151] However, treatment of methyl-derivative **26a** with BH_3 formed the *Lewis* complex **26a•BH$_3$**, which is in an equilibrium with a P–B–P bridged species (Scheme 6).[157]

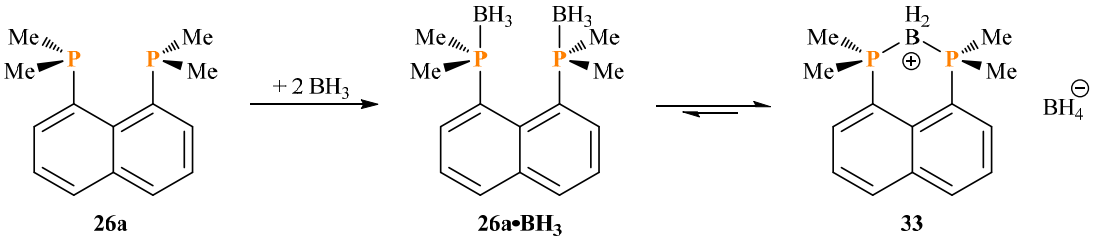

Scheme 6. Treating **26a** with an excess of thf•BH_3 results in the formation of the *Lewis* adduct **26a•BH$_3$**, which is in an equilibrium with the P–B–P bridged species **33**.

Inspired by these findings, a series of intramolecular H-bond activations of the pnictanes **34** and **36** was reported. The BH_3 adducts of the unsymmetric phosphines 1-(*i*-Pr_2P)-8-(R(H)P)-Naph (R = H **34a**, Ph **34b**, Fc **34c**) can be activated at room temperature under the release of hydrogen and the formation of P–B–P-bridged compounds **35a-c**.[153] Upon heating, phosphines **34a-c** and the corresponding phospha-arsanes 1-(*i*-Pr_2P)-8-(R(H)As)-Naph (R = H **36a**, Ph **36b**) eliminate an alkane or hydrogen, respectively, followed by the formation of a P–Pn bond (Pn = P **37**, As **38**, **39**) (Scheme 7).[154,158]

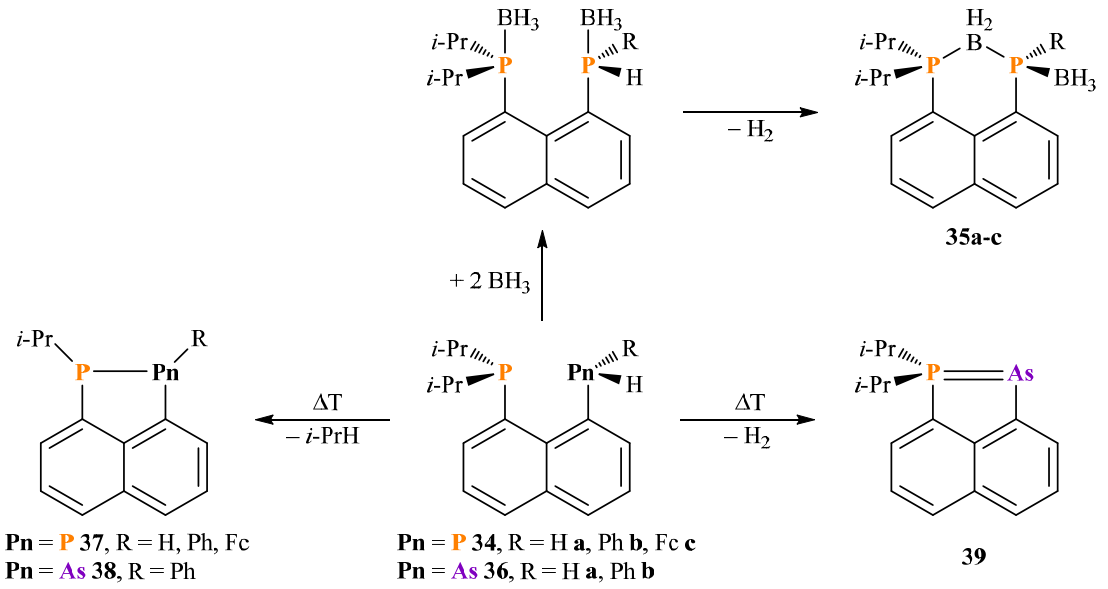

Scheme 7. Formation of P–E bonds (E = B, P, As) *via* elimination of hydrogen or *iso*-propane, respectively.

The proposed mechanism of the coupling reaction involved the formation of an intramolecularly phosphine-stabilized phosphine-radical. The P–P bond formation can then proceed with elimination of an *iso*-propane radical, which deprotonates the next phosphine to continue the chain.[154]

The studies on heteroleptic substitutions as observed in bis(phosphines) **34** and phospha-arsines **36** were extended to antimony and bismuth by using various ligands. In consequence, different orientations of the ligands were observed which showed a correlation to the *Lewis* acidity of the resulting pnictogen center. While the halide atoms in X_2Pn groups typically assume a perpendicular orientation to the Pn–P axis, the substituents in the XRPn groups (X = halide, R = alkyl/aryl; X = R = alkyl/aryl) adopt a parallel (X) and perpendicular (R) orientation to the Pn–P moiety, respectively.[91,159,160,161]

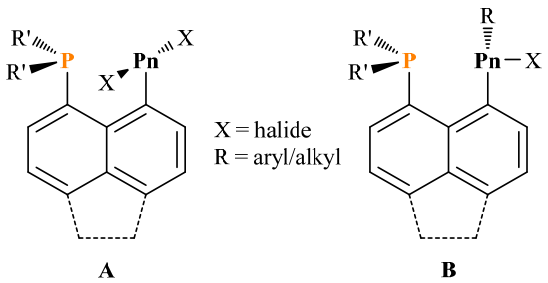

Figure 10. Typical orientations of heteroleptic substituted phospha-pnictines. An exception is found with 5-(Cl_2Sb)-6-(Ph_2P)-Acenaph, which adopts motif **B** instead of **A**.[161]

Unlike phospha-(III)-naphthalenes and acenaphthenes, similar homoleptic substituted compounds for As-Bi are barely investigated. In an attempt to prepare a chiral bis(stibine) for the coordination to transition metals, 1,8-$(Me_2Sb)_2$Naph (**40**) and 1,8-$(Ph_2Sb)_2$Naph (**41**) were synthesized. Unfortunately, only the oxidated species of **40** was characterized by sc-XRD.[162]

3.2. Interactions in Bis(naphthalenediyls)

Although the degree of freedom is already limited in *peri*-substituted naphthalenes, it can be further restricted by the introduction of a second naphthalene ligand. In an attempt to synthesize 1,8-bridged naphthalenes by reacting R_2EX_2 (E = Si **42**, R = Me **a**, Et **b**; E = Sn **43**, R = Me **a**, Ph **b**) with **25**, the corresponding "dimer" was generated for tin, while the monomer was isolated for silicon (Scheme 8).

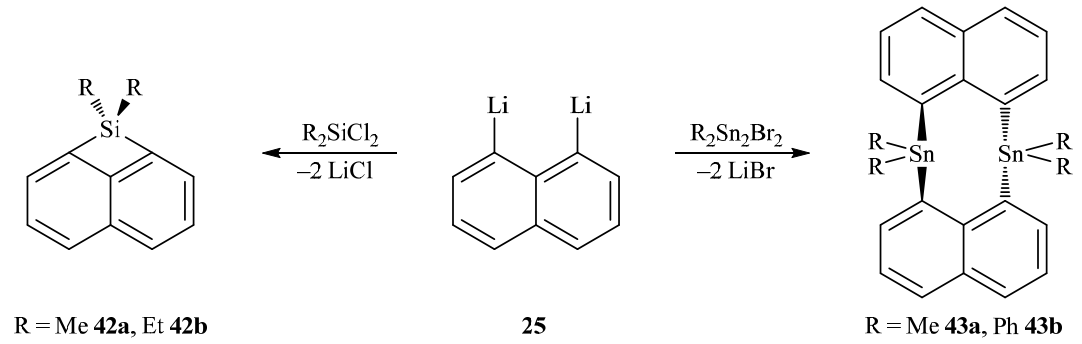

Scheme 8. Synthesis of monomeric and dimeric *peri*-substituted naphthalenes.

43a showed mostly signs of steric repulsion and upon irradiation with UV-light, the Me_2Sn groups were eliminated under C–C coupling to form the 1,8-bonded naphthalene dimer perylene (**44**).[163] Unfortunately, **25** provides a comparably hard transmetallation reagent; a softer alternative represents the 1,8-$(R_3Sn)_2$Naph (R = Me **22**, *n*-Bu **45**). Reacting tin derivative **22** with group 13 halides EX_3 (E = Ga, In) allowed the formation of digallacycle **46** and diindacycles **47** (Scheme 9).[164,165]

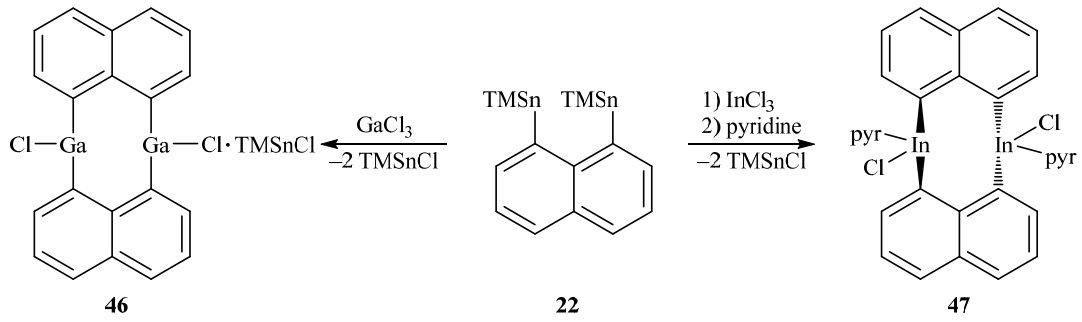

Scheme 9. Employing $TMSn_2$Naph (**22**) results in the formation of **46** and **47**.

The diindacycle $(ClInNaph)_2$ (**46**) was isolated as a pyridine (pyr) adduct exhibiting a slight deflection from the In atoms above and below the naphthalene plane,[164] as well as a thf complex in which the indium centers were situated in-plane with the naphthalene ligands.[166] In contrast, the digallacycle $(ClGaNaph)_2$ (**47**) formed a complex with the TMSnCl by-product. The TMSnCl acts as a linker between two gallium centers of different fragments forming Ga–Cl–Sn–Cl–Ga chains, while a chlorine atom is bridging the *peri*-gallium centers of the same fragment.[165] The structural motif of a *peri*-bridged Ga–Cl–E unit was also observed in heteroleptic substituted galla-stannanes **48**, which act as polyfunctional *Lewis* acids with cooperating interactions between the two metal centers. As a result, the addition of *Lewis* bases led to the formation of donor-acceptor complexes. However, in reactions with $[PPh_4][X]$ (X = Cl-I) the resulting complexes **49a-c** retain the briding chloride, while complex **50** with the stronger *Lewis* base pyridine exhibits a significant distortion (Scheme 10).[167,168]

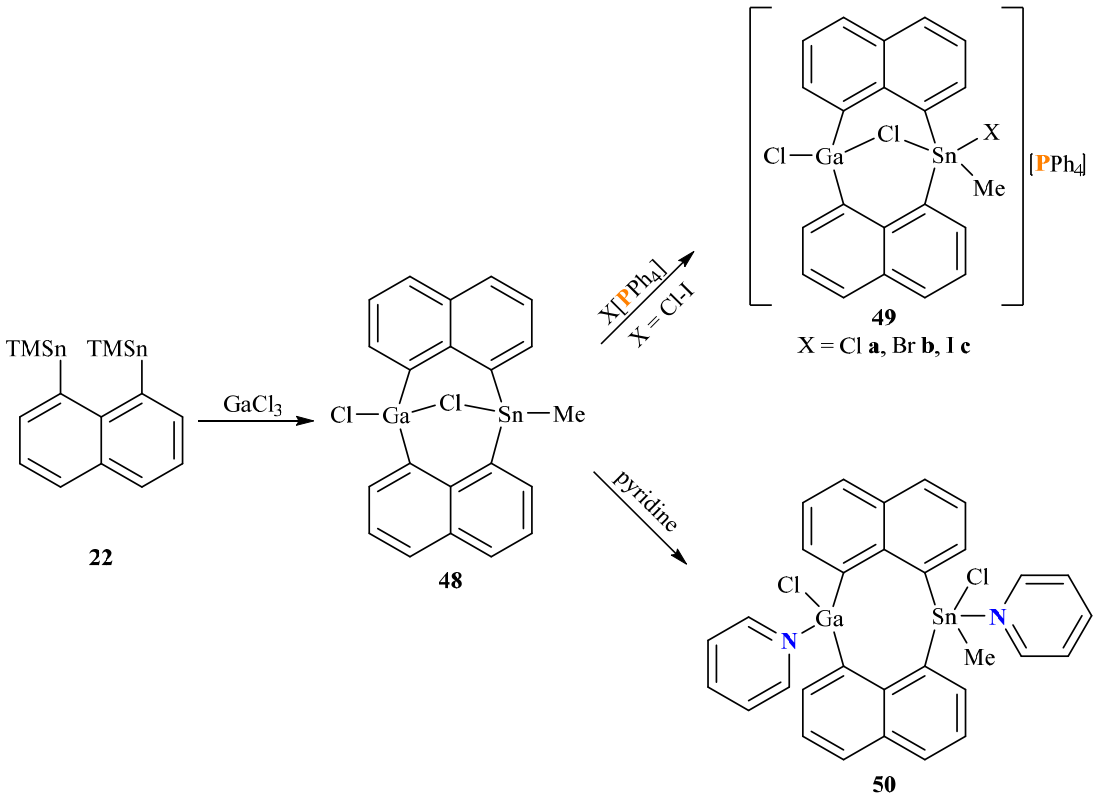

Scheme 10. The galla-stannane **48** acts as a polyfunctional *Lewis* acid.

In addition to group 13/14 element complexes, transition metals have also been incorporated in a bis(naphthalenediyl)-ligand scaffold. The homolytic substituted dimercuracycle **51** is a planar molecule with small deflections with redard to the mercury centers. The Hg···Hg *peri*-distances are shorter than the bonding distance of

metallic mercury, but longer than the sum of covalent radii.[49] Substitution of one mercury center with InX (X = Cl **52**, Br **53**) led to an increase in the metal···metal distance compared to **51**. However, the sc-XRD data was collected from adducts containing $InCl_3$ and thf, which have an influence on the metal-metal interaction through donor-acceptor interactions (Scheme 11).[166]

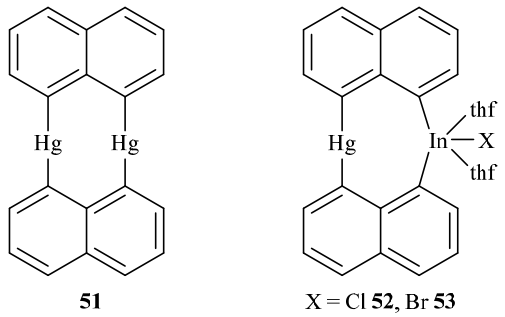

51 X = Cl **52**, Br **53**

Scheme 11. 51 exhibits short intramolecular M···M contacts, which are elongated upon substitution of a mercury atom with indium.

Unsupported metal-metal interactions in the bis(naphthalenediyl) scaffold were achieved in the form of diphenylstiboranyl-mercury **54** and -gold **55** bis(naphthalenediyl) complexes. Although the naphthalenes are *peri*-substituted with heavy elements of the sixth row, relatively short Sb···M distances (M = Au 2.7486(7) Å,[169] Hg 3.0601(7) Å[170]) were found. As the covalent radii of gold and mercury are comparable in size (r_{cov}(Au) = 1.36 Å; r_{cov}(Hg) = 1.32 Å)[171] the authors suspected significantly stronger interactions between the Sb(V) and Au(III) center.[169] However, while the addition of *Lewis* bases to **55** gives no significant change in the Au–Sb interaction,[169] a significant amplification was computed for **54** (Figure 11).[172]

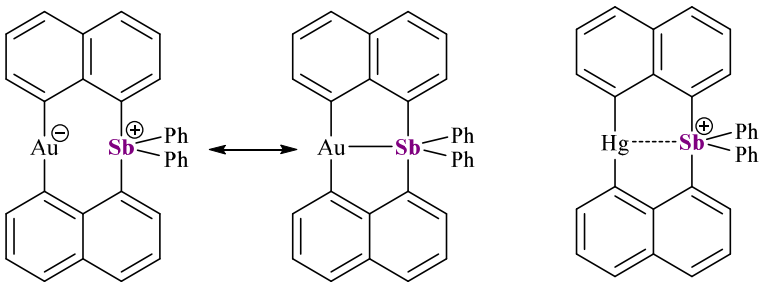

55 **54**

Figure 11. Intramolecular Sb···M interactions in **54** and **55**.

In addition to intramolecular interactions in the bis(naphthalenediyl) scaffold, dominant intermolecular interactions were reported for naphthalenediyl-substituted

dipnictanes Pn_2Naph_2 (Pn = P **56**, As **57**, Sb **58**).[173–175] While **56** and **57** adopted the same structural motif, Sb_2Naph_2 (**58**) crystallized in a different packing mode. Both motifs contained intermolecular CH···π (blue) and π···π contacts (red), however additional Sb···π contacts (green) were reported for **58** (Figure 12).[174,175]

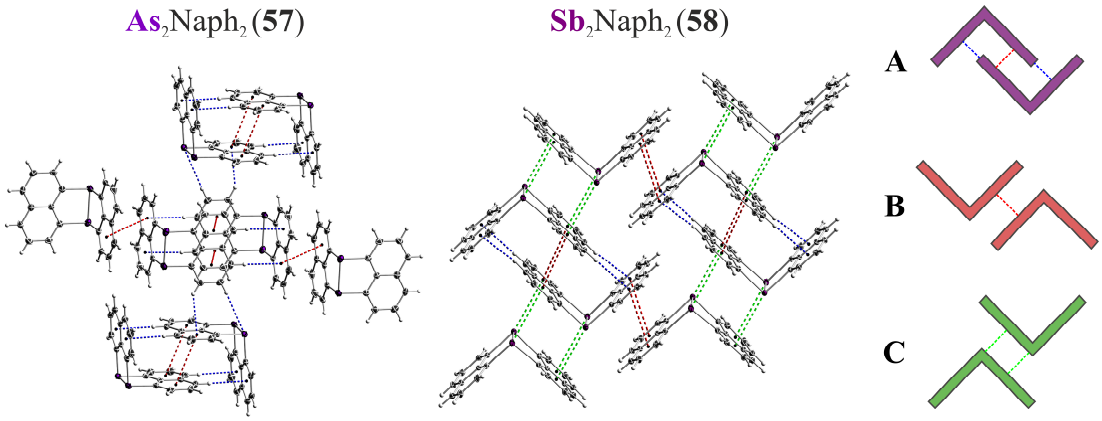

Figure 12. The crystal packing of As_2Naph_2 (**57**) and Sb_2Naph_2 (**58**). Both packings contain intermolecular CH···π (blue) and π···π contacts (red) forming back-to-back (A) and entwined-L-dimers (B). For **58** additional back-to-back dimers through Sb···π interactions are formed (C).

The reaction between As_2Naph_2 (**57**) and gold-(I) chloride yielded the oxidated species $(ClAsNaph)_2$ (**59**) and elemental gold. In contrast to its reduced parent compound **57**, **59** forms a dimer *via* As···π contacts comparable to **58**. The As···As distance is elongated by approximately 0.4 Å to 2.8383(4) Å, which is above the sum of covalent radii (r_{cov}(As) = 1.19 Å),[171] but significantly below the sum of van der Waals radii (r_{vdW}(As) = 1.85 Å) (Figure 13).[87,175]

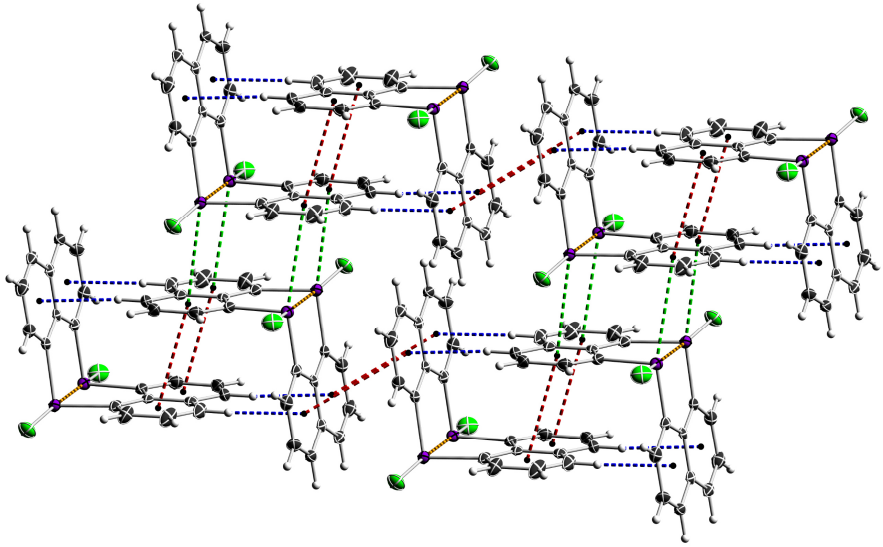

Figure 13. The crystal packing of **59** contains the same type of dimers as **58**, including the Pn···π contacts.

The dimers of type **C** (Figure 12) were analyzed in detail *via* quantum chemical methods. Even though a corresponding As-dimer was not reported and the respective Bi compound Bi_2Naph_2 (**60**) could not be isolated, theoretical dimers allowed a comparison between the elements of group 15. In conjunction with the literature reports, the computations concluded a dominant dispersive interaction between the naphthalene-ligand and the pnictogen-center. Furthermore, an increase of interaction energy with growing atomic number was reported, which is consistent with the described characteristics of *London* dispersion forces. However, since the used dimer is of theoretical nature, the experimental evidence is still pending. Additionally, the dimers of **59** and **57** showed a significant increase in *London* dispersion, while a slight increase in non-dispersive interaction was present. The enlarged LD energy stems from Cl···π interactions, while an overall loss in As···π from **57** to **59** was reported, demonstrating the huge influence of the ligands on LDFs.[175]

4. Research Objectives

Within the last decade, the knowledge and understanding of molecular interactions, especially *London* dispersion, significantly increased. However, in contrast to ligand-ligand contacts, interactions dominated by heavy elements are far less explored. The goal of this work was the synthesis of different *peri*-substituted naphthalenediyls of the heavy group 15 elements in order to study the occurring inter- and intramolecular interactions and their relation to *London* dispersion with respect to the heavy group 15 elements. The experimental results will be supported by quantum chemical computations, which allow the identification and characterization of occurring interactions. Due to the lack of experimental data on the bismuth derivative Bi_2Naph_2 (**60**), a synthetic approach to **60** needed to be developed first. For this purpose, the reported synthesis of **57** and **58** will be adapted and modified by varying the reaction conditions to prevent the formation of bismuth metal. Furthermore, interactions in $(ClAsNaph)_2$ (**58**) demonstrated that the influence of the ligand plays a vital role in the strength of the overall interaction energies. In consequence, the scope of the *peri*-substituted bis(pnicta)naphthalenediyls shall be extended to the heavier elements antimony and bismuth. A suitable start would be the synthesis of bis-1,8-(diphenylstiba)naphthalene (**41**), which was already synthesized but not structurally characterized by *Webster* et al. In addition, the variation of the halogen-to-ligand ratio will allow an evaluation of the behavior of the heavy elements antimony and bismuth relative to their lighter congener phosphorous. Since previous reports of bis(phospha)naphthalenes showed a dependency between the ligand size and the resulting molecular structure, the influence of an increasing ligand size will also be investigated. Finally, the behavior of the resulting bis(pnicta)naphthalenes towards one-electron oxidation agents was of interest (Scheme 12).

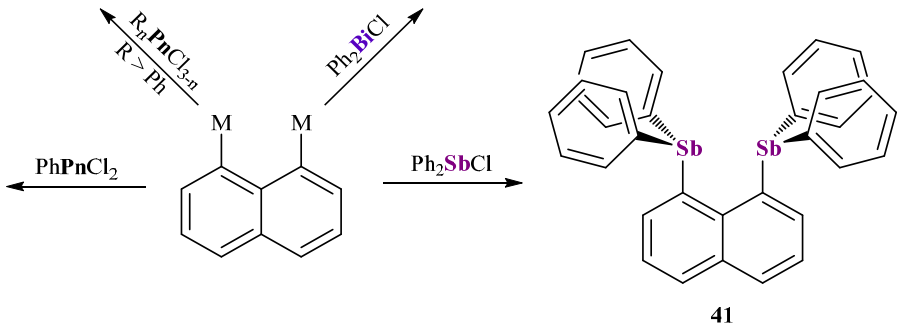

Scheme 12. Synthesis of homoleptic substituted bis(pnicta)naphthalenediyls.

5. Results and Discussion

5.1. Bis(naphthalenediyl)dipnictanes

The synthesis and isolation of the bis(naphthalenediyl)dipnictanes Pn_2Naph_2 was successfully accomplished by employing two different routes. The diphosphine **56** was obtained from oxidation of the four-membered ring **28** with oxygen and water, followed by reduction with $HSiCl_3$.[173] In contrast, the heavier congeners **57** and **58** were obtained from a reductive coupling between a TMEDA complex of 1,8-dilithionaphthalene (**25**) and the respective pnictogen-(III) halide at low temperatures (Scheme 13).[174,175]

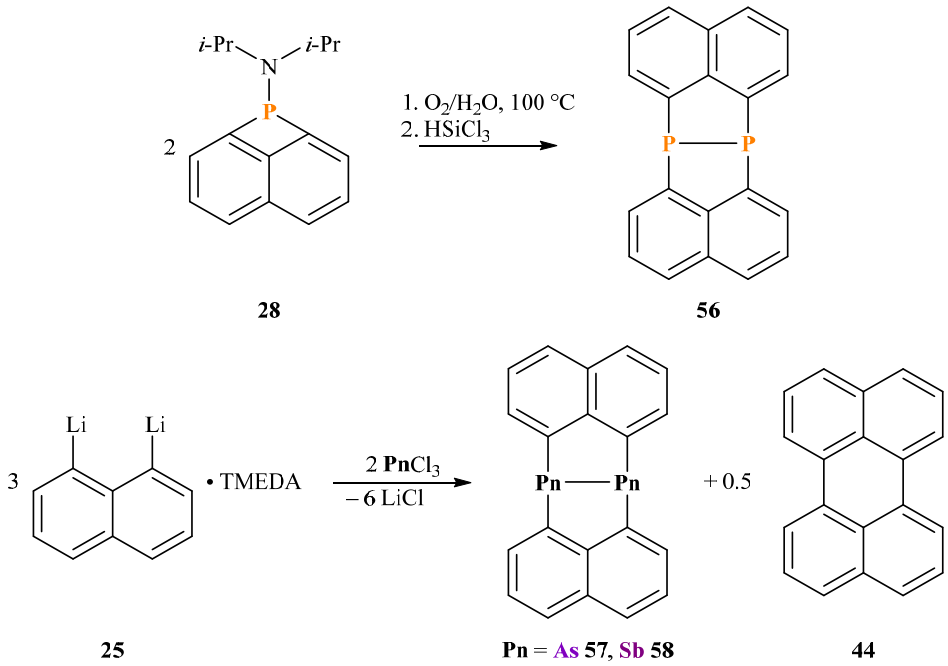

Scheme 13. Current synthetic pathways to bis(naphthalenediyl)dipnictanes **56-58**.

However, all attempts to generate the bismuth derivative Bi_2Naph_2 (**60**) with similar protocols resulted in the formation of elemental bismuth.[175] The procedure was therefore modified by adding a solution of $BiCl_3$ in thf dropwise to a cooled (–30 °C) solution of a diethyl ether complex of Li_2Naph to facilitate the work-up. Although P_2Naph_2 (**56**) was reported to react with water and air at elevated temperatures, such reactivity was not observed for the arsenic (**57**) and antimony (**58**) derivatives. The crude reaction mixture of **60** was therefore washed with degassed water, and *n*-hexane, and was finally extracted with hot toluene. The resulting solution was cooled slowly in an oil bath forming yellow needles. The needles were isolated and identified as Bi_2Naph_2 (**60**).[176]

The ^{1}H NMR spectrum is consistent with those previously reported for Pn_2Naph_2 (**56**-**58**) showing three doublet of doublets (8.11 ppm, 7.35 ppm, 7.31 ppm). **60** crystallized with eight molecules per unit cell in the monoclinic space group *C*2/c. The Bi–Bi bond distance (2.8964(8) Å) is at the shorter end of reported Bi–Bi single bond lengths. In comparison to its lighter congeners, the average sum of C–Pn–E bond angles (E = C, Pn) is smaller (Pn = P 286.11°, As 278.11°, Sb 267.23°, Bi 261.25°),[173–176] showing the increasing *p*-orbital character of the Pn–C bonds and the increasing *s*-orbital character in the pnictogen lone pair (Figure 14).[176]

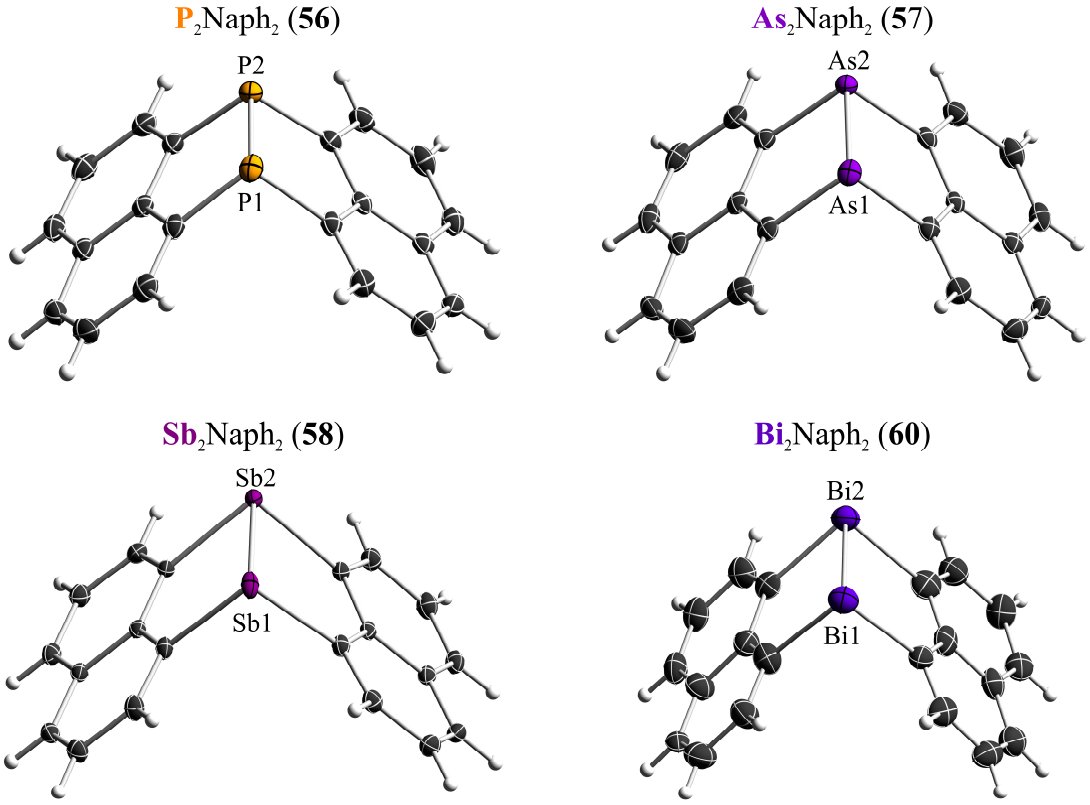

Figure 14. Solid-state structures of Pn_2Naph_2 (Pn = P **56**, As **57**, Sb **58**, Bi **60**) with displacement ellipsoids drawn at the 50 % probability level. Selected bond lengths [Å] and angles [°], **56**: P–P 2.2517(6), avg. C–P–C 99.62;[173] **57**: As–As 2.4326(4), avg. C–As–C 96.64;[175] **58**: Sb–Sb 2.7972(3), avg. C–Sb–C 94.82;[174] **60**: Bi–Bi 2.8964(8), avg. C–Bi–C 90.65.[176]

The crystal packing of **60** deviates significantly from the previously reported Pn_2Naph_2.[173–175] While $\pi\cdots\pi$ contacts played a dominant role for the lighter homologs, Bi_2Naph_2 (**60**) lacks any $\pi\cdots\pi$ contacts, but shows two Bi$\cdots\pi$ contacts per Bi atom, while Pn$\cdots\pi$ contacts were completely absent in the lightest congeners of phosphorous (**56**) and arsenic (**57**). Solely, Sb_2Naph_2 (**58**) exhibited one Sb$\cdots\pi$ contact per atom *via* back-to-back dimers (Figure 12, page 22). The Bi$\cdots\pi$ distances (3.69 Å/3.58 Å, 3.81 Å/3.80 Å) are almost identical to the Sb$\cdots\pi$ distances in **58** (3.65 Å, 3.86 Å), yet despite the larger atomic radius of Bi indicating stronger

intermolecular interactions. In contrast to **58**, Bi_2Naph_2 (**60**) forms no back-to-back dimers but assumes a V-like stacking (Figure 15.**4**). Moreover, Bi···H contacts similar to those in **57** are observed forming a zig-zag-like chain *via* the interaction of two hydrogens with a Bi atom. These chains are further connected *via* H···H and CH···π contacts (Figure 15).[176]

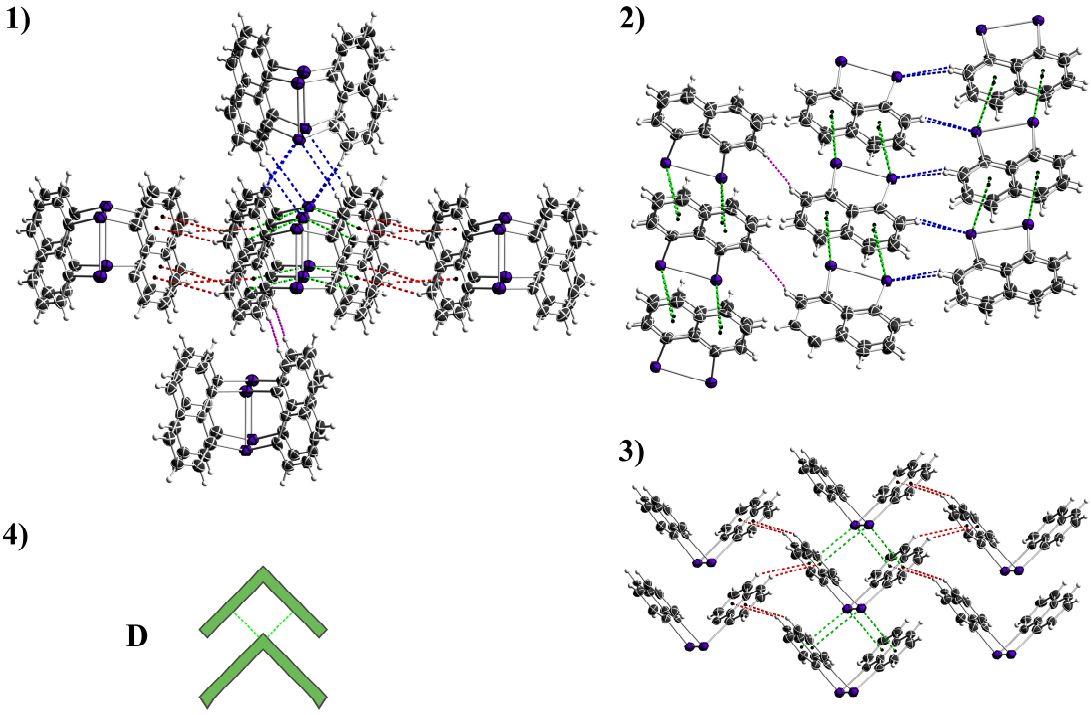

Figure 15. Crystal packing of Bi_2Naph_2 (**60**). **1-3)** A Bi_2Naph_2 (**60**) molecule is connected *via* H···H (pink), CH···π (red), Bi···H (blue), and Bi···π (green) contacts to the surrounding molecules. **4)** The molecules form dimer **D** instead of the back-to-back dimer **C** (Figure 12, page 22).

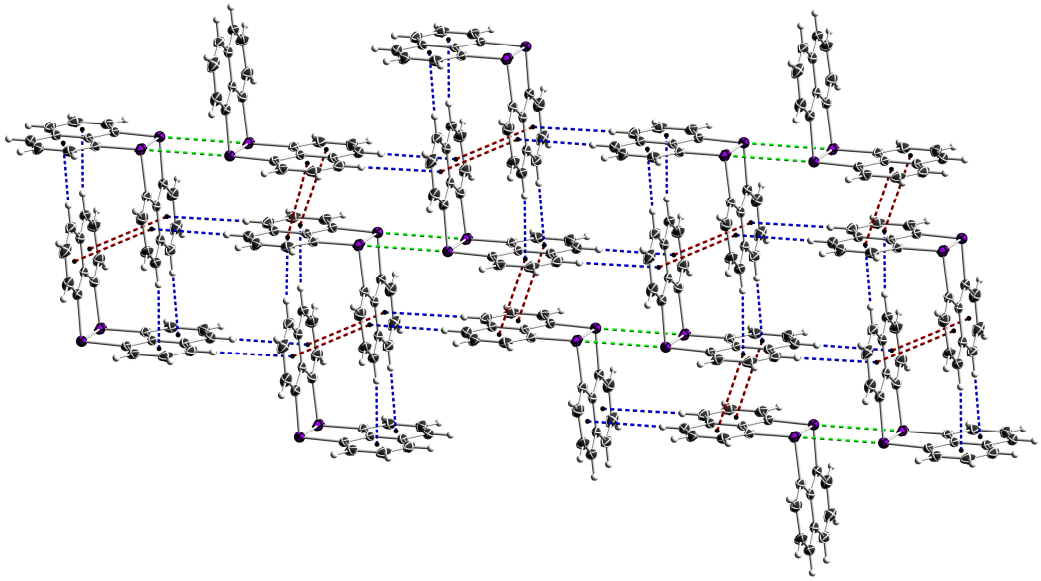

Figure 16. Crystal packing for the new polymorph of As_2Naph_2 (**57b**). In addition to CH···π (blue) and π···π (red) contacts, dimers are formed through As···As (green) contacts.

All in all, the crystal packing of Bi_2Naph_2 (**60**) deviates significantly from its lighter homologs as well as from the theoretical prediction.[68,175]

The synthetic procedure for **60** was also applied to diarsane **57** and distibane **58**. After recrystallizing a sample of **57** from fluorobenzene, a new polymorph (**57b**), which crystallized in the triclinic space group $P\bar{1}$ was obtained. The bonding parameters of the new polymorph are close to the original report (As–As: **57** 2.4326(4) Å, **57b** 2.4471(4) Å; avg. C–As–C: **57** 278.11°, **57b** 277.78°),[175] however, the crystal packing deviates due to the occurrence of As···As contacts along with the common $\pi\cdots\pi$ and CH$\cdots\pi$ contacts (Figure 16).[176]

In order to understand the reason behind the formation of the different structure motifs, quantum chemical computations with ORCA 5.0.[177–180] were performed in collaboration with *Prof. Dr. A. A. Auer*[*] and *Dr. E. Schiavo*.[*] A cluster approach was used whereby all relevant intermolecular interactions and cohesion energies of a central molecule with its closest neighbors are calculated for **60** and **57b**. The dimers were used as found in the sc-XRD structures and kept frozen throughout all computations. Energies were computed at the DLPNO-CCSD(T)/cc-pVTZ level of theory[181,182,183] and with the PBE0 functional,[184] which was selected after thorough benchmarking.[176] The computations further employed the def2-TZVPP basis set[185] utilizing the atom-pairwise dispersion correction with Becke-Johnson damping scheme (D3BJ).[22,36] To extract the portion of *London* dispersion the local energy decomposition analysis (LED) was employed.[23,24]

In conjunction with previous reports,[125,174,175] the dimer interactions were found to be dominated by LD, however the cluster approach also allowed a more detailed view at the dimers involved. For Bi_2Naph_2 (**60**) seven unique dimers were identified, which were cut from a 13-molecule cluster, while a 14-molecule cluster with eleven unique dimers was found for **57b**. In addition to the number of dimers, the respective number of occurrences per cluster needed to be considered. The major contribution in **60** comes from the "Top Y" dimer, which occurs twice per cluster and includes the Bi$\cdots\pi$ contacts providing roughly half of the total energy. Other dimers of importance are "Side Z", which occurs twice, and "Side X" appearing four times per cluster. In contrast, the contributions in the **57b** cluster are more evenly distributed. The dimers "Side X-like" and "Front Upright" occur twice per cluster, while all other dimers appear only once. Interestingly, the total cohesion energy is also smaller for As

[*]Max-Planck-Institut für Kohlenforschung, 45470 Mülheim an der Ruhr, Germany. E-mail: alexander.auer@kofo.mpg.de

(–305.28 kJ mol^{-1}) than for Bi (–334 kJ mol^{-1}), despite **57b** forming an additional contact. The dimer with the largest contribution is "UpsDwn", providing ~25 % of the cohesion energy (Figure 17).[176]

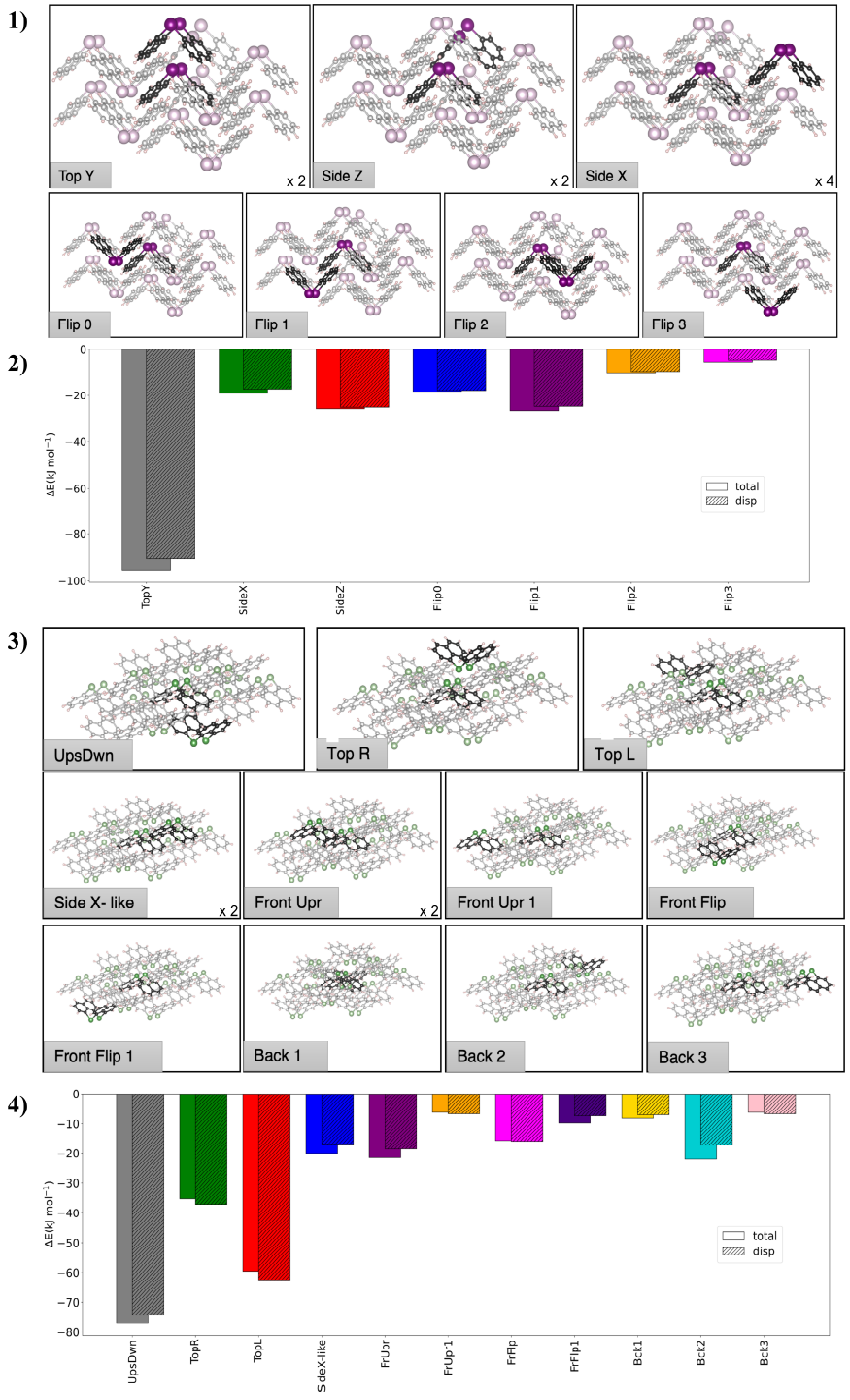

Figure 17. 1/3) Dimers as cut from the 13- and 14-molecule cluster of Pn_2Naph_2 (Pn = As **57b 1)**, Bi **60 3)**) with the geometries frozen at the experimental crystallographic ones. The highlighted molecules are the ones included in the computations, while the rest of the cluster is shown to illustrate how the dimers were extracted. C (black), As (green), Bi (purple), H (light pink). **2**/**4)** Comparison between the different dimer formation energies at the PBE0/def2-TZVPP level of theory.[176]

After evaluating the dimers in the different motifs of **57b** and **60**, the influence of the pnictogen center was closely examined. The most significant dimers from the As-cluster ("UpsDwn" and "Top L") and Bi-cluster ("Top Y") were taken and optimized for P, As, Sb, and Bi (Figure 18).[176]

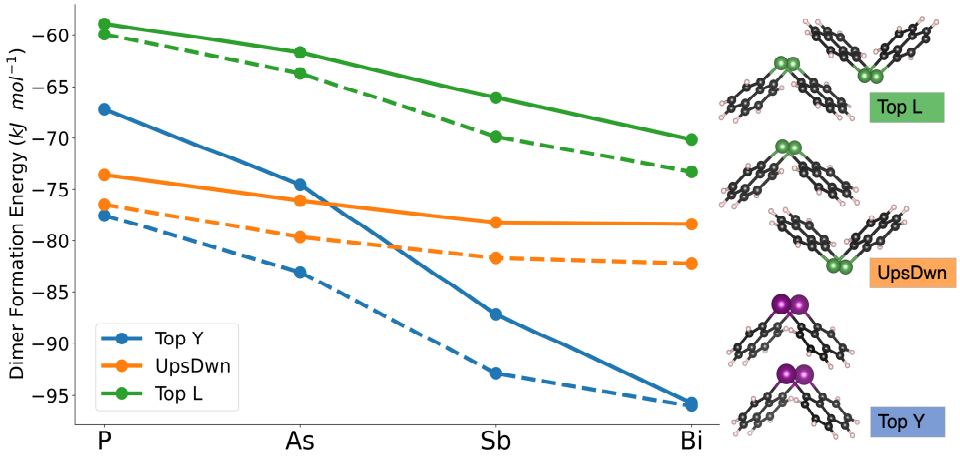

Figure 18. The total formation energies (solid lines) and dispersion contribution (dashed lines) of the Pn_2Naph_2 dimers (Pn = P-Bi). The dimers were optimized at the PBE0/def2-TZVPP level of theory. The color of the pnictogen center represents the origin of the dimer: Bi (purple), As (green).[176]

In conjunction with the experimental observations, the "Top Y" dimer is the most stable for bismuth. Going through the pnictogen group, a switch between "UpsDwn" and "Top Y" is observed, even though the dispersive portion for "Top Y" is larger than for "UpsDwn" for all pnictogens. With "Top Y" occurring twice in the cluster, this emphasizes the significance of "Top Y" in the formation of the Bi structure motif. This also explains the more even distribution for arsenic, especially since the formation energies are much closer for the lighter elements. Nevertheless, *London* dispersion plays a leading role for all dimers for which the different structural motifs can be explained by the attempt to maximize the *London* dispersion forces. With the switch of "Top Y" and "UpsDwn" occurring after arsenic, the structural motif of antimony is presumed as a crossover of arsenic and bismuth.[176]

In conclusion, the initial prediction for similarities of Sb_2Naph_2 (**58**) and Bi_2Naph_2 (**60**) was debunked, but the occurrence of Pn···π contacts stayed true. More importantly, the growing significance of LDFs was successfully demonstrated by Pn-based interactions of growing atomic number up to Bi, which was previously described only by theoretical means. Additionally, the dimer formation energies become less diverse with lighter elements, which explains the observation of a new As_2Naph_2 polymorph (**57b**), hence emphasizing a flat energy hyper surface for the structure formation.

5.2. Bis(pnicta)naphthalenes

To further investigate the ligand influence on inter- and intramolecular interactions, bis(diphenylpnicta)naphthalenes were chosen as a starting point and prepared *via* a previously reported synthesis by *Webster* and co-workers for the diphenylstiban species 1,8-$(Ph_2Sb)_2$Naph (**41**).[162] Furthermore, to evaluate the role of the ligand scaffold itself, we also became interested in $(Ph_2Sb)_2$Acenaph (**61**), due to the increased rigidity of the acenaphthene ligand. The stibanes **41** and **61** were synthesized by addition of Ph_2SbCl to solutions of Li_2L (L = Naph (**25**), Acenaph (**62**)) in thf at –78 °C (Scheme 14).[186]

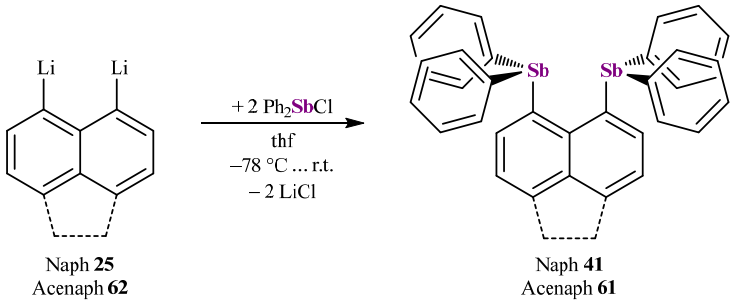

Scheme 14. Synthesis of a stibanaphthalene (**41**) and -acenaphthene (**61**).[186]

Colorless crystals of the stibanes were received upon crystallization from hot toluene (**41**) and storage at 4 °C in thf/hexane (1:1) (**61**), respectively. The ^{1}H NMR spectrum of **41** in CD_2Cl_2 displays the expected doublet of doublets for a symmetric naphthalene framework (7.88 ppm, 7.72 ppm), as well as overlapping signals for the remaining naphthalenediyl and phenyl protons (7.37-7.40 ppm, 7.26-7.35 ppm). The corresponding ^{1}H NMR spectrum of **61** contains doublets for the acenaphthenediyl CH protons (7.58 ppm, 7.18 ppm), a singlet for the CH_2 protons (3.38 ppm), as well as multiplets for the phenyl protons (7.34-7.36 ppm, 7.26-7.30 ppm). Both compounds crystallized isomorphous in the orthorhombic space group $P2_12_12_1$ and the Sb atoms adopt trigonal-pyramidal coordination spheres with C–Sb–C bond angles (**41**: 94.74(10)-101.03(12)°, **61**: 95.22(15)-100.05(14)°) and bond angular sums (**41**: Sb1 292.67°, Sb2 293.45°; **61**: Sb1 293.6°, Sb2 291.95°) indicating a high *p*-orbital character in the Sb–C bonds and hence a high *s*-orbital character for the Sb lone pair. The Sb–C bond lengths (**41**: 2.134(3)-2.179(3) Å, **61**: 2.137(4)-2.165(4) Å) are in the typical range of Sb–C single bonds. The phenyl rings assume two different alignments. Two rings are parallel to the Sb···Sb axis (**41**: 173.75(7)°/170.98(7)°, **61**: 175.28°/172.24°), while the remaining two are in orthogonal allignment to the axis (**41**: 89.12(7)°/92.91(7)°, **61**: 88.08°/90.33°). To compare the influence of the ligand

scaffold the Sb···Sb distance and dihedral angles Sb1C1/5–C8/6–Sb2 are employed. The distances between the Sb atoms (**41**: 3.2983(6) Å, **61**: 3.341 Å) are in both compounds well below the sum of the van der Waals radii (r_{vdW}(Sb) = 2.06 Å)[87] with a difference of roughly 0.05 Å between naphthalene and acenaphthene. The measured dihedral angles (**41**: 33.70(14)°, **61**: 28.58(16)°) indicate a significant distortion of the ligand framework and have a more significant difference of roughly 5°. More interestingly, **41** and **61** form neither $\pi\cdots\pi$ nor Pn$\cdots\pi$ or other metal-ligand contacts, but instead CH$\cdots\pi$ contacts were observed (Figure 19).[186]

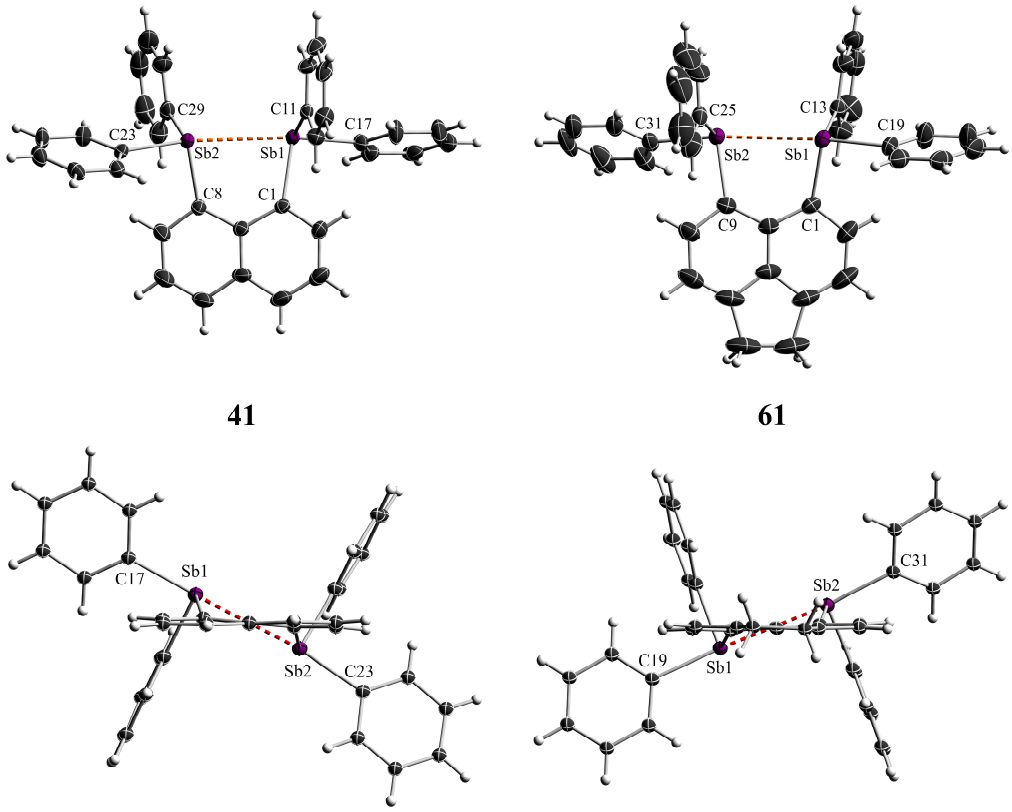

Figure 19. Solid-state structure of $(Ph_2Sb)_2$Naph (**41**, left) and $(Ph_2Sb)_2$Acenaph (**61**, right). The higher grade of distortion in naphthalene (bottom left) is visible due to a larger deflection of the hydrogen atoms. The displacement ellipsoids are drawn at a 50 % probability level. Selected distances [Å], bond angles [°] and dihedral angles [°], **41**: Sb1–Sb2 3.2983(6), Sb1–C1 2.179(3), Sb1–C11 2.134(3), Sb1–C17 2.158(3), Sb2–C8 2.159(3), Sb2–C23 2.160(3), Sb2–C29 2.142(3), C1–Sb1–C11 100.35(10), C1–Sb1–C17 97.58(10), C11–Sb1–C17 94.74(10), C11–Sb1–Sb2 89.12(7), C17–Sb1–Sb2 173.75(7), C8–Sb2–C23 96.87(10), C8–Sb2–C29 101.03(12), C23–Sb2–C29 95.55(10), C23–Sb2–Sb1 170.98(7), C29–Sb1–Sb2 92.91(7), Sb1–C1–C8–Sb2 33.70(14); **61**: Sb1–Sb2 3.341(1), Sb1–C1 2.165(4), Sb1–C13 2.140(4), Sb1–C19 2.154(4), Sb2–C9 2.151(3), Sb2–C25 2.137(4), Sb2–C31 2.158(4), C1–Sb1–C13 100.05(14), C1–Sb1–C19 98.33(16), C13–Sb1–C19 95.22(15), C13–Sb1–Sb2 88.08(9), C19–Sb1–Sb2 175.28(11), C9–Sb2–C25 99.62(17), C9–Sb2–C31 96.15(16), C25–Sb2–C31 96.18(17), C25–Sb2–Sb1 90.31(10), C31–Sb2–Sb1 172.245(13), Sb1–C1-C9–Sb2 28.58(16).[186]

Attempts to synthesize $(Ph_2Bi)_2Naph$ (**63**) by reacting Ph_2BiCl with Li_2Naph at –78 °C failed and only yielded complex reaction mixtures. *In situ* ^1H NMR spectroscopy confirmed the formation of $BiPh_3$, indicating dismutation reactions in solution, which is supported by a recent study reporting that Ph_2BiCl acts as a catalyst for these types of ligand exchange reactions.[83] In consequence, the reaction conditions were modified to keep the concentration of Ph_2BiCl as low as possible. A diluted solution of Ph_2BiCl was added slowly to a cooled solution of Li_2Naph at –30 °C yielding bis(bisma)naphthalene **63** as colorless crystals after crystallization from a CH_2Cl_2/*n*-hexane solution (1:5). The yield was improved from 17 % to 30 % by replacing Ph_2BiCl with Ph_2BiI. The ^1H NMR spectrum in CD_2Cl_2 displays the expected signals and integral ratio, as observed for **41**, but the resonance is significantly downshifted to lower field (Scheme 15).[186]

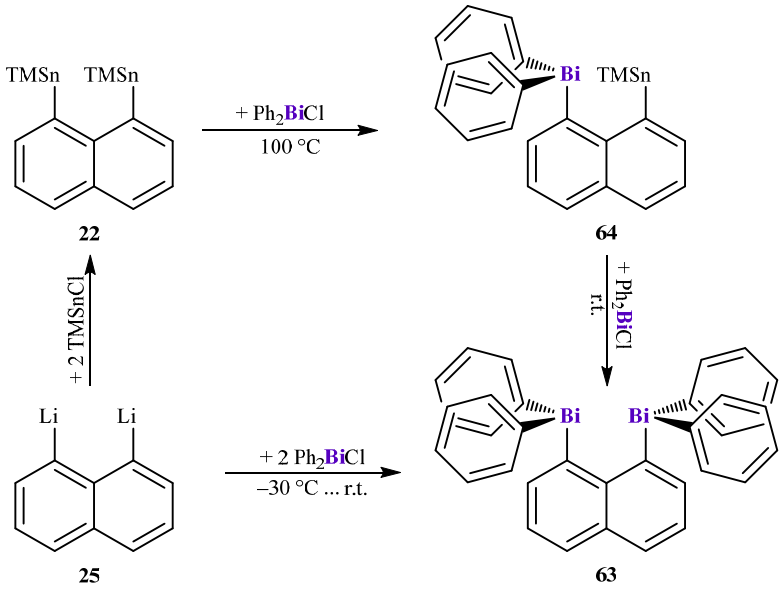

Scheme 15. Formation of (diphenylbisma)naphthalenediyls *via* two different routes.

An alternate route using $TMSn_2Naph$ (**22**) was applied to decrease the amount of dismutation. **22** is less reactive than Li_2Naph (**25**), and therefore acts as a softer naphthyl-transfer reagent.[164,168] No reaction was observed at ambient temperatures in toluene, while a complex mixture including $BiPh_3$ formed at 100 °C. One equivalent of Ph_2BiCl was therefore added dropwise at 100 °C to $TMSn_2Naph$ (**22**). Extraction and crystallization from *n*-hexane yielded a bright yellow solid which was identified as 1-(Ph_2Bi)-8-(TMSn)-Naph (**64**). The ^1H NMR spectrum of **64** in CD_2Cl_2 displays a unique signal for each naphthalenediyl proton, which is in conjunction with an asymmetric ligand structure, while a multiplet is observed for the phenyl groups that overlaps with a signal for a naphthyl proton. The Me_3Sn groups generate a triplet due

to $^{1}H–^{119/117}Sn$ coupling. In comparison with **41** and **61**, the signals are shifted to lower field, while the proton closest to Bi exhibits the largest downfield shift (8.37 ppm). The signal in the ^{119}Sn NMR spectrum is also shifted significantly to lower field when compared to Me_3SnPh[187] and $TMSn_2Naph$ (**22**) (**64**: –47.1 ppm, **22**: –25.7 ppm, Me_3SnPh: –28.6 ppm†).[186]

63 and **64** crystallized in the monoclinic space groups $P2_1$ and $P2_1n$, respectively, with the Bi atoms adopting trigonal-pyramidal coordination spheres. The C–Bi–Bi bond angles in **63** range from 92.0(3)° to 99.1(3)° with the bond angular sum (Bi1: 282.9°, Bi2: 288.6°) indicating high *p*-orbital character in the Bi–C bonds. The intramolecular Bi···Bi distance of 3.4461(4) Å is well below the sum of van der Waals radii (r_{vdW}(Bi) = 2.07 Å[87]). In contrast to its antimony derivatives **41** and **61** intermolecular Bi···π contacts are formed in addition to inter- and intramolecular CH···π contacts. Furthermore, the dihedral angle Bi1–C1–C8–Bi2 (8.98(37)°) is significantly smaller than for **41** and **61**, hence indicating far less steric strain despite the heavier element used. Comparing the orientation of the Ph_2Pn groups reveals, that **63** assumes structure motif **B** (Figure 10, page 18). This is in parallel with **26d**, which shows the same orientation, but indicates intramolecular Bi···Bi interaction. This again is supported by an elongated Bi1–C11 bond length (Bi1–C11 2.281(8) Å, Bi1–C17 2.252(7) Å, Bi2–C23 2.257(8) Å, Bi2–C29 2.268(8) Å), especially since an interaction of the Bi lone pair with an antibonding Bi–C orbital can be the origin. Since the ^{1}H NMR spectrum displays the expected signals for a symmetric species, a possible interaction is too weak to be sustained in solution. Moreover, one has to keep in mind that the orientation of the Ph_2Bi groups can also be a consequence of the observed inter- and intramolecular interactions since the maximization of LD energy was reported as a significant driving force in *e.g.* Pn_2Naph_2.[176] **64** also forms dimers *via* CH···π contacts. The intramolecular Bi···Sn distance (3.5312(7) Å) is well below the sum of *van der Waals* radii (r_{vdW}(Bi) = 2.07 Å, r_{vdW}(Sn) = 2.17 Å)[87] but is slightly elongated compared to **63**, which is probably due to the larger *van der Waals* radius of tin. Similar to the bis(bisma) species **63**, the dihedral angle Bi–C1–C8–Sn (33.92(11)°) is significantly larger which points to larger steric stress and therefore stronger repulsive interaction. The bond angular sum of bismuth (284.89°) is comparable to **63**, thus indicating high *p*-orbital character (Figure 20).[186]

†The ^{119}Sn NMR spectrum was recorded with a solution of 20 % Me_3SnPh in CH_2Cl_2.[187].

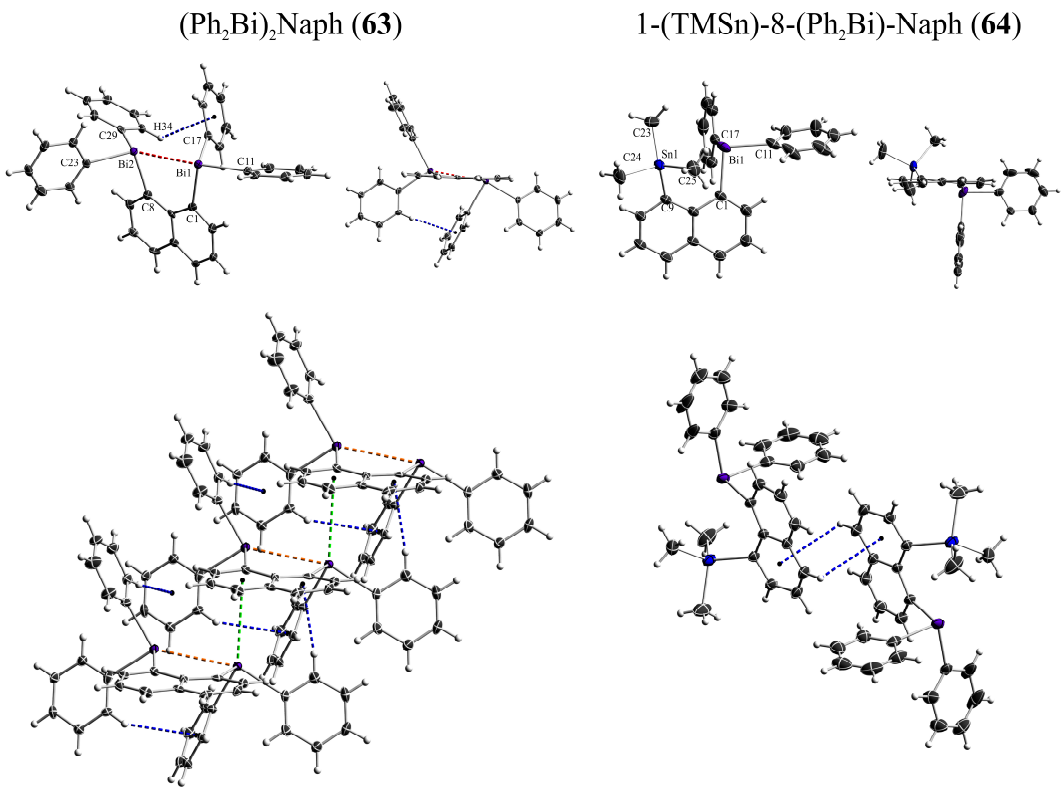

Figure 20. Solid-state structures of $(Ph_2Bi)_2Naph$ (**63**, left) and 1-(Ph_2Bi)-8-TMSn-Naph (**64**, right). The displacement ellipsoids are drawn at a 50 % probability level. **63** forms an intramolecular CH···π contact (blue), while a two-dimensional chain formed by Bi···π (green) and CH···π contacts is observed (bottom left). **64** forms a dimeric unit through CH···π contacts (bottom right). The distortion of the naphthalene ligand is significantly smaller in **63**, as seen by the deflections of the hydrogens and *peri*-bonded groups. Selected distances [Å], bond angles [°] and dihedral angles [°], **63**: Bi1–Bi2 3.4461(4), Bi1–C1 2.289(8), Bi1–C11 2.281(8), Bi1–C17 2.252(7), Bi2–C8 2.270(9), Bi2–C23 2.257(8), Bi2–C29 2.268(8), C1–Bi1–Bi2 77.4(2), C11–Bi1–Bi2 159.9(2), C17–Bi1–Bi2 70.4(2), C1–Bi1–C11 95.5(3), C1–Bi1–C17 95.4(3), C11–Bi1–C17 92.0(3), C8–Bi2–Bi1 80.2(2), C23–Bi2–Bi1 129.3(2), C29–Bi2–Bi1 136.6(2), C8–Bi2–C23 99.1(3), C8–Bi2–C29 95.4(3), C23–Bi2–C29 94.1(3), Bi1–C1–C8–Bi2 8.98(37); **64**: Bi–Sn 3.5312(7), Bi–C1 2.252(3), Bi–C11 2.246(4), Bi–C17 2.245(4), C1–Bi–C11 96.68(13), C1–Bi–C17 93.25(12), C11–Bi–C17 94.46(13), Bi–C1–C8–Sn 33.92(11).[186]

Compared to $(Ph_2P)_2Naph$ (**26d**), the Pn···Pn distances in **41**, **61**, and **63** are significantly elongated, while the dihedral angles φ in **41** and **61** are also larger. Surprisingly, the dihedral angle of **63** is significantly smaller compared to **26d**. This may be due to less steric strain between the phenyl ligands, since the distance between the ligands is increased. However, the dihedral angles of $(Ph_2B)_2Naph$[144] and $(PhTe)_2Naph$[188] are both larger than that of **26d**, independent from the steric load. Moreover, $(Ph_2Bi)_2Naph$ (**63**) shows the smallest dihedral angle in the presence of a naphthalenediyl ligand, even though the compound contains the heaviest atom and does not have the largest E···E distance.[186] The introduction of the acenaphthenediyl led to a significant decrease in the dihedral angle φ, which demonstrates the higher

rigidity of the ligand. However, while for Sn[133,189] and Sb[186] this is accompanied by an increase in the E···E distance, a slight decrease is reported for P (Table 4).[146,190]

Table 4. E···E distances [Å] and dihedral angles φ [°] of selected homoleptic *peri*-substituted naphthalenediyl complexes. The sum of *van der Waals* radii[87] $\Sigma r_{vdW}(E)$ [Å] is given as a reference.

	E···E	$\Sigma r_{vdW}(E)$	φ(E1–C1–C2–E2)[a]
$(Ph_2B)_2Naph$[144]	3.003	3.84	23.42
$(TMSn)_2Naph$ (22)[189]	3.864	4.34	51.28
$(TMSn)_2Acenaph$[133]	3.969	4.34	42.22
$(Ph_2P)_2Naph$ (**26d**)[146]	3.052	3.60	17.69
$(Ph_2P)_2Acenaph$[190]	3.028	3.60	6.23
$(Ph_2Sb)_2Naph$ (**41**)[186]	3.298	4.12	33.70
$(Ph_2Sb)_2Acenaph$ (**61**)[186]	3.341	4.12	28.55
$(Ph_2Bi)_2Naph$ (**63**)[186]	3.446	4.14	8.98
$(PhTe)_2Naph$[188]	3.287	4.12	23.71

[a]C1 and C2 represent the carbons in the *peri*-position of the respective ligand.

Using the Orca 5.0 program package, quantum chemical computations were performed to study the electronic nature of **41**, **61**, and **63**.[177] Natural bond order (NBO) analysis was performed with the NBO program package version 7.0.[191] Quantum theory of atoms in molecules (QTAIM) analysis was performed using the program package Multiwfn version 3.8[192] and the visualization was generated with VMD version 1.9.3.[193] Geometries were taken from sc-XRD data and computed at the def2-TZVPP[185] level of theory (def2-QZVP[185] for E>Ne) with the def2/J[194] auxiliary basis set utilizing atom-pairwise dispersion correction with Becke-Johnson damping (D3BJ).[22,36] The functionals BP86[195,196] and PBE[197] were already chosen before in computations for comparable systems[174,176,186] but were found to potentially describe either antimony or bismuth inaccurately (*vide infra*). For this reason, the systems were computed with both functionals. The geometries obtained from the calculations show small but significant deviations from the sc-XRD data, as indicated by the root-mean-square deviation (RSMD). While the Sb···Sb distance and torsion angles in both Sb compounds are diminished, virtually no change for the Bi···Bi distance was observed for **63**, however, the dihedral angle φ is significantly increased. In general, the Pn–C bonds are elongated compared to the sc-XRD data. Interestingly, the largest deviation for the Sb systems was found with the PBE functional, however it described the geometric parameters of **63** more accurately, which is in conjunction with recent reports (*vide infra*) (Table 5).[186]

Table 5. Comparison of selected geometric parameters derived from computations and sc-XRD data including distances [Å], bond angles [°], and dihedral angles [°] and RMSD.

		sc-XRD	BP86	PBE
$(Ph_2Sb)_2Naph$ (**41**)	Pn···Pn	3.298	3.284	3.285
	C–Pn	2.134, 2.142, 2.158, 2.159, 2.160, 2.179,	2.167, 2.167, 2.175, 2.175, 2.190, 2.190	2.169, 2.169, 2.178, 2.179, 2.194, 2.195,
	C–Pn–E	89.12, 92.91, 94.74, 95.55, 96.87, 97.58, 100.35, 101.03, 170.98, 173.75,	79.42, 79.46, 80.15, 80.23, 93.68, 93.77, 94.67, 94.68, 95.53, 95.58, 172.36, 172.49	79.96, 80.08, 83.93, 84.64, 94.62, 94.77, 95.34, 95.46, 95.91, 95.96, 175.71, 176.02
	Pn–C–C–Pn	33.70	21.42	15.80
	RMSD		1.24	1.12
$(Ph_2Sb)_2Acenaph$ (**61**)	Pn···Pn	3.341	3.324	3.324
	C–Pn	2.137, 2.140, 2.151, 2.154, 2.158, 2.165	2.168, 2.169, 2.174, 2.174, 2.182, 2.183	2.169, 2.169, 2.178, 2.179, 2.187, 2.187
	C–Pn–E	88.08, 90.31, 95.22, 96.15, 96.18, 98.33, 99.62, 100.05, 172.25, 175.28	79.40, 79.94, 80.14, 80.46, 93.86, 93.98, 95.02, 95.08, 95.19, 95.25, 172.17, 173.37	80.50, 80.54, 84.67, 86.81, 95.26, 95.21, 95.42, 95.43, 96.30, 96.31, 176.30, 176.77
	Pn–C–C–Pn	28.58	13.39	2.65
	RMSD	–	0.95	0.72
$(Ph_2Bi)_2Naph$ (**63**)	Pn···Pn	3.446	3.441	3.447
	C–Pn	2.252, 2.257, 2.268, 2.270, 2.281, 2.289	2.263, 2.270, 2.273, 2.280, 2.290, 2.296	2.269, 2.273, 2.275, 2.283, 2.295, 2.300
	C–Pn–E	70.4, 77.4, 80.2, 92.0, 94.1, 95.4, 95.4, 95.5, 99.1, 129.3, 136.6, 159.9	72.1, 77.2, 78.4, 92.0, 92.1, 92.7, 93.1, 94.5, 94.6, 131.1, 133.4, 160.3	73.7, 78.0, 78.6, 93.3, 93.6, 93.7, 93.9, 94.2, 95.2, 129.0, 135.2, 164.0,
	Pn–C–C–Pn	8.98	22.45	16.51
	RMSD	–	0.53	0.45

Nevertheless, both functionals seem to overestimate the intramolecular attraction for antimony. This can be seen from the decreased Sb···Sb distance and dihedral angle, as well as the intramolecular repulsion for bismuth since the dihedral angle increased significantly in **63**. In this respect, further computations with the PBE0 functional[198] were performed. Overall, the geometries of **41** and **61** showed a significantly better fit to the experimental sc-XRD data, while slight deterioration in the geometry of **63** occurred. Nevertheless, an overestimation of attraction is found also with the PBE0

functional in **41** and **61**. Since attractive interaction in the form of *London* dispersion is expected, comparative computations without the D3 correction were performed. Surprisingly, the resulting geometries were a better fit with significantly diminished RMSDs, which implies an overestimation of *London* dispersion through the D3 correction term (Table 6).

Table 6. Comparison of selected geometric parameters derived from computations and sc-XRD data including distances [Å], bond angles [°], dihedral angles [°], and RMSD.

		sc-XRD	**PBE0**	**PBE0–D3**
$(Ph_2Sb)_2Naph$ (**41**)	Pn···Pn	3.298	3.262	3.304
	C–Pn	2.134, 2.142, 2.158, 2.159, 2.160, 2.179,	2.142, 2.142, 2.153, 2.153, 2.168, 2.169	2.148, 2.148, 2.160, 2.161, 2.173, 2.173
	C–Pn–E	89.12, 92.91, 94.74, 95.55, 96.87, 97.58, 100.35, 101.03, 170.98, 173.75,	80.06, 80.12, 88.26, 88.30, 95.64, 95.64, 96.47, 96.52, 96.84, 96.89, 175.09, 175.12	79.19, 79.28, 91.44, 92.09, 96.26 96.79, 98.29, 96.27, 96.83, 98.39, 171.22, 171.79
	Pn–C–C–Pn	33.70	14.94	19.70
	RMSD	–	0.50	0.37
$(Ph_2Sb)_2Acenaph$ (**61**)	Pn···Pn	3.341	3.323	3.362
	C–Pn	2.137, 2.140, 2.151, 2.154, 2.158, 2.165	2.145, 2.145, 2.151, 2.151, 2.162, 2.162	2.149, 2.149, 2.159, 2.160, 2.166, 2.167
	C–Pn–E	88.08, 90.31, 95.22, 96.15, 96.18, 98.33, 99.62, 100.05, 172.25, 175.28	80.22, 83.72, 87.41, 95.57, 95.87, 95.87, 95.92, 96.77, 96.84, 175.78, 176.94	79.45, 79.48, 90.72, 91.95, 96.31, 96.35, 97.10, 97.11, 98.12, 98.13, 171.40, 172.57
	Pn–C–C–Pn	28.58	2.63	12.42
	RMSD	–	0.72	0.39
$(Ph_2Bi)_2Naph$ (**63**)	Pn···Pn	3.446	3.472	3.468
	C–Pn	2.252, 2.257, 2.268, 2.270, 2.281, 2.289	2.238, 2.244, 2.247, 2.261, 2.252, 2.271	2.247, 2.250, 2.251, 2.259, 2.272, 2.280
	C–Pn–E	70.4, 77.4, 80.2, 92.0, 94.1, 95.4, 95.4, 95.5, 99.1, 129.3, 136.6, 159.9	73.1, 76.1, 77.9, 93.0, 93.0, 93.1, 94.4, 95.1, 95.5, 130.9, 133.3, 161.2	75.9, 77.6, 94.5, 95.2, 95.3, 95.5, 95.6, 96.0, 122.1, 141.7, 167.4, 178.6
	Pn–C–C–Pn	8.98	24.13	13.88
	RMSD	–	0.54	0.46

The resulting LUMOs of all three compounds were found located on the naphthalene-type ligand L with an antibonding orbital. When calculated without the dispersion correction D3BJ, a slight deviation in the orbital shape for **41** and **61** was observed *via* a slight extension to the Sb centers. For **61** and **63**, a significant portion of the HOMO was found on L as well, however, the Bi1 lone pair of **63** and the Sb lone pairs including an Sb–C_{Ph} bond of **61** are also reflected by the respective frontier orbital. In contrast, the HOMO of **41** is not located on the naphthalenediyl ligand but is instead primarily located on the antimony lone pairs, while also stretching to Sb–C_{peri} and Sb–C_{Ph} bonds. Without the dispersion correction, the HOMO of **61** is more comparable to the HOMO of **41** than **63** (Figure 21).

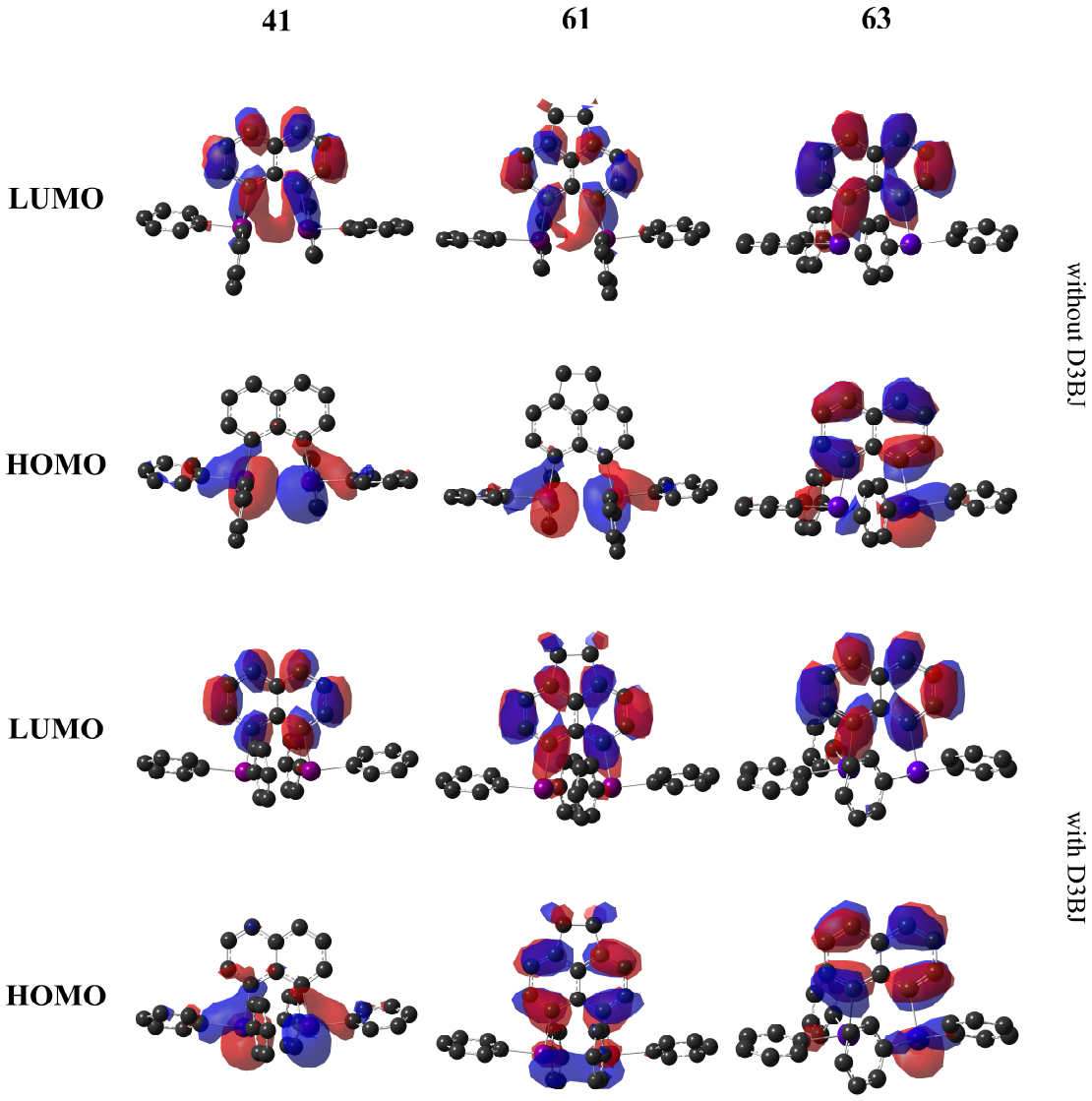

Figure 21. Frontier orbitals of $(Ph_2Pn)_2L$ (L = Naph, Pn = Sb **41**, Bi **63**; L = Acenaph, Pn = Sb **61**). The hydrogen atoms are omitted for clarity. ΔE_{HL} were computed with BP86/PBE/PBE0/PBE0–D3 and are given in Table 7. Isovalues: **41**: 0.025; **61**: 0.02 (bottom), 0.025 (top); **63**: 0.02.

The HOMO-LUMO gaps ΔE_{HL} are in close range and show no significant deviation when calculated with BP86 or PBE. In contrast, ΔE_{HL} is significantly larger, when computed with PBE0 regardless of applied dispersion correction. Although the overall differences are small, the HOMO-LUMO gaps increase from **41** to **63**. With the NBO analysis giving small Wiberg bond indices (WBI) and Mayer bond orders (MBO) between the Pn center may indicate shared electron density and therefore attractive interaction (Table 7, Figure 22).

Table 7. NBO analysis of $(Ph_2Pn)_2L$ (L = Naph, Pn = Sb **41**, Bi **63**; L = Acenaph, Pn = Sb **61**) performed with the BP86 and PBE functionals including the HOMO-LUMO gap ΔE_{HL}, Wiberg bond indices (WBI), Mayer bond orders (MBO), natural partial charges and NBO interactions.

			41	**61**	**63**
BP86	ΔE_{HL} [kcal mol^{-1}]		3.12	3.06	3.15
	WBI (MBO) [a.u.]	Pn···Pn	0.12 (0.19)	0.11 (0.26)	0.10 (0.15)
	Natural partial charge [e]	Pn	+1.02/+1.02	+1.02/+1.02	+0.98/+1.01
	$n_{Pn}\rightarrow\sigma^*_{Pn-C}$ [kcal mol^{-1}]		4.53/4.54	3.95/4.01	4.41
PBE	ΔE_{HL} [kcal mol^{-1}]		3.02	3.07	3.16
	WBI (MBO) [a.u.]	Pn···Pn	0.14 (0.31)	0.13 (0.31)	0.10 (0.15)
	Natural partial charge [e]	Pn	+1.02/+1.02	+1.02/+1.02	+0.98/+1.01
	$n_{Pn}\rightarrow\sigma^*_{Pn-C}$ [kcal mol^{-1}]		5.26/5.20	4.83/4.93	4.58
PBE0	ΔE_{HL} [kcal mol^{-1}]		4.57	4.74	4.84
	WBI (MBO) [a.u.]	Pn···Pn	0.14 (0.31)	0.12 (0.28)	0.08 (0.13)
	Natural partial charge [e]	Pn	+1.07/+1.07	+1.07/+1.07	+1.04/+1.06
	$n_{Pn}\rightarrow\sigma^*_{Pn-C}$ [kcal mol^{-1}]		6.96/6.95	5.64/5.82	5.19
PBE0–D3	ΔE_{HL} [kcal mol^{-1}]		4.52	4.66	4.89
	WBI (MBO) [a.u.]	Pn···Pn	0.14 (0.30)	0.12 (0.27)	0.09 (0.13)
	Natural partial charge [e]	Pn	+1.07/+1.06	+1.06/+1.06	+1.04/+1.05
	$n_{Pn}\rightarrow\sigma^*_{Pn-C}$ [kcal mol^{-1}]		6.85/6.79	5.93/6.00	5.39

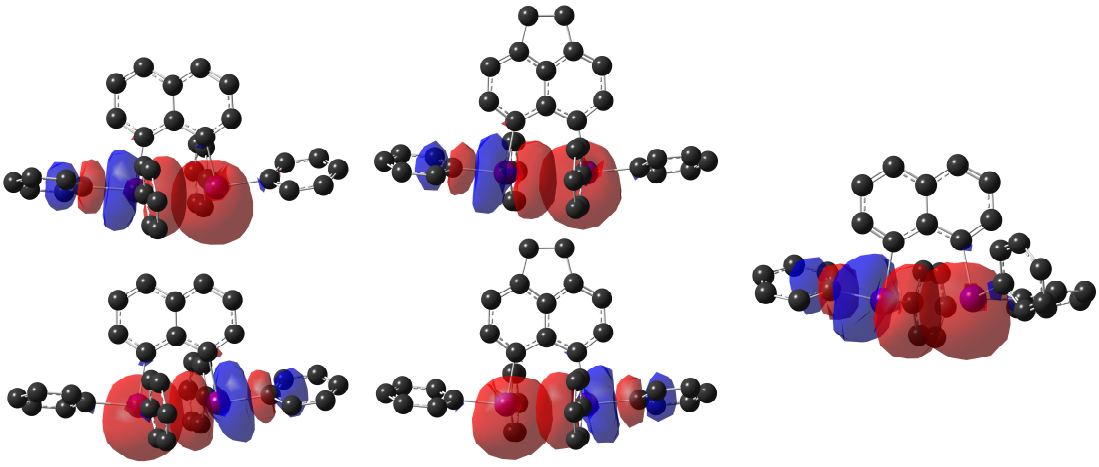

Figure 22. NBO orbital interactions (isovalue 0.025, **63**: 0.02) of $(Ph_2Pn)_2L$ (L = Naph, Pn = Sb **41**, Bi **63**; L = Acenaph, Pn = Sb **61**). A symmetric interaction between the Sb lone pairs n_{Sb} and antibonding Sb–C_{Ph} orbital is shown, while a significant interaction (>3 kcal mol^{-1}) for Bi was only found from the Bi2 lone pair n_{Bi2} to the Bi1–C11 antibonding orbital $\sigma^*_{Bi1-C11}$.

A second-order perturbation theory analysis in NBO basis identified an interaction between the Sb lone pairs n_{Sb} and the opposing Sb–C_{Ph} antibonding orbital $\sigma^*_{Sb–C}$. For **63**, only one interaction between the Bi2 center and Bi1–C11 antibonding orbital was found. The strengths of the interactions are in the range of weak hydrogen bonds and are of comparable magnitude. Moreover, the pnictogen centers bear a similar charge. In summary, only small hints for covalent interaction between the pnictogen center are observed, whereas electrostatics play no part.

In addition, QTAIM analysis was performed to gain more insights into the covalent and closed-shell nature of the interaction. At the bond critical points (BCP) between the Pn centers, the *Laplacian* of the electron density $\nabla^2\rho_{CP}$ was >0 with low electron density, which indicates closed-shell interactions. Since NBO analysis did not show a significant charge difference, an ionic nature of the interaction can be excluded, which then leaves *van der Waals* interactions. However, the total energy density $H_{CP}(r)$ was <0, which is an indication of covalent interactions, *i.e.* electron sharing, and therefore supports the observed NBO interactions. In summary, the QTAIM analysis suggests a combination of *van der Waals* ($\nabla^2\rho_{CP}$) and covalent interactions (H_{CP}). This is supported by the ratio of the absolute potential and the *Lagrangian* kinetic energy $\frac{|V_{CP}|}{G_{CP}}$; in this case, a range of $1.1 < \frac{|V_{CP}|}{G_{CP}} < 2$ for intermediate interactions in the analysis of various hydrogen bonds was determined (Figure 23, Table 8).[199]

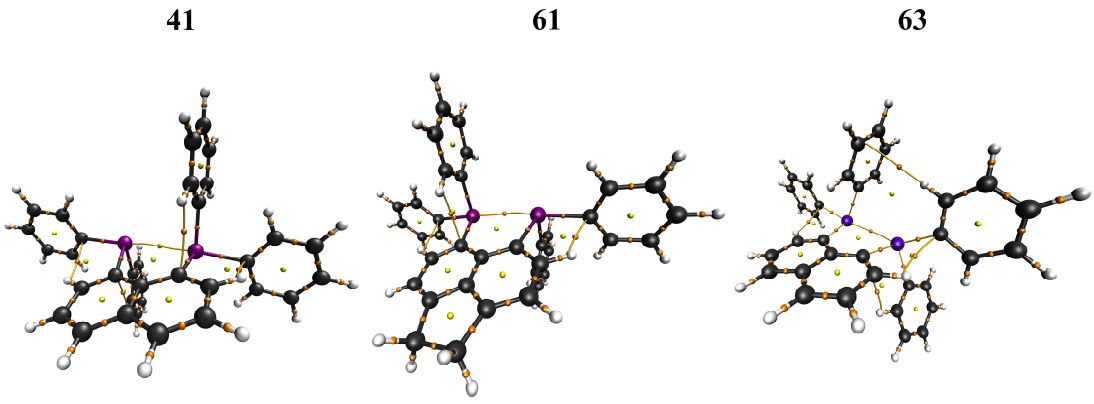

Figure 23. Molecular graphs (PBE0) of **41** (left), **61** (middle), and **63** (right) showing the bond paths (lines), bond critical points (orange).

Table 8. The topological and energetic properties of the electron density $\rho(\mathbf{r})$ computed at the bond critical points between the Pn centers for **41**, **61**, and **63**. The electron density (ρ_{CP}), the *Laplacian* of the electron density ($\nabla^2\rho_{CP}$), the *Lagrangian* kinetic (G_{CP}), potential (V_{CP}), and total energy densities (H_{CP}) at the BCPs are given in atomic units (a.u.).

		ρ_{CP}(r)	$\nabla^2\rho_{CP}$	G_{CP}	V_{CP}	H_{CP}	$\frac{\lvert V_{CP}\rvert}{G_{CP}}$
41	BP86	0.0220	0.0273	0.00880	–0.0108	–0.00198	1.22
	PBE	0.0228	0.0258	0.00874	–0.0110	–0.00229	1.26
	PBE0	0.0240	0.0263	0.00926	–0.0120	–0.00270	1.30
	PBE0–D3	0.0227	0.0252	0.00866	–0.0110	–0.00235	1.27
61	BP86	0.0218	0.0261	0.00820	–0.00988	–0.00167	1.20
	PBE	0.0207	0.0245	0.00818	–0.0102	–0.00204	1.25
	PBE0	0.0215	0.0251	0.00830	–0.0103	–0.00203	1.24
	PBE0–D3	0.0208	0.0239	0.00783	–0.0969	–0.00186	1.24
63	BP86	0.0185	0.0309	0.00849	–0.00924	–0.000853	1.09
	PBE	0.0186	0.0300	0.00835	–0.00920	–0.000751	1.10
	PBE0	0.0174	0.0300	0.00811	–0.00871	–0.000608	1.07
	PBE0–D3	0.0178	0.0297	0.00814	–0.00886	–0.000715	1.09

In one instance, the recrystallization of **63** yielded a few orange crystals in addition to the colorless needles of **63**. sc-XRD identified the orange crystals as $(PhBiNaph)_2$ (**65**), which is probably formed *via* dismutation reactions. To explore the reaction in more detail, *in situ* ^{1}H NMR experiments were conducted. A solution of **63** in toluene stored at ambient temperatures for ten days yielded only small amounts of **65**, whereas heating the toluene solution to 80 °C gave no **65**. Contrarily, heating a sample to 100 °C yielded a complex reaction mixture including **65**. As dismutation did not seem to be a feasible and selective route to generate **65**, a different approach was chosen. Although the addition of $RPCl_2$ to Li_2Naph (**25**), yielded the reduced species $(PhP)_2Naph$ (**27**) or the four-membered ring $(i\text{-}Pr)_2NPNaph$ (**28**),[155] the synthesis of **65** *via* dropwise addition of equimolar amounts of $PhBiCl_2$ to **25** at –30 °C was performed. The ^{1}H NMR spectrum of **65** in thf-d_8 contained the expected signals for the phenyl and naphthalenediyl substituents showing all magnetically unique protons without overlapping. However, some impurities remained after recrystallization since the product and by-products showed comparable solubilities in common organic solvents. One of the impurities was identified as Bi_2Naph_2 (**60**). Unfortunately, the reaction of $PhSbCl_2$ with Li_2Naph (**25**) and $TMSn_2Naph$ (**22**) only yielded complex reaction mixtures and no product could be isolated (Scheme 16).[186]

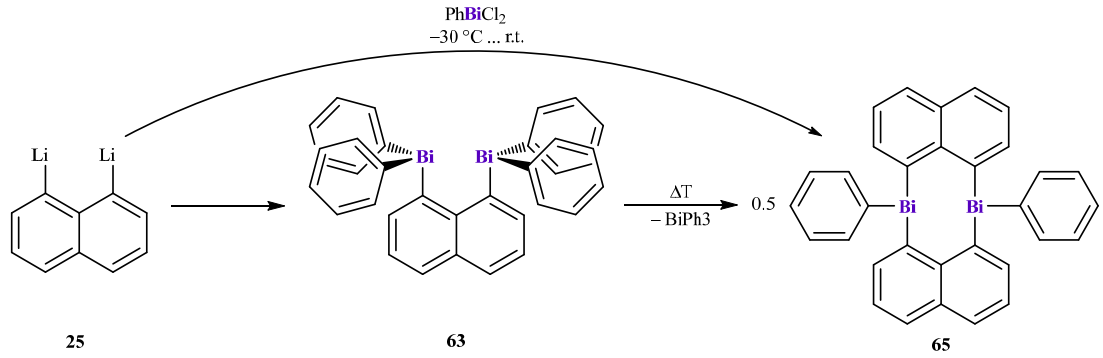

Scheme 16. The formation of **65** is observed *via* dismutation and salt-metathesis reactions.

(PhBiNaph)$_2$ (**65**) crystallized in the triclinic space group $P\bar{1}$. As observed in **63** and **64**, the Bi atoms adopt a trigonal-pyramidal coordination sphere with the bond angular sums (Bi1 289.36°, Bi2 285.32°) indicating a high *p*-orbital character for the Bi–C bonds (Figure 24).

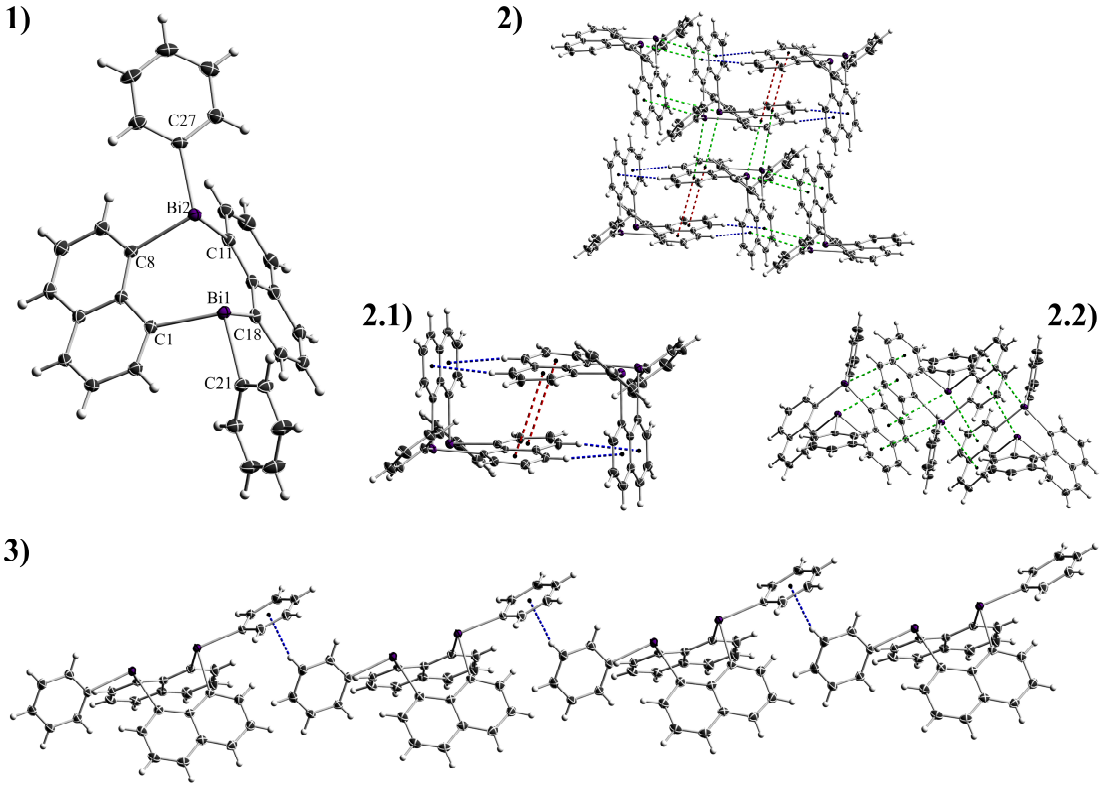

Figure 24. The solid-state structure of (PhBiNaph)$_2$ (**65**) with displacement ellipsoids drawn at a 50 % probability level. **1)** The molecular unit of **65**. **2)** The molecules of **65** form a two-dimensional network through CH···π (blue, **2.1**), π···π (red, **2.1**), and Bi···π (green, **2.2**) contacts. **C)** The two-dimensional layers are interconnected through $C_{Ph}H$···π contacts. Selected distances [Å], bond angles [°]: Bi1–Bi2 3.2273(4), Bi1–C1 2.306(3), Bi1–C18 2.303(3), Bi1–C21 2.279(3), Bi2–C8 2.267(3), Bi2–C11 2.267(3), Bi2–C27 2.268(3), C1–Bi1–C18 95.02(10), C1–Bi1–C21 97.63(11), C18–Bi1–C21 96.71(11), C21–Bi1–Bi2 173.96(7), C8–Bi2–C11 87.38(11), C8–Bi2–C27 100.70(11), C11–Bi2–C27 97.24(11), C27–Bi2–Bi1 174.62(8).

While the Bi–C bonds in **65** (2.267(3) Å-2.306(3) Å) are significantly longer than in **63**, the Bi···Bi distance is drastically shortened (3.2273(4) Å) even surpassing the Sb···Sb distance of **41**. $(PhBiNaph)_2$ (**65**) assumes a butterfly-type structure, which is comparable to $(ClAsNaph)_2$ (**59**),[175] whereas the packing motif similar to the dipnictanes Pn_2Naph_2 (Pn = As, Sb).[174,175] Analogous to **60**, one Bi atom forms two π contacts with rather large Bi···π distances (Bi1 4.05 Å/4.08 Å, Bi2 4.11 Å/3.71 Å). However, in contrast to **60**, these contacts are formed *via* two back-to-back dimers (type **C**, Figure 12, page 22) instead of the V-like type **D** (Figure 15, page 29), thus resulting in an overall trimeric unit. Moreover, the common dimer **A**, which is formed through CH···π and π···π contacts, is also observed. These interactions result in two-dimensional layers, which are also connected by CH···π contacts between the phenyl substituents.

To analyze the non-covalent interactions within the Bi(III) species **65** in more detail, quantum chemical computations were performed in cooperation with *Prof. Dr. G. Jansen*[‡] and *F. van der Vight*[‡] using the Orca 5.0[177–180] and Molpro 2015.1[200] program packages. To identify the interaction with the largest contribution, the dimeric units were studied. The trimeric unit (Figure 24, **B.2**) was split into two dimers **D1** and **D2** with different Bi···Bi distances (**D1**: 6.274 Å, 6.578 Å, 7.512 Å; **D2**: 4.680 Å, 5.627 Å, 5.743 Å), while the third unit **D3** under consideration was found in the type **A** dimer (Figure 24, **B.1**) (Figure 25). The dimer interaction energies were computed in the def2-TZVP basis set[185,194] with the BP[195,196] and PBE[197] functionals utilizing the atom-pairwise dispersion correction with Becke-Johnson damping (D3BJ) (Table 9).[22,36,186]

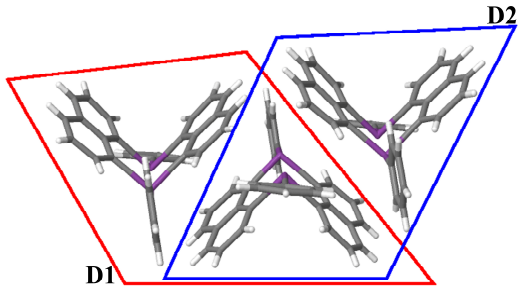

Figure 25. Separation of the trimeric unit into the dimers **D1** and **D2**.[186]

Table 9. Computed interaction energies [kJ mol^{-1}] for the dimers D1-D3.[186]

	BP+D3	PBE+D3
D1	–147.9	–88.2
D2	–182.9	–110.0
D3	–106.2	–80.2

‡Theoretical Organic Chemistry, University of Duisburg-Essen, 45141 Essen, E-mail: georg.jansen@uni-due.de

Although both functionals identified the interactions within **D2** as the leading contributor to the overall stabilization, the magnitudes deviate significantly (Table 9). As a result, higher-level methods were applied. The dimers were simplified by replacing a varying number of substituents with hydrogen atoms, giving four different dimers. Replacement of the distant naphthalenediyl and the phenyl substituent gives the $[Naph(BiH_2)_2]_2$ dimer (**D4**), which was further simplified to the $Bi_2H_6\cdots Naph$ dimer (**D5**). Compared to **D4**, the resulting energy of **D5** will have to be multiplied by two as it contains only half of the interactions involved. Further simplification led to the $(Bi_2H_6)_2$ dimer (**D6**) and $(Naph)_2$ dimer (**D7**), which account for the Bi···Bi interactions, and the $\pi\cdots\pi$ interactions, respectively. In addition to the previously used method, the energies were calculated at the DLPNO-CCSD(T)[182,183,201] and DFT-SAPT[202] level of theory with the asymptotically-corrected PBE0AC hybrid functional[203] in the TZVPP basis-set[185,194,204] with counterpoise-correction[205] (Table 10).[186]

Table 10. Computed interaction energies [kJ mol^{-1}] for the dimers **D4**-**D7**.[186]

	$[Naph(BiH_2)_2]_2$ (D4)	**$Bi_2H_6\cdots Naph$ (D5)**	**$(Bi_2H_6)_2$ (D6)**	**$(Naph)_2$ (D7)**
BP+D3	–110.5	–45.1	–25.8	–11.3
PBE+D3	–58.7	–27.0	–14.8	–11.6
DLPNO-CCSD(T)	–48.1	–19.0	–9.9	–10.0
DFT-SAPT (PBE0AC)	–41.3	–17.7	–8.9	–8.3

At first glance, a significant deviation of the BP+D3 interaction energies is observed, while the PBE+D3 energies agree reasonably with the applied higher level methods. It is important to note, that the interaction energies for the higher methods are not yet converged, while the applied D3 methods are nearly converged. Therefore, the "true" interaction energies for **D1**-**D3** are expected to be fairly well represented by the PBE+D3 method (Table 9).[186]

A comparison of the interaction energies for the dimers **D4**-**D7** shows that the Bi···π contacts give the main stabilizing contribution, however, the interactions in dimers **D6** and **D7** also contribute considerably to the overall stabilization. These results are in agreement with the previously reported Pn_2Naph_2 (Pn = Sb **58**, Bi **60**) and $(ClAsNaph)_2$ (**59**), where a dominating Pn···π interaction was reported.[174–176] In contrast to the results obtained for Sb_2Naph_2 (**58**), PBE+D3 agree very well with the higher level methods, while it underestimated the Sb···π interactions.[186]

The nature of the dimer interactions was investigated *via* a decomposition of the DFT-SAPT energies, which yielded the electrostatic, exchange, induction, and dispersion contributions. In accordance with the previously investigated bisnaphthalenediyls **58-60**, *London* dispersion provides the leading attractive contribution to the interaction energies of the dimers **D4**-**D7**. In addition, a significant amount of electrostatic interaction was found, while the induction energies are less significant (Figure 26).

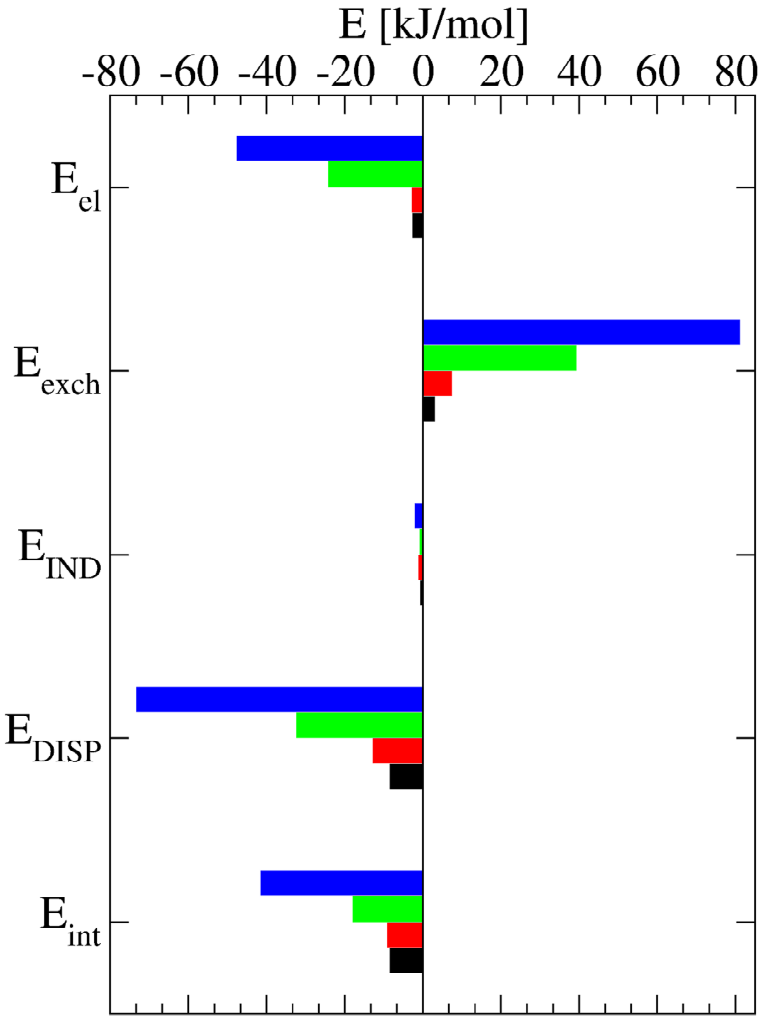

Figure 26. Interaction energy contributions as obtained with DFT-SAPT for the dimers Naph(BiH_2)$_2$ (**D4**, blue), Bi_2H_6···Naph (**D5**, green), Bi_2H_6···Bi_2H_6 (**D6**, red), Naph···Naph (**D7**, black). E_{el} represents the first-order electrostatic interaction energy, E_{exch} is the first-order exchange contribution, E_{IND} is the total induction energy, E_{DISP} represents the total dispersion energy and E_{int} is the total SAPT interaction energy.[186]

5.3. One-Electron Oxidation

Since a degree of intramolecular Pn···Pn interaction was found in compounds **41**, **61**, and **63**, their behavior towards one-electron oxidation was investigated. In this respect, the phenyl-substituted species $(Ph_2Sb)_2Naph$ (**41**) and $(Ph_2Bi)_2Naph$ (**63**) were analyzed *via* cyclic voltammetry (CV) (Figure 27).

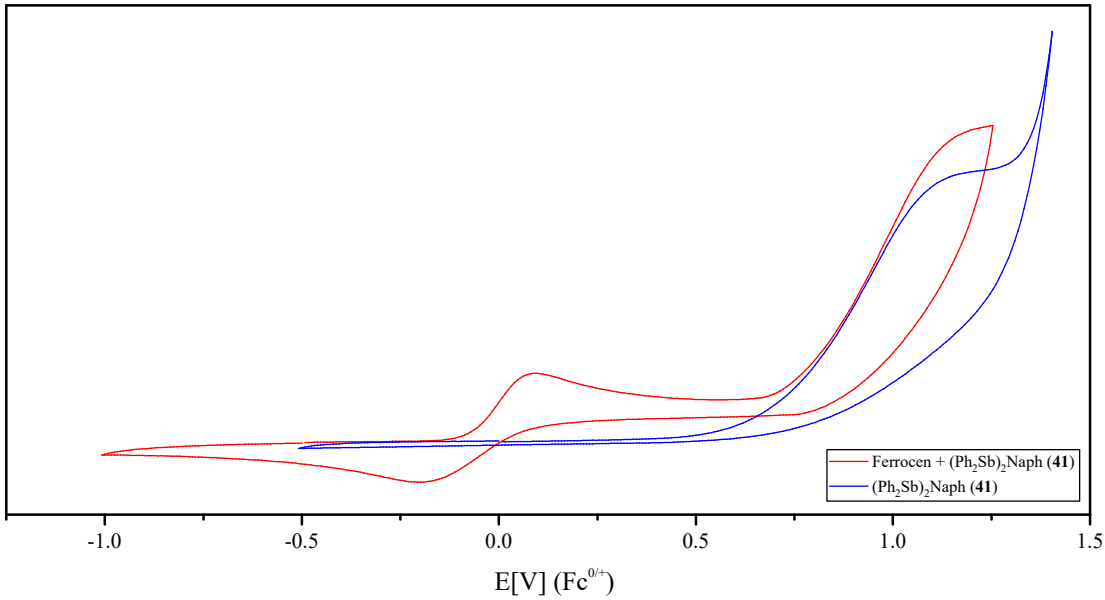

Figure 27. Cyclic voltammogram of $(Ph_2Sb)_2Naph$ (**41**) in DCM solution (1 mM) at ambient temperature containing [*n*-Bu_4N][$B(3,5\text{-}(CF_3)_2\text{-}C_6H_3)_4$] (50 mM) as electrolyte. Values are referenced to ferrocene (Fc).

A single irreversible oxidation event was observed for **41** ($E_{p,a}(Fc^{0/+1})$ = 1.17 V) and **63** ($E_{p,a}(Fc^{0/+1})$ = 0.94 V) whereby the oxidation of Bi occurred at a slightly lower voltage than for Sb. The CV studies indicate that a rather strong oxidizing agent is needed, therefore **41** was reacted with [NO][SbF_6].[206] The solids were suspended in dichloromethane and an immediate reaction was indicated by the evolution of NO gas. However, a rather complex reaction mixture was obtained and unfortunately no product could be isolated. Therefore, $AgSbF_6$ as a milder oxidation agent was employed. **41** and were suspended in CH_2Cl_2 under the exclusion of light. After 30 minutes, the solvent was removed and the residue extracted with CH_3CN yielding colorless needles upon concentrating and storing at 4 °C. sc-XRD identified the crystals as the chelated silver complex {[$(Ph_2Sb)_2Naph]_2Ag$}[SbF_6] (**66**). By performing the reaction in acetonitrile instead of DCM, the yield increased up to 84 %. The ^1H NMR spectrum of **66** in CD_2Cl_2 displays the expected doublet of doublets for the naphthyl protons (8.09 ppm, 7.74 ppm, 7.46 ppm), however, in contrast to **41** the signals for the phenyl protons do not overlap and split into a triplet

of triplets (7.37 ppm,), a triplet (7.15 ppm) and a doublet of doublets (7.09 ppm). Interestingly, no reaction was observed when **41** was reacted with $[(CH_3CN)_4Cu][BAr^{F\text{-}20}]$ ($Ar^{F\text{-}20} = (C_6F_5)_4$) or copper-(I) chloride, whereas the reaction with gold-(I) chloride yielded a complex mixture along with the precipitation of elemental gold. However, when MCl (M = Cu, Au) was reacted with **66**, transmetallation occured yielding the respective copper species $\{[(Ph_2Sb)_2Naph]_2Cu\}[SbF_6]$ (**67**), as well as a co-crystallized silver and gold species $\{[(Ph_2Sb)_2Naph]_2$"Au"$\}[SbF_6]$ (**68**, "Au" = $Ag_{0.66}Au_{0.34}$). Despite several recrystallization and synthesis attempts, no pure gold derivative of **68** could be obtained (Scheme 17).

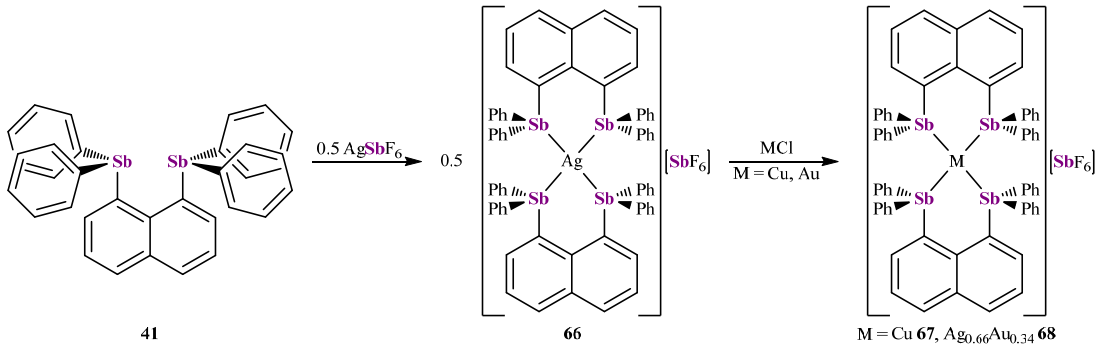

Scheme 17. Synthesis of coinage metal coordination complexes with **41** as chelating ligand.

While the signals in the ^{1}H NMR spectrum of **67** experienced a significant chemical shift compared to **66**, the ^{1}H NMR spectrum of **68** confirms the presence of two species, with a greater proportion of **66** than for the pure gold compound. $\{[(Ph_2Sb)_2Naph]_2M\}[SbF_6]$ (M = Ag **66**, Cu **67**, "Au" **68**) crystallized in the monoclinic space groups $P2_1/c$ (**66**, **68**) and $P2_1/n$ (**67**), with one and two CH_3CN molecules in the unit cell of **66** and **68**, respectively, whereas no solvent molecules were observed in the unit cell of **67**. The coinage metal centers are coordinated by two **41** molecules, which act as bidentate ligands and result in distorted tetrahedral coordination spheres of the metals. The Sb–M bond lengths are at the shorter end of known Sb–M single bonds and increase from **67** to **66**, while a slight decrease occurs when introducing gold. This is in agreement with the covalent radii of the respective elements (r_{cov}(Cu) = 1.32 Å, r_{cov}(Ag) = 1.45 Å, r_{cov}(Au) = 1.36 Å).[207] However, it is important to note, that the changes from **66** to **68** are less significant, which is probably due to partial occupation of the metal center with silver and gold in a 66:34 percent ratio (Figure 28, Table 11).

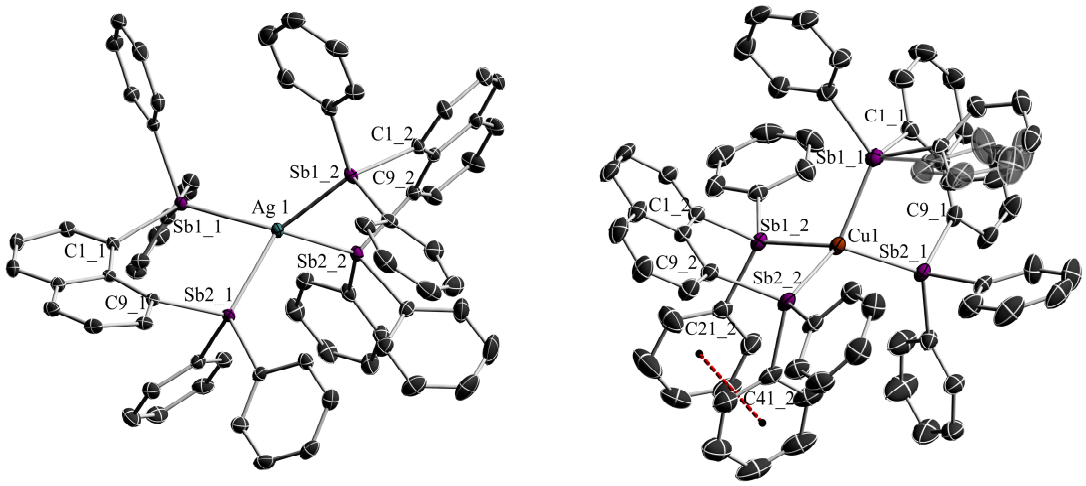

66 **67**

Figure 28. Solid-state structures of {[$(Ph_2Sb)_2Naph]_2M$}[SbF_6] (M = Cu **67**, Ag **66**) with displacement ellipsoids drawn at the 50 % probability level. The hydrogen atoms, anions, and solvent molecules are omitted for clarity.

Table 11. Selected distances [Å], bond angles [°], and dihedral angles [°] of **66-68**.

	Cu 67		**Ag 66**		**"Au" 68**	
Sb–M	2.4981(5)	2.5005(5)	2.6824(3)	2.6636(3)	2.66421(15)	2.64462(15)
	2.4740(5)	2.4759(5)	2.6786(3)	2.6861(3)	2.64438(15)	2.66237(14)
Sb···Sb	3.4698(3)	3.4393(3)	3.5931(5)	3.5814(5)	3.5931(2)	3.5792(2)
Sb–C_{peri}	2.150(3)	2.154(3)	2.171(2)	2.163(2)	2.1714(14)	2.1646(15)
	2.145(3)	2.151(3)	2.145(2)	2.145(2)	2.1409(14)	2.1411(15)
Sb–M–Sb	88.507(15)		84.170(12)		85.196(5)	
	87.437(15)		84.048(11)		84.819(5)	
	111.243(17)		131.573(9)		129.831(5)	
	129.540(19)		122.366(10)		121.527(5)	
	120.282(18)		124.360(10)		124.864(5)	
	122.797(18)		113.878(11)		114.132(5)	
M–Sb–C	108.92(9)	105.90(9)	119.00(6)	118.96(7)	117.98(4)	118.43(4)
	122.50(9)	120.18(9)	120.26(6)	119.66(7)	121.30(4)	120.58(5)
	121.42(14)	122.91(9)	114.59(6)	113.04(7)	114.80(4)	112.82(4)
	112.78(8)	112.55(9)	114.64(6)	117.99(6)	114.57(4)	117.79(4)
	120.60(9)	123.04(9)	127.66(7)	108.42(7)	126.84(4)	125.75(4)
	116.37(9)	111.49(10)	109.36(7)	125.66(7)	109.79(4)	108.44(4)
C–Sb–C	101.10(13)	105.52(12)	97.96(9)	100.72(9)	97.61(6)	100.88(6)
	95.57(16)	99.40(12)	99.74(9)	100.62(9)	99.63(6)	100.44(6)
	107.65(5)	100.04(12)	101.75(9)	100.67(10)	101.87(6)	100.43(6)
	100.88(13)	104.05(13)	102.51(9)	98.88(10)	102.81(6)	103.05(6)
	102.70(12)	101.77(13)	94.97(9)	103.13(9)	95.12(6)	98.83(6)
	100.92(12)	101.42(13)	102.35(9)	97.81(10)	102.65(6)	98.10(6)
Sb–C_{peri}–C_{peri}–Sb	9.85(16)	15.48(16)	32.73(11)	13.60(13)	32.88(7)	14.80(9)

The Sb–M–Sb angles are found in a range of roughly 110°-130°, while the bite angles are significantly more acute (~90°). The bite angles become smaller with increasing *van der Waals* radii, whereas the Sb···Sb distances follow the covalent radii trend. In comparison with **41**, the Sb···Sb distances are significantly enlarged, while a decrease in the dihedral angle Sb–C_{peri}–C_{peri}–Sb is observed. Intramolecular $\pi\cdots\pi$ contacts are formed through two neighboring phenyl rings of the same ligand in **67**. Additionally, the cationic parts of **66**-**68** form intermolecular CH···π contacts, which suggests little to no charge distribution to the organic ligands. Within **66** and **68**, one $[SbF_6]^-$ anion forms C_{Ph}H···F contacts, while the cation of **67** is connected with six $[SbF_6]^-$ units, forming a three-dimensional network (Figure 29).

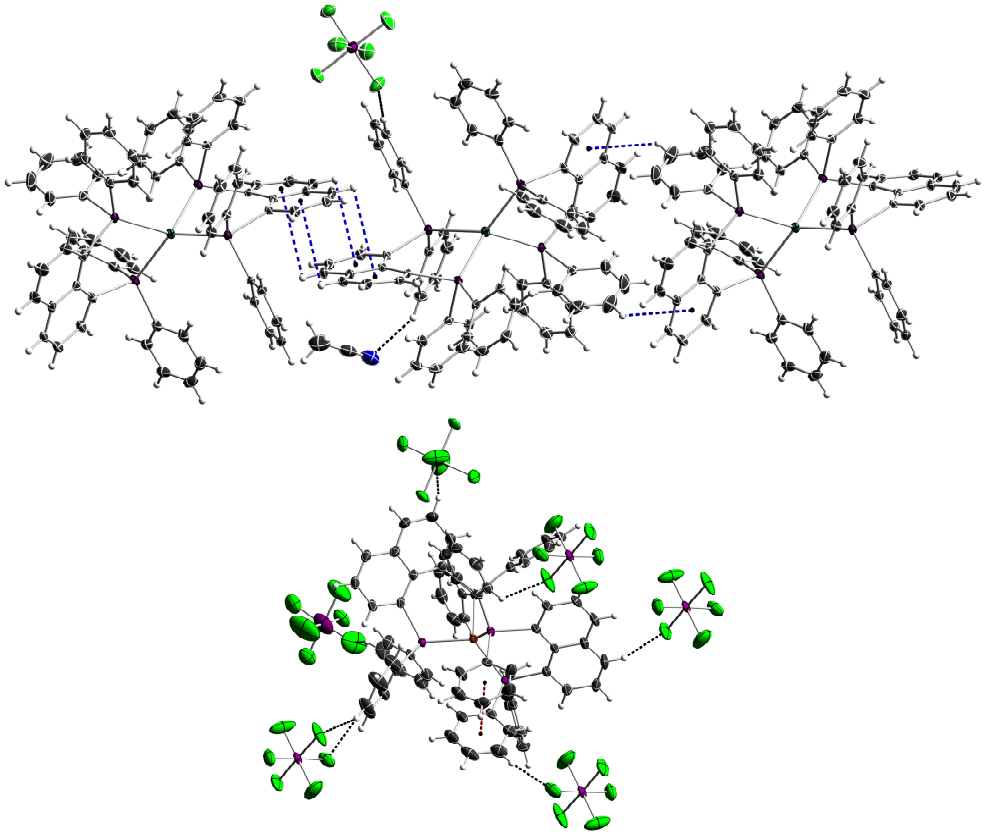

Figure 29. Intermolecular contacts in **66** (top) and **67** (bottom). Disordered groups are omitted for clarity. The complex form three-dimensional networks, through various contacts like CH···π (blue) and CH···F (black).

Reactions with strong oxidants were found to yield mixtures, whereas mild oxidants in the form of coinage metal halides led to coordination complexes: with that, the size of the ligand bonded to the pnictogen center was increased. Based on the reported stabilization of antimony-centered radicals of the type •PnR_3 (R = 2,4,6-tri-*iso*-propylphenyl = Trip),[208] the synthesis of the respective bis(diarylpnicta)naphthalene was attempted.

Analogous to the synthesis of $(Ph_2Pn)_2Naph$ (Pn = Sb **41**, Bi **63**), $Trip_2PnCl$ was reacted with Li_2Naph to yield $(Trip_2Pn)_2Naph$ (Pn = Sb **69**, Bi **70**) at –78 °C (**69**) and –30 °C (**70**), respectively.[209]

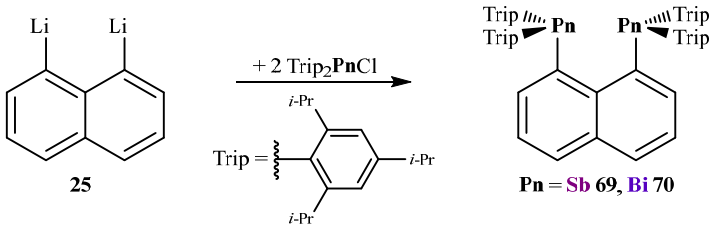

Scheme 18. Synthesis of sterically more crowded bis(diarylpnicta)naphthalenes **69** and **70**.

Despite the increased ligand size, the ^{1}H NMR spectrum of **70** displays the expected signals for a highly symmetric species, which includes three signals for the naphthalenediyl protons and the corresponding signals for the Trip-ligand. In contrast, the signals in the ^{1}H NMR spectrum of **69** indicate a molecule of lower symmetry, as the signals for the Trip-ligand are broad and splitted into more signals (Figure 30).[209]

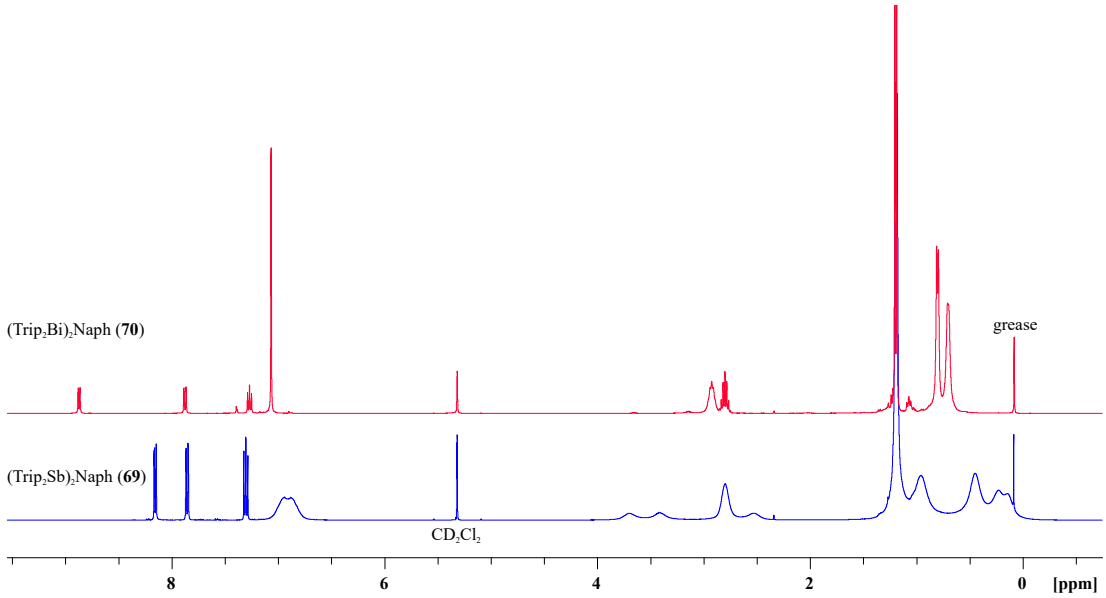

Figure 30. The ^{1}H NMR spectrum of $(Trip_2Pn)_2Naph$ (Pn = Sb **69**, Bi **70**) recorded in CD_2Cl_2 at ambient temperature. The spectrum of **70** (red) indicates a highly symmetric species, while a molecule of lower symmetry is implied by the signal splitting in the ^{1}H NMR spectrum of **69** (blue).

To gain more insight into the present molecular dynamics variable temperature (VT) NMR measurements were performed in toluene. The VT studies showed that the signal for the *ortho-iso*-propyl group undergoes two coalescence points. Initially, only one signal is observed for the group, which then splitted into two broad signals (T_c = 70 °C **69**, 0 °C **70**), each of which further split into two signals (T_c = 50 °C **69**, –60 °C **70**) (Figure 31).[209]

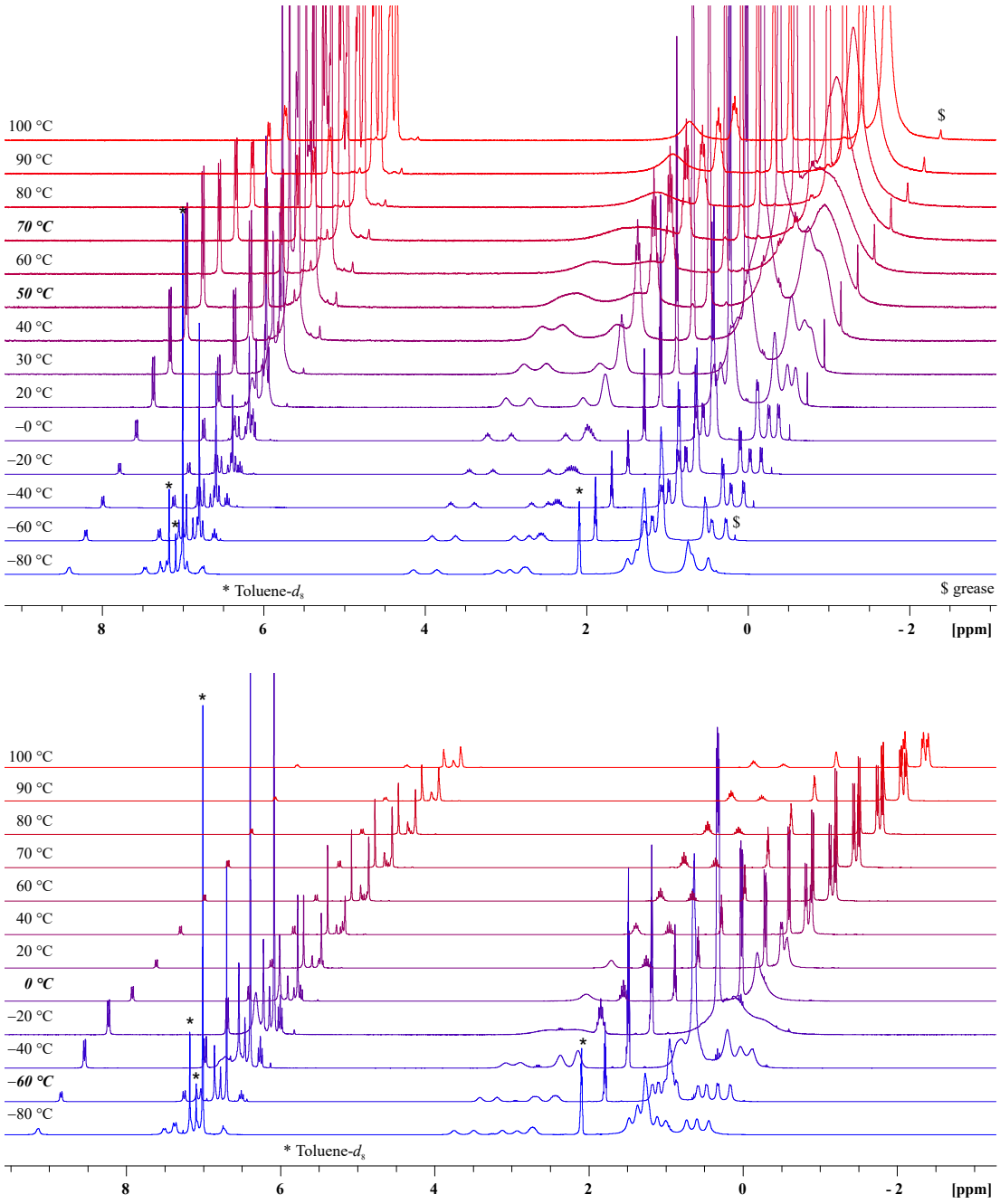

Figure 31. ^{1}H VT NMR studies of (Trip$_2$Sb)$_2$Naph (**69**, top) and (Trip$_2$Bi)$_2$Naph (**70**, bottom) in toluene-d_8.[209]

According to the following equations

$$\Delta G^{\neq} = -RT_c \ln\left(\frac{k_c h}{k_B}\right) \qquad (2)^{[210]}$$

$R = 8.314$ J mol^{-1} K^{-1}; $h = 6.626 \cdot 10^{-34}$ J Hz^{-1}; $k_B = 1.381 \cdot 10^{-23}$ J K^{-1}

with

$$k_c = \frac{\pi}{\sqrt{2}} \Delta\nu \qquad (3)^{[210]}$$

the free energies of activation $\Delta G^{\neq}$ were calculated. Herein, $\Delta\nu$ is defined as the chemical shift difference in Hz between the fully separated signals. For **69**, $\Delta G^{\neq}$ values of 15.6 and 15.9 kcal mol^{-1} were calculated at the coalescence temperatures (50 °C, 70 °C), while 12.9 and 13.3 kcal mol^{-1} were calculated for **70** (0 °C, –60 °C). The hindered rotation in both molecules most likely stems from ligand-ligand interactions between the Trip groups. The larger barriers observed for **69** can be explained by the different atom sizes of the pnictogen centers in **69** and **70**, which result in different distances between the ligands.[209]

Both $(Trip_2Pn)_2Naph$ (Pn = Sb **69**, Bi **70**) were crystallized from saturated ethanol solutions upon storage at 4 °C. They crystallized in the orthorhombic and monoclinic space groups $P2_12_12$ (**69**) and $C2/c$ (**70**) with two (**69**) and four (**70**) molecules per unit cell, respectively (Figure 32).[209]

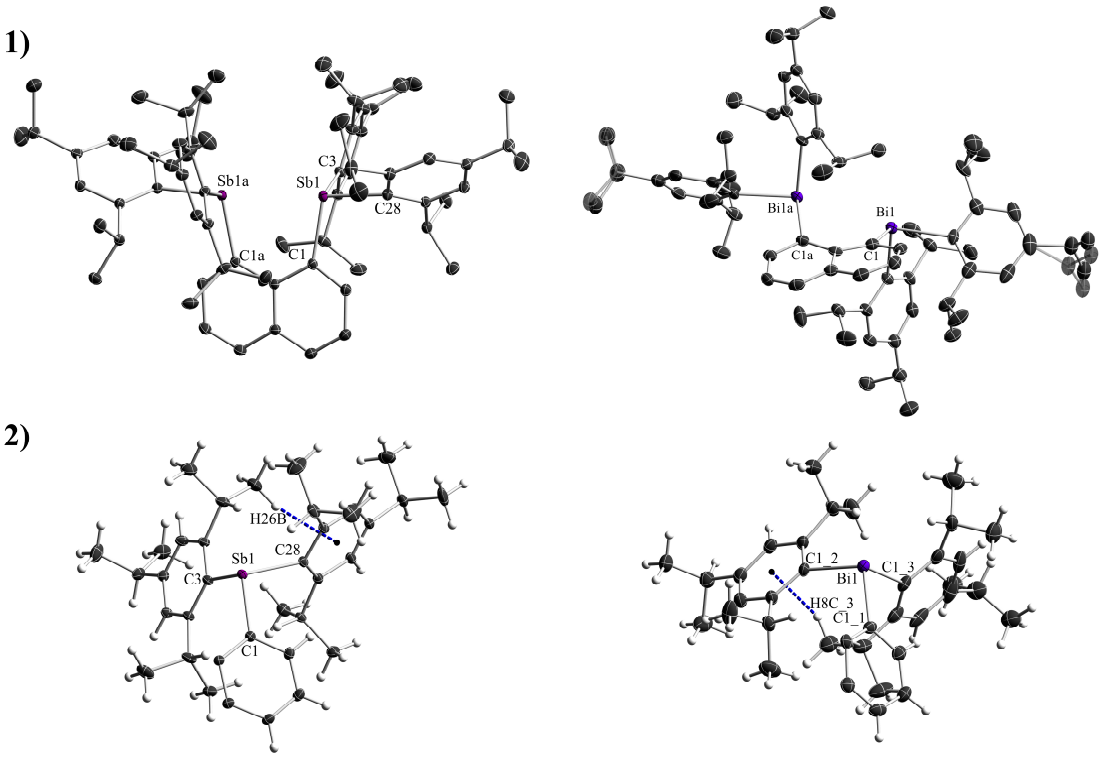

Figure 32. 1) Solid-state structures of $(Trip_2Pn)_2Naph$ (Pn = Sb **69** (left), Bi **70** (right)) with displacements ellipsoids drawn at the 50 % probability level. The hydrogen atoms are omitted for clarity. **2)** The asymmetric units of **69** and **70**. The formation of intramolecular CH···π contacts (blue) is observed. Selected distances [Å], bond angles [°], and dihedral angles [°], **69**: Sb1–Sb1a 3.2328(2), Sb1–C1, 2.1769(11), Sb1–C3 2.2019(11), Sb1–C28 2.1902(10), C1–Sb1–Sb1a 80.89(3), C3–Sb1–Sb1a 93.23(3), C28–Sb1–Sb1a 167.59(3), C1–Sb1–C3 106.84(4), C1–Sb1–C28 101.51(4), C3–Sb1–C28 97.64(4), Sb1–C1–C1a–Sb1a 12.78(7); **70**: Bi1–Bi1a 3.6742(4), Bi1–C11 2.318(4), Bi1–C12 2.326(5), Bi1–C13 2.326(5), C11–Bi1–Bi1a 74.73(11), C12–Bi1–Bi1a 92.31(19), C13–Bi1–Bi1a 164.20(13), C11–Bi1–C12 107.53(16), C11–Bi1–C13 96.72(17), C12–Bi1–C13 92.31(19), Bi1–C11–C1a–Bi1a 28.13(29).[209]

As seen in **41** and **63**, the pnictogen atoms adopt trigonal-pyramidal coordination spheres with C–Pn–C bond angles between 92.31(9)° and 107.53(16)°; the smallest angles are observed between the phenyl *ipso*-carbons. The sum of bond angles (**69**: 306.02°, **70**: 296.56°) indicate a high *p*-orbital character for the bonding electrons. In comparison with previously reported Pn–C single bonds, the observed Sb–C bond lengths (2.1769(11) Å, 2.2019(11) Å, 2.1902(10) Å) and Bi–C bond lengths (2.318(4) Å, 2.326(5) Å, 2.326(5) Å) are slightly elongated, which can be explained by repulsive interactions due to the steric crowding. However, despite the steric hindrance, a decrease in the Sb···Sb distance compared to **41** is observed (**69**: 3.2327(2) Å **41**: 3.2983(6) Å[186]), which consequently points to stronger attractive forces, such as ligand···ligand dispersion interactions. In contrast, the Bi···Bi distance in **70** (3.6742(4) Å) is significantly elongated compared to **63** (3.4461(4) Å), which instead suggests a stronger repulsive interaction between the Bi atoms. This is also reflected by the dihedral angles Pn1–C1–C1a–Pn1a of the Naph ligands indicating a larger distortion in **70** (**69**: 12.78(7)°, **70**: 28.13(29)°) (Figure 33).[209]

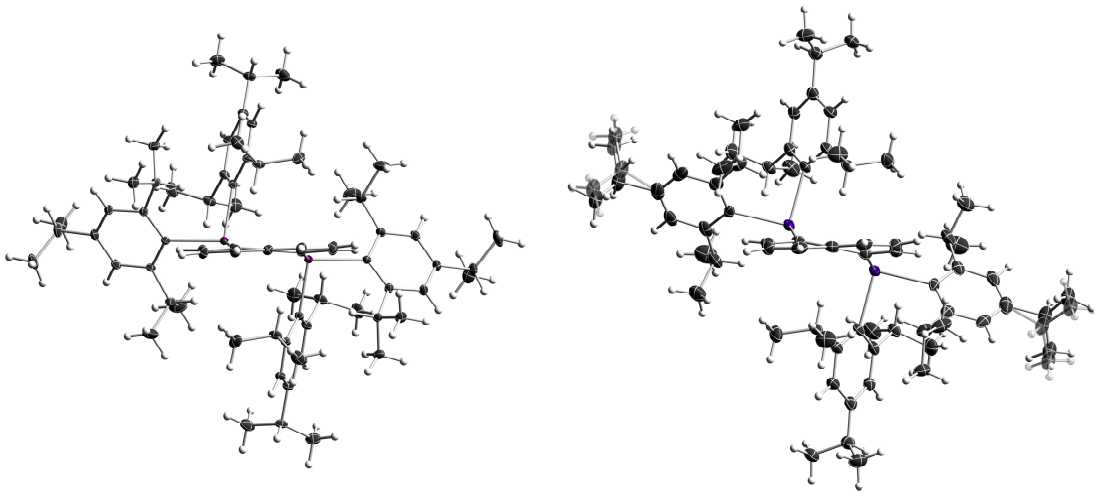

Figure 33. The present greater distortion of the naphthalene ligand in **70** (right) is clearly visible through the reflection of the *ortho*- and *meta*-hydrogen atom. The larger reflection of the Bi centers compared to Sb is visible.

Similar to the phenyl groups in **41**, both **69** and **70** assume a similar orientation for the Trip ligands, whereby two Trip groups are roughly situated parallel to the Pn···Pn axis. The remaining two Trip groups are aligned orthogonally to the axis and are point symmetric to each other. In addition, intramolecular CH···π contacts are observed in both structures between an *iso*-propyl and a Trip group, while intermolecular H···H contacts are only found in **70**.[209]

Subsequently, **69** and **70** were studied *via* CV to determine their redox properties. With respect to $(Trip_2Sb)_2Naph$ (**69**), two oxidation events were observed. The first event ($E_{1/2}(Fc^{0/+1})$ = –0.1 V) is determined pseudo-reversible since the peak-to-peak distance ΔE_p increased significantly with higher scan rates, followed by an irreversible event ($E_{p,a}(Fc^{0/+1})$ = 0.74 V). In contrast, only one irreversible event was observed for **70** ($E_{p,a}(Fc^{0/+1})$ = 0.66 V), which also occurred at a slightly lower voltage compared to the irreversible event of **69**. Moreover, two reduction events were observed for **70** ($E_{p,c}(Fc^{0/+1})$ = –0.79 V, –2.16 V), however the first event at –0.79 V only occurred, when the sample was scanned in oxidative direction. Based on these CV studies, $[Fc][Bar^{F\text{-}20}]$ was selected as a mild oxidizing agent for **69** (Figure 34).[206,209]

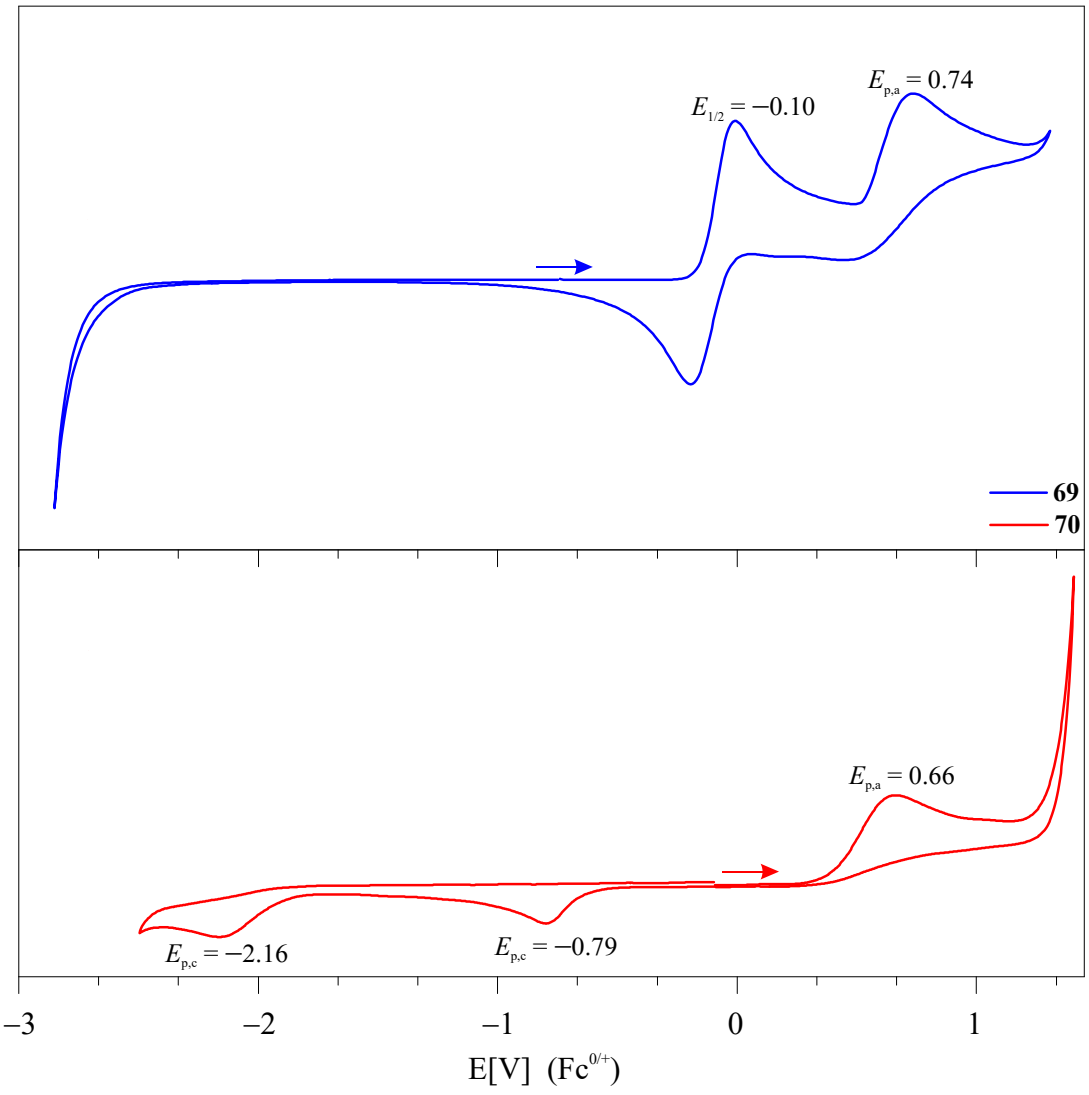

Figure 34. Cyclic voltammograms measured with solutions of $(Trip_2Pn)_2Naph$ (Pn = Sb **69**, Bi **70**) (1 mM) in DCM with $[n\text{-}Bu_4N][B(3,5\text{-}(CF_3)_2\text{-}C_6H_3)_4]$ (100 mM) as the electrolyte. Two oxidation events are observed for **69** (top), while only one occurred for **70** (bottom). The values are referenced to ferrocene.[209]

The reaction of **69** with [Fc][Bar$^{F\text{-}20}$] proceeded with an immediate color change from yellow to green. After workup, green crystals were isolated from a concentrated DCM solution, which was layered with ten equivalents of *n*-hexane. Surprisingly, no paramagnetic characteristics were observed and sc-XRD identified the compound as [1-(Trip$_2$Sb)-8-(TripSb)-Naph][BAr$^{F\text{-}20}$] (**71**) (Scheme 19).[209]

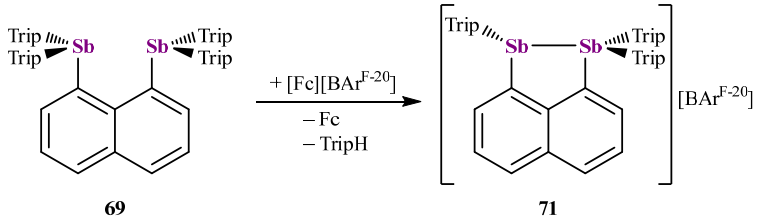

69 **71**

Scheme 19. The synthesis of **71** proceeds *via* elimination of ferrocene (Fc) and 2,4,6-tri-*iso*-propylbenzene (TripH).

TripH was identified as a by-product of the reaction, which implies a protonation during the reaction. Since the reaction proceeded faster in CH_2Cl_2 or thf than in benzene, the protonation of Trip by the solvent seems reasonable especially since the aforementioned solvents are much easier to deprotonate. The splitting of the Naph protons in the ^{1}H NMR spectrum of **71** indicates an unsymmetric species. Aside from that, sharp and broad signals in a 2:1 ratio were observed, for which ^{1}H VT NMR studies in CD_2Cl_2 were performed. The sharp signals displayed a coalescence temperature T_c of –70 °C was determined, while the broad signals became sharper at lower temperatures (Figure 35).[209]

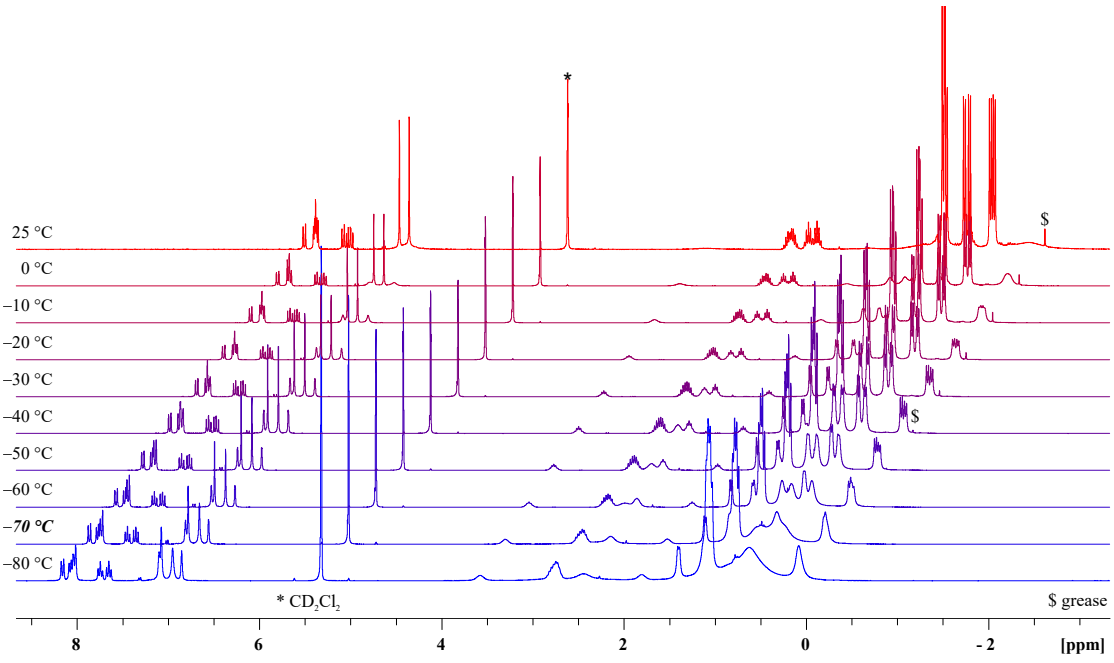

Figure 35. ^{1}H VT NMR studies of [(Trip$_2$Sb)(TripSb)Naph][Bar$^{F\text{-}20}$] (**71**) in CD_2Cl_2.[209]

The resulting rotational barrier of $\Delta G^{\neq}$ = 10.1 kcal mol^{-1} is roughly 5 kcal mol^{-1} smaller than in **69**; this is expected due to the decreased steric hindrance and *London* dispersion energy with the removal of one Trip group (Table 12).[209]

Table 12. Rotational barriers $\Delta G^{\neq}$ of **69**-**71** calculated at the coalescence temperatures obtained by ^{1}H VT NMR spectroscopy.[209]

	$T_{c\text{-}1}$ [°C] ($\Delta G^{\neq}$ [kcal mol^{-1}])	$T_{c\text{-}2}$ [°C] ($\Delta G^{\neq}$ [kcal mol^{-1}])
(Trip$_2$Sb)$_2$Naph (**69**)	70 (15.9)	50 (15.6)
(Trip$_2$Bi)$_2$Naph (**70**)	0 (12.9)	–60 (13.3)
[(TripSb)(Trip$_2$Sb)Naph][BAr$^{F\text{-}20}$] (**71**)	–70 (10.1)	–

Since the initial goal was to convert **69** into a paramagnetic species, we attempted the conversion of **71** into a neutral radical *via* one-electron reduction. In this case, **71** was reacted with KC_8, after which a yellow solid was isolated, which was identified by sc-XRD as (TripSb)$_2$Naph (**72**), while TripH and K[BAr$^{F\text{-}20}$] were identified as by-products by NMR spectroscopy. In contrast to its predecessors, the ^{1}H NMR spectrum of **72** displays the expected signals for a highly symmetric species (Scheme 20).[209]

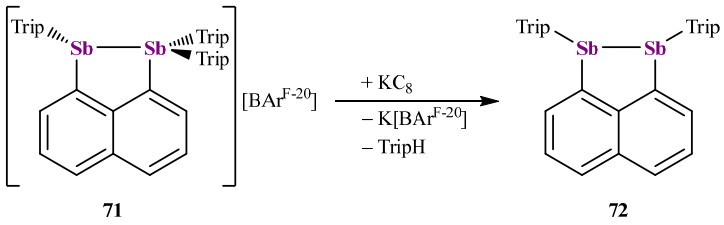

71 **72**

Scheme 20. The reaction of **71** with KC_8 again proceeds under elimination of TripH, as well as K[BAr$^{F\text{-}20}$] to form the distibane **72**.

[(Trip$_2$Sb)(TripSb)Naph][BAr$^{F\text{-}20}$] (**71**) crystallized in the triclinic space group $P\bar{1}$ with two molecules per unit cell, while (TripSb)$_2$Naph (**72**) crystallized in the orthorhombic space group *Pbca* with eight molecules per unit cell. In comparison to **69**, the Sb–C bond lengths are significantly shortened, with the tetrahedrally-coordinated Sb1_1 atom showing shorter Sb–C bond lengths (Sb1_1–C11_1 2.1170(15) Å, Sb1_1–C11_1 2.1367(15) Å, Sb1_1–C26_1 2.1465(15) Å) than the three-coordinated antimony center Sb2_1 (Sb2_1–C3_1 2.1647(17) Å, Sb2_1–C41_1 2.1708(16) Å). Compared to **69**, the Sb–Sb distance in **71** is significantly shorter and in the range of typical Sb-(II)–Sb-(II) bond lengths, which indicates a strong donor-acceptor interaction between the antimony centers. Moreover, the Sb–Sb distance in **72** (2.7991(6) Å), which bears a covalent Sb–Sb bond, is more or less identical to **71** (2.7980(4) Å). Both distances are found at the shorter end of reported Sb–Sb bond

lengths for distibanes.[§] In both compounds, intramolecular CH···π contacts are observed, as well as intermolecular CH···F contacts in **71** and CH···π contacts in **72** (Table 13).[209]

Table 13. Comparison of selected distances [Å], bond angles [°], and dihedral angles [°] between **69**, **71**, and **72**.[209]

	69	**71**	**72**
Sb–Sb	3.2327(2)	2.7980(4)	2.7991(6)
Sb–C	2.1769(11), 2.2019(11), 2.1902(10)	2.1170(15), 2.1367(15), 2.1465(15), 2.1647(17), 2.1708(16)	2.149(6), 2.196(6), 2.153(6), 2.192(6)
C–Sb–Sb	80.89(3), 93.23(3), 167.59(3)	91.26(4), 137.25(4), 98.29(4), 80.51(4), 106.31(4)	86.18(16), 100.81(17), 85.91(15), 102.91(15)
Sb–C–C–Sb	12.78(7)	13.77(6)	5.49(24)

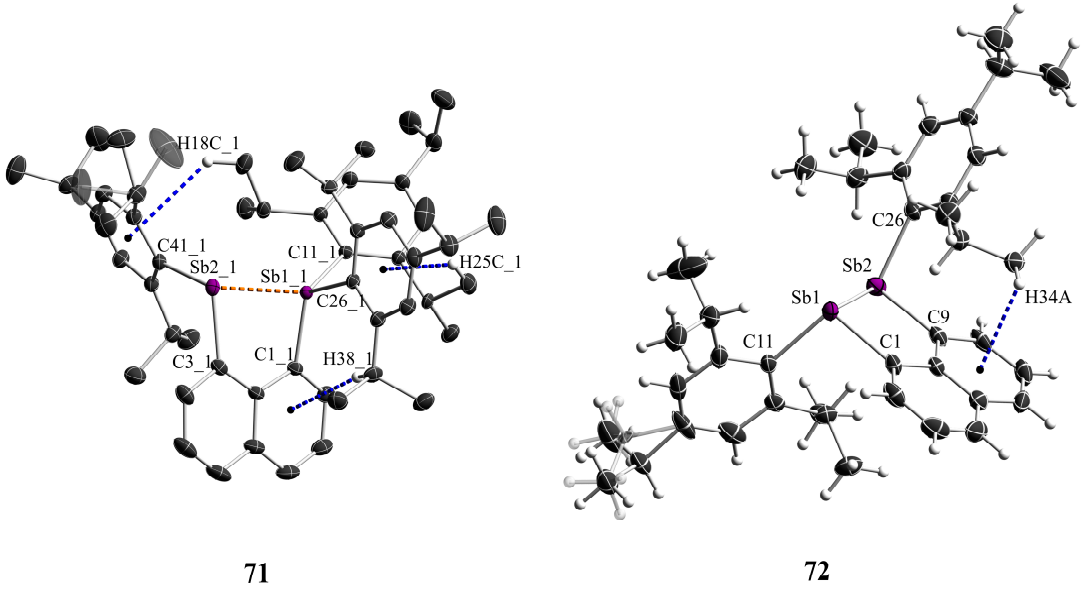

71 **72**

Figure 36. Solid-state structure of [1-(Trip$_2$Sb)-8-(TripSb)-Naph][BAr$^{F\text{-}20}$] (**71**) and (TripSb)$_2$Naph (**72**) with displacement ellipsoids drawn at the 50 % probability level. The [BAr$^{F\text{-}20}$] anion and the majority of hydrogen atoms of **71** were omitted for clarity.

The Trip groups in **71** and **72** do not adopt parallel orientations to the Sb–Sb axis but are rather aligned approximately orthonormal to the naphthalenediyl plane. Thereby it is not possible to distinguish whether the orientation of the ligands is caused by the CH···π contacts or if the orientation benefits them only. The distortion of the naphthalenediyl ligand with respect to the dihedral angle Sb–C$_{peri}$–C$_{peri}$–Sb increases

[§]*Breunig* et al. reported [(CO)$_4$Cr(Sb$_2$Et$_4$)]$_2$ with a Sb–Sb bond length significantly below any reported disitibane. However, the authors present a highly disordered structure and can not exclude the presence of a second species. Therefore, the values have to be treated with care.[211].

slightly from **69** to **71**, before decreasing in **72**. Despite the significant steric hindrance, the increase in **71** is probably due to the short Sb–Sb distance. On the other hand, the steric strain in **72** is significantly reduced since the Trip groups are aligned at opposite sides of the naphthalenediyl plane and thereby causing the decrease in distortion.[209]

Since only one oxidation event of higher voltage was observed for **70**, comparable reactions were performed with [NO][SbF_6]. Although no product could be isolated from the reaction mixture, TripH was identified as a by-product, which indicates a comparable reaction mechanism to the reaction between **69** and [Fc][BAr^{F-20}].[209]

To gain more insight into the Sb–Sb interactions in **71** and **72** quantum chemical computations were performed in collaboration with *Prof. Dr. G. Haberhauer*[**] and *N. Semleit*[*] using the Gaussian 16,[212] Amsterdam Density Functional (ADF)[213] and AIMAll[214] program packages. Geometries were optimized at the def2-TZVP level of theory[185,194] with the B3LYP[195,215] functionals utilizing the atom-pairwise dispersion correction with Becke-Johnson damping (D3BJ).[22,36] NBO analysis was performed using NBO 3.1[216] implemented in Gaussian 16. The bond energy analysis computations[217] were conducted using ADF at the B3LYP-D3BJ/TZP level of theory. Quantum theory of atoms in molecules (QTAIM)[218] analysis (B3LYP-D3BJ/TZP and B3LYP-D3BJ/def2-TZVP) were performed using ADF and AIMAll. Finally, interacting quantum atoms (IQA)[219] computations were performed using ADF. The computations were conducted for **69**-**72**, as well as phenyl substituted reference systems **S1**-**S4**. Since the pnictogen centers in **S1**-**S4** are not connected *via* the naphthalenediyl ligand, the pnictogen interactions can be determined by dividing the system into two fragments. In addition, attractive *London* dispersion through *i*-Pr-H···π contacts was excluded. The computations agreed with the sc-XRD data revealing shorter Sb···Sb distances for **71**/**S3** (2.806 Å/2.848 Å) than in **72**/**S4** (2.820 Å/2.860 Å). These results support the hypothesis of strong charge-transfer interaction and even indicate that the charge-transfer interaction of **71**/**S3** is stronger than the covalent Sb–Sb bond in **72**/**S4** (Figure 37).[209]

[**]Insitute of Organic Chemistry, University of Duisburg-Essen, 45117 Essen, Germany. E-mail: gebhard.haberhauer@uni-due.de

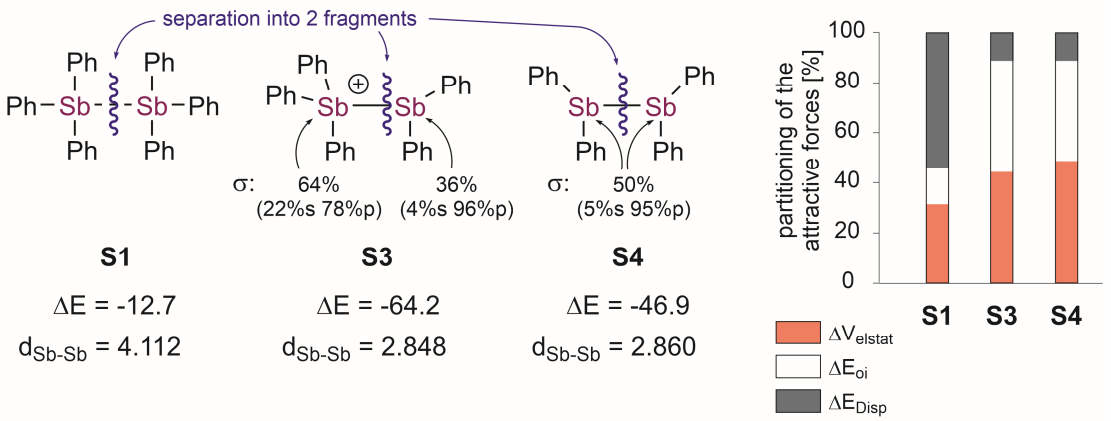

Figure 37. Sb···Sb distances [Å] computed at the B3LYP-D3BJ/def2-TZVP level of theory in the reference systems **S1**, **S3**, and **S4**. The contributions of the attractive forces (ΔV_{elstat}, ΔE_{oi}, ΔE_{Disp}) and total binding energies (ΔE in kcal mol^{-1}) between the Ph_nSb fragments originate from bond energy analysis computations at the B3LYP-D3BJ/TZP level of theory.[209]

Moreover, a bond energy analysis computed larger total binding energies ΔE for **S3** (–64.2 kcal mol^{-1}) than for **S4** (–46.9 kcal mol^{-1}), hence emphasizing the strong charge transfer interaction. Notably, the nature of the Sb···Sb interaction indicates that **S1** is an LD driven dimer, whereas **S3** and **S4** share similar binding characteristics. More specifically, both have negligible LD terms with major contributions from electrostatics (ΔV_{elstat}) and orbital interactions (ΔE_{oi}). Surprisingly, the term of orbital interactions is larger for **S3** than for **S4**, which indicates that the dative bond of **S3** is stronger than the covalent bond of **S4**. The NBO analysis of **S3** suggests a polarized Sb–Sb bond towards the tetravalent Sb center (64 %) with 22 % *s*-orbital character versus 4 % *s*-orbital character for the trivalent Sb center. Conversely, no signs of polarization were observed for the covalent bond of **S4** with 95 % *p*-orbital character. These findings are supported by QTAIM, which gives a negative *Laplacian* of the electron density ($\nabla^2\rho_{CP}$) between the Sb atoms at the bond critical points (BCP) and therefore indicates polar covalent interactions. The BCPs are closer to the tetravalent Sb center which agrees well with the polarization from the NBO analysis.[209]

5.4. Increasing the Steric Demand

Under comparable reaction conditions, the reaction of **25** with $PhBiCl_2$ instead of the phosphorous derivative[155] yielded a different type of reaction product. Correspondingly, to increase the ligand size on the pnictogen center and investigate the resulting reactivity, $TTPPnCl_2$ (TTP = 2,6-Trip-C_6H_3) was prepared[220] and reacted with M_2Naph (M = Li **25**, TMSn **22**). As previous reactions between $PhSbCl_2$ and M_2Naph yielded rather complex mixtures, $TTPSbCl_2$ was alternatively reacted with the milder transmetallation reagent $TMSn_2Naph$ (**22**) in toluene. At room temperature, no immediate reaction was observed, therefore the mixture was heated to 100 °C. After work-up, a colorless crystalline solid was obtained. The ^1H NMR spectrum of the solid in C_6D_6 shows the TTP and Naph ligand in a 1:1 ratio, which is consistent with the ^1H NMR spectrum of $(PhBiNaph)_2$ (**65**). However, sc-XRD identified the compound as TTPSbNaph (**73**) (Scheme 21).

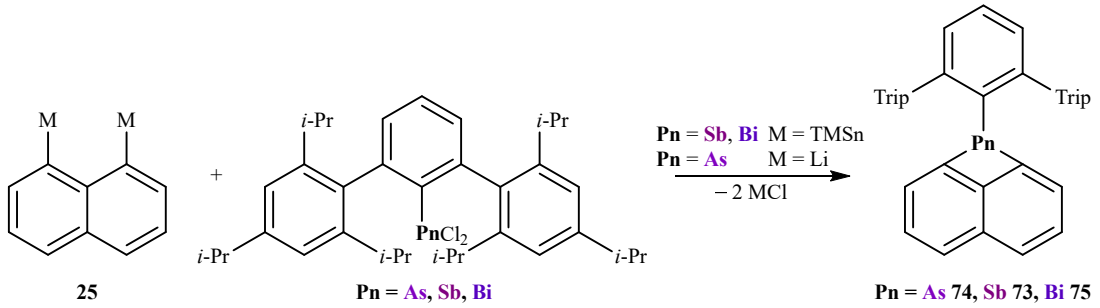

Scheme 21. Synthesis of sterically highly-strained four-membered rings including the pnictogen centers [PnC_3] (Pn = As, Sb, Bi).

In contrast to **65**, the naphthalenediyl ligand in **73** acts as a bidentate ligand forming a highly strained four-membered ring *via* the *peri*-positions; this is the first example of a [C_3Sb] four-membered ring. **73** can be seen as the monomeric unit of an $(RPnNaph)_2$ derivative, however no sign or evidence of a possible equilibrium have been observed to date. Because the formation of **73** is consistent with the reactivity of sterically crowded phosphine dihalides with Li_2Naph,[155] consequently the preparation of the arsenic and bismuth derivatives was attempted. Accordingly, the reaction of $TTPAsCl_2$ with Li_2Naph (**25**) proceeded immediately at room temperature, yielding TTPAsNaph (**74**) after work-up and recrystallization from ethanol. On the other hand, reaction of $TTPBiCl_2$ with $TMSn_2Naph$ (**22**), in analogy to **73**, required elevated temperatures and resulted in the formation of TTPBiNaph (**75**). In addition to **75**, the formation of a pink to red solid was observed, which was identified as the dibismuthene TTPBi=BiTTP.[220]

The compounds crystallized in the monoclinic space group $P2_1n$ (Sb **73**, Bi **75**) and triclinic space group $P\bar{1}$ (As **74**), respectively, and contain two (**74**), four (**75**), and eight (**73**) molecules per unit cell. The Pn–C bond lengths are at the higher end of reported Pn–C single bonds. The bond angular sums (As **74**: 283.76°; Sb **73**: 274.49°; Bi **75**: 273.35°) indicate high *p*-orbital character, however, the C1–Pn–C8 angles (As **74**: 69.68(4)°, Sb **73**: 64.87(9)°, Bi **75**: 62.27(9)°) are significantly smaller than typical C–Pn–C angles of three-coordinated pnictogen centers and decrease with ascending atomic number. The sharper bond angle for heavier elements is not surprising since the distance between the *peri*-positions is fixed, while the distance between ligand and element successively increases. The Trip groups are roughly orthogonal to the naphthalene plane as indicated by the C9–Pn–C11 angle (As **74**: 112.77(3)°, Sb **73**: 108.76(7)°, Bi **75**: 109.31(7)°) (Figure 38).

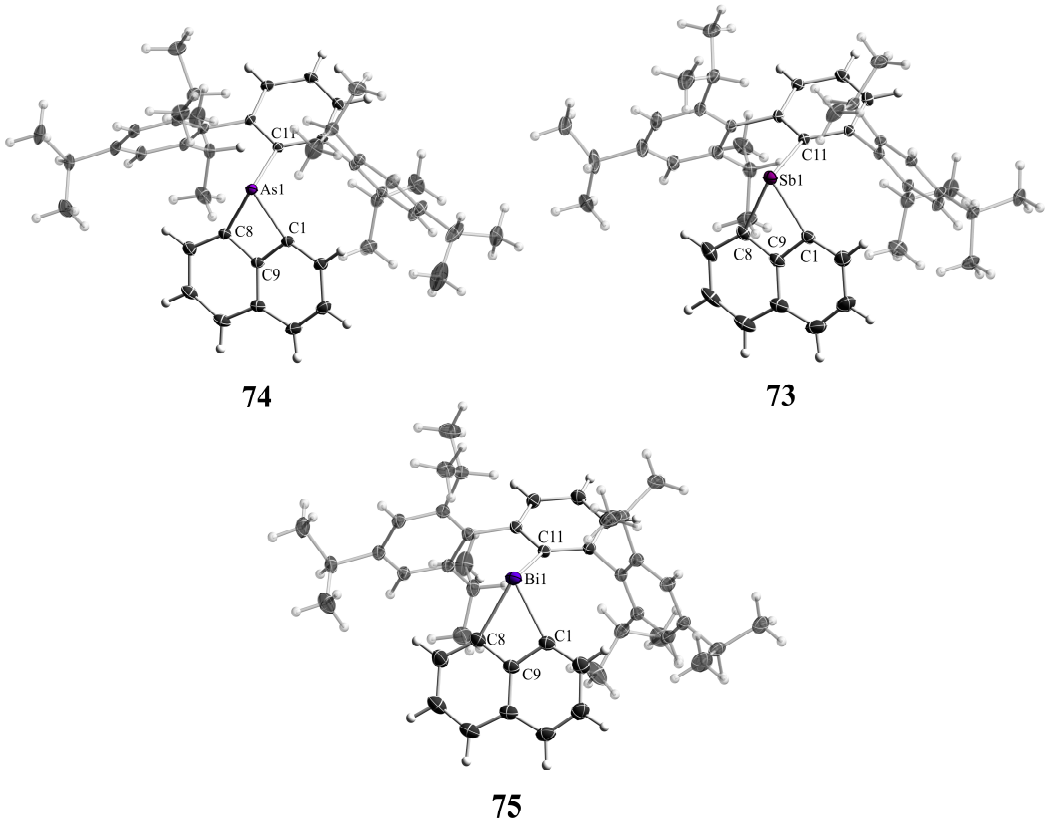

Figure 38. Solid-state structure of TTPPnNaph (Pn = As **74**, Sb **73**, Bi **75**) with displacement ellipsoids drawn at the 50 % probability level. The Trip groups are displayed at a 50 % transparency level for clarity. Selected distances [Å] and angles [°], TTPAsNaph (**74**): C1–As1 1.9919(10), C8–As1 2.0014(10), C9–As1 2.4612(9), C11–As1 1.9667(9), C1–As1–C8 69.68(4), C1–As1–C11 107.04(4), C8–As1–C11 107.04(4), C9–As1–C11 112.77(3); TTPSbNaph (**73**): C1–Sb1 2.173(2), C8–Sb1 2.184(2), C9–Sb1 2.625(2), C11–Sb1 2.171(2), C1–Sb1–C8 64.87(9), C1–Sb1–C11 104.11(8), C8–Sb1–C11 105.51(8), C9–Sb1–C11 108.76(7); TTPBiNaph (**75**): C1–Bi1 2.279(2), C8–Bi1 2.288(2), C9–Bi1 2.725(2), C11–Bi1 2.261(2), C1–Bi1–C8 62.27(9), C1–Bi1–C11 105.24(8), C8–Bi1–C11 105.84(8), C9–Bi1–C11 109.31(7).

The crystal packings of **73**-**75** are quite different. TTPSbNaph (**73**) crystallized with a highly disordered molecule of thf in the packing, however, no interactions between molecules of **73** were observed. In contrast, the arsenic derivative **74** formed dimers *via* CH···π contacts, whereas TTPBiNaph (**75**) exhibited a three-dimensional network *via* CH···π and Bi···H contacts (Figure 39).

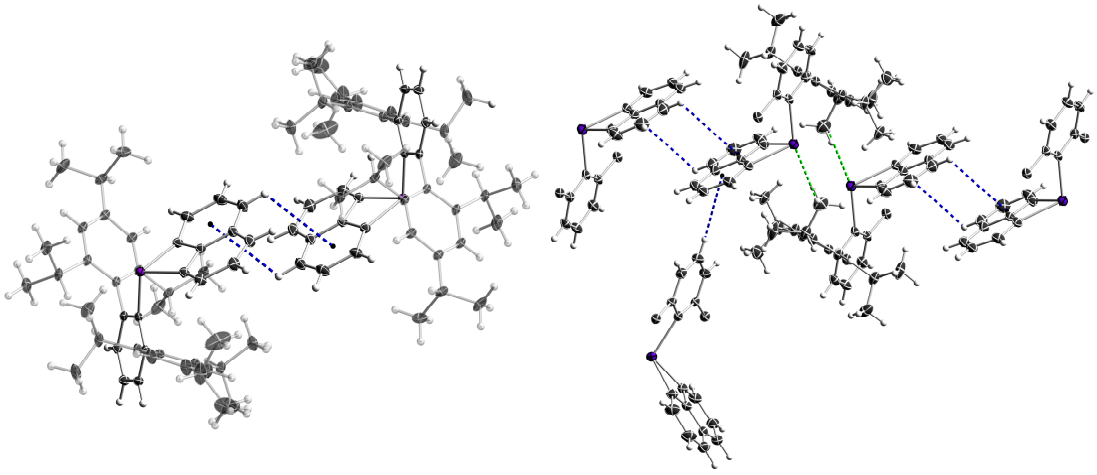

TTPAsNaph (**74**) TTPBiNaph (**75**)

Figure 39. Extracts from the crystal packing of **74** (left) and **75** (right). TTPAsNaph (**74**) forms a dimer *via* CH···π contacts (blue), while a three-dimensional network in **75** is formed *via* CH···π and Bi···H contacts (green). The Trip groups are displayed at a 50 % transparency level (**74**) or are omitted for clarity (**75**).

Increasing the ligand size on the pnictogen center resulted in the formation of three-coordinated pnictogen compounds in which the naphthalenediyl framework acts as a chelating ligand. Comparable compounds of the type R_nENaph have been reported in the literature with elements including B,[221] C,[222] Si,[223] P,[155,156,224] S,[225] Ti,[226] and Pt.[226] The prepared compounds represent the first examples for As-Bi, as well as the first examples of carbon-based strained four-membered rings containing Sb and Bi, respectively.

6. Summary, Conclusion and Outlook

The goal of this work was to expand the understanding of non-covalent interactions in organometallic chemistry by preparing a variety of pnictogen-substituted naphthalenediyls. The systems were fully characterized and further investigated by quantum chemical means. Thereby, the series of Pn_2Naph_2 was completed and the rather underexplored group of bis(pnicta)naphthalenediyls was successfully expanded.

Bi_2Naph_2 (**60**) was finally isolated after succesful modifications of the synthetic procedure and work-up. The new synthetic protocol was also successfully applied for the preparation of As_2Naph_2 (**57**) and Sb_2Naph_2 (**58**) and recrystallization attempts of As_2Naph_2 (**57**) yielded a new polymorph with different intermolecular contacts. Theoretical investigations in cooperation with *Prof. Dr. A. A. Auer* and *Dr. E. Schiavo* showed a correlation between crystal packing and maximizing *London* dispersion. These studies also explained the different crystal packings of As-Bi, as well as the occurrence of different polymorphs of As conclusively based on the occurring dimer interactions.[176]

Furthermore, *peri*-substituted bis(diphenylpnicta)naphthalenediyl derivatives $(Ph_2Pn)_2L$ (L = Naph, Pn = Sb **41**, Bi **63**; L = Acenaph, Pn = Sb **61**) were prepared *via* the reaction of Ph_2PnCl with M_2L (L = Naph, M = TMSn **22**, Li **25**; L = Acenaph, M = Li **62**). In contrast to the respective Pn_2Naph_2 derivatives, intermolecular Bi$\cdots\pi$ contacts were observed instead of Sb$\cdots\pi$ contacts, which highlights the importance of these interactions for Bi. In addition, weak intramolecular Pn$\cdots$Pn interactions were suggested by theoretical computations. The reaction of $PhBiCl_2$ resulted in the formation of the bisnaphthalenediyl species $(PhBiNaph)_2$ (**65**), which deviated from the reactivity of $PhPCl_2$ towards Li_2Naph.[155] **65** assumed a packing motif closely resembling that of Pn_2Naph_2. Two Bi$\cdots\pi$ contacts per atom as well as $\pi\cdots\pi$ contacts were observed, of which the latter were absent in Bi_2Naph_2 (**60**). Theoretical investigations performed in cooperation with *Prof. Dr. G. Jansen* and *F. van der Vight* underlined not only the importance of specific dimer interactions but also the maximization of LD as a driving force in crystal packings.[186]

Moreover, the redox potential of the bis(diphenylpnicta)naphthalenediyls was investigated with a particular emphasis on the one-electron oxidation since the HOMO was located on the pnictogen center. While CV studies only revealed irreversible behavior, oxidation reactions with stronger oxidation agents only yielded product mixtures. In contrast, softer oxidation agents like $AgSbF_6$ resulted in the

formation of coordination complexes, in which **41** acted as a bidentate ligand. The Ag–Sb interaction in complex **66** not only allowed its isolation and crystallization but also for metal exchange reactions with CuCl and AuCl. The latter, however, gave no complete substitution of the silver atom, but the formation of a co-crystal. Since the oxidation of phenyl-substituted species proved to be unsuccessful, the ligand size was increased.

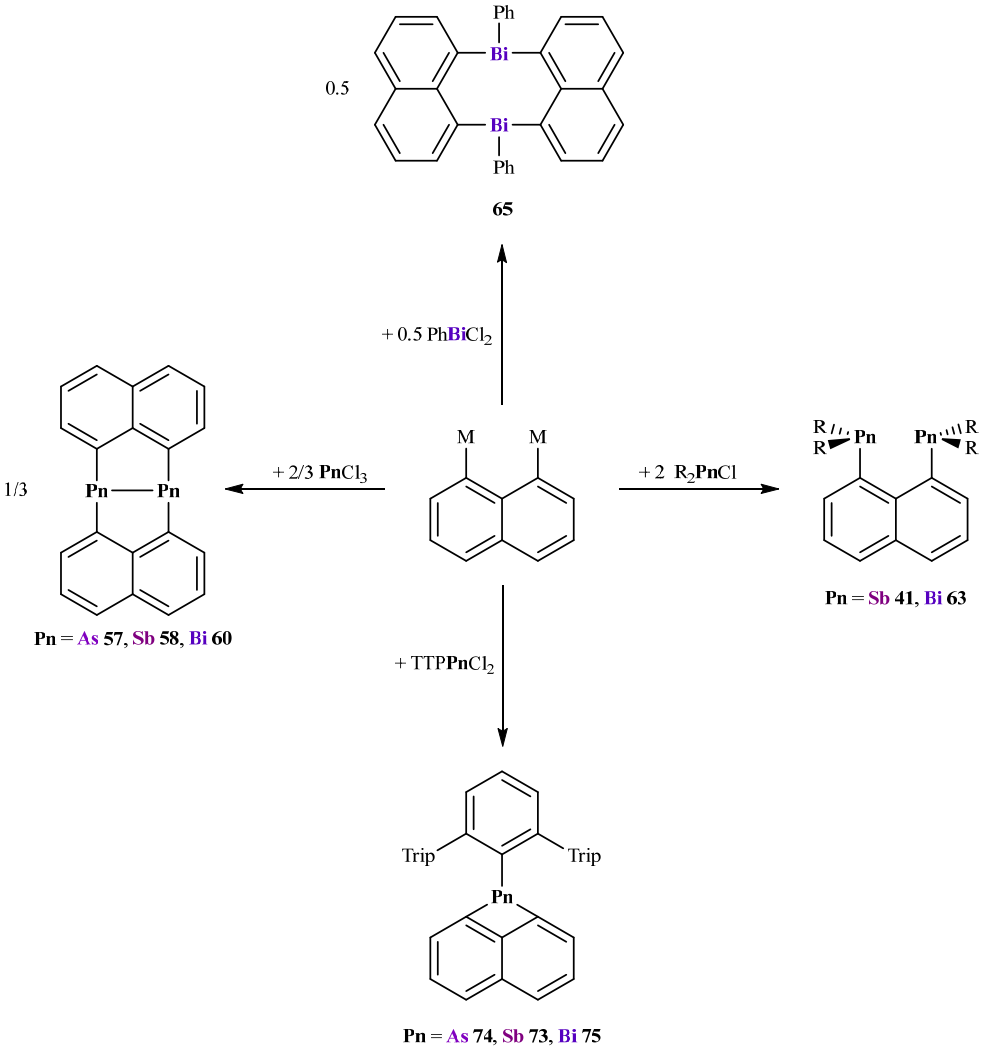

Scheme 22. Overview of the different reactivities from R_nPnCl_{x-n} with 1,8-M_2Naph.

$(Trip_2Pn)_2$Naph compounds (Pn = Sb **69**, Bi **70**) showed that the Bi···Bi distance in **70** was elongated compared to **63**, while the Sb···Sb distance in **69** contracted in comparison to **41**. This difference was also visible in the ^{1}H NMR spectra; **70** showed the expected signals of a symmetric species, whereas signal broadening and signals corresponding to a species of lower symmetry were observed for **69**. Although no product could be isolated from the oxidation of **70**, a clean product was obtained from reacting **69** with [Fc][BAr^{F-20}]. However, in both cases, the elimination of TripH was observed, which indicates a comparable reaction for the Bi compound.

[(Trip$_2$Sb)(TripSb)Naph][BAr$^{F\text{-}20}$] (**71**) contains a surprisingly short Sb···Sb distance due to a rather strong attractive interaction. One-electron reduction with KC_8 led to further elimination of TripH and formation of distibane (TripSb)$_2$Naph (**72**). Interestingly, the Sb–Sb distance virtually did not change compared to **71**. Quantum chemical computations in cooperation with *Prof. Dr. G. Haberhauer* and *N. Semleit*, showed that the dative Sb–Sb interaction in **71** is even stronger than the "regular" covalent bond in **72**.[209]

Finally, the ligand size was further increased to investigate the reactivity of RPnCl$_2$ towards bis-1,8-metallated naphthalenediyls. The reaction of TTPPnCl$_2$ (Pn = As-Bi) with 1,8-M$_2$Naph (M = TMSn **22**, Li **25**) yielded TTPPnNaph (Pn = As **74**, Sb **73**, Bi **75**). Bearing the naphthalenediyl fragment as a bidentate ligand, **73-75** formed strained four-membered rings, which were unprecedented for antimony and bismuth. This matches the reported reactivity of RPCl$_2$ in which R bears higher steric demand and a stronger electron donating effect.

For future studies, TTPPnNaph (Pn = As **74**, Sb **73**, Bi **75**) are the most promising starting materials. Compounds with a chelating naphthalenediyl ligand were shown to undergo ring opening reactions,[223–225,227] which would allow the introduction of different elements and/or substituents and would most importantly give further insight into the *peri*-interaction of homo- and heterosubstituted naphthalenediyls of heavy pnictogens (Scheme 23).

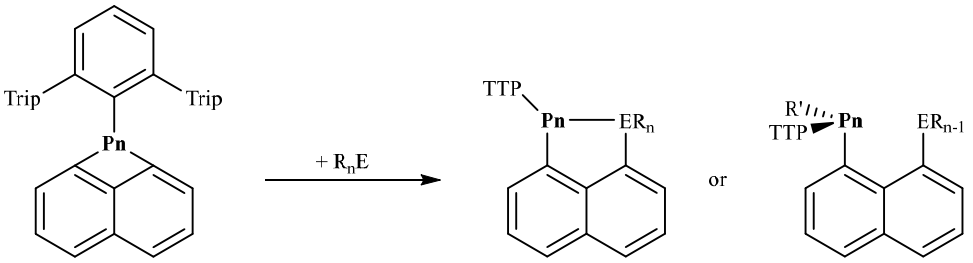

Scheme 23. Possible ring-opening reaction of TTPPnNaph (Pn = As-Bi).

Moreover, an alternative route for the generation of strained four-membered rings, as reported in the literature, involves the monosubstitution of 1,8-dibromoacenaphthene, with subsequent P–C bond formation *via* the addition of RLi.[156] Transfering the process to the heavy elements may form RPnNaph with various ligands and may also offer more insight into a possible monomer-dimer equilibrium of RPnNaph and (RPnNaph)$_2$.

7. Experimental Details

General Procedure. All manipulations were performed in an atmosphere of purified argon using standard Schlenk and glovebox techniques. Toluene, *n*-hexane, and diethyl ether were dried using a mBraun Solvent Purification System (SPS). Dichloromethane and acetonitrile were carefully dried over CaH_2. THF was carefully dried over NaK. The dried solvents were stored over appropriate, activated molecular sieves. Deuterated solvents were dried over activated molecular sieves (4 Å, 3 Å for CD_2Cl_2) and degassed prior to use. The anhydrous nature of the solvents was verified by *Karl Fischer* titration.

Instrumentation. NMR spectra were recorded using a Bruker Avance DPX 300, a Bruker Avance Neo 400 or a Bruker Avance DRX 600 spectrometer.

IR spectra were recorded in a glove box with an ALPHA-T FT-IR spectrometer equipped with a single-reflection ATR sampling module.

Microanalyses were performed at the elemental analysis laboratory of the University of Duisburg-Essen. Melting points were measured in wax-sealed glass capillaries under argon atmosphere using a Thermo Scientific 9300 apparatus and are uncorrected.

CV studies were performed in a glovebox using a Metrohm Autolab PGSTAT 204 potentiostat with a three-electrode setup consisting of a Pt-disk (d = 1 mm) working electrode, a Pt-wire counter electrode, and an Ag-wire pseudoreference electrode; ferrocene was used as an internal standard. For **69**, the ferrocene redox couple was obscured; hence, decamethylferrocene was used as the internal reference (440 mV vs Fc in THF/0.1 M NBu_4PF_6).[228]

Single-crystal X-ray diffraction. The crystals were mounted on nylon loops in inert oil. Crystallographic data were collected on a Bruker AXS D8 Kappa diffractometer with APEX2 detector (monochromated $Mo_{K\alpha}$ radiation, λ = 0.71073 Å) or a Bruker AXS D8 Venture diffractometer with Photon II detector (monochromated $Cu_{K\alpha}$ radiation, λ = 1.54178 Å, micro-focus source) at 100(2) K and are summarized in Table 15-19. The structures were solved with direct methods (SHELXS-2013)[229] and refined anisotropically by full-matrix least-squares on F^2 (SHELXL-2017).[230] Absorption corrections were performed semi-empirically from equivalent reflections on basis of multi-scans and numerical from indexed faces (**60**, **63**, **65**) (Bruker AXS APEX2/3). Hydrogen atoms were refined using a riding model or rigid methyl groups.

On the crystal of **64** grew a satellite crystal that could not be removed. Treatment as twin component revealed very low intensities (mean < 1 · I/σ) for the non-overlapped reflections. The resulting model did not show any improvements and thus was discarded. For **67** a phenyl ring is disordered over two positions. The corresponding bond lengths were restrained to be equal (SADI) and RIGU restraints were applied to the anisotropic displacement parameters of the phenyl rings' atoms. The anion is fully disordered with the fluorine atoms' electron density spread out over a shell around the central antimony atom. In this density, two alternate positions could be identified and refined, however, the anisotropic displacement parameters show that this is still a rather crude model. All Sb–F bond lengths were restrained to be equal (SADI) and the four equatorial fluorine atoms plus the antimony atom were restrained to lie on a mutual plane (FLAT) for each axis of the octahedron. RIGU restraints were used for the anisotropic displacement parameters of both orientations of the anion and additional ISOR restraints for the smaller component. In **68** the Ag position is also occupied by Au. The ratio is approx. Ag:Au 66:34. Position and displacement of Au and Ag were constrained to be equal (EXYZ, EADP). In **70** an *iso*-propyl group is disordered over two positions. Its bond lengths and angles were restrained to be equal (SADI). The atoms were refined with common displacement parameters (EADP) to which RIGU restraints were applied. In **71** an *iso*-propyl group is disordered over two positions. Its bond lengths and angles were restrained to be equal (SADI) and RIGU and SIMU restraints were applied to its anisotropic displacement parameters. The high residual electron density in **70** and **72** is likely caused by absorption. Several methods and parameters were tried to improve the absorption correction, however, the residual density could not be reduced any further. The highest residual density maxima in **71** are a straight line with the heavy atoms and evenly spaced thus they are likely artifacts caused by *Fourier* series truncation. For **73** the anisotropic displacement parameters of the *iso*-propyl groups suggest disorder, however, the displacement ellipsoids are not yet elongated enough to find and refine two split positions. Moreover, the structure contains two highly disordered tetrahydrofurane molecules. The final refinement was done with a solvent free dataset from a PLATON/SQUEEZE run. (For details see: A. L. Spek, *Acta Cryst*. **1990**, *46*, 194-201). The molecules were included in the sum formula for completeness.

Commercially Available Substances. The following substances were commercially available and purified as described.

Table 14. List of commercially available substances.

Substance	Molecular formula	Purification
1,8-Dibromonaphthalene	$C_{10}H_6Br_2$	
2,4,6-Tri-*iso*-propylbromobenzene	$C_{15}H_{23}Br$	
Acenaphthene	$C_{12}H_{10}$	
Antimony-(III) chloride	$SbCl_3$	Sublimation
Arsenic-(III) chloride	$AsCl_3$	Distillation
Bismuth-(III) chloride	$BiCl_3$	Sublimation
n-Butyllithium (2.5 M in hexane)	C_4H_9Li	
t-Butyllithium (1.9 M in Pentane)	C_4H_9Li	
Copper-(I) bromide	CuBr	
Copper-(I) chloride	CuCl	
Gold-(I) chloride	AuCl	
Magnesium (turnings)	Mg	
N-Bromosuccinimide	$C_4H_4BrNO_2$	
Nitroso hexafluoroantimonate-(V)	$NOSbF_6$	
Potassium	K	
Silver hexafluoroantimonate-(V)	$AgSbF_6$	
Sodium iodide	NaI	
Trimethyltin-(IV) chloride	C_3H_9ClSn	
Triphenyl antimony-(III)	$C_{18}H_{15}Sb$	
Triphenyl arsenic-(III)	$C_{18}H_{15}As$	
Triphenyl bismuth-(III)	$C_{18}H_{15}Bi$	

7.1. Precursor Synthesis

The compounds potassium graphite (KC_8),[231] 1-iodo-2,6-bis(2,4,6-tri-*iso*-propylphenyl)benzene (TTPI), 2,6-bis(2,4,6-tri-*iso*-propylphenyl)phenyl lithium ethyl etherate (TTPLi)[232] and 2,6-bis(2,4,6-tri-*iso*-propylphenyl)phenyl pnictogen dichlorides ($TTPPnCl_2$, Pn = As-Bi)[220] were prepared according to literature procedure without significant modification.

Synthesis of 1,8-Dilithionaphthalene · n ethyl etherate (25).[233] 1,8-Dibromonaphthalene (35.2 mmol, 10 g) was weighed into a 100-mL-Schlenk tube and 30 mL of diethyl ether were added. The suspension was cooled to –78 °C and a solution of *n*-butyl lithium (2.5 M in hexane, 70.4 mmol, 28.2 mL) was added slowly. The suspension was allowed to warm to room temperature overnight turning into a yellow solution. All volatiles were removed *in vacuo* and the yellow residue was washed with *n*-hexane. Removing the remaining volatiles *in vacuo* gave **25· 0.635 Et_2O** as a pyrophoric, yellow powder. **Yield:** 6.32 g (96 %); **^{1}H NMR (thf-d_8, 400.1 MHz, 297 K) δ [ppm]:** 8.03 (dd, 2 H, Naph-*H*), 7.41 (dd, 2 H, Naph-*H*), 7.07 (dd, 2 H, Naph-*H*), 3.39 (q, O-C*H*$_2$CH$_3$), 1.12 (t, O-CH$_2$C*H*$_3$).

Synthesis of 1,8-Bis(trimethyltin)naphthalene (22).[131] 1,8-Dibromonaphthalene (10 mmol, 2.83 g) was weighed into a Schlenk tube and dissolved in 30 mL of diethyl ether. The solution was cooled to –78 °C and *n*-butyllithium (2.5 M in hexane, 20 mmol, 8 mL) was added via syringe. The mixture was stirred 30 minutes at –30 °C and one hour at room temperature after which the solution was cooled to –30 °C. Solid trimethyltin chloride (20 mmol, 3.99 g) was added to the reaction mixture which resulted in the immediate formation of a white precipitate. The mixture was stirred overnight and allowed to come to room temperature. All volatiles were removed *in vacuo* and the product was extracted with hexane (2 x 20 mL). The hexane solution was concentrated until a white precipitate was formed, which was redissolved in the heat. Storing the solution at –30 °C gave **22** as colorless needles. **Yield:** 2.96 g (65 %); **^{1}H NMR (C_6D_6, 400.1 MHz, 297 K) δ [ppm]:** 7.73 (dd, 2 H, Naph-*H*), 7.59 (dd, 2 H, Naph-*H*), 7.23 (dd, 2 H, Naph-*H*), 0.31 (t, 18 H, Sn-C*H*$_3$).

Synthesis of 5,6-Dibromoacenaphthen.[234] *N*-Bromosuccinimide (287.12 mmol, 51.108 g) was dissolved in 100 mL of DMF and cooled in an ice bath. Acenaphthene (129.7 mmol, 20 g) was weighed into a flask and suspended in 30 mL of DMF. The suspension of acenaphthene was added to the NBS solution and residues were transferred with an additional 20 mL of DMF. After two hours of stirring the mixture

was heated to 35 °C and stirred overnight. The resulting suspension was filtered via *Büchner* funnel, the solid washed with hexane (50 mL) and ethanol (3 x 20 mL), and the volatiles were removed *in vacuo* resulting in a pale-yellow powder. **Yield:** 6.603 g (16 %); **^{1}H NMR ($CDCl_3$, 300.1 MHz, 297 K) δ [ppm]:** 7.80 (d, 2 H, Naph-*H*), 7.10 (d, 2 H, Naph-*H*), 3.32 (s, 4 H, CH_2).

Synthesis of 5,6-Dilithioacenaphthen ethyl etherate (62).[142] 5,6-Br_2Acenaph (6.4 mmol, 2 g) was suspended in 15 mL of diethyl ether and cooled to –78 °C. To the suspension was added a solution of *n*-butyllithium (2.5 M in hexane, 12.8 mmol, 5.12 mL) via syringe. The reaction mixture was stirred overnight and allowed to warm to room temperature. All volatiles were removed *in vacuo* and the residue washed with hexane (2 x 20 mL). Removing all solvents *in vacuo* resulted in **62** as a brown powder. **Yield:** 1.23 g (80 %); **^{1}H NMR (thf-d_8, 300.1 MHz, 297 K) δ [ppm]:** 7.96 (d, 2 H, Naph-*H*), 6.96 (d, 2 H, Naph-*H*), 3.39 (q, 4 H, O-CH_2-CH_3), 3.19 (s, 4 H, Ace-CH_2), 1.12 (t, 6 H, O-CH_2-CH_3).

Synthesis of Diphenylantimony-(III) chloride.[159] Ph_2SbCl was prepared according to literature procedures. Colorless crystals were obtained upon storing the melt for a week at 4 °C. **Yield:** 9.07 g (98 %); **^{1}H NMR (C_6D_6, 400.1 MHz, 297 K) δ [ppm]:** 7.80 (dd, 2 H, Naph-*H*), 7.25 (dd, 2 H, Naph-*H*), 7.07 (dd, 2 H, Naph-*H*).

Synthesis of Phenylantimony-(III) dichloride.[159] $PhSbCl_2$ was prepared according to literature procedures. Colorless crystals were obtained upon heating the melt to 100 °C for 6 h followed by storing at 4 °C overnight. **Yield:** ; **^{1}H NMR (C_6D_6, 400.1 MHz, 297 K) δ [ppm]:** 7.46-7.44 (m, 2 H, Ph-*H*), 7.09 (t, 2 H, Ph-*H*), 7.05-6.99 (m, 3 H, Ph-*H*).

Synthesis of Diphenylbismuth-(III) chloride.[235] $BiCl_3$ (10 mmol, 3.15 g) and $BiPh_3$ (20 mmol, 8.80 g) were weighed into a 250-mL-Schlenk tube and suspended in 100 mL of diethyl ether. The mixture was stirred overnight, and the solvent removed by filtration. The residue was washed with diethyl ether (3 x 30 mL) and the volatiles were removed *in vacuo* to give Ph_2BiCl as a white, crystalline powder. **Yield:** 10.99 g (92 %); **^{1}H NMR (C_6D_6, 400.1 MHz, 297 K) δ [ppm]:** 7.99 (d, 2 H, Ph-*o*-*H*), 7.37 (t, 2 H, Ph-*m*-*H*), 7.07 (tt, 1 H, Ph-*p*-*H*).

Synthesis of Diphenylbismuth-(II) iodide.[236] $BiPh_3$ (11.4 mmol, 5.018 g) was weighed into a Schlenk tube and suspended in a mixture of diethyl ether (40 mL) and *n*-hexane (20 mL). I_2 (11.4 mmol, 2.89 g) was added to give an orange suspension,

which was stirred for 3 h. The solution was removed by filtration and the residue dried *in vacuo* to give Ph_2BiI as an orange solid. **Yield:** 4.58 g (82 %); **^{1}H NMR (C_6D_6, 400.1 MHz, 297 K) δ [ppm]:** 8.05 (dd, 2 H, Ph-*o*-*H*), 7.25 (t, 2 H, Ph-*m*-*H*), 7.04 (tt, 1 H, Ph-*p*-*H*).

Synthesis of Phenylbismuth-(III) dichloride.[235] $BiCl_3$ (10 mmol, 3.15 g) and Ph_3Bi (5 mmol, 2.20 g) were weighed into a 100-mL-Schlenk tube and suspended in 80 mL of diethyl ether. The mixture was stirred overnight resulting in a yellow coloring. The diethyl ether was filtered off and the residue dried *in vacuo*. The product was extracted with hot toluene (2 x 100 mL). Crystallization set in, while the filtrate was cooling down giving $PhBiCl_2$ as a crystalline, white solid. **Yield:** 1.82 g (34 %); **^{1}H NMR (C_6D_6, 400.1 MHz, 297 K) δ [ppm]:** 8.45 (dd, 2 H, Ph-*o*-*H*), 7.68 (t, 2 H, Ph-*m*-*H*), 7.09 (tt, 1 H, Ph-*p*-*H*).

Synthesis of 2,4,6-Tri-*iso*-propylphenyl copper-(I).[237] TripBr (10 mmol, 2.83 g, 2.53 mL) was dissolved in 20 mL of diethyl ether and cooled to –78 °C. To the cooled solution, *t*-butyllithium (1.9 M in pentane, 20 mmol, 10.5 mL) added via syringe and the mixture was stirred overnight. The yellow solution was cooled to –78 °C and CuBr (10 mmol, 1.43 g) was suspended in a separate flask in 20 mL of diethyl ether. The TripLi solution was then added to the copper bromide over the course of five minutes and the reaction mixture was stirred for 72 hours, which resulted in a green suspension. All volatiles were removed *in vacuo* and the product was extracted with *n*-hexane (2 x 20 mL). The solution was concentrated to 20 mL leading to the formation of a white precipitate, which was redissolved in the heat. Storage at –30 °C resulted in TripCu as a white, crystalline solid. Concentrating the mother liquor resulted in another crop of the desired product. **Yield:** 1.44 g (54 %). **^{1}H NMR (C_6D_6, 400.1 MHz, 297 K) δ [ppm]:** 7.07 (s, 2 H, Ph-*m*-*H*), 3.94 (br-s, 2 H, *o*-C*H*-CH_3), 2.77 (sept, 1 H, $^3J_{HH}$ = 6.87 Hz, *p*-C*H*-CH_3), 1.33 (br-d, 12 H, $^3J_{HH}$ = 7.13 Hz, *o*-CH-CH_3), 1.22 (d, 6 H, $^3J_{HH}$ = 8.08 Hz, *p*-CH-CH_3).

Synthesis of Bis(2,4,6-tri-*iso*-propylphenyl)pnictogen-(III) chloride (Pn = Sb, Bi).[208] TripCu (10 mmol, 2.66 g) and $PnCl_3$ (Sb: 5 mmol, 1.14 g, Bi: 1 mmol, 315 mg) were each weighed into a Schlenk tube and dissolved in 30 mL of thf. The solutions were cooled to –50 °C after which TripCu was added to the $PnCl_3$ solution. The mixture was stirred for two days and allowed to warm to room temperature. The volatiles were removed *in vacuo*, followed by extraction with hexane (4 x 20 mL). After the solvent had been removed *in vacuo*, the residue was washed with diethyl

ether (2 x 15 mL). The residue was dried *in vacuo* to give a yellow powder. **Yield:** Sb: 2.29 g (82 %). Bi: 360 mg (55 %).

Synthesis of 1,8-Bis(naphthalenediyl)dipnictane-(II) (Pn = As 57, Sb 58).[174,175] **25** (As: 12 mmol, 2.245 g; Sb: 3 mmol, 544 mg) was weighed into a 100-mL-Schlenk tube, dissolved in 20 mL of thf and cooled to –40 °C. The tube was fitted with a dropping funnel, which already contained the pnictogen-(III) trichloride (As: 8 mmol, 1.45 g, 0.67 mL; Sb: 2 mmol, 456 mg). 50 mL of thf were added and the solution was added dropwise over the course of two hours. The reaction mixture was allowed to warm to room temperature overnight. All volatiles were removed *in vacuo* of the resulting orange suspension and 50 mL of degassed water were added and the mixture stirred for 30 minutes. The water was removed by filtration and the residue washed with hexane (2 x 50 mL). After the solvent was removed *in vacuo* the product was extracted with hot toluene and stored at –30 °C to give the desired product. Concentrating the mother liquor results in the precipitation of further product. **57**: **Yield:** 300 mg (19 %); **^{1}H NMR (C_6D_6, 400.1 MHz, 297 K) δ [ppm]:** 7.80 (dd, 2 H, Naph-*H*), 7.25 (dd, 2 H, Naph-*H*), 7.07 (dd, 2 H, Naph-*H*); **58**: **Yield:** 132 mg (27 %); **^{1}H NMR (C_6D_6, 400.1 MHz, 297 K) δ [ppm]:** 7.88 (dd, 2 H, Naph-*H*), 7.22 (dd, 2 H, Naph-*H*), 7.06 (dd, 2 H, Naph-*H*).

7.2. Experimental Procedures

7.2.1. Synthesis of 1,8-Bis(naphthalenediyl)dibismuthane-(II) (**60**)

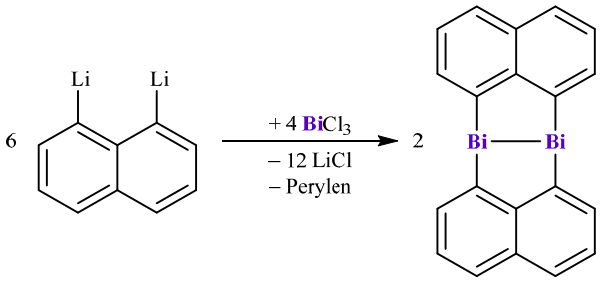

Li_2Naph (6 mmol, 1.107 g) was weighed into a Schlenk tube and dissolved in 20 mL of thf. The green solution was cooled to –30 °C and the tube fitted with a dropping funnel loaded with $BiCl_3$ (4 mmol, 1.241 g). $BiCl_3$ was then dissolved in 50 mL of thf and the solution was added dropwise over two hours. The mixture was stirred overnight and allowed to warm to room temperature giving an orange suspension. The volatiles were removed *in vacuo* and 50 mL of water were added and heated to 50 °C. The suspension was stirred for 30 minutes giving a yellow powder. The water was removed by filtration and the powder washed with hot *n*-hexane (4 x 25 mL). After the solvent was removed *in vacuo* the product was extracted with hot toluene. The hot toluene solutions were filtered into a preheated Schlenk tube and allowed to cool in an oil bath leading to the formation of yellow, crystalline needles, which were suitable for X-ray diffraction. Toluene was removed by filtration and the needles dried *in vacuo*. **Yield:** 45 mg (3 %); **m.p.:** 320 °C (dec.); **elemental analysis [wt-%]:** calcd. for: $C_{20}H_{12}Bi_2$: C 35.8, H 1.80; found: C 34.2, H 1.56; **^{1}H NMR (600.1 MHz, 297 K, thf-d_8) δ [ppm]:** 8.11 (dd, $^3J_{HH}$ = 6.59 Hz, $^4J_{HH}$ = 1.09 Hz, 2 H, Naph-2,7-C*H*), 7.35 (dd, $^3J_{HH}$ = 7.98 Hz, $^4J_{HH}$ = 0.95 Hz, 2 H, Naph-4,5-C*H*), 7.31 (dd, $^3J_{HH}$ = 7.84 Hz, $^3J_{HH}$ = 6.75 Hz, 2 H, Naph-3,6-C*H*); **^{13}C{^{1}H} NMR (150.9 MHz, 297 K, thf-d_8) δ [ppm]:** 142.66 (Naph-2,7-*C*H), 127.74 (Naph-3,6-*C*H), 127.28 (Naph-4,5-*C*H); **IR ν [cm^{-1}]:** 3032 (w), 1529 (w), 1478 (w), 1424 (w), 1343 (w), 1187 (w), 1129 (w), 974 (w), 907 (w), 800 (s), 767 (s), 728 (w), 538 (w), 520 (w), 424 (m), 379 (w).

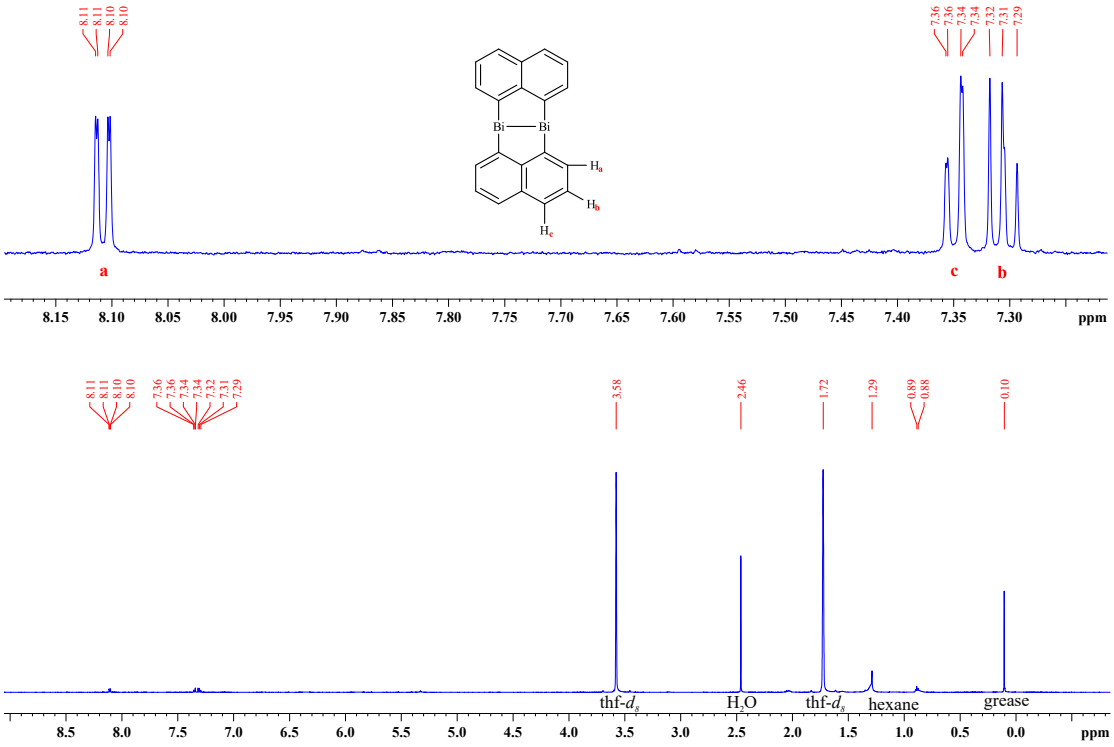

Figure E1. ^{1}H NMR spectrum of Bi_2Naph_2 (**60**) in thf-d_8.

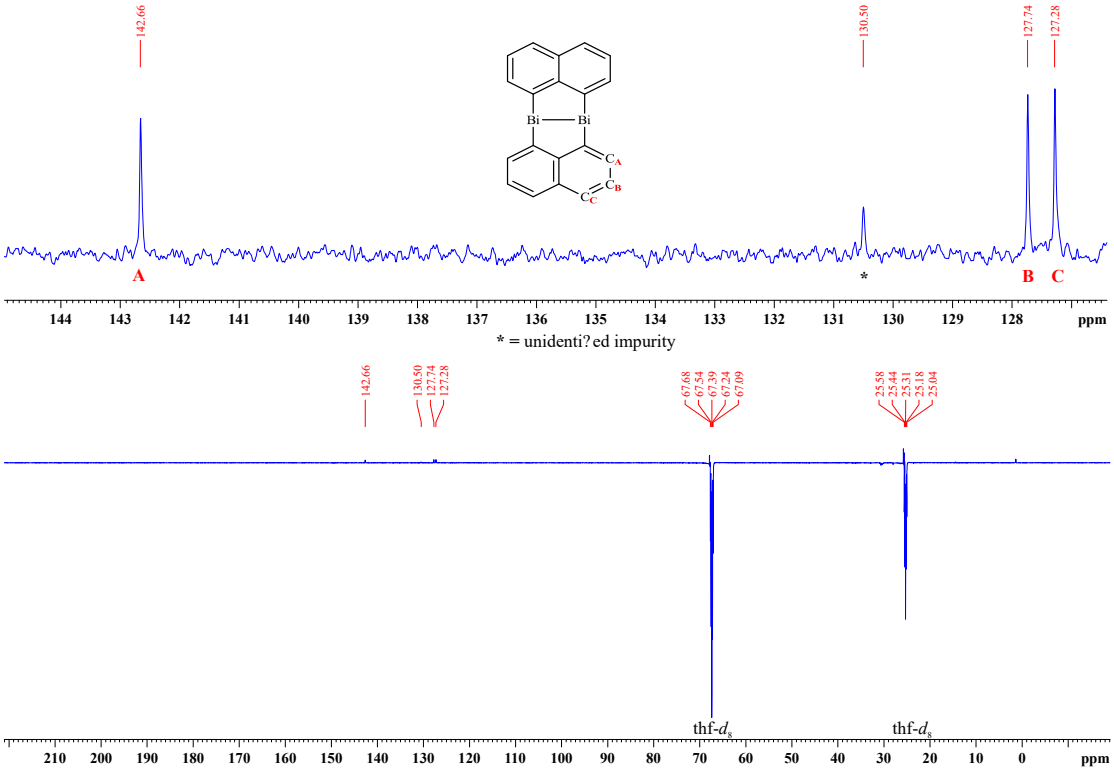

Figure E2. DEPT-135 ^{13}C{^{1}H} NMR spectrum of Bi_2Naph_2 (**60**) in thf-d_8.

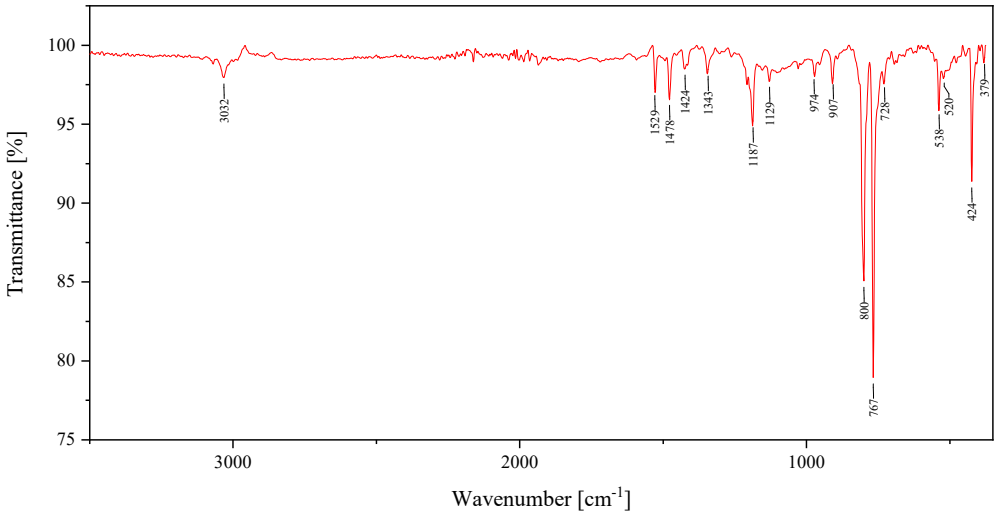

Figure E3. IR spectrum of neat Bi_2Naph_2 (**60**).

7.2.2. Synthesis of 1,8-Bis(diphenylstiba-(III))naphthalene (**41**)[162]

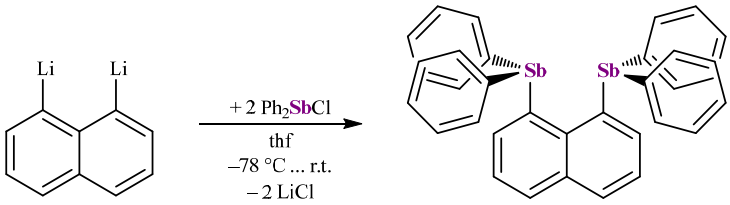

1,8-Li_2Naph · 0.6 Et_2O (922.75 mg, 5 mmol) and Ph_2SbCl (3.11 g, 10 mmol) were dissolved in 15 mL thf each and cooled to –78 °C. The green solution of 1,8-Li_2Naph was added dropwise to the stirred solution of Ph_2SbCl, which resulted in a yellow suspension. The mixture was allowed to warm to ambient temperature and stirred for 12 h. After the solvent was removed *in vacuo*, the yellow residue was extracted with hot toluene (2 x 20 mL). Concentrating the solution to 10 mL resulted in a white precipitate, which was redissolved through heating. Storing at 4 °C gave colorless crystals of **41**. The mother liquor was filtered off and the crystals were washed with *n*-hexane (2 x 10 mL) and dried *in vacuo*. Concentrating the mother liquor to 5 mL and storing at –30 °C gave another crop of **41**, which was purified as described. **Yield:** 2.03 g (60 %); **^{1}H NMR (CD_2Cl_2, 400.1 MHz, 25 °C) δ [ppm]:** 7.88 (dd, $^3J_{HH}$ = 8.12 Hz, $^4J_{HH}$ = 1.08 Hz, 2 H, Naph-4-*H*), 7.72 (dd, $^3J_{HH}$ = 7.03 Hz, $^4J_{HH}$ = 1.62 Hz, 2 H, Naph-2-*H*), 7.37-7.40 (m, 8 H, Ph-*m*-*H*), 7.26-7.35 (m, 14 H, Naph-3-*H*, Ph-*o*/*p*-*H*); **^{13}C{^{1}H} NMR (CD_2Cl_2, 100.6 MHz, 25 °C) δ [ppm]:** 143.56 (Naph-9-*C*), 141.73 (Ph-*ipso*-*C*), 140.98 (Naph-1,8-*C*), 140.15 (Naph-4,5-*C*H), 136.63 (Ph-*m*-*C*H), 135.70 (Naph-10-*C*), 131.34 (Naph-2,7-*C*H), 129.24 (Ph-*o*/*p*-*C*), 128.81 (Ph-*o*/*p*-*C*), 126.16 (Naph-3,6-*C*H).

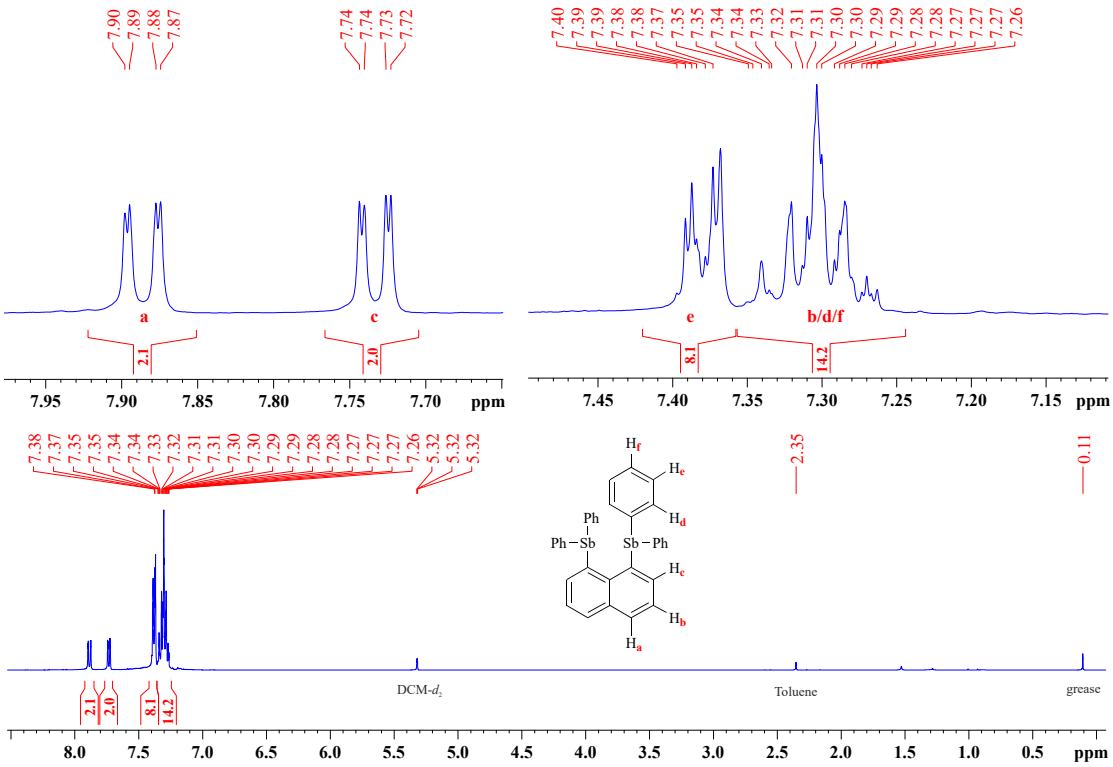

Figure E4. ^{1}H NMR spectrum of 1,8-$(Ph_2Sb)_2$Naph (**41**) in CD_2Cl_2.

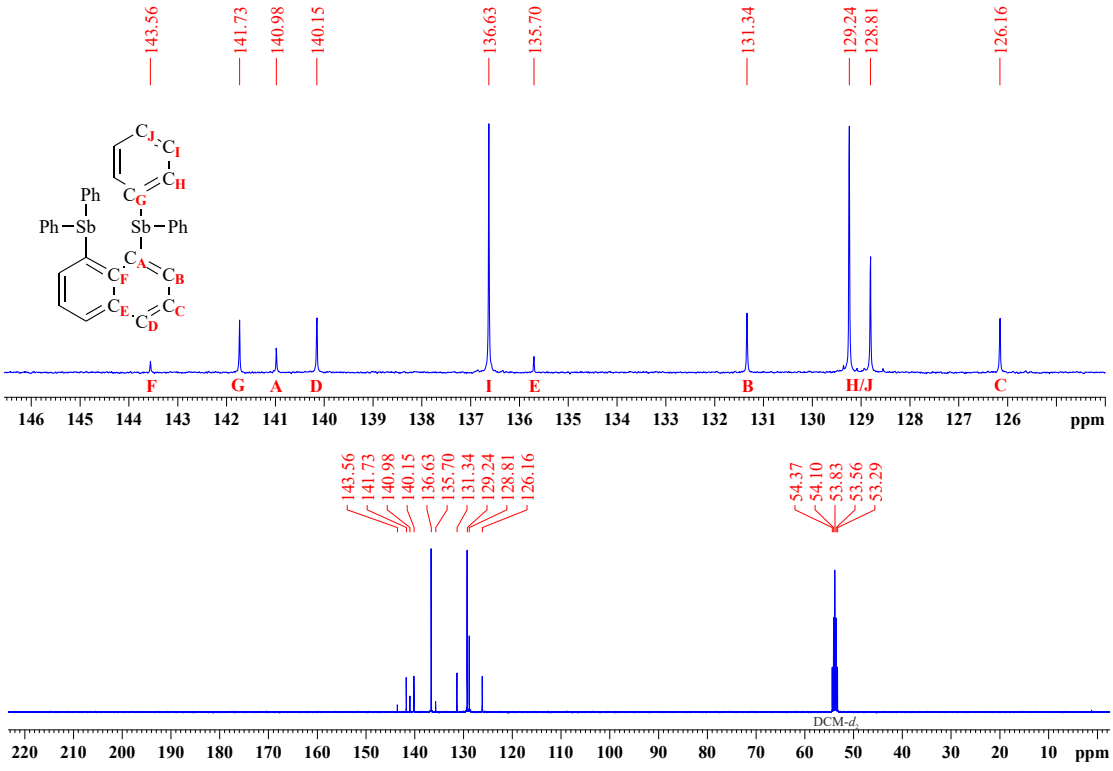

Figure E5. $^{13}C\{^{1}H\}$ NMR spectrum of 1,8-$(Ph_2Sb)_2$Naph (**41**) in CD_2Cl_2.

7.2.3. Synthesis of 5,6-Bis(diphenylstiba-(III))acenaphthene (**61**)

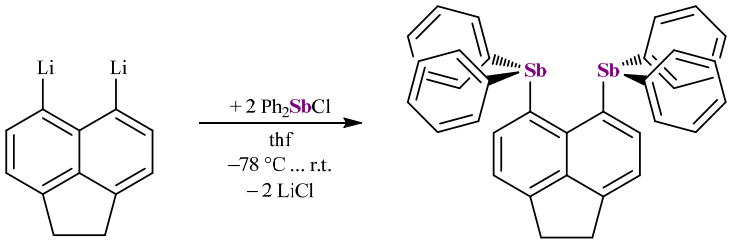

5,6-Li_2Acenaph (120.1 mg, 0.5 mmol) and Ph_2SbCl (311.42 mg, 1 mmol) were each weighed into a 25-mL-Schlenk tube and dissolved in 10 mL of thf each. The solutions were cooled to –78 °C and Ph_2SbCl was slowly added to Li_2Acenaph. A color change from red to yellow was observed after complete addition. The resulting mixture was warmed to room temperature and stirred overnight. The solvent was removed *in vacuo* giving a red oily residue. Resting for one hour resulted in the formation of colorless needles. The needles were washed with toluene (2 x 15 mL), 15 mL of hexane, and dried *in vacuo*. The residue was dissolved in 0.6 mL of thf and was mixed with 0.6 mL of hexane. Storing at 4 °C resulted in **61** as colorless needles. **Yield:** 95 mg (27 %); **m.p.:** 228 °C; **elemental analysis [wt-%]:** calcd. for $C_{36}H_{28}Sb_2$: C 61.41, H 4.01. Found: C 61.45, H 3.76; **^{1}H NMR (CD_2Cl_2, 400.1 MHz, 25 °C) δ [ppm]:** 7.58 (d, $^3J_{HH}$ = 6.94 Hz, 2 H, Naph-*o*-*H*), 7.36-7.34 (m, 8 H, Ph-*o*-*H*), 7.30-7.26 (m, 12 H, Ph-*m*/*p*-*H*), 7.18 (d, $^3J_{HH}$ = 7.08 Hz, 2 H, Naph-*m*-*H*), 3.38 (s, 4 H, CH_2); **^{13}C{^{1}H} NMR (CD_2Cl_2, 100.6 MHz, 25 °C) δ [ppm]:** 149.55 (Naph-9-*C*), 142.44 (Naph-1,8-*C*), 141.54 (Ph-*ipso*-*C*), 141.23 (Naph-2,7-*C*H), 141.00 (Naph-10-*C*), 136.86 (Ph-*m*-*C*H), 135.17 (Naph-4,5-*C*), 129.36 (Ph-*o*-*C*H), 128.89 (Ph-*p*-*C*H), 120.95 (Naph-3,6-*C*H), 30.48 (*C*H_2); **IR ν [cm^{-1}]:** 3055 (w), 3040 (w), 2961 (w), 2917 (w), 2870 (w), 2839 (w), 1951 (w), 1877 (w), 1815 (w), 1763 (w), 1642 (w), 1573 (w), 1551 (w), 1521 (w), 1477 (w), 1428 (m), 1378 (w), 1326 (w), 1301 (w), 1262 (w), 1247 (w), 1220 (w), 1181 (w), 1153 (w), 1106 (w), 1060 (m), 1018 (m), 996 (m), 970 (w), 943 (w), 911 (w), 842 (m), 817 (m), 730 (s), 695 (s), 616 (w), 602 (m), 569 (w), 530 (w), 481 (w), 457 (m), 450 (m), 394 (w).

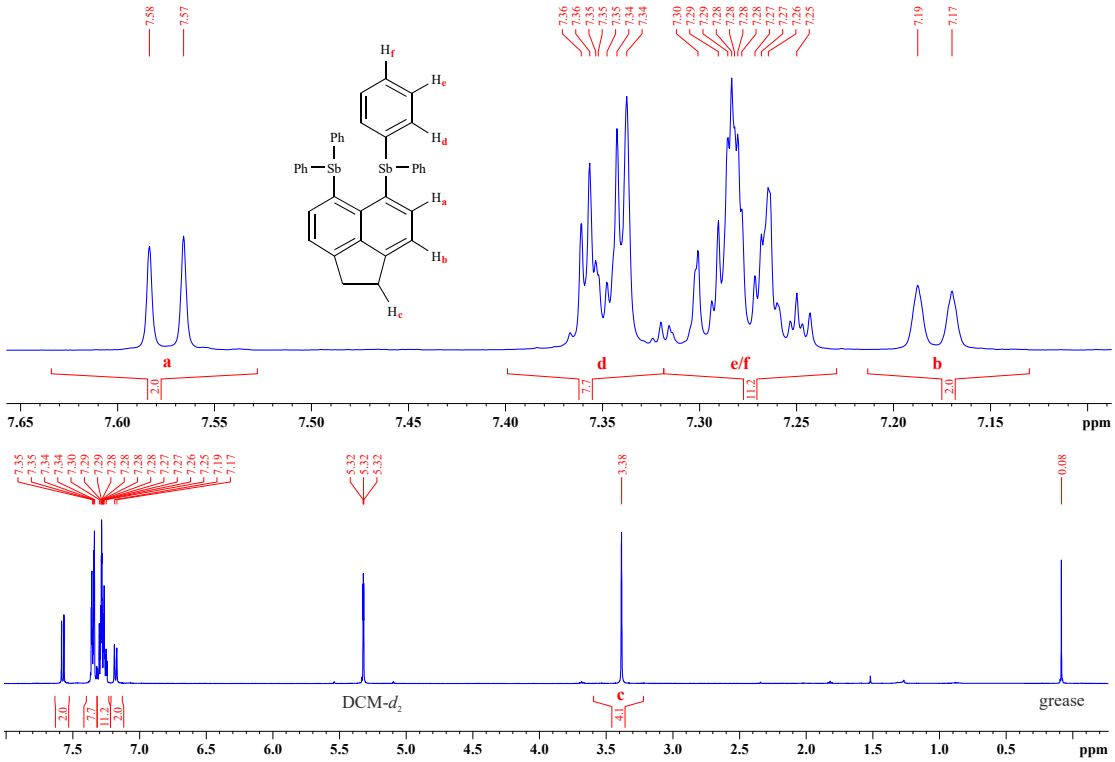

Figure E6. ^{1}H NMR spectrum of 5,6-(Ph$_2$Sb)$_2$Acenaph (**61**) in CD_2Cl_2.

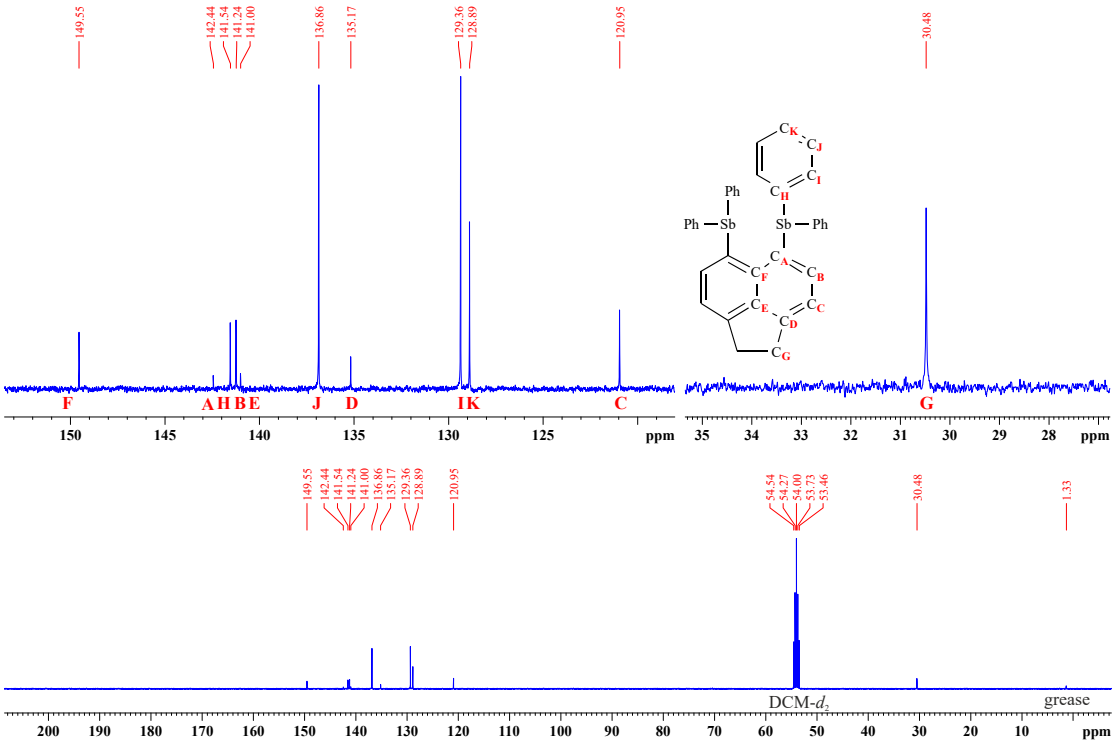

Figure E7. ^{13}C{^{1}H} NMR spectrum of 5,6-(Ph$_2$Sb)$_2$Acenaph (**61**) in CD_2Cl_2.

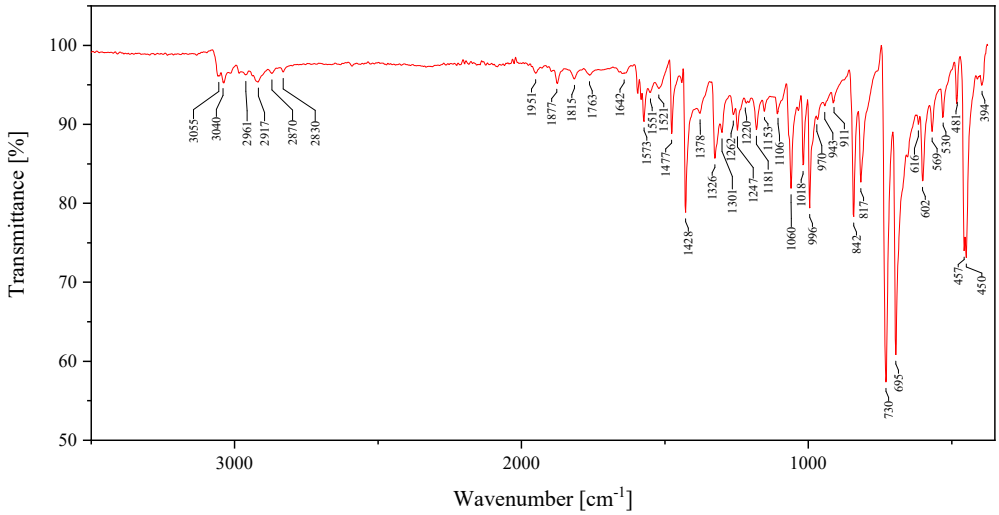

Figure E8. IR spectrum of neat 5,6-$(Ph_2Sb)_2$Acenaph (**61**).

7.2.1. Synthesis of 1,8-Bis(diphenylbisma-(III))naphthalene (**63**)

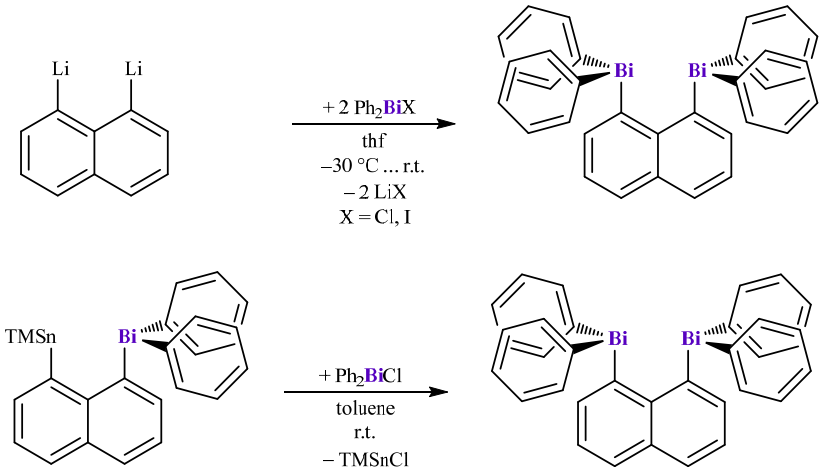

Method A. 1,8-Li_2Naph · 0.69 Et_2O (95.52 mg, 0.5 mmol) was weighed into a 100-mL-Schlenk tube, dissolved in 20 mL of thf, and cooled to –30 °C. In a dropping funnel Ph_2BiCl (398.64 mg, 1 mmol) was dissolved in 30 mL of thf and added over the course of 2 h resulting in a yellow suspension. The mixture was warmed to ambient temperature and stirred for an additional 12 h. After the solvent was removed *in vacuo,* the yellow residue was extracted with toluene (2 x 20 mL). The solution was dried *in vacuo* and the residue washed with diethyl ether (2 x 20 mL) resulting in **63** as an off-white solid. **Yield:** 72 mg (17 %); **Method B.** (Ph_2Bi)(TMSn)Naph was dissolved in 15 mL of toluene. Ph_2BiCl was weighed in a dropping funnel, dissolved in 30 mL of toluene, and added over the course of 4 h resulting in a yellow suspension. The mixture was dried *in vacuo* and the residue washed with diethyl ether (2 x 20 mL). **Yield:** 30 %; **Method C**. 1,8-Li_2Naph · 0.69 Et_2O (272 mg, 1.5 mmol) was weighed in a 100-mL-Schlenk tube, dissolved in 20 mL thf, and cooled to –30 °C. In a dropping funnel Ph_2BiI (1.47 g, 3 mmol) was dissolved in 50 mL thf and added over the course of 2 h resulting in a yellow suspension. The solvent was removed *in vacuo* and the oily residue washed with 30 mL of degassed water and dried *in vacuo*. The yellow solid was washed with *n*-hexane (20 mL) and diethyl ether (2 x 20 mL) and the volatiles were removed *in vacuo.* After extraction with toluene (2 x 20 mL) and removing the solvent *in vacuo* the product was dissolved in dichloromethane (20 mL), layered with *n*-hexane (30 mL), and stored at 4 °C leading to the formation of yellow crystals (**65**) and colorless needles. After filtration, the volume of the mother liquor was reduced resulting in the precipitation of a white solid. **Yield:** 345 mg (27 %); **m.p.:** 172.5 °C (dec.); **elemental analysis [wt-%]:** calcd. for $C_{34}H_{26}Bi_2$: C 47.9, H 3.07; found: C 47.1, H 2.92; **^{1}H NMR (400.1 MHz,**

297 K, thf-d_8) δ [ppm]: 8.34 (dd, $^3J_{HH}$ = 6.96 Hz, $^4J_{HH}$ = 1.28 Hz, 2 H, Naph-2,7-C*H*), 7.91 (dd, $^3J_{HH}$ = 8.10 Hz, $^4J_{HH}$ = 1.23 Hz, 2 H, Naph-4,5-C*H*), 7.62 (dd, $^3J_{HH}$ = 7.80 Hz, $^4J_{HH}$ = 1.58 Hz, 8 H, Ph-*m*-C*H*), 7.35-7.27 (m, 14 H, Naph-3,6-*H*, Ph-*o*/*p*-C*H*); **$^{13}C\{^1H\}$ NMR (100.6 MHz, 297 K, thf-d_8) δ [ppm]:** 162.21 (Naph-1,8-*C*), 145.08 (Naph-9-*C*), 142.74 (Naph-2,7-*C*H), 139.11 (Naph-10-*C*), 138.32 (Ph-*m*-*C*H), 131.24 (Ph-*o*/*p*-*C*H), 130.82 (Naph-4,5-*C*H), 129.09 (Naph-3,6-*C*H), 128.31 (Ph-*o*/*p*-*C*); **IR ν [cm^{-1}]:** 3060 (w), 3038 (w), 2955 (w), 1632 (w), 1566 (w), 1526 (w), 1472 (w), 1429 (m), 1380 (w), 1330 (w), 1254 (w), 1188 (w), 1156 (w), 1132 (w), 1055 (w), 1011 (w), 996 (m), 817 (m), 790 (w), 771 (m), 724 (s), 698 (m), 542 (w), 451 (m), 440 (m), 425 (w), 404 (w), 395 (w).

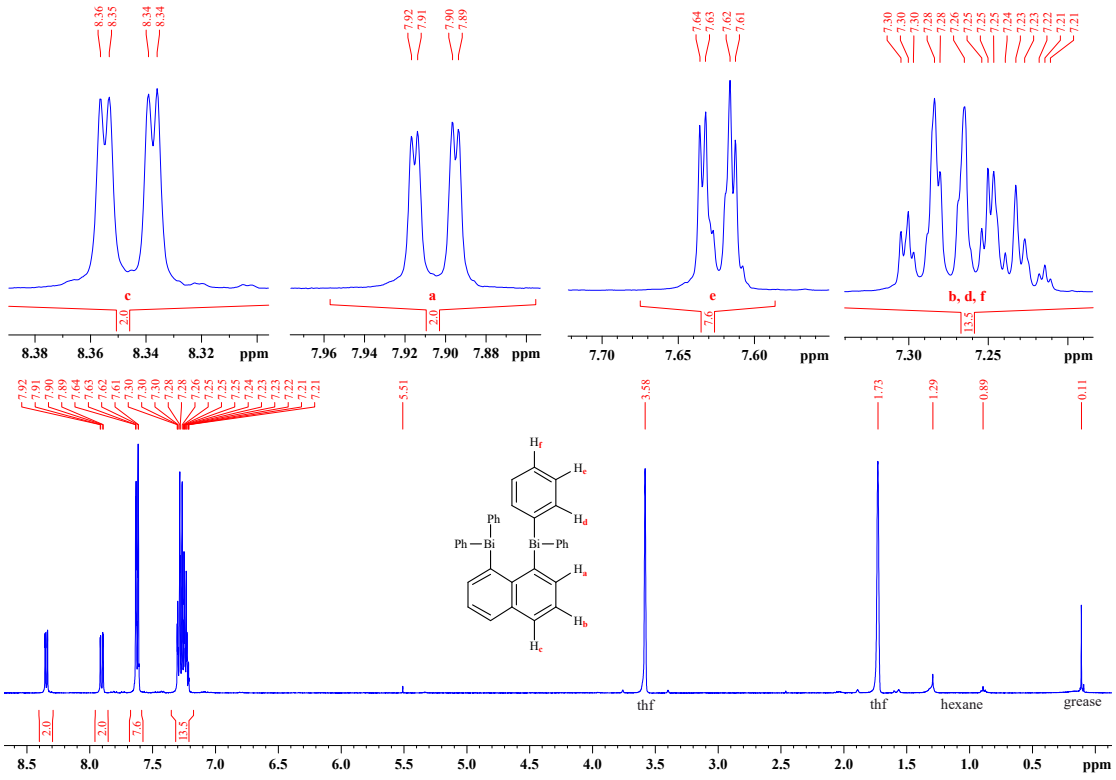

Figure E9. ^{1}H NMR spectrum of 1,8-(Ph$_2$Bi)$_2$Naph (**63**) in thf-d_8.

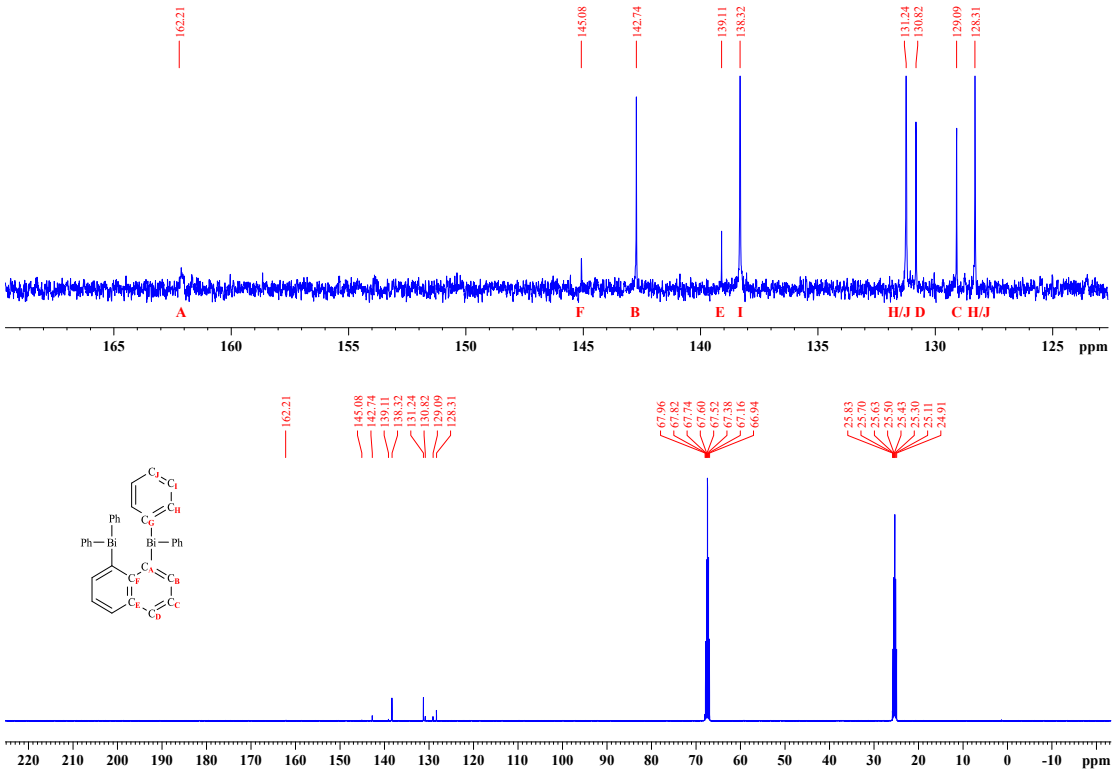

Figure E10. $^{13}C\{^{1}H\}$ NMR spectrum of 1,8-$(Ph_2Bi)_2$Naph (**63**) in thf-d_8.

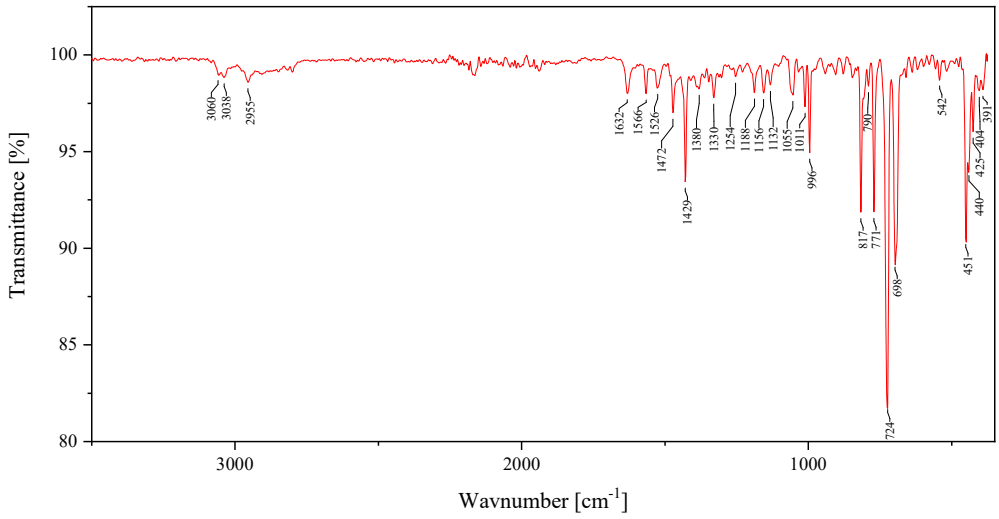

Figure E11. IR spectrum of neat 1,8-$(Ph_2Bi)_2$Naph (**63**).

7.2.1. Synthesis of 1-(Diphenylbisma-(III))-8-(trimethyltin-(IV))-naphthalene (**64**)

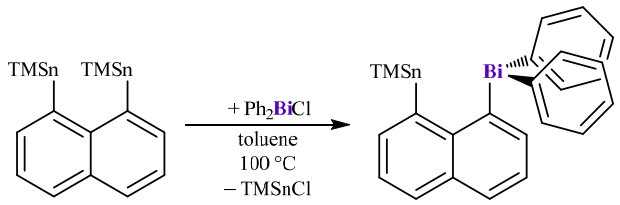

A stirred solution of $TMSn_2Naph$ (130.6 mg, 0.2 mmol) in 30 mL toluene was heated to 100 °C and 50 mL of a solution of Ph_2BiCl (79.73 mg, 0.2 mmol) in toluene was added dropwise over a course of three hours. The mixture was stirred and heated for three days. The solvent was removed *in vacuo* and the residue extracted with *n*-hexane (3 x 10 mL). The hexane solution was concentrated to 10 mL and stored at –30 °C to yield **64** as a yellow, crystalline solid. **Yield:** 27 mg (28 %); **m.p.:** 98 °C; **elemental analysis [wt-%]:** calcd. for $C_{23}H_{25}BiSn$: C 46.0, H 3.86. found: C 48.7, H 3.76; **^{1}H NMR (400.1 MHz, 297 K, C_6D_6) δ [ppm]:** 8.67 (dd, $^3J_{HH}$ = 6.86 Hz, $^4J_{HH}$ = 1.36 Hz, 1 H, Naph-*o/m*-C*H),* 7.77 (dd, $^3J_{HH}$ = 6.73 Hz, $^4J_{HH}$ = 1.36 Hz, 1 H, Naph-*o/m*-C*H*), 7.67 (dt, $^3J_{HH}$ = 8.02 Hz, 2 H), 7.61 (dd, $^3J_{HH}$ = 7.89 Hz, $^4J_{HH}$ = 1.58 Hz, 4 H, Ph-C*H*), 7.24 (d, $^3J_{HH}$ = 6.77 Hz, 1 H, Naph-*o/m*-C*H*), 7.21 (dd, $^3J_{HH}$ = 8.07 Hz, $^3J_{HH}$ = 6.82 Hz, 1 H, Naph-*o/m*-C*H*), 7.06-7.14 (m, 6 H, Ph-C*H*), 0.50 (s, 9 H, Sn–CH_3); **^{1}H NMR (400.1 MHz, 297 K, CD_2Cl_2) δ [ppm]:** 8.37 (dd, $^3J_{HH}$ = 6.92 Hz, $^4J_{HH}$ = 1.37 Hz, 1 H, Naph-2-C*H*), 7.88 (td, $^3J_{HH}$ = 7.53 Hz, $^4J_{HH}$ = 1.37 Hz, 2 H, Naph-4,5-C*H*), 7.79 (dd, $^3J_{HH}$ = 6.77 Hz, $^4J_{HH}$ = 1.37 Hz, 1 H, Naph-6-C*H*), 7.56 (dd, $^3J_{HH}$ = 7.91 Hz, $^4J_{HH}$ = 1.37 Hz, 4 H, Ph-*m*-C*H*), 7.40 (dd, $^3J_{HH}$ = 8.06 Hz, $^3J_{HH}$ = 6.97 Hz, 1 H, Naph-7-C*H*), 7.27-7.36 (m, 7 H, Naph-3-H, Ph-*o/p*-C*H*), 0.57 (t, $^2J_{HSn}$ = 26.62 Hz, $^2J_{HSn}$ = 25.49 Hz. 9 H, Sn–CH_3); **^{13}C{^{1}H} NMR (100.6 MHz, 297 K, CD_2Cl_2) δ [ppm]:** 158.18 (Naph-1-*C*Bi), 145.50 (Naph-8-*C*Sn), 144.61 (Naph-9-*C*), 141.58 (Naph-2-*C*H), 138.35 (Naph-4-*C*H), 137.84 (Naph-6-*C*H), 137.45 (Ph-*m*-*C*H), 136.51 (Naph-10-*C*), 131.00 (Naph-3-*C*H), 130.81 (Ph-*ipso*-*C*), 130.36 (Naph-5-*C*H), 128.96 (Ph-*o/p*-*C*H), 128.14 (Ph-*o/p*-*C*H), 125.03 (Naph-7-*C*H), –2.28 (Sn-*C*H_3); **^{119}Sn{^{1}H} NMR (111.9 MHz, 297 K, CD_2Cl_2) δ [ppm]:** –47.12; **IR ν [cm^{-1}]:** 3044 (w), 2979 (w), 2901 (w), 1593 (w), 1569 (w), 1531 (w), 1472 (w), 1426 (m), 1352 (w), 1324 (w), 1300 (w), 1280 (w), 1184 (w), 1154 (w), 1136 (w), 1054 (w), 1034 (w), 1013 (w), 996 (m), 964 (w), 844 (w), 815 (m), 769 (s), 723 (s), 694 (s), 519 (s), 503 (m), 442 (m), 418 (m).

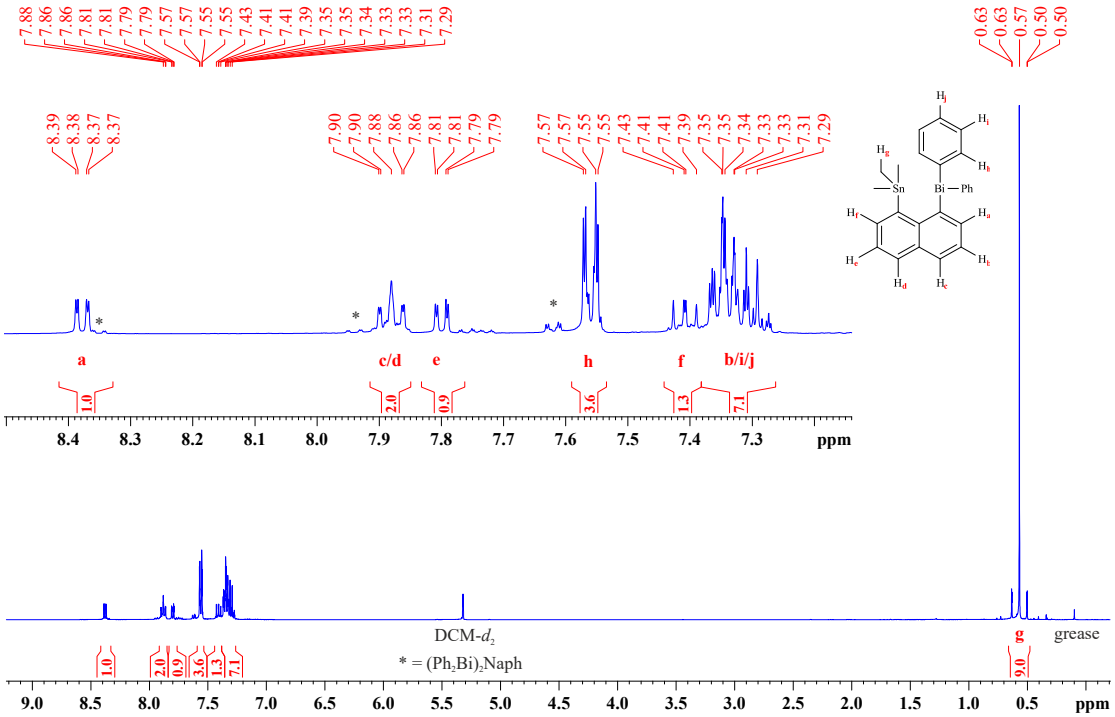

Figure E12. ^{1}H NMR spectrum of 1-(Ph_2Bi)-8-(TMSn)Naph (**64**) in CD_2Cl_2.

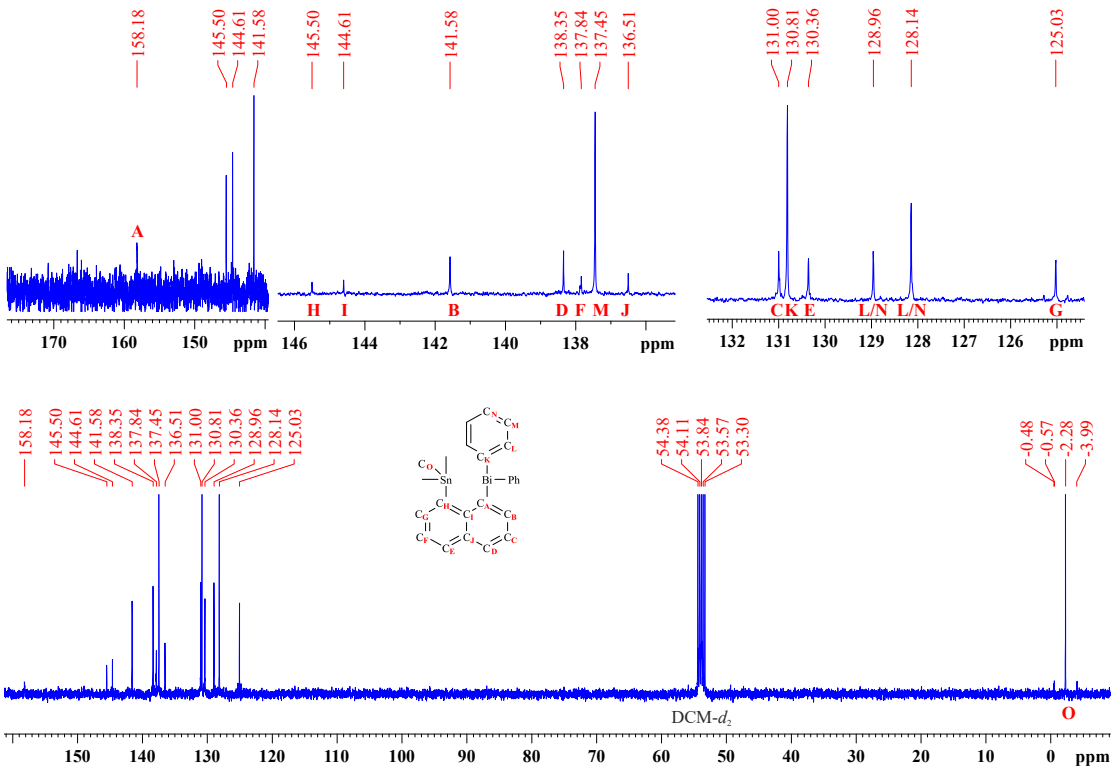

Figure E13. $^{13}C\{^{1}H\}$ NMR spectrum of 1-(Ph_2Bi)-8-(TMSn)Naph (**64**) in CD_2Cl_2.

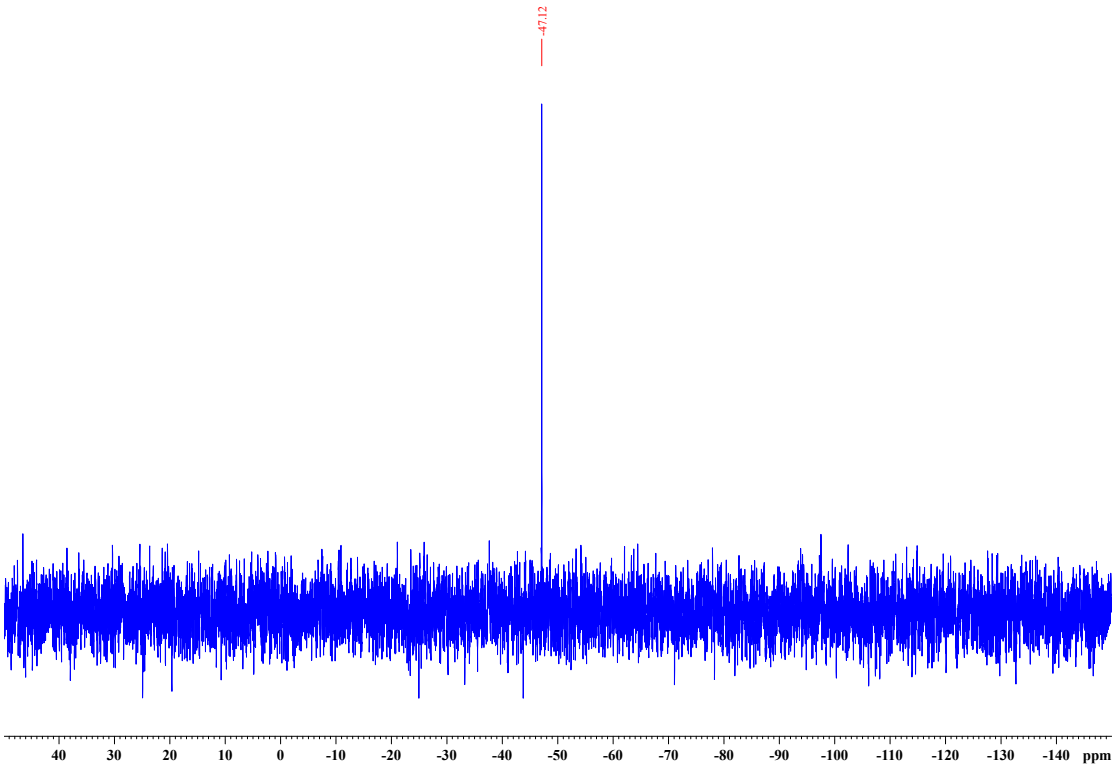

Figure E14. $^{119}Sn\{^{1}H\}$ NMR spectrum of 1-(Ph_2Bi)-8-(TMSn)Naph (**64**) in CD_2Cl_2.

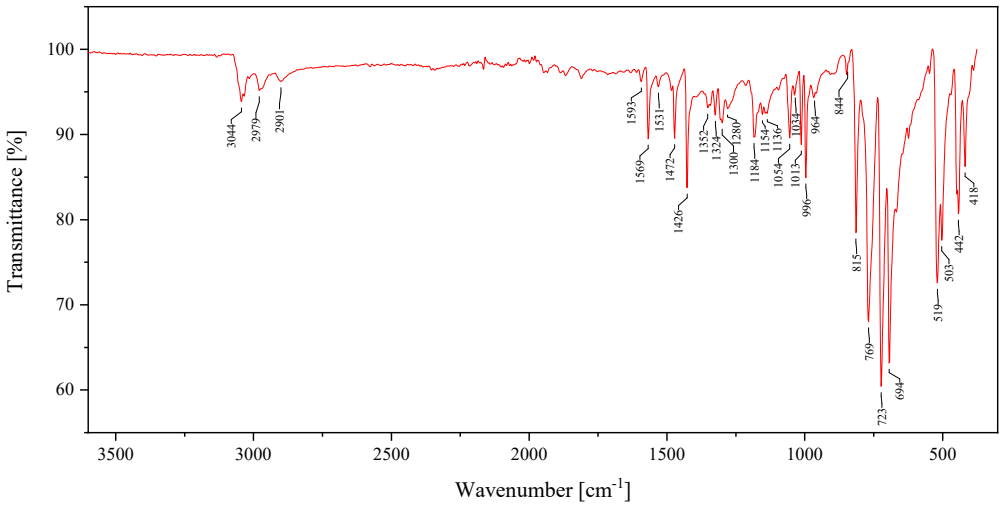

Figure E15. IR spectrum of neat 1-(Ph_2Bi)-8-(TMSn)Naph (**64**).

7.2.2. Synthesis of 1,1',8,8'-Bis(phenylbisma-(III))bisnaphthalenediyl (**65**)

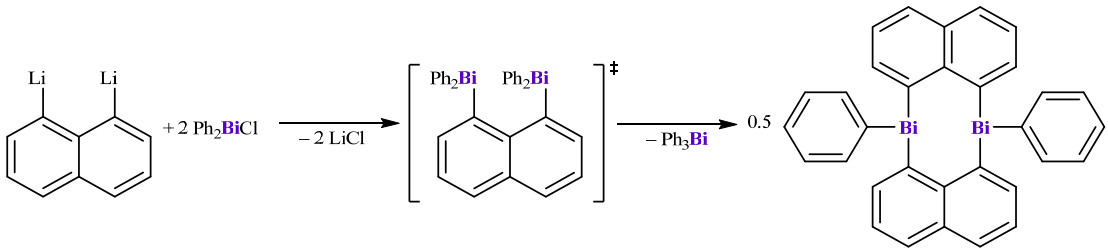

1,8-Li_2Naph · 0.69 Et_2O (191.04 mg, 1 mmol) was weighed in a 100-mL-three-necked flask, dissolved in 20 mL thf, and cooled to 30 °C. In a dropping funnel $PhBiCl_2$ (356.94 mg, 1 mmol) was dissolved in 30 mL thf and added over the course of 2 h resulting in a yellow suspension. The mixture was warmed to ambient temperature and stirred for an additional 12 h. After removal of the solvent *in vacuo* the yellow residue was extracted with toluene (2 x 20 mL). The solution was dried *in vacuo* and the residue washed with diethyl ether (2 x 20 mL) giving **65** as a yellow solid. **Yield:** 148 mg (18 %); **m.p.:** 236.3 °C (dec.); **elemental analysis [wt-%]:** calcd. for $C_{34}H_{26}Bi_2$: C 46.6, H 2.69; found: C 44.0, H 2.58; **^{1}H NMR (400.1 MHz, 297 K, thf-d_8) δ [ppm]:** 8.31 (dd, $^3J_{HH}$ = 6.90 Hz, $^4J_{HH}$ = 1.12 Hz, 2 H, Naph-2/7-C*H*), 7.80 (dd, $^3J_{HH}$ = 7.76 Hz, $^4J_{HH}$ = 1.25 Hz, 2 H, Ph-*o*-C*H*), 7.74 (dd, $^3J_{HH}$ = 8.05 Hz, $^4J_{HH}$ = 1.05 Hz, 2 H, Naph-4/5-C*H*), 7.57 (t, $^3J_{HH}$ = 7.59 Hz, 2 H, Ph-*m*-C*H*), 7.43 (tt, $^3J_{HH}$ = 7.40 Hz, $^4J_{HH}$ = 1.27 Hz, 1 H, Ph-*p*-C*H*), 7.21 (dd, $^3J_{HH}$ = 7.92 Hz, $^3J_{HH}$ = 6.91 Hz, 2 H, Naph-3/6-C*H*); **^{13}C{^{1}H} NMR (100.6 MHz, 297 K, thf-d_8) δ [ppm]:** 171.34 (Ph-*ipso*-*C*), 163.47 (Naph-1,8-*C*), 146.06 (Naph-9-*C*), 139.48 (Naph-2,7-*C*H), 138.80 (Naph-10-*C*), 138.67 (Ph-*o*-*C*H), 131.39 (Ph-*m*-*C*H), 130.01 (Naph-4,5-*C*H), 129.21 (Ph-*p*-*C*H); 128.31 (Naph-3,6-*C*); **IR ν [cm^{-1}]:** 3038 (w), 1566 (w), 1527 (m), 1472 (w), 1428 (m), 1336 (w), 1307 (w), 1186 (m), 1130 (w), 1075 (w), 1050 (w), 1036 (w), 1010 (w), 995 (m), 948 (w), 911 (w), 806 (s), 767 (s), 724 (s), 699 (s), 535 (w), 512 (w), 463 (w), 451 (w), 426 (m).

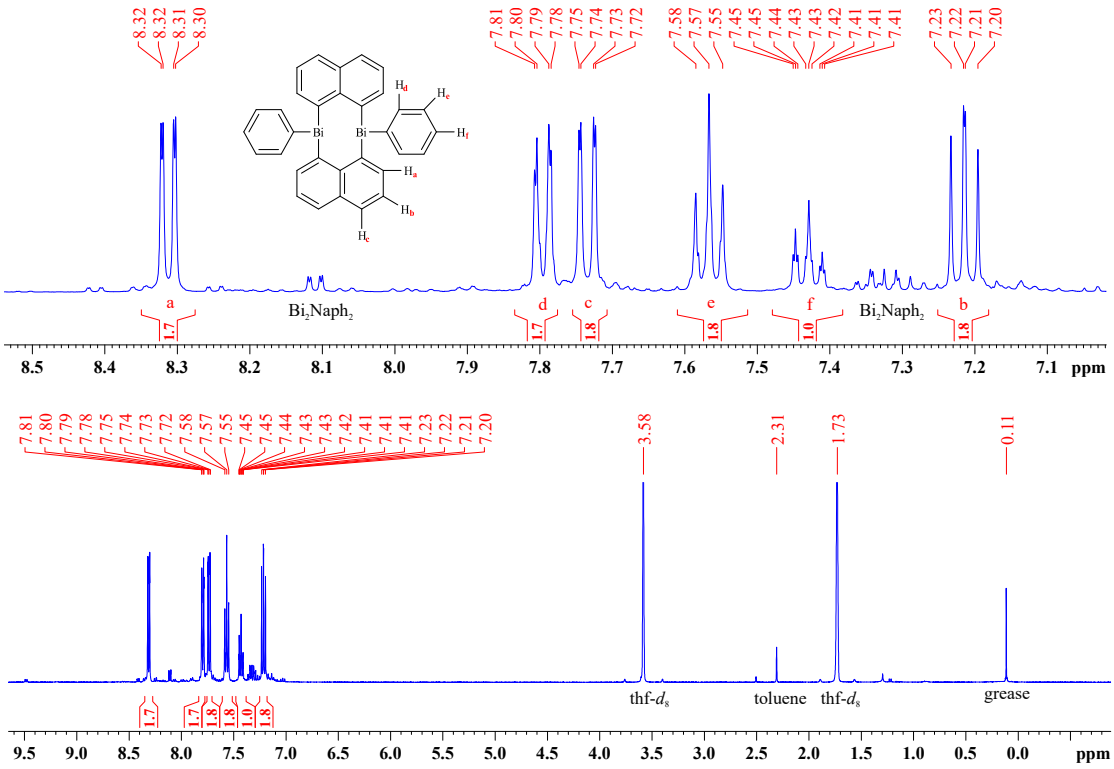

Figure E16. ^{1}H NMR spectrum of (PhBiNaph)$_2$ (**65**) in thf-d_8.

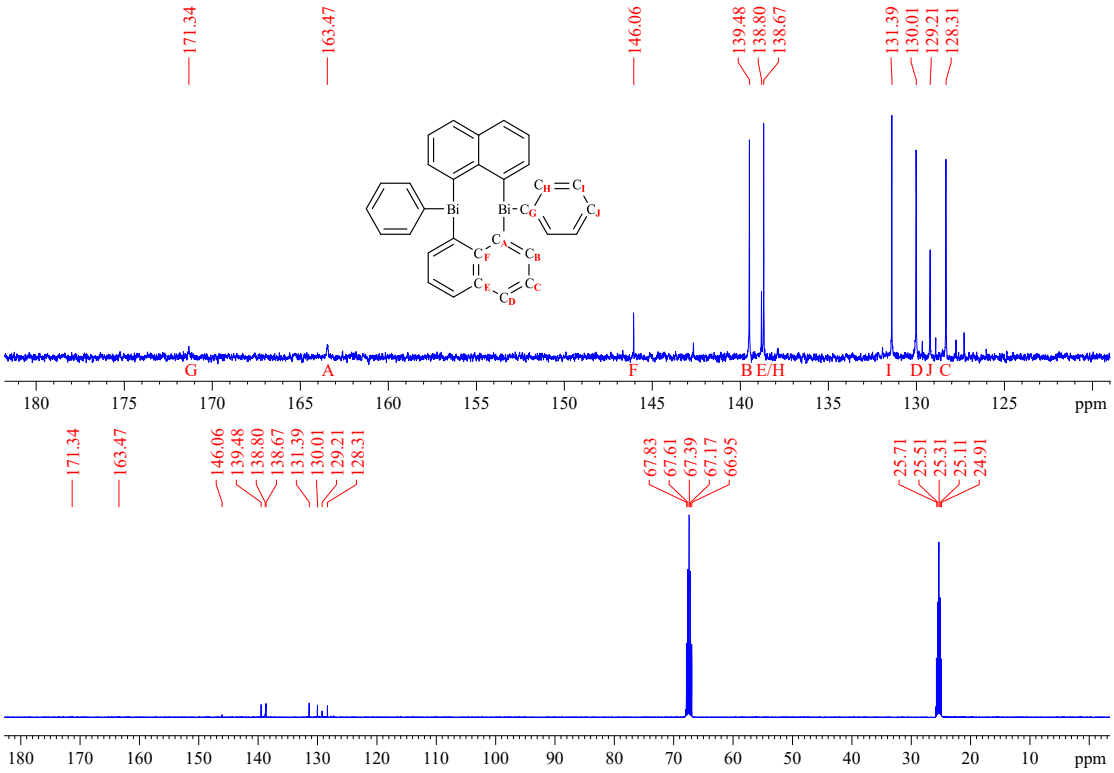

Figure E17. ^{13}C{^{1}H} NMR spectrum of (PhBiNaph)$_2$ (**65**) in thf-d_8.

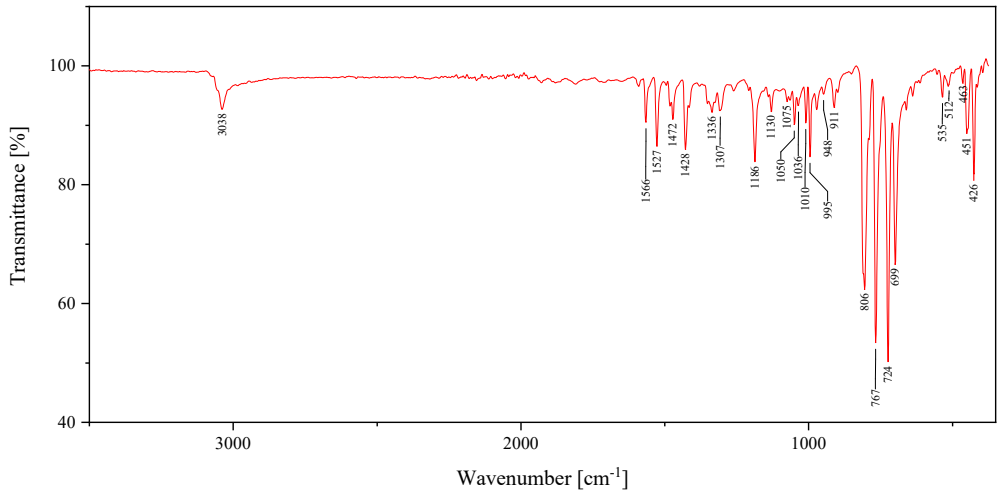

Figure E18. IR spectrum of neat $(PhBiNaph)_2$ (**65**).

7.2.3. Synthesis of Bis(1,8-bis(diphenylstiba-(III))naphthalene)silver-(I) hexafluoroantimonate-(V) (**66**)

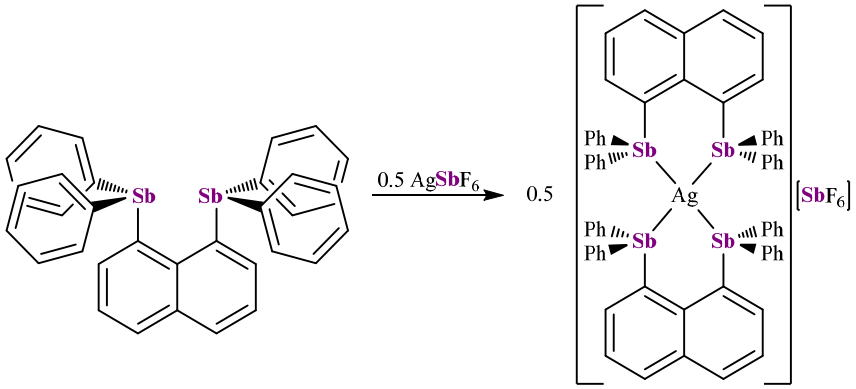

41 (2 mmol, 1.356 g) and $AgSbF_6$ (1 mmol, 341.8 mg) were weighed in a Schlenk flask and suspended in 15 mL of acetonitrile. After stirring for 2 h under the exclusion of light, the mixture was filtered and concentrated to 10 mL. The resulting precipitate was dissolved in heat and the solution stored at 4 °C to give colorless crystals of **66**. **Yield:** 1.278 g (71 %); **m.p.:** 158 °C (dec.); **elemental analysis [wt-%]:** calcd. for $C_{70}H_{55}AgF_6NSb_5$: C 48.5, H 3.28, N 1.57. found: C 48.7, H 3.41, N 1.60; **^{1}H NMR (400.1 MHz, 297 K, CD_2Cl_2) δ [ppm]:** 8.09 (dd, $^3J_{HH}$ = 8.21 Hz, $^4J_{HH}$ = 1.27 Hz, 2 H, Naph-*o*-C*H*), 7.74 (dd, $^3J_{HH}$ = 7.09 Hz, $^4J_{HH}$ = 1.25 Hz, 2 H, Naph-*m*-C*H*), 7.46 (dd, $^3J_{HH}$ = 7.99 Hz, $^4J_{HH}$ = 7.28 Hz, 2 H, Naph-*p*-C*H*), 7.37 (tt, $^3J_{HH}$ = 7.28 Hz, $^4J_{HH}$ = 1.47 Hz, 4 H, Ph-*p*-C*H*), 7.15 (t, $^3J_{HH}$ = 7.69 Hz, 8 H, Ph-*m*-C*H*), 7.09 (dd, $^3J_{HH}$ = 7.97 Hz, $^4J_{HH}$ = 1.46 Hz, 8 H, Ph-*o*-C*H*), 1.98 (s, 3 H, CH_3CN); **^{13}C{^{1}H} NMR (100.6 MHz, 297 K, CD_2Cl_2) δ [ppm]:** 142.34 (Naph-1,8-*C*), 140.70 (Naph-3,6-*C*H), 137.23 (Naph-9-*C*), 135.87 (Ph-*o*-*C*H), 133.84 (Naph-2,7-*C*H), 133.81(Ph-*ipso*-*C*), 131.36 (Naph-10-*C*), 130.84 (Ph-*p*-*C*H), 130.22 (Ph-*m*-*C*H), 126.51 (Naph-4,5-*C*H), 117.05 (CH$_3$*C*N), 2.07 (*C*H$_3$CN); **^{19}F NMR (282.4 MHz, 297 K, CD_2Cl_2) δ [ppm]:** –107.42, –111.40, –114.14, –119.01, –121.20, –122.66 –126.44, –128.03, –130.27, –134.94, –137.78, –141.88; **IR ν [cm^{-1}]**: 3040 (w), 2963 (w), 1575 (w), 1477 (m), 1432 (m), 1350 (w), 1329 (w), 1261 (w), 1194 (w), 1157 (w), 1095 (w), 1063 (m), 1018 (m), 997 (m), 918 (w), 848 (w), 819 (m), 770 (m), 730 (s), 692 (s), 652 (s), 521 (m), 448 (m).

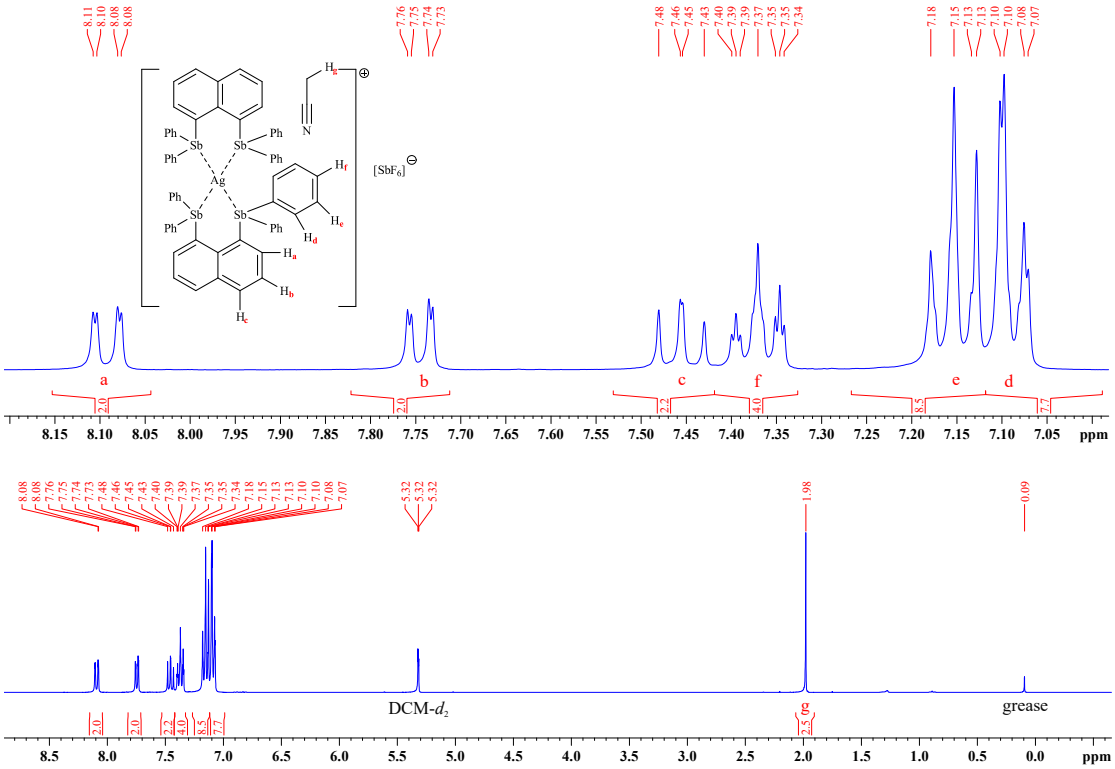

Figure E19. ^{1}H NMR spectrum of {[(Ph$_2$Sb)$_2$Naph]$_2$Ag}[SbF$_6$] (**66**) in CD$_2$Cl$_2$.

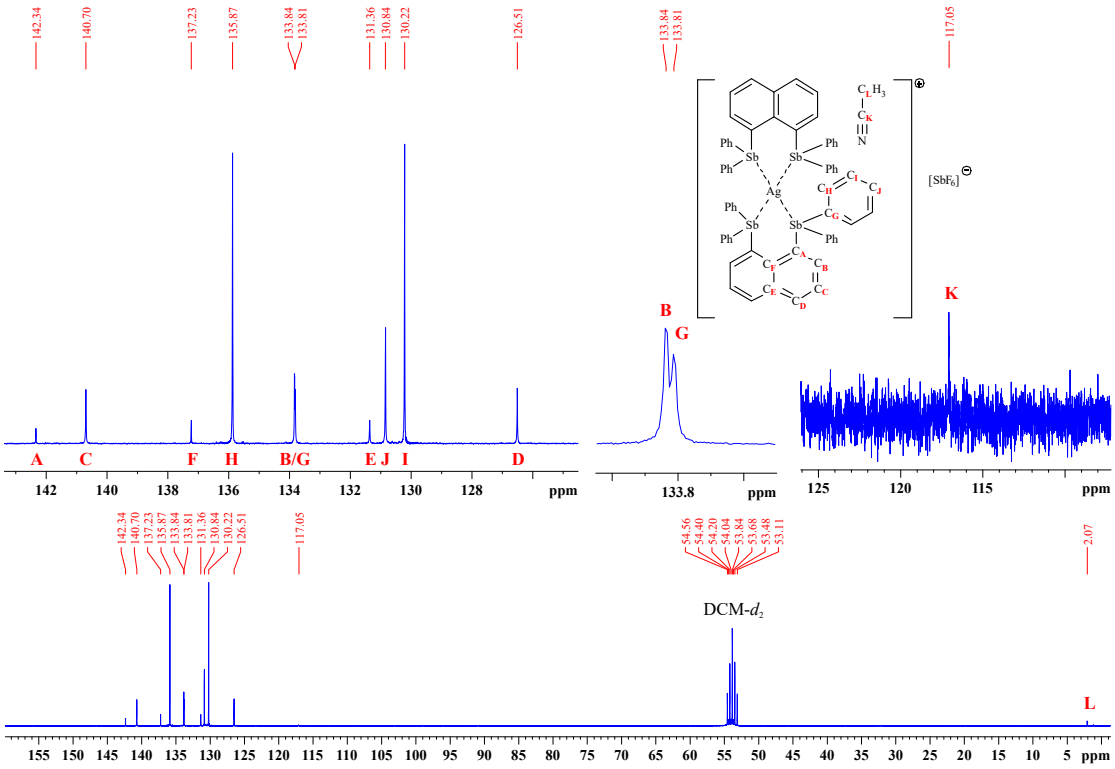

Figure E20. ^{13}C{^{1}H} NMR spectrum of {[(Ph$_2$Sb)$_2$Naph]$_2$Ag}[SbF$_6$] (**66**) in CD$_2$Cl$_2$.

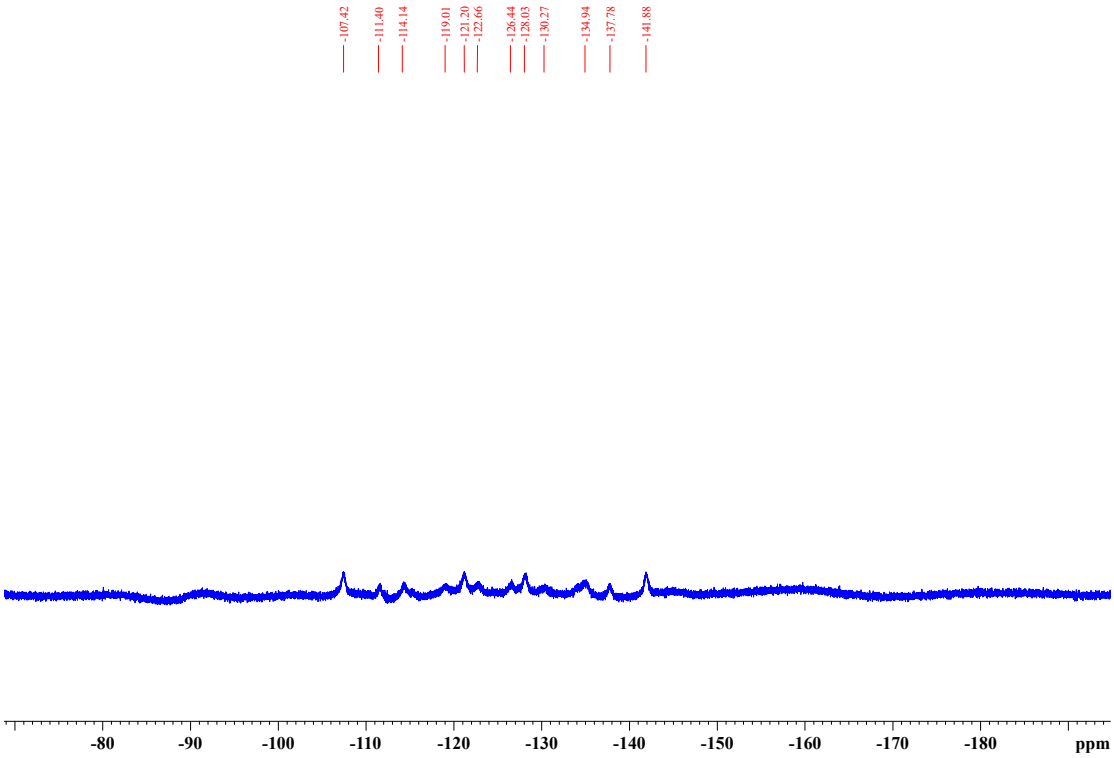

Figure E21. ^{19}F NMR spectrum of $\{[(Ph_2Sb)_2Naph]_2Ag\}[SbF_6]$ (**66**) in CD_2Cl_2.

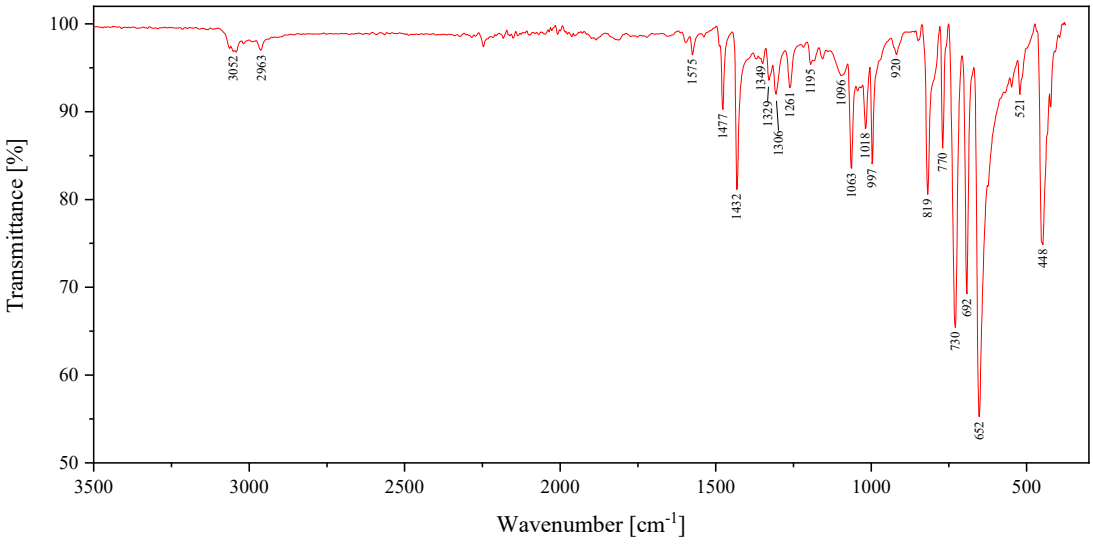

Figure E22. IR spectrum of neat $\{[(Ph_2Sb)_2Naph]_2Ag\}[SbF_6]$ (**66**).

7.2.4. Synthesis of Bis(1,8-bis(diphenylstiba-(III))naphthalene)copper-(I) hexafluoroantimonate-(V) (**67**)

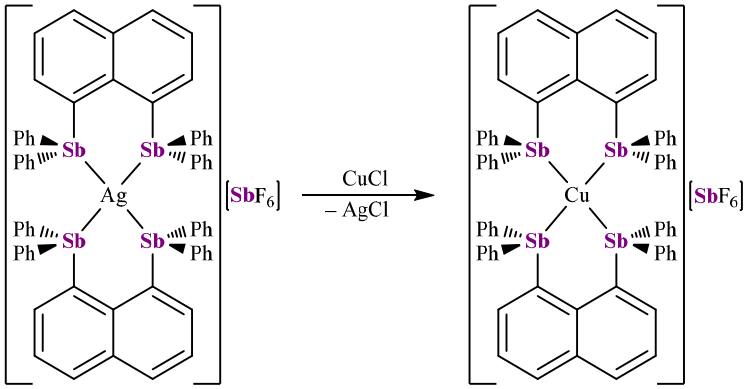

66 (0.12 mmol, 207 mg) and CuCl (0.3 mmol, 30 mg) were weighed into a Schlenk tube and dissolved in 15 mL of acetonitrile. After stirring overnight, the solvent was removed *in vacuo* and the residue dispersed in 10 mL of dichloromethane. The suspension was filtered, all volatiles were removed *in vacuo*, and the residue was washed with *n*-hexane (3 x 5 mL). The solid was dried *in vacuo* to give **67** as a white powder. Crystals suitable for X-ray analysis were collected from a thf solution layered with *n*-hexane at 4 °C. **Yield:** 115 mg (58 %); **m.p.:** 215.6 °C (dec.); **elemental analysis [wt-%]:** calcd. for $C_{68}H_{52}CuF_6Sb_5$: C 49.3, H 3.17. found: C 48.6, H 2.97; **^{1}H NMR (400.1 MHz, 297 K, CD_2Cl_2) δ [ppm]:** 8.12 (dd, $^3J_{HH}$ = 8.12 Hz, $^4J_{HH}$ = 1.10 Hz, 2 H, Naph-2,7-C*H*), 7.70 (dd, $^3J_{HH}$ = 7.05 Hz, $^4J_{HH}$ = 1.21 Hz, 2 H, Naph-4,5-C*H*), 7.48 (dd, $^3J_{HH}$ = 8.00 Hz, $^3J_{HH}$ = 7.21 Hz, 2 H, Naph-3,6-C*H*), 7.33 (tt, $^3J_{HH}$ = 7.48 Hz, $^4J_{HH}$ = 1.20 Hz, 4 H, Ph-*p*-C*H*), 7.08 (t, $^3J_{HH}$ = 7.61 Hz, 8 H, Ph-*m*-C*H*), 6.98 (dd, $^3J_{HH}$ = 7.74 Hz, $^4J_{HH}$ = 1.03 Hz, 8 H, Ph-*o*-C*H*); **^{13}C{^{1}H} NMR (100.6 MHz, 297 K, CD_2Cl_2) δ [ppm]:** 142.88 (Naph-1,8-*C*), 140.33 (Naph-4,5-*C*H), 137.02 (Naph-9-*C*), 135.67 (Ph-*o*-*C*H), 133.99 (Naph-2,7-*C*H), 133.17 (Ph-*ipso*-*C*), 130.87 (Naph-10-*C*), 130.19 (Ph-*p*-*C*H), 129.82 (Ph-*m*-*C*H), 126.53 (Naph-3,6-*C*H); **^{19}F NMR (282.4 MHz, 297 K, CD_2Cl_2) δ [ppm]:** –111.77, –114.80, –116.85, –120.43, –122.10, –123.29, –125.99, –127.20, –128.79, –132.30, –134.39, –137.54; **IR ν [cm^{-1}]**: 1574 (w), 1510(m), 1467 (m), 1421 (m), 1356 (w), 1332 (w), 1320 (w), 1283 (m), 1218 (m), 1195 (m), 1155 (m), 1142 (m), 1109 (m), 1064 (w), 1040 (w), 1031 (w), 990 (s), 873 (w), 810 (w), 790 (m), 774 (m), 731 (m), 677 (m), 655 (s), 618 (m), 586 (w), 570 (w), 539 (w), 453 (w), 421 (w).

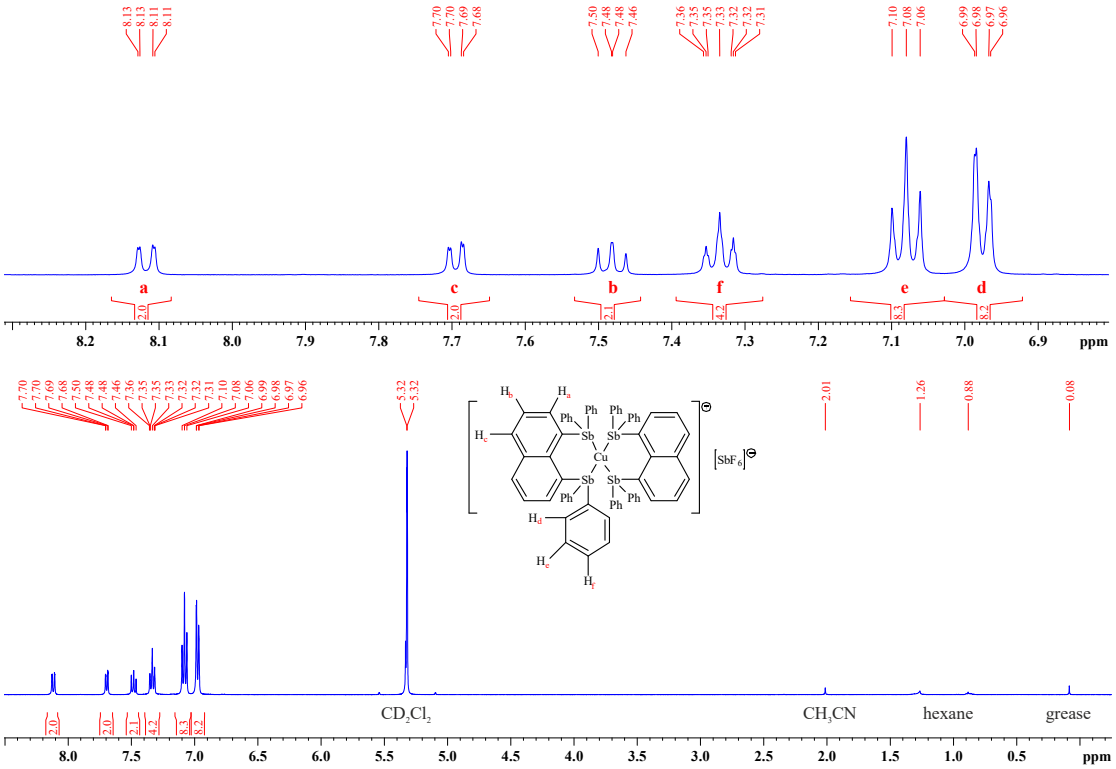

Figure E23. ^{1}H NMR spectrum of $\{[(Ph_2Sb)_2Naph]_2Cu\}[SbF_6]$ (**67**) in CD_2Cl_2.

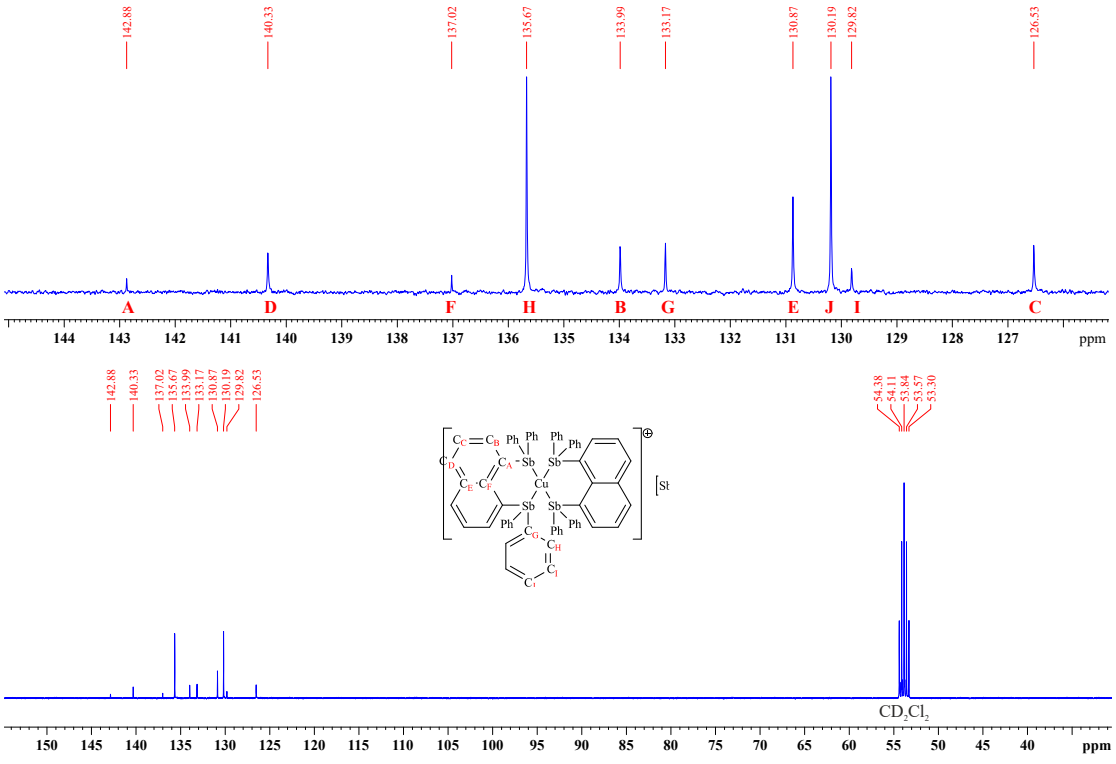

Figure E24. $^{13}C\{^{1}H\}$ NMR spectrum of $\{[(Ph_2Sb)_2Naph]_2Cu\}[SbF_6]$ (**67**) in CD_2Cl_2.

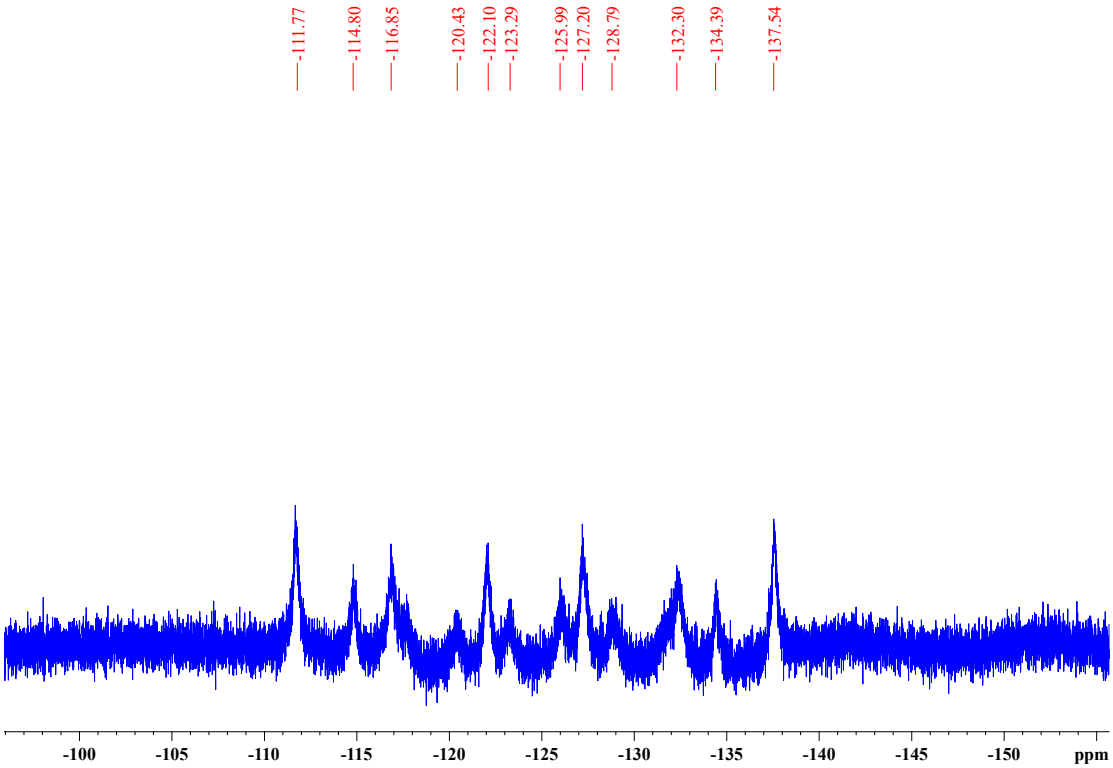

Figure E25. ^{19}F NMR spectrum of $\{[(Ph_2Sb)_2Naph]_2Cu\}[SbF_6]$ (**67**) in CD_2Cl_2.

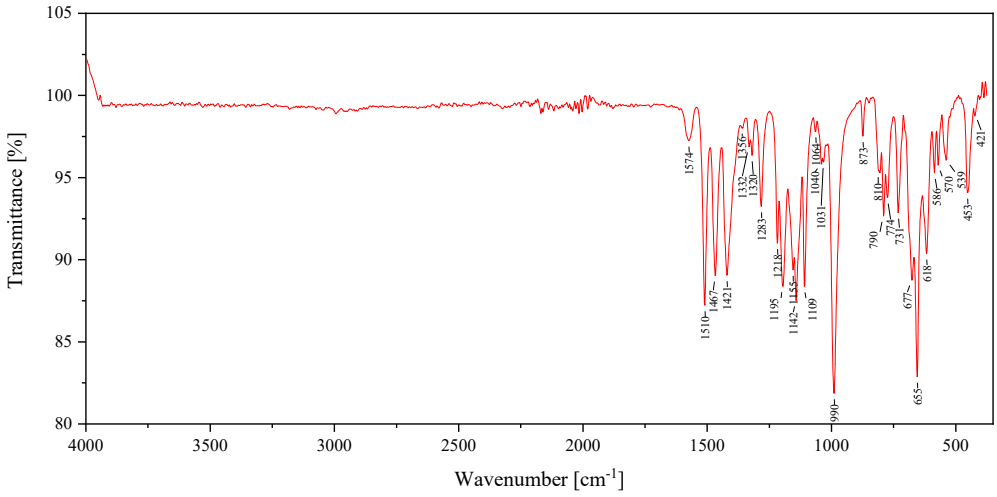

Figure E26. IR spectrum of neat $\{[(Ph_2Sb)_2Naph]_2Cu\}[SbF_6]$ (**67**).

7.2.5. Synthesis of Bis(1,8-bis(diphenylstiba-(III))naphthalene)gold-(I) hexafluoroantimonate-(V) (**68**)

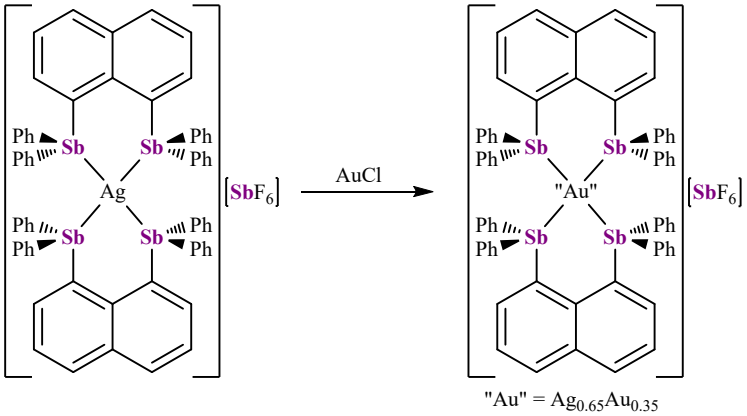

66 (0.1 mmol, 173.5 mg) and AuCl (0.1 mmol, 23 mg) were weighed into a Schlenk tube and dissolved in 15 mL of dichloromethane. After stirring overnight, the mixture was filtered, and the solvent removed *in vacuo*. The residue was dissolved in 1 mL of hot acetonitrile and stored at 4 °C to give **68** as colorless blocks. **Yield:** 61 mg (34 %); **m.p.:** 204.7 °C (dec.); **elemental analysis [wt-%]:** calcd. for $C_{72}H_{58}Ag_{0.65}Au_{0.35}F_6N_2Sb_5$: C 47.7, H 3.22, N 1.55. found: C 48.1, H 3.15, N 1.59; **^{1}H NMR (400.1 MHz, 297 K, CD_2Cl_2) δ [ppm]:** 8.11 (dd, $^3J_{HH}$ = 8.17 Hz, $^4J_{HH}$ = 1.14 Hz, 1 H, Naph-2,7-*H*), 8.09 (dd, $^3J_{HH}$ = 8.23 Hz, $^4J_{HH}$ = 1.14 Hz, 1 H, **66,** Naph-2,7-*H*), 7.77 (dd, $^3J_{HH}$ = 7.14 Hz, $^4J_{HH}$ = 1.32 Hz, 1 H, Naph-4,5-*H*), 7.74 (dd, $^3J_{HH}$ = 7.14 Hz, $^4J_{HH}$ = 1.21 Hz, 1 H, **66**, Naph-4,5-*H*) 7.46 (q, $^3J_{HH}$ = 7.68 Hz, 2 H, **66** and **68**, Naph-3,6-*H*), 7.37 (m, 4 H, Ph-*p*-*H*, **66** and **68**, 4 H), 7.14 (m, 8 H, **66** and **68**, Ph-*o*-*H*), 7.08 (m, 8 H, **66** and **68**, Ph-*m*-*H*), 1.98 (s, 3 H, C*H*$_3$CN); **^{13}C{^{1}H} NMR (100.6 MHz, 297 K, CD_2Cl_2) δ [ppm]:** 143.02 (Naph-1,8-*C*), 142.32 (**66**, Naph-1,8-*C*), 140.68 (**66**, Naph-3,6-*C*H), 139.98 (Naph-3,6-*C*H), 137.47 (Naph-9-*C*), 137.20 (**66**, Naph-9-*C*), 135.87 (**66**, Ph-*o*-*C*H), 135.41 (Ph-*o*-*C*H), 134.29 (Ph-*ipso*-*C*), 133.96 (Naph-2,7-*C*H), 133.80 (**66**), 131.34 (**66**, Naph-10-*C*), 131.31 (Naph-10-*C*), 130.95 (Ph-*p*-*C*H), 130.83 (**66**, Ph-*p*-*C*H), 130.19 (**66**, Ph-*m*-*C*H), 130.15 (Ph-*m*-*C*H), 126.50 (**66**, Naph-4,5-*C*H), 126.32 (Naph-4,5-*C*H), 117.02 (CH$_3$*C*N), 2.08 (*C*H$_3$CN); **^{19}F NMR (282.4 MHz, 297 K, CD_2Cl_2) δ [ppm]:** –111.68, –114.83, –116.92, –120.35, –122.05, –123.15, –126.02, –127.22, –128.74, –131.55, –132.30, –134.35, –137.47; **IR ν [cm^{-1}]**: 3054 (w), 2248 (w), 1576 (w), 1477 (w), 1431 (m), 1370 (w), 1349 (w), 1329 (w), 1307 (w), 1263 (w), 1243 (w), 1183 (w), 1155 (w), 1064 (m), 1018 (w), 997 (m), 954 (w), 918 (w), 842 (w), 819 (m), 770 (m), 730 (s), 692 (s), 652 (s), 549 (w), 521 (w), 451 (m).

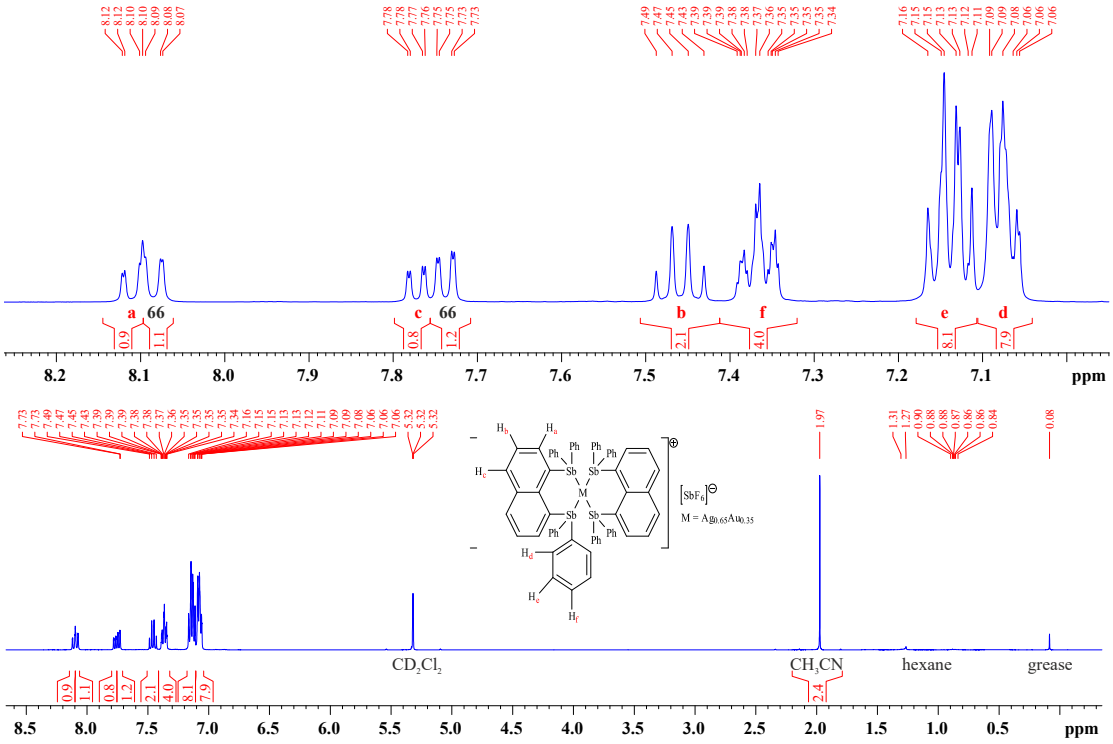

Figure E27. ^{1}H NMR spectrum of {[(Ph$_2$Sb)$_2$Naph]$_2$"Au"}[SbF$_6$] (**68**) in CD$_2$Cl$_2$.

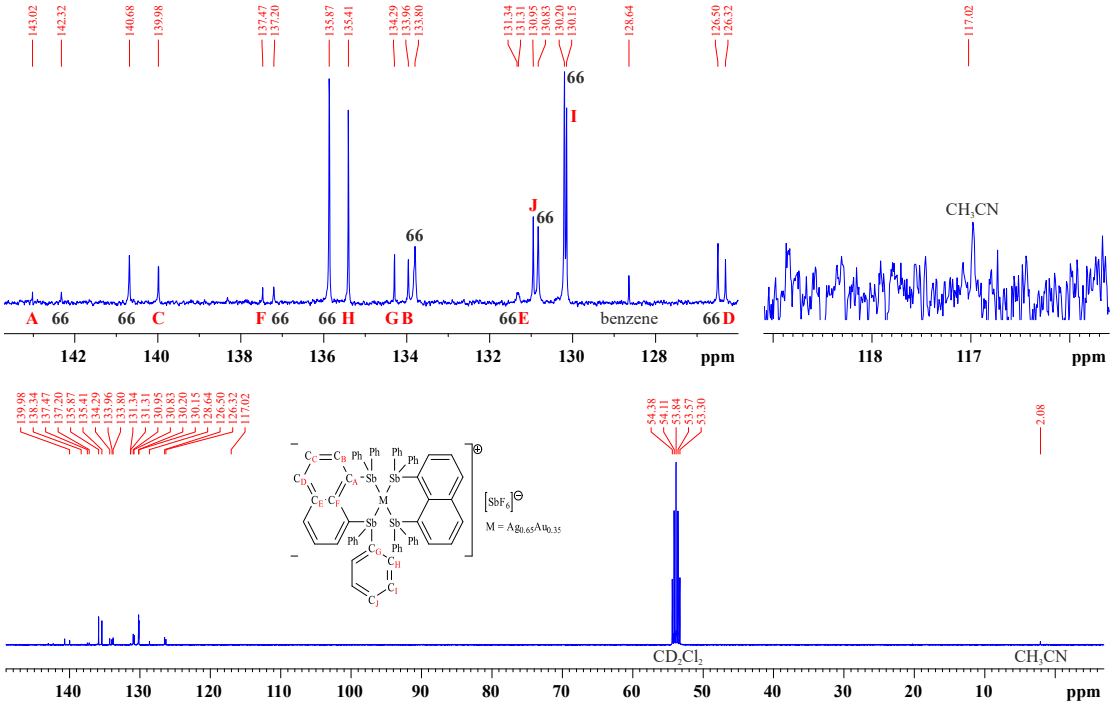

Figure E28. ^{13}C{^{1}H} NMR spectrum of {[(Ph$_2$Sb)$_2$Naph]$_2$"Au"}[SbF$_6$] (**68**) in CD$_2$Cl$_2$.

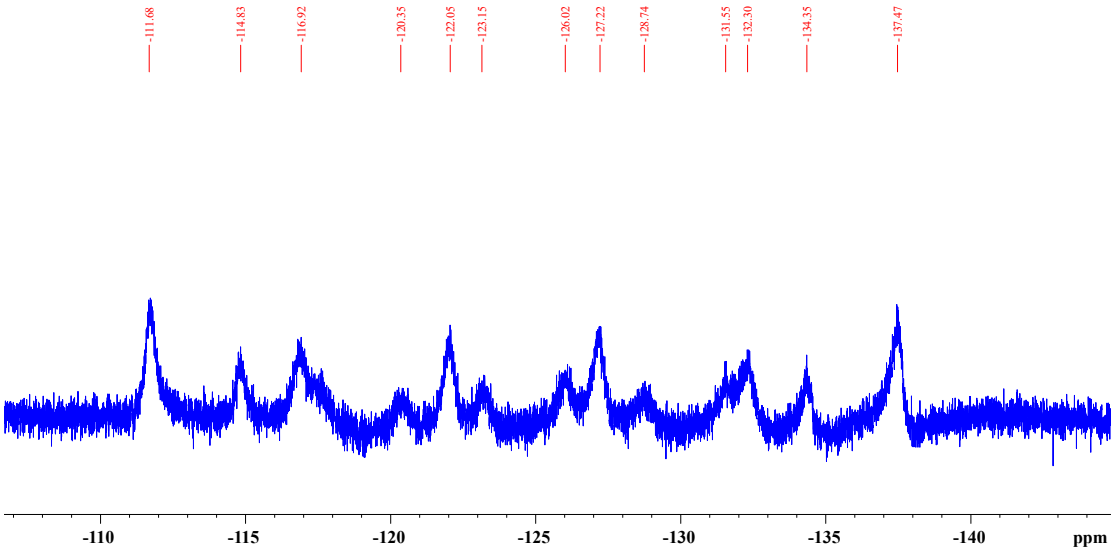

Figure E29. ^{19}F NMR spectrum of {[$(Ph_2Sb)_2Naph]_2$"Au"}[SbF_6] (**68**) in CD_2Cl_2.

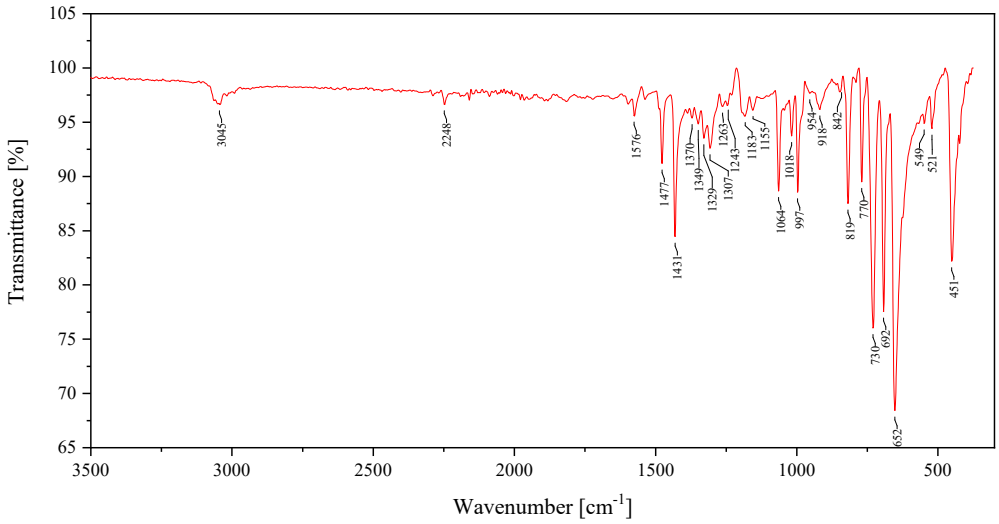

Figure E30. IR spectrum of neat {[$(Ph_2Sb)_2Naph]_2$"Au"}[SbF_6] (**68**).

7.2.6. Synthesis of 1,8-Bis(bis(2,4,6-tri-iso-propylphenyl)stiba-(III))naphthalene (**69**)

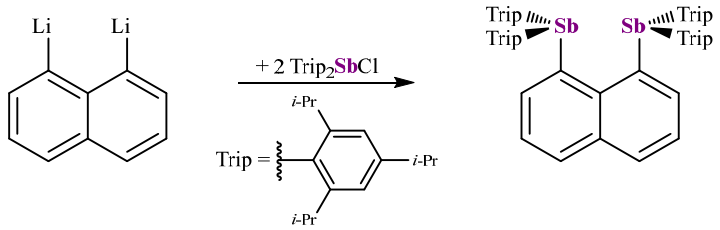

Li_2Naph (2 mmol, 369.8 mg) and $Trip_2SbCl$ (4 mmol, 2.29 g) were weighed into a Schlenk tube and dissolved in 20 mL of thf each. The solutions were cooled to –78 °C and united giving a yellow reaction mixture. After stirring overnight, the volatiles were removed *in vacuo* and 20 mL of degassed water was added. The mixture was stirred for 30 minutes after which the water was removed by filtration and the residue dried *in vacuo*. Washing with ethanol (2 x 15 mL) and removing all volatiles *in vacuo* gave **69** as a yellow powder. **Yield:** 1.565 g (65 %); **m.p.:** 265.8 °C; **elemental analysis [wt-%]:** calcd. for $C_{70}H_{98}Sb_2$: C 71.1, H 8.35. found: C 70.7, H 8.43; **^{1}H NMR (400.1 MHz, 297 K, CD_2Cl_2): δ [ppm]** 8.16 (dd, $^3J_{HH}$ = 6.95 Hz, $^4J_{HH}$ = 1.07 Hz, 2 H, Naph-2,7-*H*), 7.86 (dd, $^3J_{HH}$ = 8.15 Hz, $^4J_{HH}$ = 1.26 Hz, 2 H, Naph-4,5-*H*), 7.31 (dd, $^3J_{HH}$ = 7.96 Hz, $^3J_{HH}$ = 7.04 Hz, 2 H, Naph-3,6-*H*), 6.91 (s (br), 8 H, Ph-*m*-*H*), 3.70 (s (br), 2 H, *o*-C*H*$(CH_3)_2$), 3.41 (s (br), 2 H, *o*-C*H*$(CH_3)_2$), 2.80 (s (br), 6 H, *o/p*-C*H*$(CH_3)_2$), 2.53 (s (br), 2 H, *o*-C*H*$(CH_3)_2$), 1.19 (d, $^3J_{HH}$ = 6.61 Hz, 36 H, *o/p*-CH(C*H*$_3)_2$), 0.96 (s (br), 12 H, *o*-CH(C*H*$_3)_2$), 0.45 (s (br), 12 H, *o*-CH(C*H*$_3)_2$), 0.19 (s (br), 12 H, *o*-CH(C*H*$_3)_2$); **^{13}C{^{1}H} NMR (100.6 MHz, 297 K, CD_2Cl_2): δ [ppm]** 156.27 (br), 154.96 (br), 150.41 (br), 148.85 (br), 143.53, 143.30, 139.59 (Naph-2,7-*C*H), 137.26 (br), 136.94, 130.81 (Naph-4,5-*C*H), 125.12 (Naph-3,6-*C*H), 123.21 (br, Ph-*m*-*C*H), 122.22 (br, Ph-*m*-*C*H), 37.97 (br), 36.59 (br, *o*-*C*H$(CH_3)_2$), 34.93 (br, *o*-*C*H$(CH_3)_2$), 34.55 (*o/p*-*C*H$(CH_3)_2$), 26.05 (br, *o*-CH(*C*H$_3)_2$), 25.00 (br), 24.66 (br, *o*-CH(*C*H$_3)_2$), 24.22 (*o/p*-CH(*C*H$_3)_2$), 24.16 (*o*-CH(*C*H$_3)_2$), 23.21 (br, *o*-CH(*C*H$_3)_2$); **^{1}H NMR (300.1 MHz, 232 K, CD_2Cl_2): δ [ppm]** 8.08 (d, $^3J_{HH}$ = 6.78 Hz, 2 H, Naph-2,7-*H*), 7.84 (d, $^3J_{HH}$ = 7.63 Hz, 2 H, Naph-4,5-*H*), 7.29 (t, $^3J_{HH}$ = 7.38 Hz, 2 H, Naph-3,6-*H*), 6.98 (s, 2 H, Ph^1-*m*-*H*), 6.93 (s, 2 H, Ph^1-*m*-*H*), 6.79 (s, 2 H, Ph^2-*m*-*H*), 6.76 (s, 2 H, Ph^2-*m*-*H*), 3.63 (sept, $^3J_{HH}$ = 6.55 Hz, 2 H, Ph^1-*o*-C*H*$(CH_3)_2$), 3.31 (sept, $^3J_{HH}$ = 6.24 Hz, 2 H, Ph^2-*o*-C*H*$(CH_3)_2$), 2.85-2.65 (m, 6 H, Ph-*o/p*-C*H*$(CH_3)_2$), 2.48 (sept, $^3J_{HH}$ = 6.55 Hz, 2 H, Ph^2-*o*-C*H*$(CH_3)_2$), 1.16-1.10 (m, 36 H, Ph-*o/p*-CH(C*H*$_3)_2$), 0.92-0.89 (m, 12 H, Ph^1-*o*-CH(C*H*$_3)_2$), 0.38 (d, $^3J_{HH}$ = 6.69 Hz, 6 H, Ph^2-*o*-CH(C*H*$_3)_2$), 0.31 (d, $^3J_{HH}$ = 6.23 Hz, 6 H, Ph^2-*o*-CH(C*H*$_3)_2$), 0.20 (d, $^3J_{HH}$ = 6.46 Hz, 6 H, Ph^2-*o*-

CH(CH_3)$_2$), 0.02 (d, $^3J_{HH}$ = 6.23 Hz, 6 H, Ph^1-*o*-CH(CH_3)$_2$); **^{13}C{^{1}H} NMR (75.5 MHz, 232 K, CD_2Cl_2): δ [ppm]** 155.55 (Ph^1-*o*-*C*), 155.11 (Ph^2-*o*-*C*), 154.13 (Ph^1-*o*-*C*), 153.31 (Ph^2-*o*-*C*), 149.83 (Ph-*p*-*C*), 148.03 (Ph-*p*-*C*), 142.66 (Naph-1,8-*C*), 142.27 (Naph-9-*C*), 142.23 (Ph^1-*ipso*-*C*), 138.80 (Naph-2,7-*C*H), 136.40 (Ph^2-*ipso*-*C*), 136.07 (Naph-10-*C*), 130.27 (Naph-4,5-*C*H), 124.55 (Naph-3,6-*C*H), 122.98 (Ph^1-*m*-*C*H), 122.34 (Ph^1-*m*-*C*H), 121.82 (Ph^2-*m*-*C*H), 121.17 (Ph^2-*m*-*C*H), 37.62 (Ph^1-*o*-*C*H(CH$_3$)$_2$), 36.29 (Ph^2-*o*-*C*H(CH$_3$)$_2$), 36.01 (Ph^2-*o*-*C*H(CH$_3$)$_2$), 34.34 (Ph^2-*o*-*C*H(CH$_3$)$_2$), 34.09 (Ph^1-*p*-*C*H(CH$_3$)$_2$), 33.95 (Ph^2-*p*-*C*H(CH$_3$)$_2$), 25.67 (Ph^2-*o*-CH(*C*H$_3$)$_2$), 25.40 (Ph^1-*o*-CH(*C*H$_3$)$_2$), 24.50 (Ph^1-*o*-CH(*C*H$_3$)$_2$), 24.00 (Ph^1-*o*-CH(*C*H$_3$)$_2$), 23.96 (Ph-*p*-CH(*C*H$_3$)$_2$), 23.81 (Ph-*p*-CH(*C*H$_3$)$_2$), 23.75 (Ph^2-*o*-CH(*C*H$_3$)$_2$), 22.72 (Ph^2-*o*-CH(*C*H$_3$)$_2$), 22.31 (Ph^1-*o*-CH(*C*H$_3$)$_2$), 22.26 (Ph^2-*o*-CH(*C*H$_3$)$_2$); **IR ν [cm^{-1}]**: 3033 (w), 2954 (s), 2923 (m), 2864 (m), 1594 (w), 1553 (w), 1535 (w), 1459 (m), 1415 (m), 1380 (m), 1360 (m), 1306 (w), 1258 (m), 1231 (w), 1191 (w), 1155 (w), 1129 (w), 1099 (m), 1066 (m), 1051 (m), 1007 (w), 935 (w), 876 (s), 816 (m), 773 (m), 744 (m), 668 (w), 643 (w), 629 (w), 613 (w), 563 (w), 511 (m), 470 (w), 450 (w), 433 (w), 395 (m).

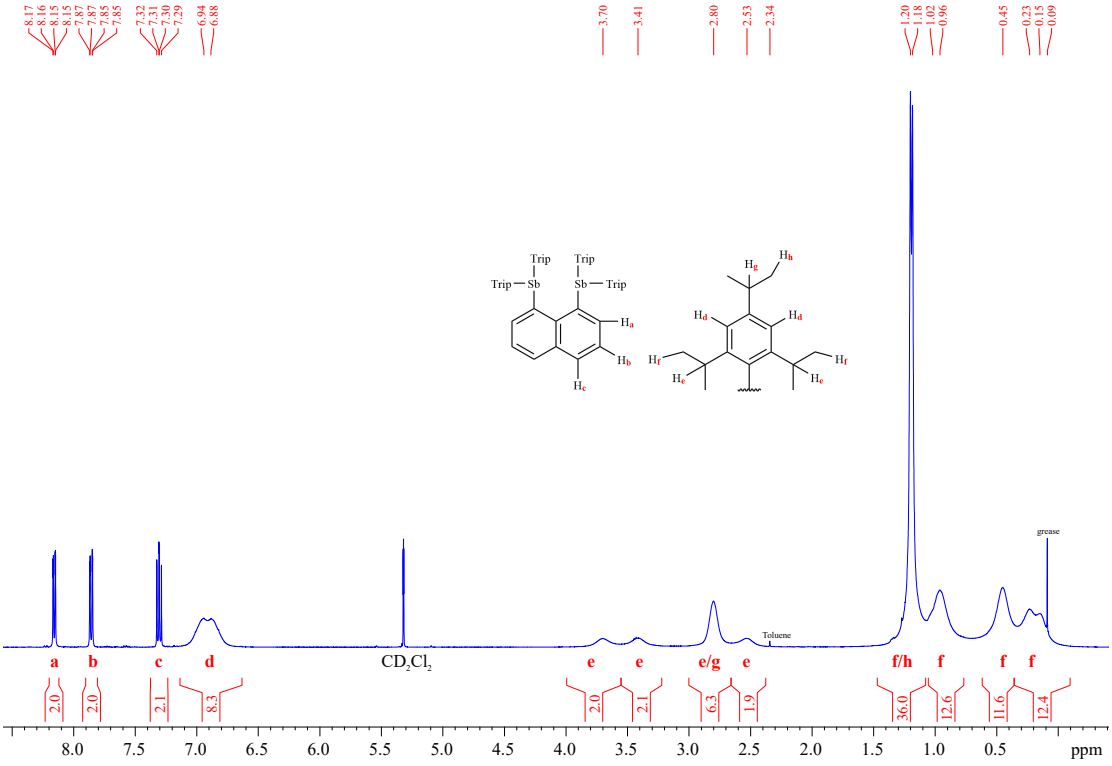

Figure E31. ^{1}H NMR spectrum of (Trip$_2$Sb)$_2$Naph (**69**) in CD_2Cl_2.

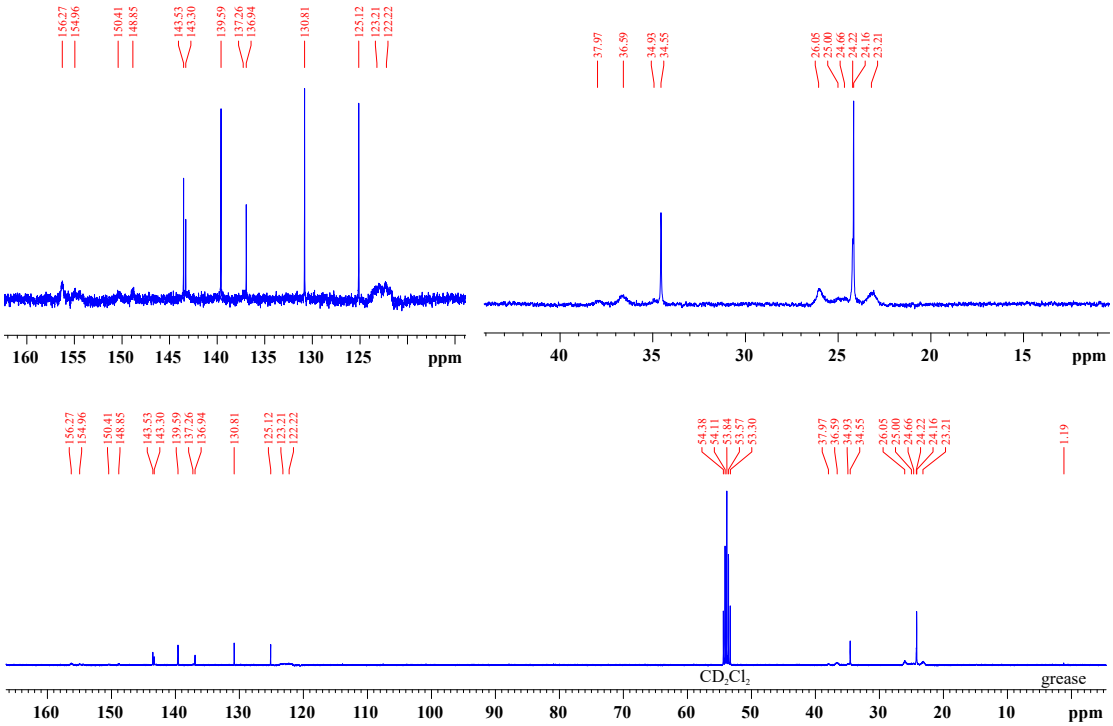

Figure E32. $^{13}C\{^{1}H\}$ NMR spectrum of $(Trip_2Sb)_2Naph$ (**69**) in CD_2Cl_2.

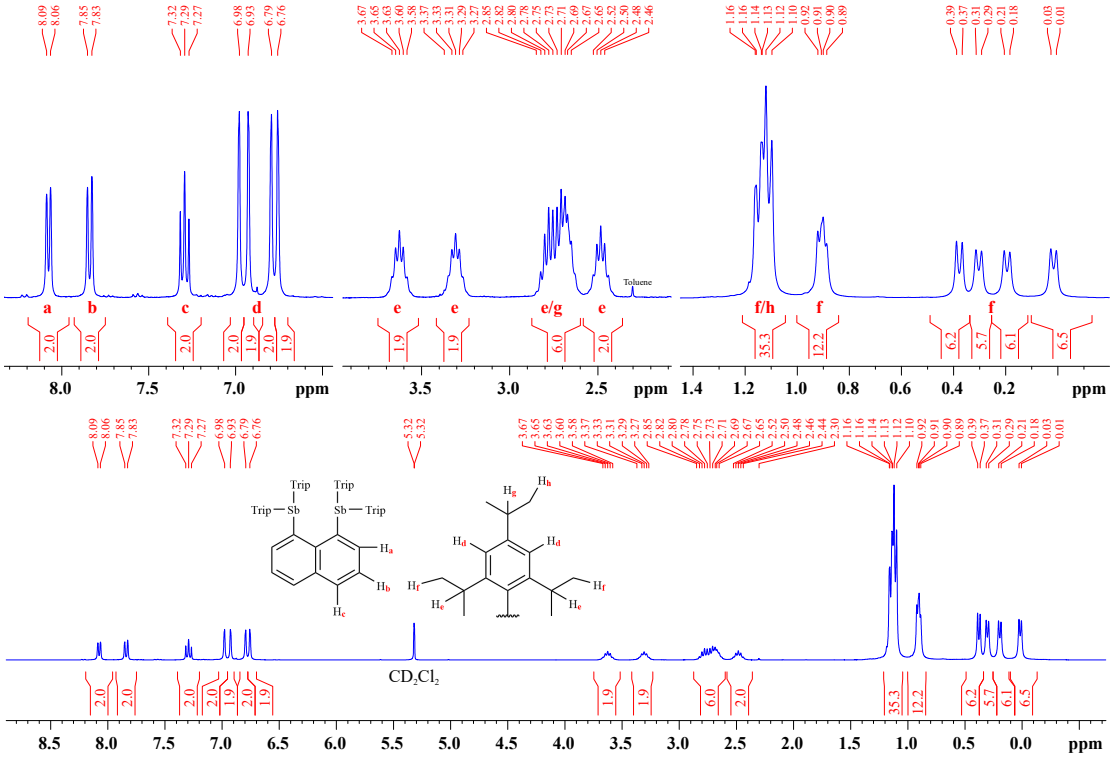

Figure E33. ^{1}H NMR spectrum of $(Trip_2Sb)_2Naph$ (**69**) in CD_2Cl_2.

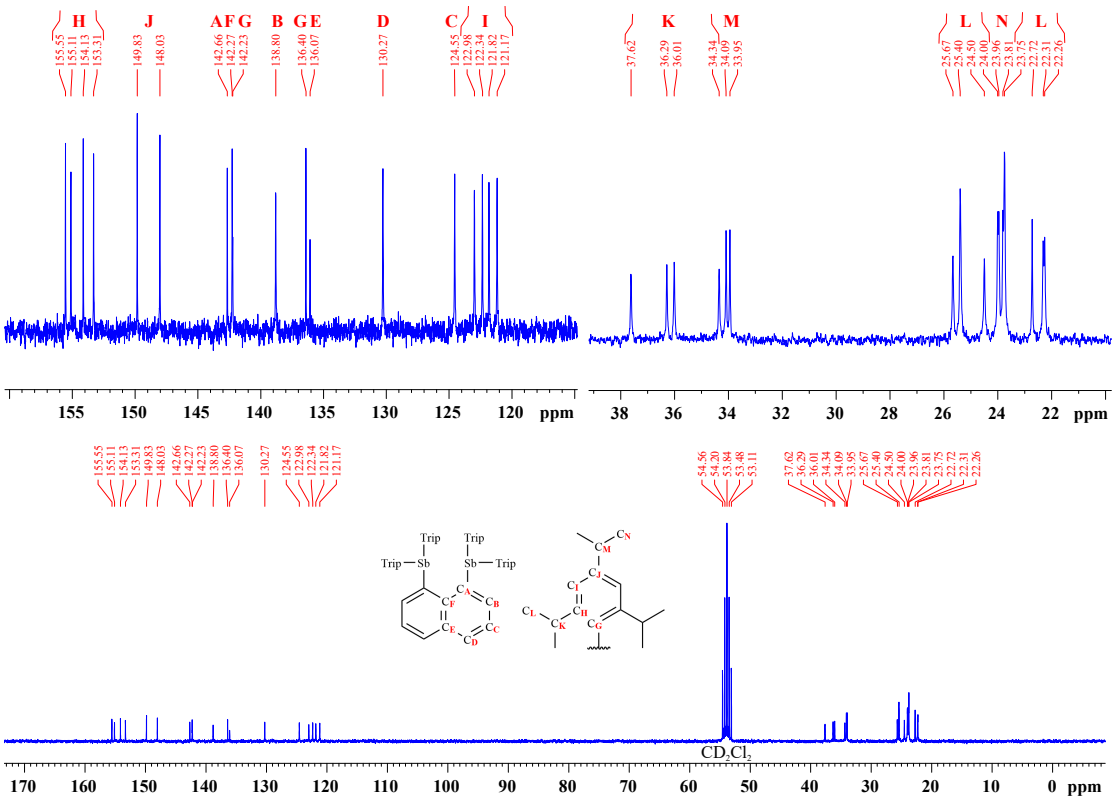

Figure E34. $^{13}C\{^{1}H\}$ NMR spectrum of $(Trip_2Sb)_2Naph$ (**69**) in CD_2Cl_2 at –40 °C.

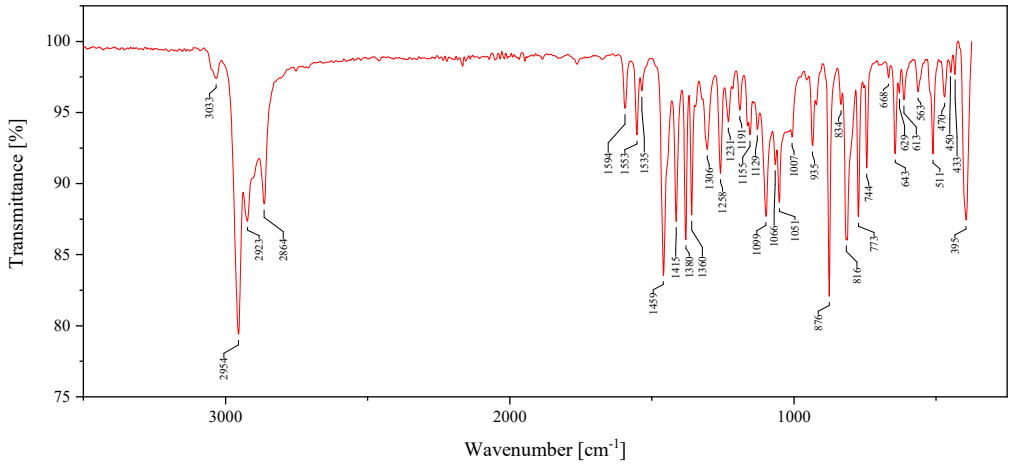

Figure E35. IR spectrum of neat $(Trip_2Sb)_2Naph$ (**69**).

7.2.1. Synthesis of 1,8-Bis(bis(2,4,6-tri-iso-propylphenyl)bisma-(III))naphthalene (**70**)

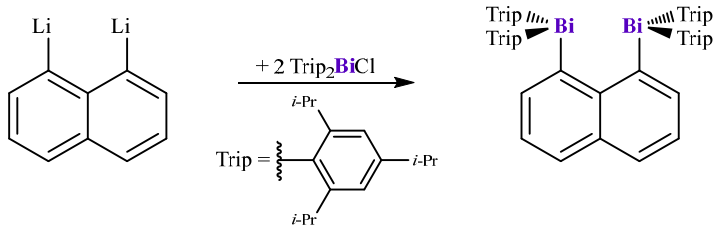

Li_2Naph (1.99 mmol, 362 mg) and $Trip_2$BiCl (2.00 mmol, 1.3 g) were weighed into a Schlenk tube, dissolved in 20 mL of thf each, and cooled to –30 °C. The yellow solution of $Trip_2$BiCl was added to Li_2Naph and stirred overnight. The reaction mixture was dried *in vacuo* and 25 mL of water were added. After the mixture was stirred for 30 minutes the solution was removed by filtration and the residue dried *in vacuo*. The solid was extracted with toluene and the resulting solution concentrated to 2 mL. Ethanol (10 mL) was added giving a precipitate, which was dissolved in the heat. Storage of the solution at 4 °C resulted in yellow crystals of **70**. **Yield:** 754.8 mg (56 %); **m.p.:** 249.6 °C (dec.); **elemental analysis [wt-%]:** calcd. for $C_{70}H_{98}Bi_2$: C 61.93, H 7.28. found: C 62.0, H 7.22; **^{1}H NMR (400.1 MHz, 297 K, CD_2Cl_2) δ [ppm]:** 8.87 (dd, $^3J_{HH}$ = 6.88 Hz, $^4J_{HH}$ = 0.96 Hz, 2 H, Naph-2,7-C*H*), 7.88 (dd, $^3J_{HH}$ = 7.96 Hz, $^4J_{HH}$ = 0.93 Hz, 2 H, Naph-4,5-C*H*), 7.27 (t, $^3J_{HH}$ = 7.41 Hz, 2 H, Naph-3,6-C*H*), 7.07 (s, 8 H, Ph-*m*-*H*), 2.93 (sept, $^3J_{HH}$ = 6.45 Hz, 8 H, *o*-C*H*$(CH_3)_2$), 2.80 (sept, $^3J_{HH}$ = 6.94 Hz, 4 H, *p*-C*H*$(CH_3)_2$), 1.20 (d, $^3J_{HH}$ = 7.01 Hz, 24 H, *p*-CH(C*H*$_3)_2$), 0.81 (d, $^3J_{HH}$ = 6.42 Hz, 24 H, *o*-CH(C*H*$_3)_2$), 0.70 (d, $^3J_{HH}$ = 4.67 Hz, 24 H, *o*-CH(C*H*$_3)_2$); **^{13}C{^{1}H} NMR (100.6 MHz, 297 K, CD_2Cl_2) δ [ppm]:** 160.75 (Naph-*ipso*-*C*), 156.17 (Trip-*ipso*/*o*-*C*), 149.12 (Trip-*p*-*C*), 145.71 (Naph-10-*C*), 143.89 (Naph-2,7-*C*H), 139.26 (Naph-9-*C*), 129.98 (Naph-4,5-*C*H), 127.71 (Naph-3,6-*C*H), 123.67 (Ph-*m*-*C*H), 39.30 (*o*-*C*H$(CH_3)_2$), 34.60 (*p*-*C*H$(CH_3)_2$), 25.12 (*o*-CH(*C*H$_3)_2$), 24.42 (*o*-CH(*C*H$_3)_2$), 24.21 (*p*-CH(*C*H$_3)_2$), 24.14 (*p*-CH(*C*H$_3)_2$); **IR ν [cm^{-1}]**: 3015 (w), 2947 (s), 2914 (m), 2890 (m), 2855 (m), 1582 (w), 1549 (w), 1523 (w), 1453 (m), 1408 (m), 1375 (m), 1355 (m), 1302 (w), 1254 (w), 1226 (w), 1187 (w), 1152 (w), 1126 (w), 1093 (m), 1048 (m), 990 (m), 935 (w), 872 (m), 833 (w), 806 (m), 764 (m), 734 (m), 640 (w), 550 (w), 550 (w), 507 (w), 471 (w), 448 (w).

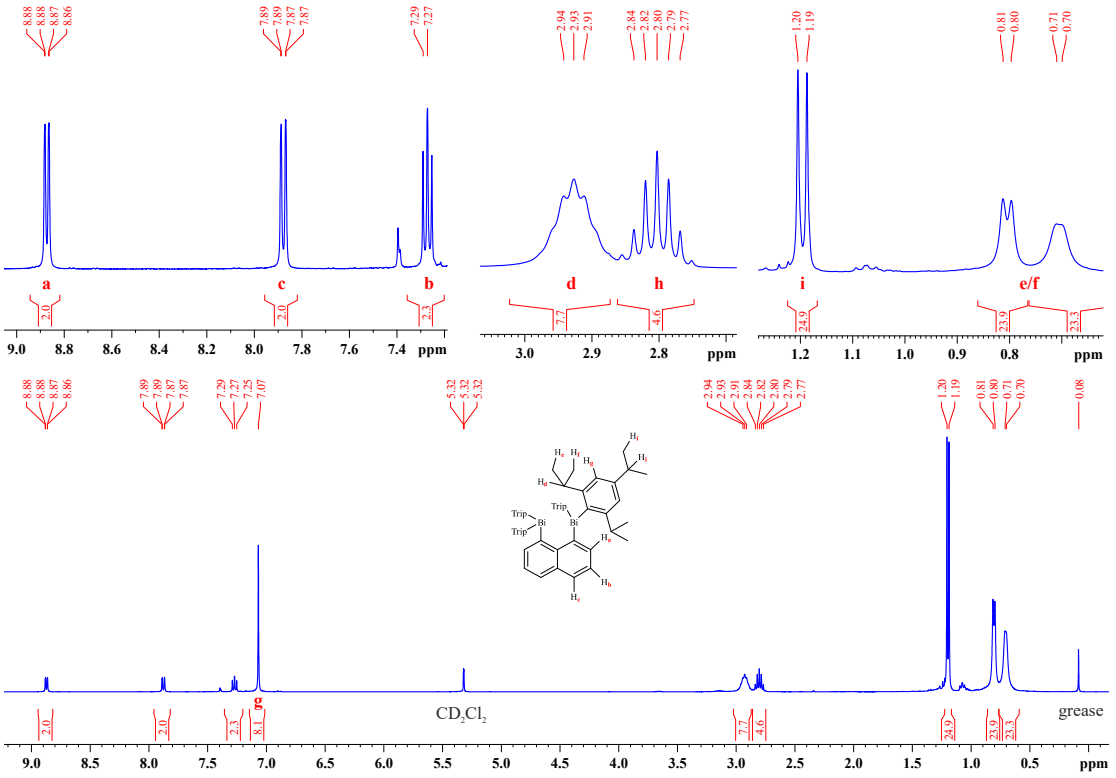

Figure E36. ^{1}H NMR spectrum of (Trip$_2$Bi)$_2$Naph (**70**) in CD_2Cl_2.

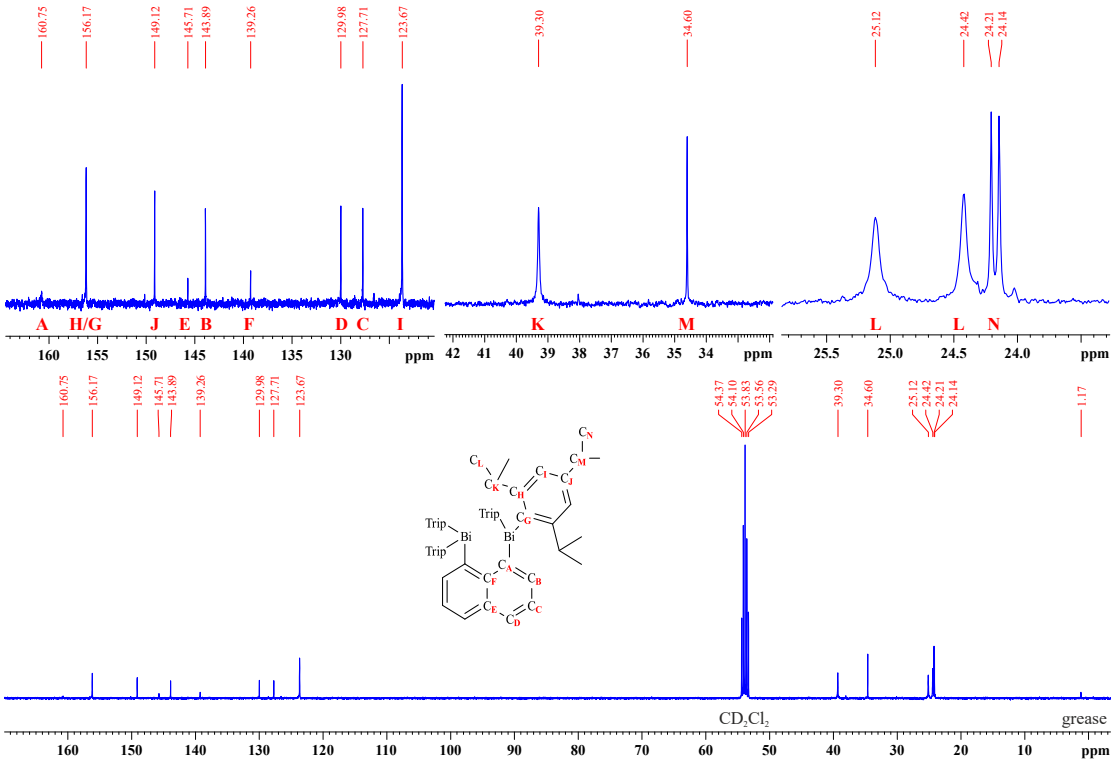

Figure E37. ^{13}C{^{1}H} NMR spectrum of (Trip$_2$Bi)$_2$Naph (**70**) in CD_2Cl_2.

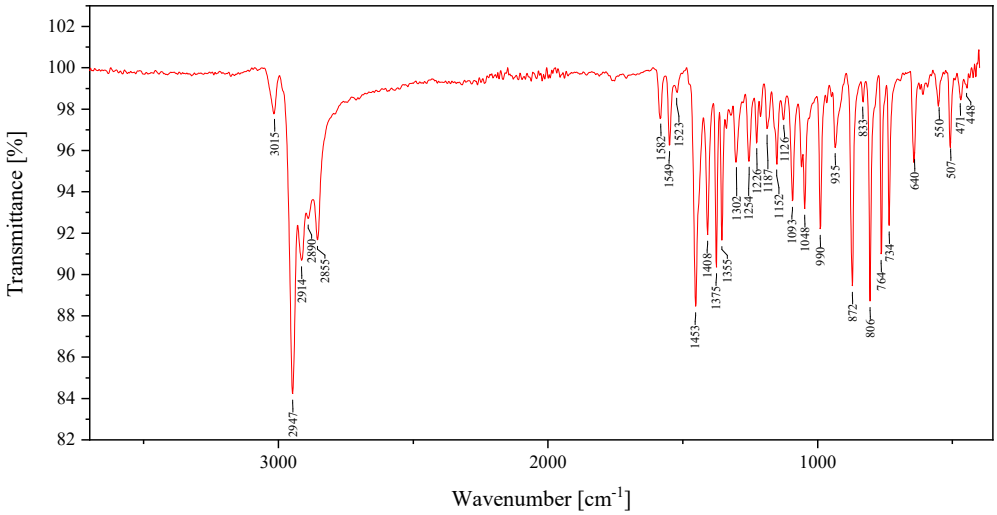

Figure E38. IR spectrum of neat $(Trip_2Bi)_2Naph$ (**70**).

7.2.2. Synthesis of 1-(2,4,6-tri-iso-propylphenyl)stibenium-(III)-8-bis(2,4,6-tri-iso-propylphenyl)stiba-(III)naphthalene tetrakis(pentafluorophenyl)borat (**76**)

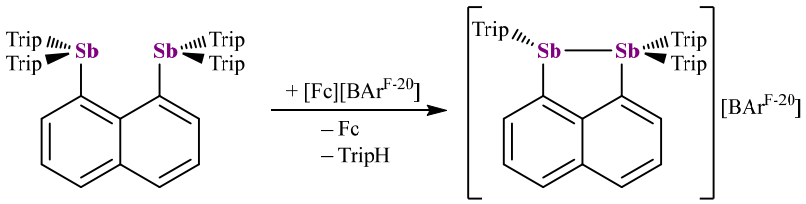

69 (0.8 mmol, 1 g) and [Fc][$BAr^{F\text{-}20}$] (0.8 mmol, 723 mg) were each weighed into a Schlenk tube and dissolved in 30 mL of thf. The solutions were cooled to –78 °C and the solution of [Fc][$BAr^{F\text{-}20}$] was added to **69** turning the reaction mixture deep purple. The mixture was stirred overnight and the solvent removed *in vacuo*. The oily residue was washed with *n*-hexane until the hexane solution stayed colorless after which further 50 mL of hexane were added. The mixture was stirred at 60 °C overnight and the solution removed by filtration. Drying *in vacuo* gave **71** as a green powder. Crystals suitable for single X-ray diffractometry were obtained by dissolving 100 mg of **71** in 2 mL of DCM, which was layered with 30 mL of *n*-hexane. Storage for a week at 4 °C resulted in green blocks of **71**. **Yield:** 1.325 g (84 %); **m.p.:** 106.0 °C; **elemental analysis [wt-%]:** calcd. for $C_{79}H_{75}BF_{20}Sb_2$: C 57.21, H 4.56. found: C 56.5, H 4.22; **^{1}H NMR (400.1 MHz, 297 K, CD_2Cl_2): δ [ppm]** 8.21 (d, $^3J_{HH}$ = 8.43 Hz, 1 H, Naph-*H*), 8.11-8.06 (m, 3 H, Naph-*H*), 7.77 (dd, $^3J_{HH}$ = 8.05 Hz, $^3J_{HH}$ = 7.21 Hz, 1 H, Naph-*m*-*H*), 7.70 (dd, $^3J_{HH}$ = 8.26 Hz, $^3J_{HH}$ = 6.95 Hz, 1 H, Naph-*m*-C*H*), 7.17 (s, 2 H, Ph-*m*-*H*), 7.09 (s (br), 2 H, Ph-*m*-*H*), 7.06 (s, 2 H, Ph-*m*-*H*), 3.82 (s (br), 1 H, *o*-C*H*(CH_3)$_2$), 2.90 (sept, $^3J_{HH}$ = 6.85 Hz, 1 H, *p*-C*H*(CH_3)$_2$), 2.84 (sept, $^3J_{HH}$ = 6.91 Hz, 2 H, *p*-C*H*(CH_3)$_2$), 2.68 (sept, $^3J_{HH}$ = 6.58 Hz, 2 H, *o*-C*H*(CH_3)$_2$), 2.58 (sept, $^3J_{HH}$ = 6.58 Hz, 2 H, *o*-C*H*(CH_3)$_2$), 2.00 (s (br), 1 H, *o*-CH(C*H*$_3$)$_2$), 1.47 (s (br), 6 H, *o*-CH(C*H*$_3$)$_2$) 1.21-1.16 (m, 18 H, *p*-CH(C*H*$_3$)$_2$), 0.97 (d, $^3J_{HH}$ = 6.75 Hz, 6 H, *o*-CH(C*H*$_3$)$_2$), 0.91 (d, $^3J_{HH}$ = 6.51 Hz, 6 H, *o*-CH(C*H*$_3$)$_2$), 0.68 (d, $^3J_{HH}$ = 6.51 Hz, 6 H, *o*-CH(C*H*$_3$)$_2$), 0.64 (d, $^3J_{HH}$ = 6.75 Hz, 6 H, *o*-CH(C*H*$_3$)$_2$), 0.25 (s (br), 6 H, *o*-CH(C*H*$_3$)$_2$); **^{11}B NMR (128.4 MHz, 297 K, CD_2Cl_2): δ [ppm]** –16.75 (s); **^{13}C{^{1}H} NMR (100.6 MHz, 297 K, CD_2Cl_2): δ [ppm]** 157.63 (br), 155.81 (Trip-*C*), 154.89 (Trip-*C*), 154.35 (Trip-*C*), 153.87 (Trip-*C*), 153.63 (Trip-*C*), 149.79 (br, Trip-*C*), 147.35 (br, Trip-*C*), 142.35 (Naph-*ipso*-*C*), 141.11 (Naph-*C*), 140.12 (Naph-*ipso*-*C*), 139.86 (br, Trip-*C*), 138.43 (Naph-*CH*), 137.87 (br, Trip-*C*), 137.37 (Naph-10-*C*), 136.03 (Naph-*C*H), 135.47 (br, Trip-*C*), 134.54 (Naph-*C*H), 134.32, 132.36 (Naph-

*C*H), 128.45 (Trip-*C*), 128.0 (Trip-*C*), 127.93 (Naph-3/5-*C*H), 127.85 (Naph-3/5-*C*H), 125.91 (Trip-*m*-*C*), 125.31 (Trip-*m*-*C*H), 124.07 (Trip-*m*-*C*H), 40.39 (*o*-C*H*(CH_3)$_2$), 38.73 (*o*-C*H*(CH_3)$_2$), 37.26 (*o*-C*H*(CH_3)$_2$), 34.78 (*p*-C*H*(CH_3)$_2$), 34.69 (*p*-C*H*(CH_3)$_2$), 34.54 (*p*-C*H*(CH_3)$_2$), 25.05 (*o*-CH(C*H*$_3$)$_2$), 24.46 (*o*-CH(C*H*$_3$)$_2$), 23.96 (*o*-CH(C*H*$_3$)$_2$), 23.83 (*p*-CH(C*H*$_3$)$_2$), 23.72 (*p*-CH(C*H*$_3$)$_2$), 23.68 (*p*-CH(C*H*$_3$)$_2$), 23.07 (br, *o*-CH(C*H*$_3$)$_2$), 14.28 (br, *o*-CH(C*H*$_3$)$_2$); **^{19}F NMR (376.5 MHz, 297 K, CD_2Cl_2): *δ* [ppm]** –133.26 (br-s, 2 F, BAr^F-*o/m*-C*F*), –163.84 (t, $^3J_{FF}$ = 20.55 Hz, 1 F, BAr^F-*p*-C*F*), –167.72 (br-t, $^3J_{FF}$ = 18.19 Hz, 2 F, BAr^F-*o/m*-C*F*); **^{1}H NMR (300.1 MHz, 242 K, CD_2Cl_2): *δ* [ppm]** 8.18 (d, $^3J_{HH}$ = 7.98 Hz, 1 H, Naph-*H*), 8.09-8.04 (m, 3 H, Naph-*H*), 7.76 (dd, $^3J_{HH}$ = 7.91 Hz, $^3J_{HH}$ = 7.38 Hz, 1 H, Naph-*m*-*H*), 7.68 (dd, $^3J_{HH}$ = 8.17 Hz, $^3J_{HH}$ = 6.81 Hz, 1 H, Naph-*m*-*H*), 7.16 (d, $^4J_{HH}$ = 1.61 Hz, 1 H, Sb^+-Ph-*m*-*H*), 7.12 (s, 2 H, Ph-*m*-*H*), 7.00 (s, 2 H, Ph-*m*-*H*), 7.00 (s, 2 H, Ph-*m*-*H*), 6.89 (d, $^4J_{HH}$ = 1.37 Hz, 1 H, Ph-*m*-*H*), 3.72 (sept, $^3J_{HH}$ = 6.57 Hz, 1 H, *o*-C*H*(CH_3)$_2$), 2.85 (sept, $^3J_{HH}$ = 6.72 Hz, 1 H, *p*-CH(CH_3)$_2$), 2.79 (sept, $^3J_{HH}$ = 6.47 Hz, 2 H, *p*-C*H*(CH_3)$_2$), 2.62 (sept, $^3J_{HH}$ = 6.22 Hz, 2 H, *o*-C*H*(CH_3)$_2$), 2.50 (sept, $^3J_{HH}$ = 6.22 Hz, 2 H, *o*-C*H*(CH_3)$_2$), 1.91 (sept, $^3J_{HH}$ = 6.72 Hz, 1 H, *o*-C*H*(CH_3)$_2$), 1.45 (d, $^3J_{HH}$ = 6.29 Hz, 3 H, CH(C*H*$_3$)$_2$), 1.26 (d, $^3J_{HH}$ = 6.29 Hz, 3 H, *o*-CH(C*H*$_3$)$_2$) 1.15-1.09 (m, 18 H, *p*-CH(C*H*$_3$)$_2$), 0.91 (d, $^3J_{HH}$ = 6.71 Hz, 6 H, *o*-CH(C*H*$_3$)$_2$), 0.82 (d, $^3J_{HH}$ = 6.29 Hz, 6 H, *o*-CH(C*H*$_3$)$_2$), 0.63 (d, $^3J_{HH}$ = 6.29 Hz, 6 H, *o*-CH(C*H*$_3$)$_2$), 0.56 (d, $^3J_{HH}$ = 6.71 Hz, 6 H, *o*-CH(C*H*$_3$)$_2$), 0.17 (d, $^3J_{HH}$ = 6.71 Hz, 3 H, *o*-CH(C*H*$_3$)$_2$), 0.12 (d, $^3J_{HH}$ = 6.71 Hz, 3 H, *o*-CH(C*H*$_3$)$_2$); **IR *ν* [cm^{-1}]**: 2955 (w), 2922 (w), 2859 (w), 1637 (w), 1587 (w), 1556 (w), 1506 (m), 1458 (s), 1412 (w), 1381 (w), 1359 (w), 1304 (w), 1255 (m), 1079 (m), 976 (s) 876 (w), 812 (m), 766 (m), 753 (m), 680 (m), 658 (m), 604 (w), 568 (w), 510 (w).

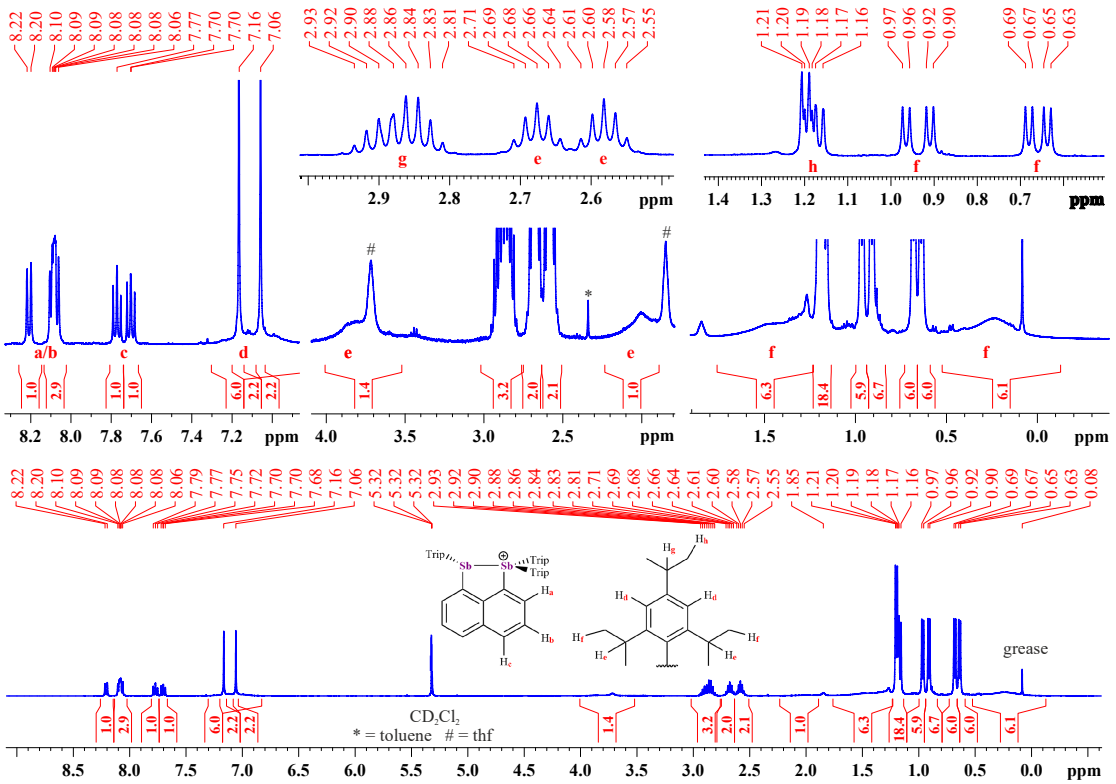

Figure E39. ^{1}H NMR spectrum of [(Trip$_2$Sb)(TripSb)Naph][BAr$^{F\text{-}20}$] (**71**) in CD_2Cl_2. Due to overlap of signals and lack of cross-peaks in 2D NMR spectra, no exact assignment of ^{1}H NMR signals to the corresponding protons could be made.

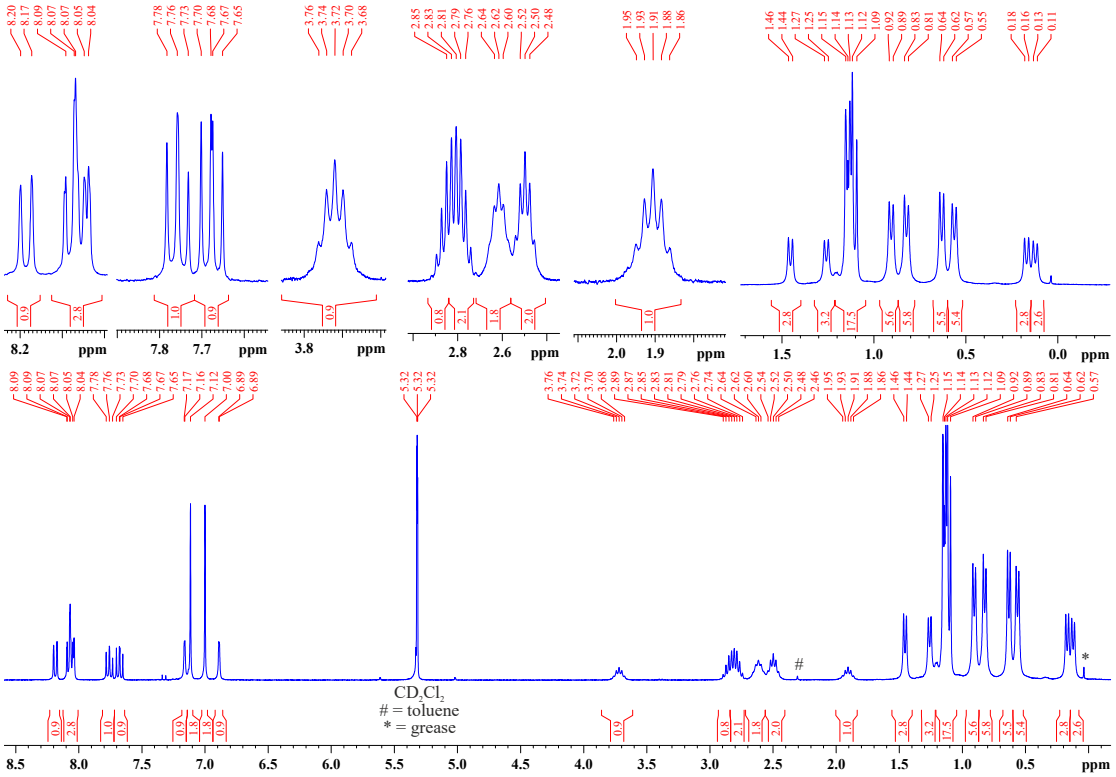

Figure E40. ^{1}H NMR spectrum of [(Trip$_2$Sb)(TripSb)Naph][BAr$^{F\text{-}20}$] (**71**) in CD_2Cl_2 at –30 °C**.** Due to low intensity in ^{13}C{^{1}H} NMR spectra, no clear assignment of ^{1}H NMR to the corresponding protons could be made.

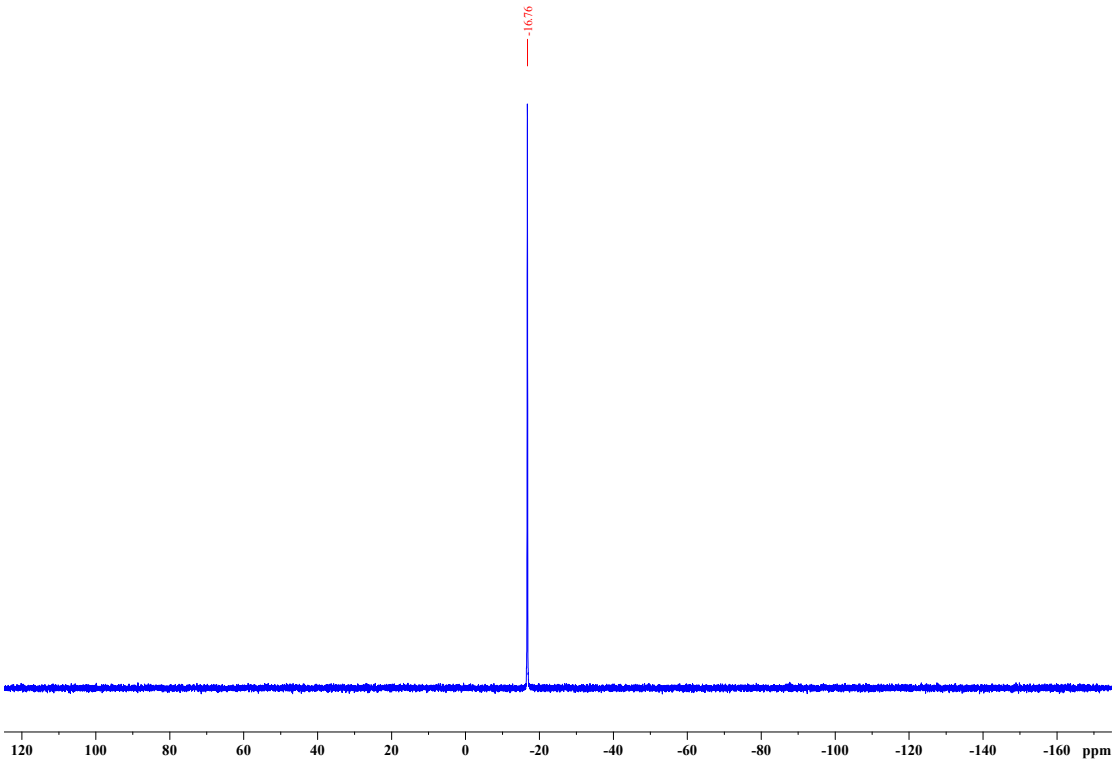

Figure E41. ^{11}B NMR spectrum of [(Trip$_2$Sb)(TripSb)Naph][BAr$^{F\text{-}20}$] (**71**) in CD_2Cl_2.

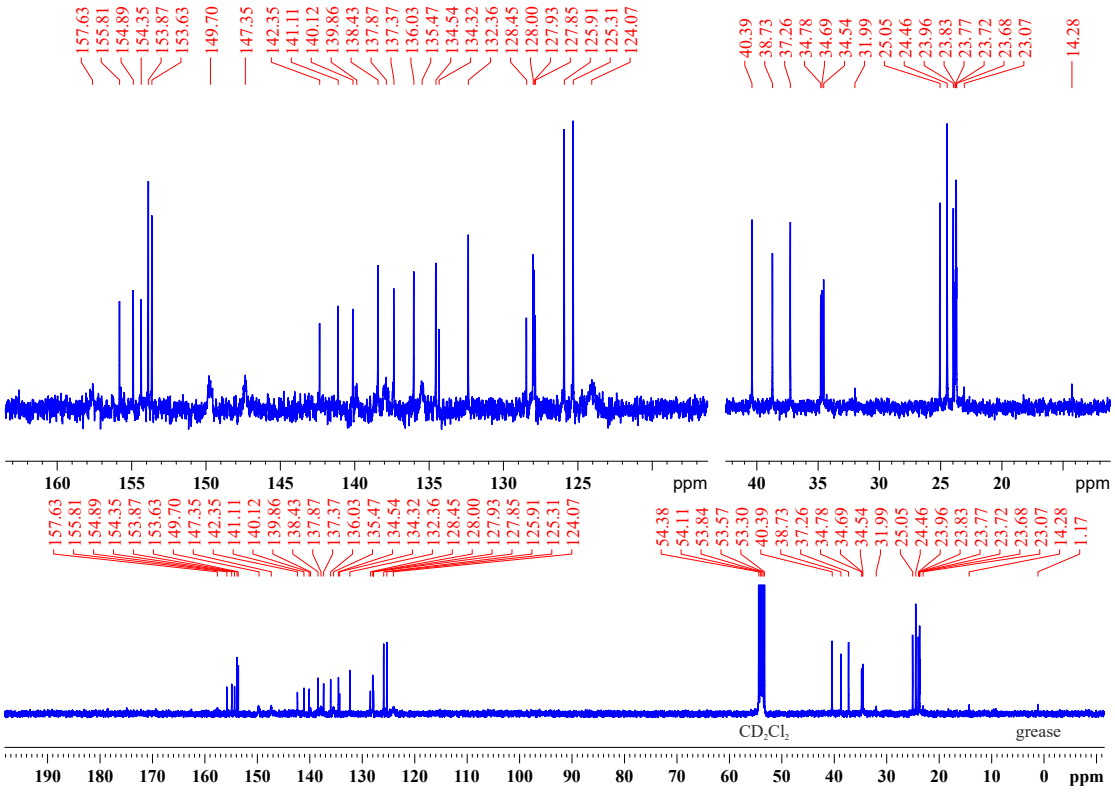

Figure E42. $^{13}C\{^1H\}$ NMR spectrum of [(Trip$_2$Sb)(TripSb)Naph][BAr$^{F\text{-}20}$] (**71**) in CD_2Cl_2.

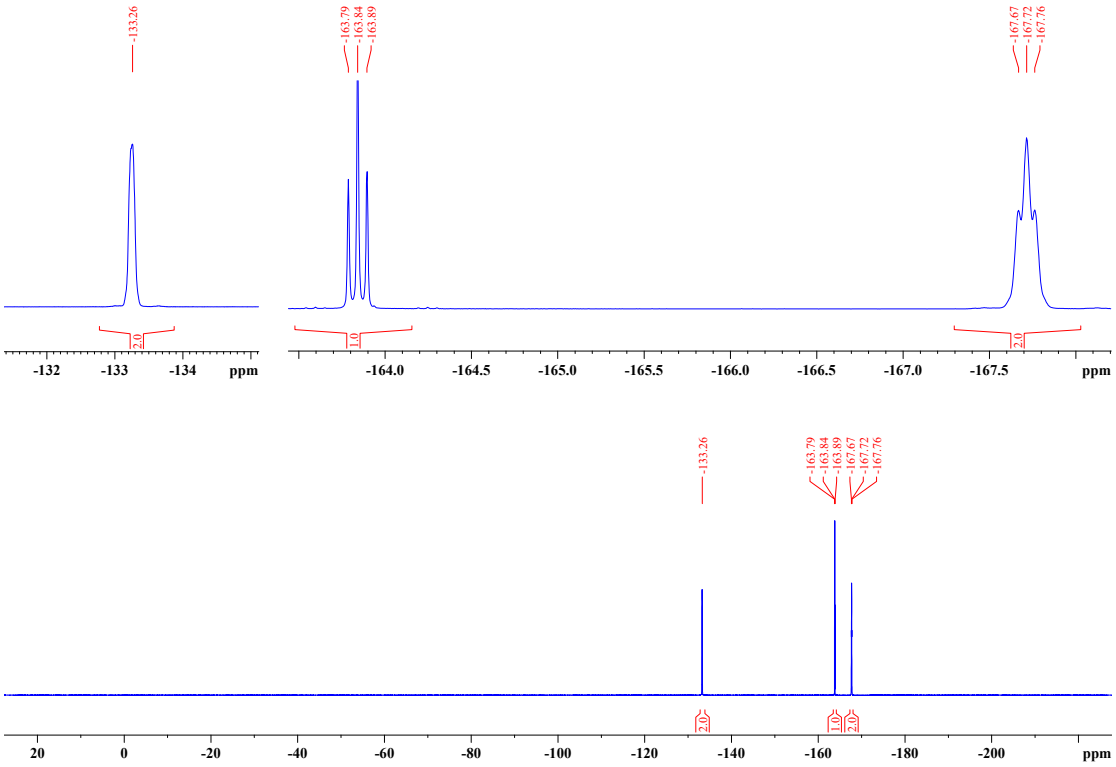

Figure E43. ^{19}F NMR spectrum of [(Trip$_2$Sb)(TripSb)Naph][BAr$^{F\text{-}20}$] (**71**) in CD_2Cl_2.

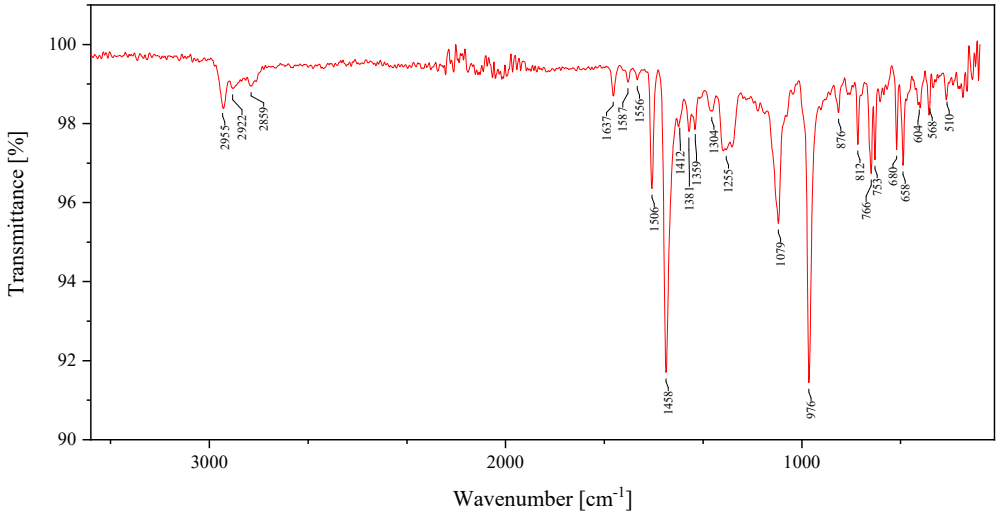

Figure E44. IR spectrum of neat [(Trip$_2$Sb)(TripSb)Naph][BAr$^{F\text{-}20}$] (**71**).

7.2.3. Synthesis of 1,8-Bis-((2,4,6-tri-*iso*-propylphenyl)stiban-(II))naphthalenediyl (**72**)

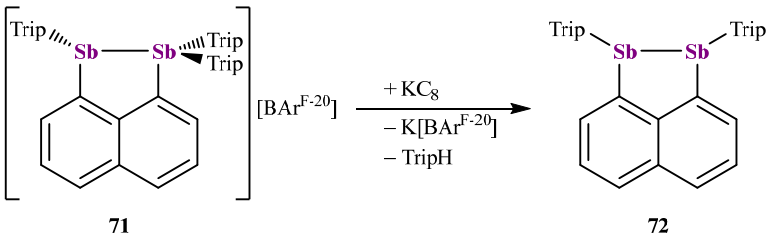

71 **72**

71 (0.06 mmol, 100 mg) and KC_8 (0.06 mmol, 8 mg) were weighed into a Schlenk tube and dissolved in 5 mL of thf. The suspension was stirred overnight and filtered giving a pale-yellow solution. After the solvent was removed *in vacuo* the residue was extracted with *n*-hexane (3 x 5 mL) and concentrated until the formation of precipitate was observed. The solid was redissolved in the heat and the solution was stored at 4 °C to give a yellow crystalline solid. **Yield:** 17 mg (37 %); **m.p.:** 245.8 °C; **elemental analysis [wt-%]:** calcd. for $C_{40}H_{52}Sb_2$: C 61.88, H 6.75. found: C 61.8, H 6.56; **^{1}H NMR (400.1 MHz, 297 K, CD_2Cl_2) δ [ppm]:** 7.86 (dd, $^3J_{HH}$ = 6.79 Hz, $^4J_{HH}$ = 1.21 Hz, 2 H, Naph-2/7-C*H*), 7.71 (dd, $^3J_{HH}$ = 8.21 Hz, $^4J_{HH}$ = 1.11 Hz, 2 H, Naph-4/5-C*H*), 7.38 (dd, $^3J_{HH}$ = 8.11 Hz, $^3J_{HH}$ = 6.85 Hz, 2 H, Naph-3/6-C*H*), 6.94 (s, 4 H, Ph-*m*-C*H*), 3.25 (sept, $^3J_{HH}$ = 6.78 Hz, 4 H, *o*-C*H*(CH_3)$_2$), 2.82 (sept, $^3J_{HH}$ = 6.97 Hz, 2 H, *p*-C*H*(CH_3)$_2$), 1.21 (dd, $^3J_{HH}$ = 6.88 Hz, $^4J_{HH}$ = 2.06 Hz, 12 H, *p*-CH(C*H*$_3$)$_2$), 1.14 (d, $^3J_{HH}$ = 6.84 Hz, 12 H, *o*-CH(C*H*$_3$)$_2$), 0.64 (d, $^3J_{HH}$ = 6.65 Hz, 12 H, *o*-CH(C*H*$_3$)$_2$); **^{13}C{^{1}H} NMR (100.6 MHz, 297 K, CD_2Cl_2) δ [ppm]:** 156.69 (Ph-*o*-*C*), 150.20 (Ph-*p*-*C*), 147.95 (Naph-9-*C*), 145.02 (Naph-10-*C*), 138.75 (Naph-2/7-*C*H), 138.47 (Naph-1/8-*C*), 134.67 (Ph-*ipso*-*C*), 128.92 (Naph-4/5-*C*H), 125.91 (Naph-3/6-*C*H), 122.34 (Ph-*m*-*C*H), 38.20 (*o*-*C*H(CH_3)$_2$), 34.48 (*p*-*C*H(CH_3)$_2$), 25.27 (*o*-CH(*C*H$_3$)$_2$), 24.39 (*o*-CH(*C*H$_3$)$_2$), 24.06 (*p*-CH(*C*H$_3$)$_2$); **IR ν [cm^{-1}]**: 3030 (w), 2943 (s), 2914 (m), 2891 (m), 2854 (m), 1585 (w), 1546 (w), 1533 (w), 1451 (m), 1408 (m), 1375 (m), 1355 (m), 1339 (w), 1296 (w), 1255 (m), 1228 (w), 1191 (w), 1163 (w), 1092 (m), 1059 (m), 1048 (m), 1018 (m), 972 (w), 931 (w), 872 (m), 806 (s), 769 (s), 740 (m), 704 (w), 670 (w), 643 (w), 620 (w), 557 (w), 509 (w), 463 (w), 444 (w), 428 (w).

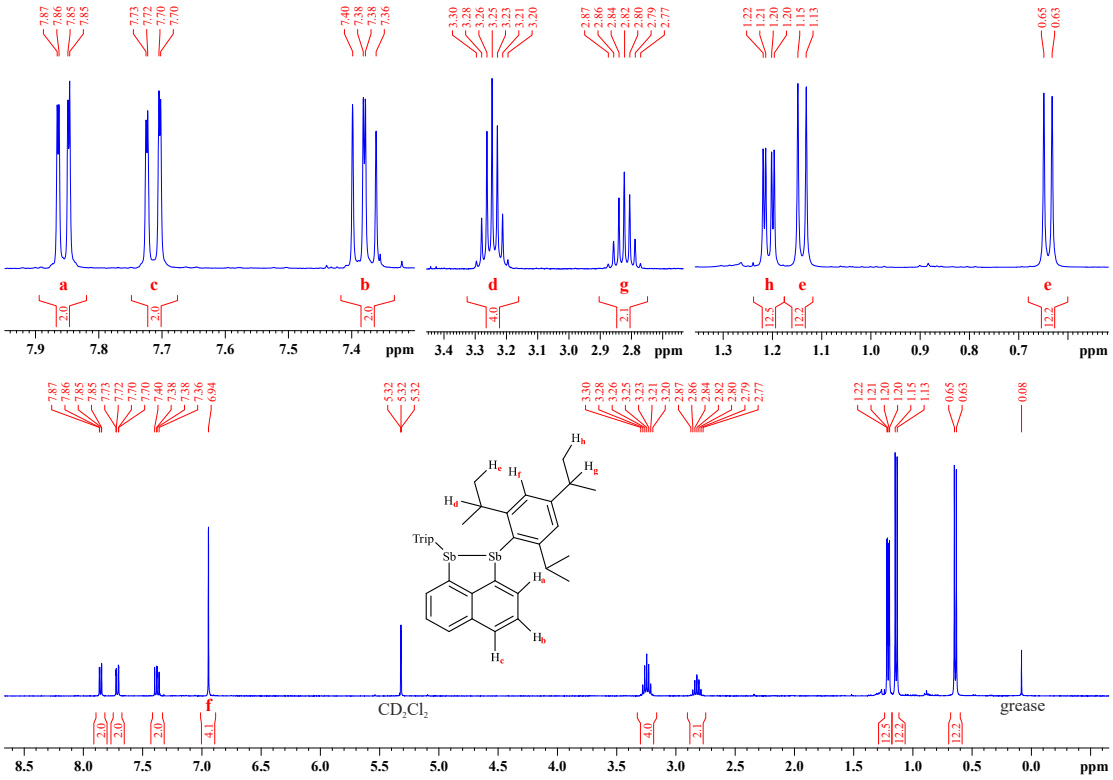

Figure E45. ^{1}H NMR spectrum of $(TripSb)_2Naph$ (**72**) in CD_2Cl_2.

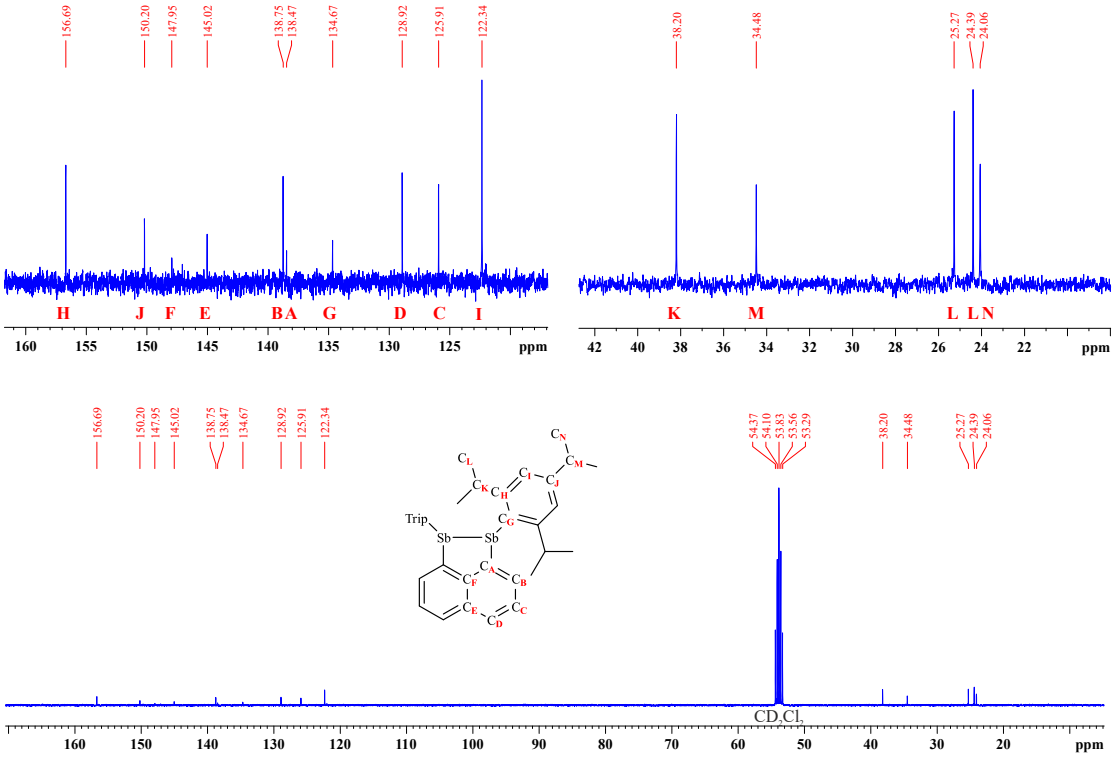

Figure E46. $^{13}C\{^{1}H\}$ NMR spectrum of $(TripSb)_2Naph$ (**72**) in CD_2Cl_2.

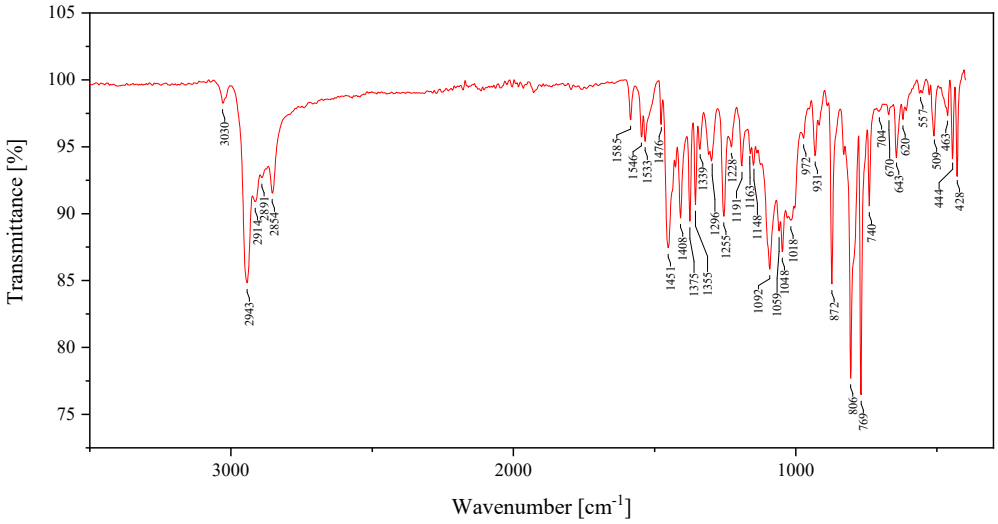

Figure E47. IR spectrum of neat $(TripSb)_2Naph$ (**72**).

7.2.4. Synthesis of 2,6-Bis(2,4,6-tri-iso-propylphenyl)phenyl-1,8-naphthalenediylarsane-(III) (**74**)

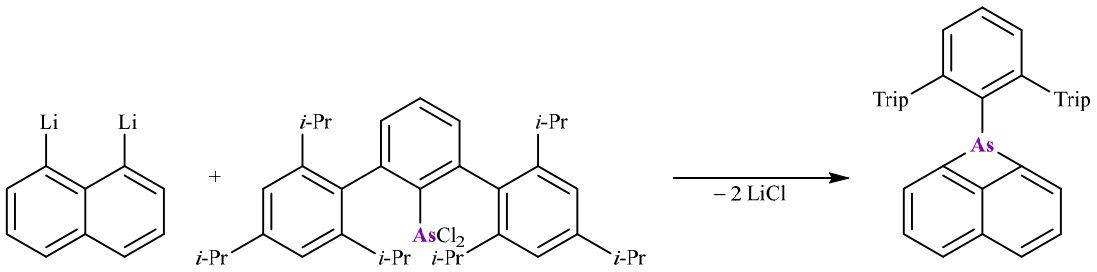

Li_2Naph (0.3 mmol, 54.5 mg) and $TTPAsCl_2$ (0.3 mmol, 187.9 mg) were weighed into a Schenk tube and dissolved in 10 mL of thf giving an orange solution. The mixture was stirred for 4 h after which the solvent was removed *in vacuo*. 10 mL of degassed water were added and the mixture stirred overnight. The solvent was removed by filtration and the *in vacuo* dried residue extracted with *n*-hexane (15 mL). The volatiles were removed *in vacuo* and redissolved in ethanol (20 mL). The mixture was separated by hot filtration and upon storing the solution at 4 °C colorless crystals were obtained. **Yield:** 37 mg (18 %); **m.p.:** 182.8 °C; **elemental analysis [wt-%]:** calcd. for $C_{46}H_{55}As$: C 80.91, H 8.12. found: C 80.9, H 7.9; **^{1}H NMR (400.1 MHz, 297 K, CD_2Cl_2) δ [ppm]:** 7.44 (d, $^3J_{HH}$ = 8.25 Hz, 2 H, Naph-2,7-C*H*), 7.34 (t, $^3J_{HH}$ = 7.50 Hz, 1 H, Terph-*p*-C*H*), 7.15 (s, 4 H, Trip-*m*-C*H*), 7.09 (d, $^3J_{HH}$ = 7.25 Hz, 2 H, Terph-*m*-C*H*), 7.04 (dd, $^3J_{HH}$ = 8.25 Hz, $^3J_{HH}$ = 6.75 Hz, 2 H, Naph-3,6-C*H*), 5.88 (d, $^3J_{HH}$ = 6.94 Hz, 2 H, Naph-4,5-C*H*), 3.05 (sept, $^3J_{HH}$ = 7.07 Hz, 2 H, Trip-*p*-C*H*$(CH_3)_2$), 2.67 (sept, $^3J_{HH}$ = 6.78 Hz, 4 H, Trip-*o*-C*H*$(CH_3)_2$), 1.42 (d, $^3J_{HH}$ = 6.93 Hz, 12 H, Trip-*p*-CH(C*H*$_3)_2$), 1.04 (d, $^3J_{HH}$ = 7.07 Hz, 12 H, Trip-*o*-CH(C*H*$_3)_2$), 0.83 (d, $^3J_{HH}$ = 6.95 Hz, 12 H, Trip-*o*-CH(C*H*$_3)_2$); **^{13}C{^{1}H} NMR (100.6 MHz, 297 K, CD_2Cl_2) δ [ppm]:** 149.96 (Naph-9-*C*), 148.92 (Trip-*o*-*C*), 147.37 (Trip-*p*-*C*), 143.06 (Terph-*o*-*C*), 142.92 (Terph-*ipso*-*C*), 138.35 (Naph-10-*C*), 137.47 (Trip-*ipso*-*C*), 130.71 (Terph-*m*-*C*H), 128.00 (Naph-3,6-*C*H), 127.58 (Naph-1,8-*C*), 127.14 (Terph-*p*-*C*H), 125.40 (Naph-4,5-*C*H), 123.69 (Naph-2,7-*C*H), 121.78 (Trip-*m*-*C*H), 35.03 (Trip-*p*-*C*H$(CH_3)_2$), 31.31 (Trip-*o*-*C*H$(CH_3)_2$), 25.58 (Trip-*o*-CH(*C*H$_3)_2$), 24.41 (Trip-*p*-CH(*C*H$_3)_2$), 22.76 (Trip-*o*-CH(*C*H$_3)_2$); **IR ν [cm^{-1}]**: 3507 (w), 3039 (w), 2946 (s), 2916 (m), 2855 (m), 1600 (m), 1559 (m), 1453 (m), 1377 (m), 1357 (m), 1309 (w), 1235 (w), 1192 (w), 1164 (w), 1095 (w), 1063 (w), 964 (w), 938 (w), 873 (s), 799 (s), 771 (s), 741 (m), 716 (w), 648 (m), 588 (w), 562 (w) 507 (w), 478 (w), 445 (m),409 (w).

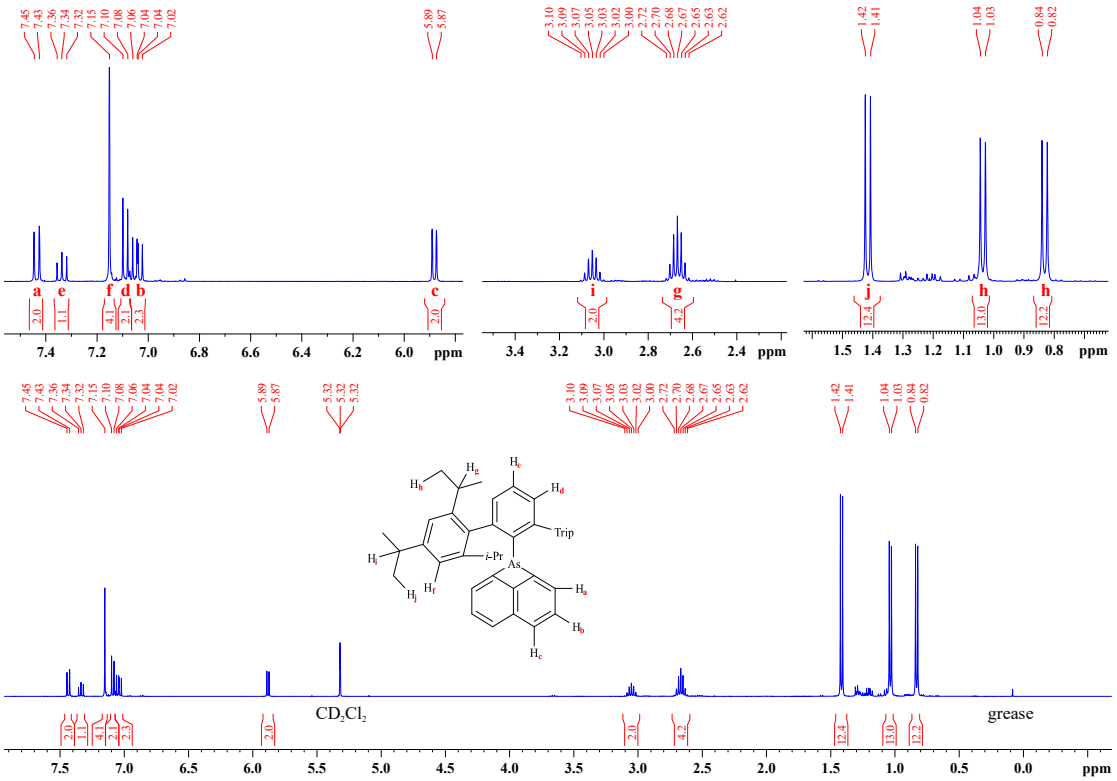

Figure E48. ^{1}H NMR spectrum of TTPAsNaph (**74**) in CD_2Cl_2.

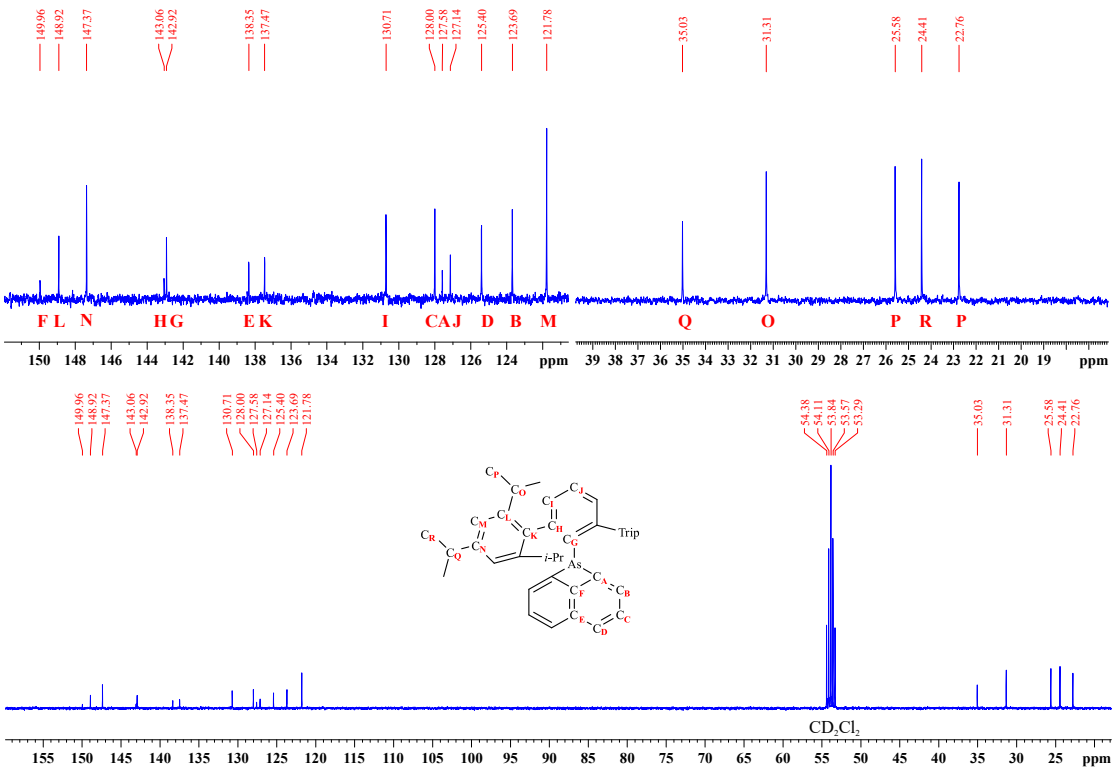

Figure E49. $^{13}C\{^{1}H\}$ NMR spectrum of TTPAsNaph (**74**) in CD_2Cl_2.

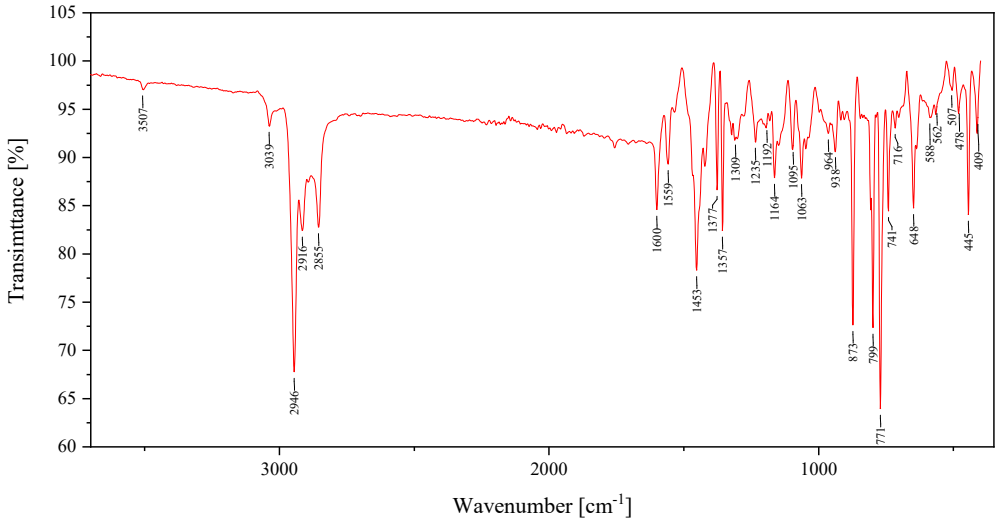

Figure E50. IR spectrum of neat TTPAsNaph (**74**).

7.2.5. Synthesis of 2,6-Bis(2,4,6-tri-iso-propylphenyl)phenyl-1,8-naphthalenediylstibane-(III) (**73**)

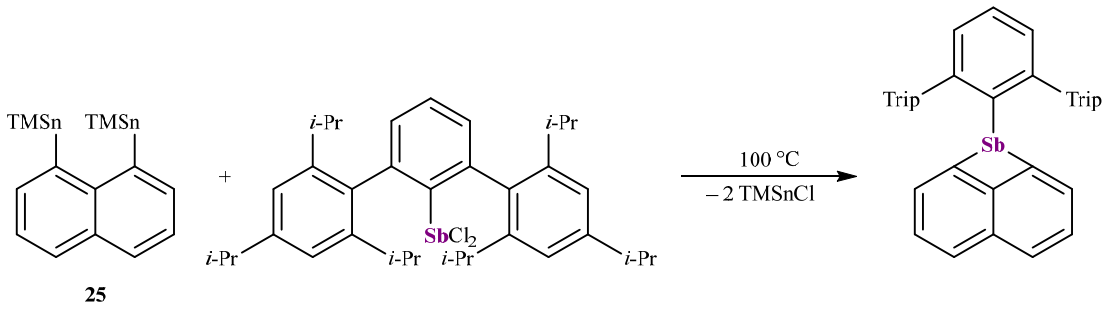

25

1,8-$TMSn_2$Naph (0.75 mmol, 500 mg) and $TTPSbCl_2$ (0.75 mmol, 407.7 mg) were dissolved in 20 mL of toluene and heated to 100 °C. After stirring for three days the solvent was removed *in vacuo* and the residue was dissolved in EtOH. The solution was concentrated until the formation of a solid precipitate was observed, which was redissolved in the heat. Storage at –20 °C gave colorless crystals of **73**. **Yield:** 317 mg (58 %); **m.p.:** 144.8 °C; **elemental analysis [wt-%]:** calcd. for $C_{46}H_{55}Sb$: C 75.72, H 7.60. found: C 76.1, H 7.64; **^{1}H NMR (400.1 MHz, 297 K, CD_2Cl_2) δ [ppm]:** 7.54 (dd, $^3J_{HH}$ = 8.39 Hz, $^4J_{HH}$ = 0.68 Hz, 2 H, Naph-2,7-C*H*), 7.37 (dd, $^3J_{HH}$ = 7.69 Hz, $^3J_{HH}$ = 7.30 Hz, 1 H, Terph-*p*-C*H*), 7.14 (s, 4 H, Trip-*m*-C*H*), 7.14 (d, $^3J_{HH}$ = 7.60 Hz, 2 H, Terph-*m*-C*H*), 7.10 (dd, $^3J_{HH}$ = 8.39 Hz, $^3J_{HH}$ = 6.73 Hz, 2 H, Naph-3,6-C*H*), 6.39 (dd, $^3J_{HH}$ = 6.78 Hz, $^4J_{HH}$ = 0.65 Hz, 2 H, Naph-4,5-C*H*), 3.05 (sept, $^3J_{HH}$ = 7.00 Hz, 2 H, *p*-C*H*$(CH_3)_2$), 2.66 (sept, $^3J_{HH}$ = 6.85 Hz, 4 H, *o*-C*H*$(CH_3)_2$), 1.42 (d, $^3J_{HH}$ = 6.99 Hz, 12 H, *p*-CH(C*H*$_3)_2$), 1.02 (d, $^3J_{HH}$ = 6.86 Hz, 12 H, *o*-CH(C*H*$_3)_2$), 0.83 (d, $^3J_{HH}$ = 6.86 Hz, 12 H, *o*-CH(C*H*$_3)_2$); **^{13}C{^{1}H} NMR (100.6 MHz, 297 K, CD_2Cl_2) δ [ppm]:** 157.13 (Naph-9-*C*), 148.88 (Trip-*o*-*C*), 147.04 (Trip-*p*-*C*), 146.08 (Terph-*o*-*C*), 145.65 (Terph-*ipso*-*C*), 138.42 (Trip-*ipso*-*C*), 131.97 (Naph-10-*C*), 130.13 (Terph-*m*-*C*H), 129.66 (Naph-1,8-*C*), 127.72 (Naph-4,5-*C*H), 127.61 (Terph-*p*-*C*H), 126.85 (Naph-3,6-*C*H), 123.87 (Naph-2,7-*C*H), 121.83 (Trip-*m*-*C*H), 35.00 (*p*-*C*H$(CH_3)_2$), 31.26 (*o*-*C*H$(CH_3)_2$), 25.75 (*o*-CH(*C*H$_3)_2$), 24.35 (*p*-CH(*C*H$_3)_2$), 22.70 (*o*-CH(*C*H$_3)_2$); **IR ν [cm^{-1}]**: 3054 (w), 3033 (w), 3013 (w), 2946 (s), 2913 (m), 2854 (m), 1598 (w), 1554 (w), 1453 (m), 1375 (m), 1354 (m), 1311 (w), 1248 (w), 1233 (w), 1163 (w), 1094 (w), 1076 (w), 1065 (w), 1044 (w), 1011 (w), 935 (w), 873 (m), 802 (s), 773 (s), 740 (m), 698 (w) 646 (w), 583 (w9, 476 (w), 426 (w), 406 (w).

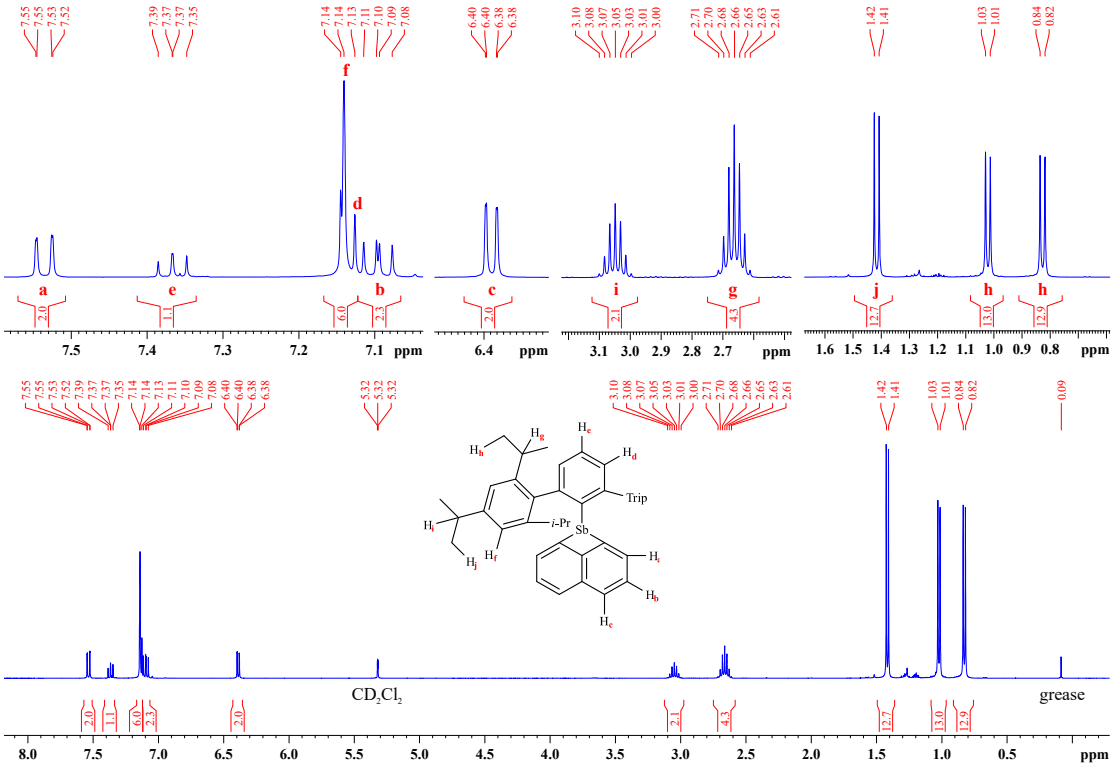

Figure E51. ^{1}H NMR spectrum of TTPSbNaph (**73**) in CD_2Cl_2.

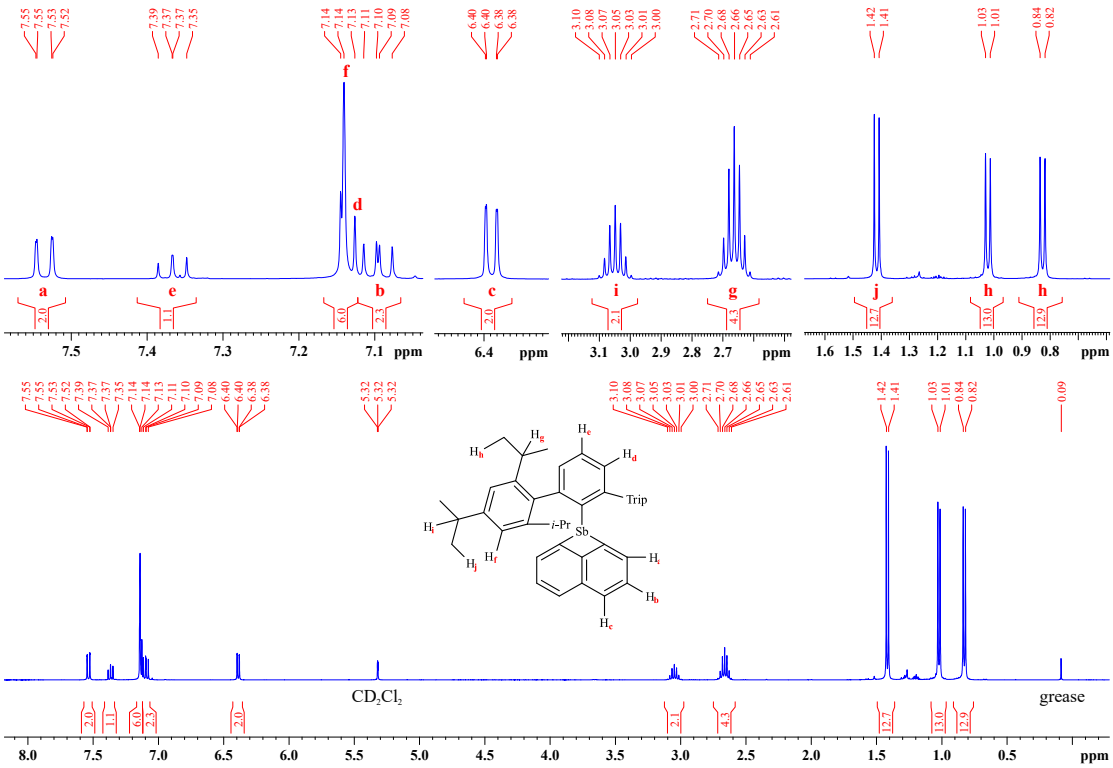

Figure E52. $^{13}C\{^{1}H\}$ NMR spectrum of TTPSbNaph (**73**) in CD_2Cl_2.

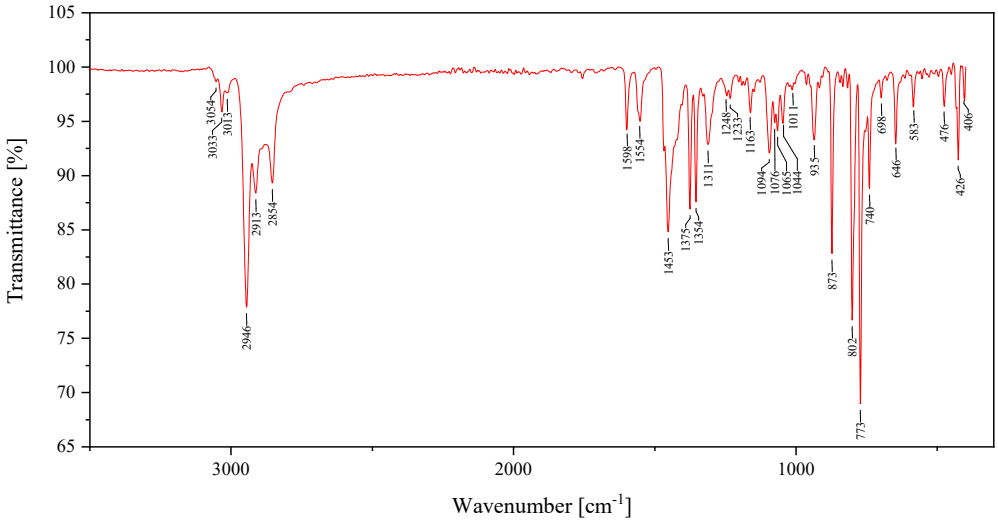

Figure E53. IR spectrum of neat TTPSbNaph (**73**).

7.2.6. Synthesis of 2,6-Bis(2,4,6-tri-iso-propylphenyl)phenyl-1,8-naphthalenediylbismuthane-(III) (**75**)

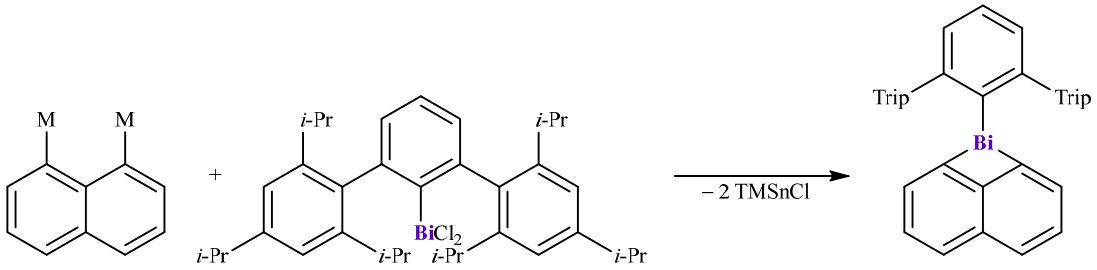

1,8-$TMSn_2$Naph (0.53 mmol, 289.3 mg) and $TTPBiCl_2$ (0.53 mmol, 400.0 mg) were dissolved in 25 mL of toluene and heated to 100 °C, giving a yellow solution, which turned red after a few hours. After stirring overnight, the solvent was removed *in vacuo* and the residue was suspended in EtOH (30 mL) and filtrated. The solution was concentrated until turbidity was visible and the solid was redissolved in the heat. Storage at –20 °C gave a mixture of colorless crystals of **75** and a deep purple solid, which was identified as $(TTPBi)_2$.[220] The mother liquor was removed by filtration and concentrated until slight turbidity was visible. The solid was redissolved in the heat and stored at –20 °C to give a clean crop of **75**. **Yield:** 161 mg (37 %); **m.p.:** 164.4 °C; **elemental analysis [wt-%]:** calcd. for $C_{46}H_{55}Bi$: C 67.63, H 6.79. found: C 67.6, H 6.45; **^{1}H NMR (400.1 MHz, 297 K, C_6D_6) δ [ppm]:** 8.07 (dd, $^3J_{HH}$ = 8.27 Hz, $^4J_{HH}$ = 0.60 Hz, 2 H, Naph-2,7-C*H*), 7.77 (dd, $^3J_{HH}$ = 6.74 Hz, $^4J_{HH}$ = 0.66 Hz, 2 H, Naph-4,5-C*H*), 7.42 (dd, $^3J_{HH}$ = 8.27 Hz, $^3J_{HH}$ = 6.74 Hz, 2 H, Naph-3,6-C*H*), 7.36 (d, $^3J_{HH}$ = 7.46 Hz, 2 H, Terph-*m*-C*H*), 7.23 (s, 4 H, Trip-*m*-C*H*), 7.19 (dd, $^3J_{HH}$ = 7.84 Hz, $^3J_{HH}$ = 7.08 Hz, 1 H, Terph-*p*-C*H*), 3.02-2.89 (m, 6 H, *o*/*p*-C*H*$(CH_3)_2$), 1.39 (d, $^3J_{HH}$ = 7.24 Hz, 12 H, *p*-CH(C*H*$_3)_2$), 1.10 (d, $^3J_{HH}$ = 6.63 Hz, 12 H, *o*-CH(C*H*$_3)_2$), 1.01 (d, $^3J_{HH}$ = 7.02 Hz, 12 H, *o*-CH(C*H*$_3)_2$); **^{13}C{^{1}H} NMR (100.6 MHz, 297 K, C_6D_6) δ [ppm]:** 172.16 (Terph-*ipso*-*C*), 165.22 (Naph-1,8-*C*), 148.63 (Trip-*o*-*C*), 147.92 (Terph-*o*-*C*), 146.88 (Trip-*p*-*C*), 139.92 (Trip-*ipso*-*C*), 137.19 (Naph-10-*C*), 133.48 (Naph-9-*C*), 131.67 (Terph-*m*-*C*H), 127.15 (Terph-*p*-*C*H), 126.80 (Naph-3,6-*C*H), 125.35 (Naph-4,5-*C*H), 122.68 (Naph-2,7-*C*H), 121.64 (Trip-*m*-*C*H), 35.04 (*p*-*C*H$(CH_3)_2$), 31.40 (*o*-*C*H$(CH_3)_2$), 25.95 (*o*-CH(*C*H$_3)_2$), 24.45 (*p*-CH(*C*H$_3)_2$), 23.18 (*o*-CH(*C*H$_3)_2$); **IR ν [cm^{-1}]**: 3054 (w), 3031 (w), 313 (w), 2946 (m), 2911 (m), 2853 (m), 1600 (w), 1556 (w), 1537 (w), 1453 (m), 1375 (m), 1354 (m), 1310 (m), 1246 (w), 1231 (w), 1198 (w), 1183 (w), 1161 (w), 1094 (m), 1076 (w), 1063 (w), 1044 (w), 1002 (w), 933 (m), 873 (m), 799 (s), 770 (s), 737 (m), 694 (w), 646 (m), 585 (w), 472 (w), 428 (w), 419 (w).

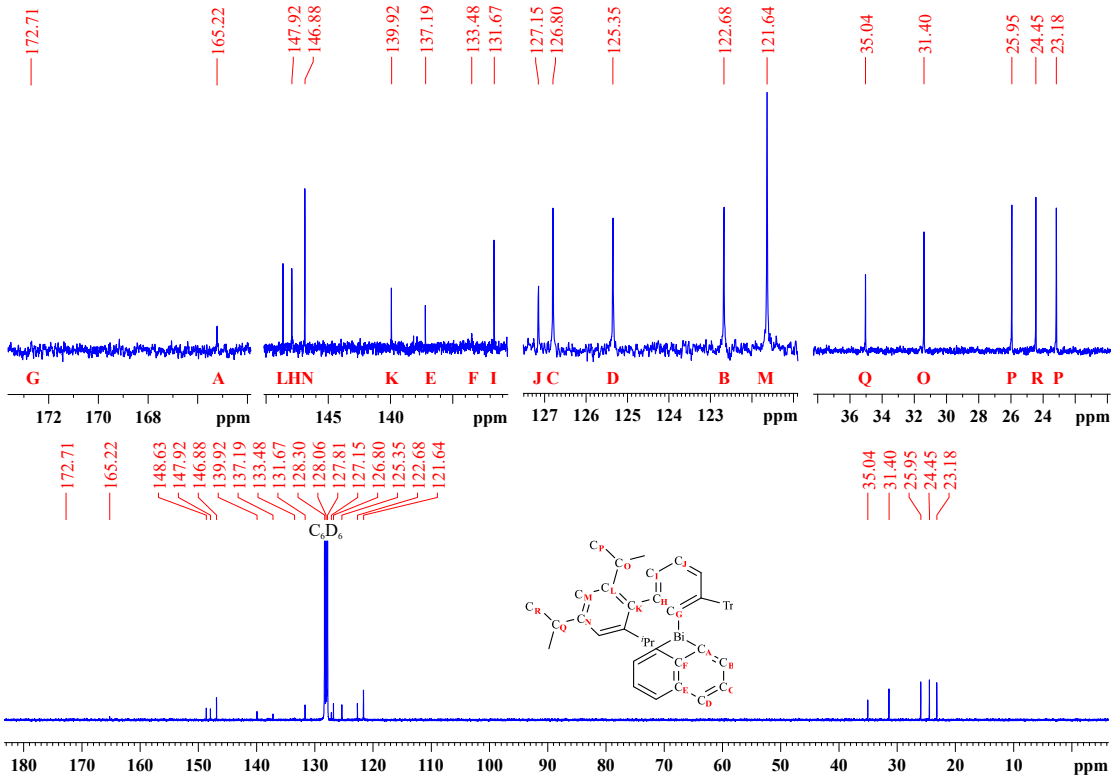

Figure E54. ^{1}H NMR spectrum of TTPBiNaph (**75**) in C_6D_6.

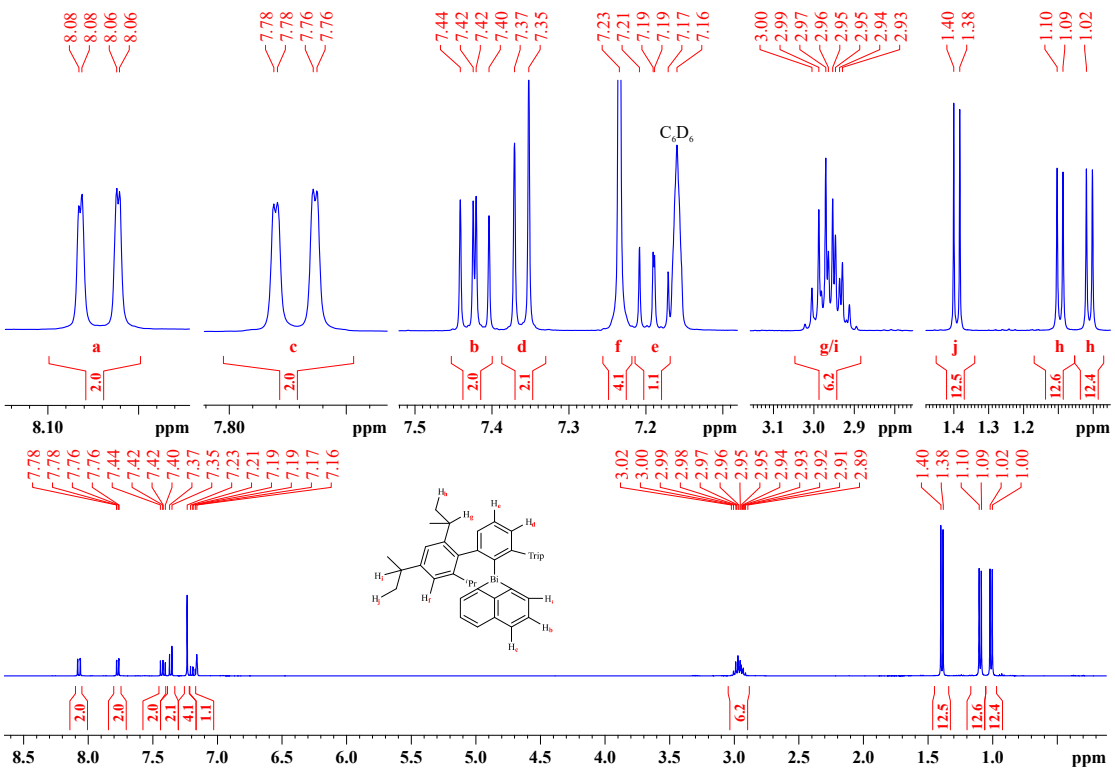

Figure E55. ^{13}C{^{1}H} NMR spectrum of TTPBiNaph (**75**) in C_6D_6.

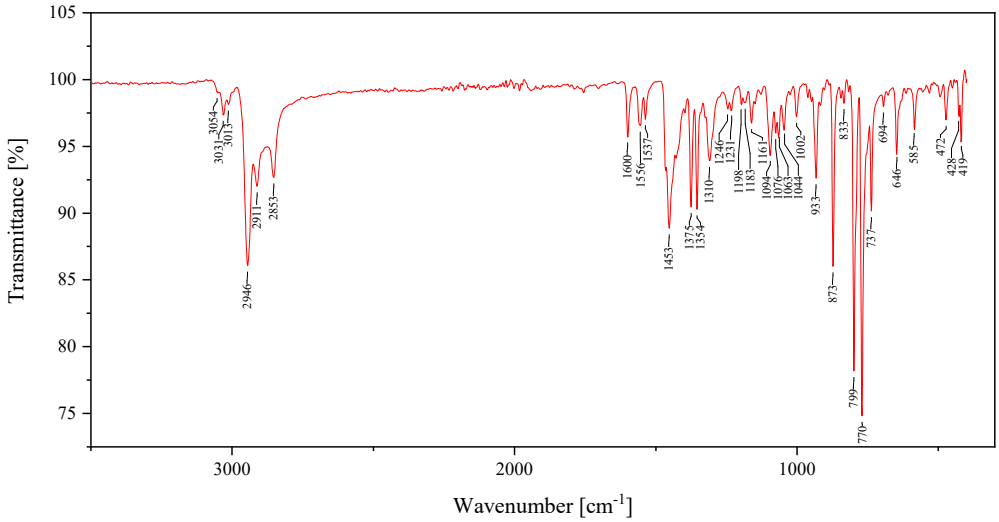

Figure E56. IR spectrum of neat TTPBiNaph (**75**).

8. References

[1] E. Riedel, C. Janiak, *Anorganische Chemie*. *Mit DVD,* 7. Aufl., de Gruyter, Berlin, **2007**.

[2] P. W. Atkins, J. de Paula, *Atkins' physical chemistry,* 8. Aufl., Oxford University Press, Oxford, **2006**.

[3] a) J. P. Wagner, P. R. Schreiner, *Angew. Chem.* **2015**, *127*, 12446; *Angew. Chem. Int. Ed.* **2015**, *54*, 12274; b) M. Giese, M. Albrecht, *ChemPlusChem* **2020**, *85*, 715.

[4] P. P. Power, *Organometallics* **2020**, *39*, 4127.

[5] D. J. Liptrot, P. P. Power, *Nat. Rev. Chem.* **2017**, *1*.

[6] K. L. Mears, P. P. Power, *Acc. Chem. Res.* **2022**, *55*, 1337.

[7] P. R. Schreiner, L. V. Chernish, P. A. Gunchenko, E. Y. Tikhonchuk, H. Hausmann, M. Serafin, S. Schlecht, J. E. P. Dahl, R. M. K. Carlson, A. A. Fokin, *Nature* **2011**, *477*, 308.

[8] A. A. Fokin, L. V. Chernish, P. A. Gunchenko, E. Y. Tikhonchuk, H. Hausmann, M. Serafin, J. E. P. Dahl, R. M. K. Carlson, P. R. Schreiner, *J. Am. Chem. Soc.* **2012**, *134*, 13641.

[9] a) J. M. Schümann, J. P. Wagner, A. K. Eckhardt, H. Quanz, P. R. Schreiner, *J. Am. Chem. Soc.* **2021**, *143*, 41; b) M. A. Strauss, H. A. Wegner, *Angew. Chem.* **2021**, *133*, 792; *Angew. Chem. Int. Ed.* **2021**, *60*, 779.

[10] N. W. Mitzel, M. Linnemannstöns, J. Schwabedissen, B. Neumann, G. Stammler, R. Berger, *Chem. Eur. J.* **2020**, *26*, 2169.

[11] A. A. Fokin, T. S. Zhuk, S. Blomeyer, C. Pérez, L. V. Chernish, A. E. Pashenko, J. Antony, Y. V. Vishnevskiy, R. J. F. Berger, S. Grimme, C. Logemann, M. Schnell, N. W. Mitzel, P. R. Schreiner, *J. Am. Chem. Soc.* **2017**, *139*, 16696.

[12] T. Glodde, Y. V. Vishnevskiy, L. Zimmermann, H.-G. Stammler, B. Neumann, N. W. Mitzel, *Angew. Chem.* **2021**, *133*, 1542; *Angew. Chem. Int. Ed.* **2021**, *60*, 1519.

[13] L. Song, J. Schoening, C. Wölper, S. Schulz, P. R. Schreiner, *Organometallics* **2019**, *38*, 1640.

[14] J. Jung, S. T. Löffler, J. Langmann, F. W. Heinemann, E. Bill, G. Bistoni, W. Scherer, M. Atanasov, K. Meyer, F. Neese, *J. Am. Chem. Soc.* **2020**, *142*, 1864.

[15] S. Rösel, H. Quanz, C. Logemann, J. Becker, E. Mossou, L. Cañadillas-Delgado, E. Caldeweyher, S. Grimme, P. R. Schreiner, *J. Am. Chem. Soc.* **2017**, *139*, 7428.

[16] P. A. Kollman, *Acc. Chem. Res.* **1977**, *10*, 365.

[17] E. V. Anslyn, D. A. Dougherty, *Modern physical organic chemistry*, University Science Books, Mill Valley, California, **2006**.

[18] a) S. A. Khan, *J. Emerg. Technol. Innov. Res.* **2014**, *1*, 52; b) K. P. Goetz, D. Vermeulen, M. E. Payne, C. Kloc, L. E. McNeil, O. D. Jurchescu, *J. Mater. Chem. C* **2014**, *2*, 3065.

[19] H. Wang, W. Wang, W. J. Jin, *Chem. Rev.* **2016**, *116*, 5072.

[20] F. Jensen, *Introduction to Computational Chemistry*, Wiley, Chichester, West Sussex, Hoboken, NJ, Oxford, **2017**.

[21] C. A. Hunter, *Angew. Chem.* **1993**, *105*, 1653; *Angew. Chem. Int. Ed.* **1993**, *32*, 1584.

[22] S. Grimme, J. Antony, S. Ehrlich, H. Krieg, *J. Chem. Phys.* **2010**, *132*, 154104.

[23] G. Bistoni, A. A. Auer, F. Neese, *Chem. Eur. J.* **2017**, *23*, 865.

[24] W. B. Schneider, G. Bistoni, M. Sparta, M. Saitow, C. Riplinger, A. A. Auer, F. Neese, *J. Chem. Theory Comput.* **2016**, *12*, 4778.

[25] a) M. Nishio, *CrystEngComm* **2004**, *6*, 130; b) M. Nishio, Y. Umezawa, K. Honda, S. Tsuboyama, H. Suezawa, *CrystEngComm* **2009**, *11*, 1757; c) M. Nishio, *Phys. Chem. Chem. Phys.* **2011**, *13*, 13873.

[26] P. Pyykkö, *Angew. Chem.* **2004**, *116*, 4512; *Angew. Chem. Int. Ed.* **2004**, *43*, 4412.

[27] P. Pyykkö, *Chem. Soc. Rev.* **2008**, *37*, 1967.

[28] a) J. E. Lennard-Jones, *Proc. R. Soc. Lond. A* **1924**, *106*, 463; b) J. E. Lennard-Jones, *Proc. R. Soc. Lond. A* **1924**, *106*, 441; c) J. E. Lennard-Jones, *Proc. Phys. Soc.* **1931**, *43*, 461.

[29] *CRC handbook of chemistry and physics*. *A ready-reference book of chemical and physical data*, CRC Press, Boca Raton, **2003**.

[30] C. A. Hunter, *Angew. Chem.* **2004**, *116*, 5424; *Angew. Chem. Int. Ed.* **2004**, *43*, 5310.

[31] R. Eisenschitz, F. London, *Z. Physik* **1930**, *60*, 491.

[32] F. London, *Trans. Faraday Soc.* **1937**, *33*, 8b-26.

[33] S. Rösel, P. R. Schreiner, *Isr. J. Chem.* **2022**, *62*, e202200002.

[34] B. Kahr, D. van Engen, K. Mislow, *J. Am. Chem. Soc.* **1986**, *108*, 8305.

[35] S. Grimme, P. R. Schreiner, *Angew. Chem.* **2011**, *123*, 12849; *Angew. Chem. Int. Ed.* **2011**, *50*, 12639.

[36] S. Grimme, S. Ehrlich, L. Goerigk, *J. Comput. Chem.* **2011**, *32*, 1456.

[37] D. E. Goldberg, D. H. Harris, M. F. Lappert, K. M. Thomas, *J. Chem. Soc., Chem. Commun.* **1976**, 261.

[38] S. L. Hinchley, C. A. Morrison, D. W. Rankin, C. L. Macdonald, R. J. Wiacek, A. Voigt, A. H. Cowley, M. F. Lappert, G. Gundersen, J. A. Clyburne, P. P. Power, *J. Am. Chem. Soc.* **2001**, *123*, 9045.

[39] J.-D. Guo, S. Nagase, P. P. Power, *Organometallics* **2015**, *34*, 2028.

[40] J.-D. Guo, D. J. Liptrot, S. Nagase, P. P. Power, *Chem. Sci.* **2015**, *6*, 6235.

[41] J. P. Wagner, P. R. Schreiner, *J. Chem. Theory Comput.* **2016**, *12*, 231.

[42] a) E. Solel, M. Ruth, P. R. Schreiner, *J. Am. Chem. Soc.* **2021**, *143*, 20837; b) B. D. Rekken, T. M. Brown, J. C. Fettinger, F. Lips, H. M. Tuononen, R. H. Herber, P. P. Power, *J. Am. Chem. Soc.* **2013**, *135*, 10134; c) M.-L. Y. Riu, G. Bistoni, C. C. Cummins, *J. Phys. Chem. A* **2021**, *125*, 6151.

[43] a) S. Grimme, *J. Comput. Chem.* **2004**, *25*, 1463; b) S. Grimme, *J. Comput. Chem.* **2006**, *27*, 1787; c) R. Haack, S. Schulz, G. Jansen, *J. Comput. Chem.* **2018**, *39*, 1413.

[44] H.-N. Adams, W. Hiller, J. Strähle, *Z. Anorg. Allg. Chem.* **1982**, *485*, 81.

[45] a) M. Jansen, *Angew. Chem.* **1987**, *99*, 1136; *Angew. Chem. Int. Ed.* **1987**, *26*, 1098; b) M. Olaru, J. Kögel, R. Aoki, R. Sakamoto, H. Nishihara, E. Lork, S. Mebs, M. Vogt, J. Beckmann, J. F. Kögel, *Chem. Eur. J.* **2019**, *26*, 275.

[46] C. Janiak, R. Hoffmann, *J. Am. Chem. Soc.* **1990**, *112*, 5924.

[47] P. Pyykkö, *Chem. Rev.* **1997**, *97*, 597.

[48] a) F. Scherbaum, A. Grohmann, B. Huber, C. Krüger, H. Schmidbaur, *Angew. Chem.* **1988**, *100*, 1602; *Angew. Chem. Int. Ed.* **1988**, *27*, 1544; b) H. Schmidbaur, *Gold Bull* **1990**, *23*, 11.

[49] H. Schmidbaur, H.-J. Öller, D. L. Wilkinson, B. Huber, G. Müller, *Chem. Ber.* **1989**, *122*, 31.

[50] S. Sculfort, P. Braunstein, *Chem. Soc. Rev.* **2011**, *40*, 2741.

[51] H. Schmidbaur, A. Schier, *Angew. Chem.* **2015**, *127*, 756; *Angew. Chem. Int. Ed.* **2015**, *54*, 746.

[52] a) Q. Zheng, S. Borsley, G. S. Nichol, F. Duarte, S. L. Cockroft, *Angew. Chem.* **2019**, *131*, 12747; *Angew. Chem. Int. Ed.* **2019**; b) R. Donamaría, V. Lippolis, J. M. López-de-Luzuriaga, M. Monge, M. Elena Olmos, *Comput. Theor. Chem* **2014**, *1030*, 53.

[53] H. Schmidbaur, A. Schier, *Organometallics* **2015**, *34*, 2048.

[54] Y. Liu, L. J. Taylor, S. P. Argent, J. McMaster, D. L. Kays, *Inorg. Chem.* **2021**, *60*, 10114.

[55] a) N. V. S. Harisomayajula, S. Makovetskyi, Y.-C. Tsai, *Chem. Eur. J.* **2019**, *25*, 8936; b) P. Woidy, A. J. Karttunen, M. Widenmeyer, R. Niewa, F. Kraus, *Chem. Eur. J.* **2015**, *21*, 3290.

[56] E. Hupf, R. Kather, M. Vogt, E. Lork, S. Mebs, J. Beckmann, *Inorg. Chem.* **2016**, *55*, 11513.

[57] a) M. Bardajía, A. Laguna, *Eur. J. Inorg. Chem.* **2003**, 3069; b) J. M. López-de-Luzuriaga, M. Monge, M. E. Olmos, D. Pascual, *Organometallics* **2015**, *34*, 3029; c) E. J. Fernández, A. Laguna, J. M. López-de-Luzuriaga, F. Mendizabal, M. Monge, M. E. Olmos, J. Pérez, *Chem. Eur. J.* **2003**, *9*, 456; d) E. Hupf, E. Lork, S. Mebs, J. Beckmann, *Inorg. Chem.* **2015**, *54*, 1847; e) O. Crespo, A. Laguna, E. J. Fernández, J. M. López-de-Luzuriaga, P. G. Jones, M. Teichert, M. Monge, P. Pyykkö, N. Runeberg, M. Schütz, H. J. Werner, *Inorg. Chem.* **2000**, *39*, 4786; f) E. J. Fernández, J. M. López-de-Luzuriaga, M. Monge, M. A. Rodríguez, O. Crespo, M. C. Gimeno, A. Laguna, P. G. Jones, *Chem. Eur. J.* **2000**, *6*, 636; g) H. Li, C. Zhou, E. Wang, X. Kang, W. W. Xu, M. Zhu, *Chem. Commun.* **2022**, *58*, 5092; h) R. Donamaría, V. Lippolis, J. M. López-de-Luzuriaga, M. Monge, M. Nieddu, M. E. Olmos, *Inorg. Chem.* **2020**, *59*, 6398.

[58] S. Raju, H. B. Singh, R. J. Butcher, *Dalton Trans.* **2020**, *49*, 9099.

[59] R. Donamaría, V. Lippolis, J. M. López-de-Luzuriaga, M. Monge, M. Nieddu, M. E. Olmos, *Chem. Eur. J.* **2018**, *24*, 13740.

[60] D. Seyferth, *Organometallics* **2001**, *20*, 1488.

[61] F. A. Paneth, H. Loleit, *J. Chem. Soc.* **1935**, 366.

[62] A. J. Ashe, E. G. Ludwig, *Organometallics* **1982**, *1*, 1408.

[63] A. J. Ashe, W. Butler, T. R. Diephouse, *J. Am. Chem. Soc.* **1981**, *103*, 207.

[64] A. J. Ashe in *Advances in Organometallic Chemistry*, *Vol. 30* (Hrsg.: R. West), Academic Press, New York, **1990**, S. 77–97.

[65] A. J. Ashe, E. G. Ludwig, J. Oleksyszyn, J. C. Huffman, *Organometallics* **1984**, *3*, 337.

[66] A. J. Ashe, E. G. Ludwig, J. Oleksyszyn, *Organometallics* **1983**, *2*, 1859.

[67] A. J. Ashe, J. W. Kampf, D. B. Puranik, S. M. Al-Taweel, *Organometallics* **1992**, *11*, 2743.

[68] A. Kuczkowski, S. Heimann, A. Weber, S. Schulz, D. Bläser, C. Wölper, *Organometallics* **2011**, *30*, 4730.

[69] F. A. Paneth, *Trans. Faraday Soc.* **1934**, *30*, 179.

[70] K. Y. Monakhov, T. Zessin, G. Linti, *Eur. J. Inorg. Chem.* **2010**, 322.

[71] T. Hughbanks, R. Hoffmann, M. H. Whangbo, K. R. Stewart, O. Eisenstein, E. Canadell, *J. Am. Chem. Soc.* **1982**, *104*, 3876.

[72] A. J. Ashe, E. G. Ludwig, *J. Organomet. Chem.* **1986**, *303*, 197.

[73] G. Balázs, H. J. Breunig, E. Lork, W. Offermann, *Organometallics* **2001**, *20*, 2666.

[74] a) R. Wolf, J. Fischer, R. C. Fischer, J. C. Fettinger, P. P. Power, *Eur. J. Inorg. Chem.* **2008**, 2515; b) L. Balazs, H. J. Breunig, E. Lork, C. Silvestru, *Eur. J. Inorg. Chem.* **2003**, 1361; c) L. Balazs, H. J. Breunig, E. Lork, A. Soran, C. Silvestru, *Inorg. Chem.* **2006**, *45*, 2341.

[75] S. Schulz, S. Heimann, A. Kuczkowski, D. Bläser, C. Wölper, *Organometallics* **2013**, *32*, 3391.

[76] K. W. Klinkhammer, P. Pyykkö, *Inorg. Chem.* **1995**, *34*, 4134.

[77] M. Bujak, H.-G. Stammler, Y. V. Vishnevskiy, N. W. Mitzel, *CrystEngComm* **2021**, *24*, 70.

[78] S. Schulz, A. Kuczkowski, D. Bläser, C. Wölper, G. Jansen, R. Haack, *Organometallics* **2013**, *32*, 5445.

[79] J. Moilanen, C. Ganesamoorthy, M. S. Balakrishna, H. M. Tuononen, *Inorg. Chem.* **2009**, *48*, 6740.

[80] C. Ganesamoorthy, M. S. Balakrishna, J. T. Mague, H. M. Tuononen, *Inorg. Chem.* **2008**, *47*, 7035.

[81] a) D. Britton, V. G. Young, E. O. Schlemper, *Acta Cryst. C* **2002**, *58*, m307-9; b) B. W. Skelton, Effendy, A. H. White, *CCDC 1851864: CSD Communication,* DOI: 10.5517/CCDC.CSD.CC2050KS; c) A. M. Christianson, F. P. Gabbaï, *Organometallics* **2017**, *36*, 3013; d) Di Lu, M. L. Coote, J. Ho, N. L. Kilah, C.-Y. Lin, G. Salem, M. L. Weir, A. C. Willis, S. B. Wild, P. J. Dilda, *Organometallics* **2012**, *31*, 1808; e) L. I. Goryunov, V. D. Shteingarts, J. Grobe, B. Krebs, M. U. Triller, *Z. Anorg. Allg. Chem.* **2002**, *628*, 1770; f) E. V. Avtomonov, K. Megges, S. Wocadlo, J. Lorberth, *J. Organomet. Chem.* **1996**, *524*, 253; g) H. J. Breunig, E. Lork, O. Moldovan, C. I. Raţ, *J. Organomet. Chem.* **2008**, *693*, 2527; h) A. C. Marr, M. Nieuwenhuyzen, C. L. Pollock, G. C. Saunders, *Organometallics* **2007**, *26*, 2659.

[82] I. Becker, M. Windhaus, R. Mattes, *Z. Naturforsch. B* **1994**, *49*, 870.

[83] T. Louis-Goff, A. L. Rheingold, J. Hyvl, *Organometallics* **2020**, *39*, 778.

[84] W. A. Baker, D. E. Williams, *Acta Cryst. B* **1978**, *34*, 3739.

[85] a) C. Jones, P. C. Junk, A. F. Richards, M. Waugh, *New J. Chem.* **2002**, *26*, 1209; b) W.-Y. Yeh, H. Seino, T. Amitsuka, S. Ohba, M. Hidai, Y. Mizobe, *J. Organomet. Chem.* **2004**, *689*, 2338.

[86] J. Bruckmann, C. Krüger, *Acta Cryst. C* **1995**, *51*, 1155.

[87] M. Mantina, A. C. Chamberlin, R. Valero, C. J. Cramer, D. G. Truhlar, *J. Phys. Chem. A* **2009**, *113*, 5806.

[88] A. P. M. Robertson, P. A. Gray, N. Burford, *Angew. Chem.* **2014**, *126*, 6162; *Angew. Chem. Int. Ed.* **2014**, *53*, 6050.

[89] a) R. Mokrai, J. Barrett, D. C. Apperley, A. S. Batsanov, Z. Benkő, D. Heift, *Chem. Eur. J.* **2019**, *25*, 4017; b) R. Mokrai, J. Barrett, D. C. Apperley, Z. Benkő, D. Heift, *Inorg. Chem.* **2020**, *59*, 8916; c) J. Burt, W. Levason, G. Reid, *Coord. Chem. Rev.* **2014**, *260*, 65; d) N. C. Norman, N. L. Pickett, *Coord. Chem. Rev.* **1995**, *145*, 27.

[90] a) J. L. Dutton, P. J. Ragogna, *Coord. Chem. Rev.* **2011**, *255*, 1414; b) S. S. Chitnis, E. MacDonald, N. Burford, U. Werner-Zwanziger, R. McDonald, *Chem. Commun.* **2012**, *48*, 7359; c) E. Conrad, N. Burford, R. McDonald, M. J. Ferguson, *J. Am. Chem. Soc.* **2009**, *131*, 17000; d) S. S. Chitnis, B. Peters, E. Conrad, N. Burford, R. McDonald, M. J. Ferguson, *Chem. Commun.* **2011**, *47*, 12331; e) S. S. Chitnis, N. Burford, R. McDonald, M. J. Ferguson, *Inorg. Chem.* **2014**, *53*, 5359; f) J. W. Wielandt, S. Petrie, N. L. Kilah, A. C. Willis, R. D. Dewhurst, F. Belaj, A. Orthaber, R. Stranger, S. B. Wild, *Aust. J. Chem.* **2016**, *69*, 524; g) N. L. Kilah, S. Petrie, R. Stranger, J. W. Wielandt, A. C. Willis, S. B. Wild, *Organometallics* **2007**, *26*, 6106; h) J. W. Wielandt, N. L. Kilah, A. C. Willis, S. B. Wild, *Chem. Commun.* **2006**, 3679; i) M. J. Ray, A. M. Z. Slawin, M. Bühl, P. Kilian, *Organometallics* **2013**, *32*, 3481; j) N. Burford, P. J.

Ragogna, R. McDonald, M. J. Ferguson, *J. Am. Chem. Soc.* **2003**, *125*, 14404; k) N. Burford, P. J. Ragogna, R. McDonald, M. J. Ferguson, *Chem. Commun.* **2003**, 2066; l) J. M. Slattery, C. Fish, M. Green, T. N. Hooper, J. C. Jeffery, R. J. Kilby, J. M. Lynam, J. E. McGrady, D. A. Pantazis, C. A. Russell, C. E. Willans, *Chem. Eur. J.* **2007**, *13*, 6967.

[91] P. S. Nejman, T. E. Curzon, M. Bühl, D. McKay, J. D. Woollins, S. E. Ashbrook, D. B. Cordes, A. M. Z. Slawin, P. Kilian, *Inorg. Chem.* **2020**, *59*, 5616.

[92] E. Conrad, N. Burford, R. McDonald, M. J. Ferguson, *J. Am. Chem. Soc.* **2009**, *131*, 5066.

[93] E. Conrad, N. Burford, R. McDonald, M. J. Ferguson, *Chem. Commun.* **2010**, *46*, 4598.

[94] a) C. Hering, M. Lehmann, A. Schulz, A. Villinger, *Inorg. Chem.* **2012**, *51*, 8212; b) H. J. Breunig, M. Denker, E. Lork, *Angew. Chem.* **1996**, *108*, 1081; *Angew. Chem. Int. Ed.* **1996**, *35*, 1005; c) H. Althaus, H. J. Breunig, E. Lork, *Chem. Commun.* **1999**, 1971.

[95] J. Ramler, F. Fantuzzi, F. Geist, A. Hanft, H. Braunschweig, B. Engels, C. Lichtenberg, *Angew. Chem.* **2021**, *133*, 24592; *Angew. Chem. Int. Ed.* **2021**, *60*, 24388.

[96] a) G. Frenking, *Angew. Chem.* **2014**, *126*, 6152; *Angew. Chem. Int. Ed.* **2014**, *53*, 6040; b) D. Himmel, I. Krossing, A. Schnepf, *Angew. Chem.* **2014**, *126*, 6159; *Angew. Chem. Int. Ed.* **2014**, *53*, 6047; c) D. Himmel, I. Krossing, A. Schnepf, *Angew. Chem.* **2014**, *126*, 378; *Angew. Chem. Int. Ed.* **2014**, *53*, 370; d) A. Nandi, S. Kozuch, *Chem. Eur. J.* **2020**, *26*, 759.

[97] J. S. Murray, P. Lane, P. Politzer, *Int. J. Quantum Chem.* **2007**, *107*, 2286.

[98] A. Bauzá, S. K. Seth, A. Frontera, *Coord. Chem. Rev.* **2019**, *384*, 107.

[99] P. Scilabra, G. Terraneo, G. Resnati, *Acc. Chem. Res.* **2019**, *52*, 1313.

[100] D. J. Pascoe, K. B. Ling, S. L. Cockroft, *J. Am. Chem. Soc.* **2017**, *139*, 15160.

[101] a) P. Politzer, J. S. Murray, T. Clark, *Phys. Chem. Chem. Phys.* **2013**, *15*, 11178; b) P. J. Costa, *Phys. Sci. Rev.* **2017**, *2*; c) R. W. Troff, T. Mäkelä, F. Topić, A. Valkonen, K. Raatikainen, K. Rissanen, *Eur. J. Org. Chem.* **2013**, *2013*, 1617.

[102] S. Scheiner, *Int. J. Quantum Chem.* **2013**, *113*, 1609.

[103] S. Scheiner, *Acc. Chem. Res.* **2013**, *46*, 280.

[104] K. T. Mahmudov, A. V. Gurbanov, V. A. Aliyeva, G. Resnati, A. J. Pombeiro, *Coord. Chem. Rev.* **2020**, *418*, 213381.

[105] L. de Azevedo Santos, T. A. Hamlin, T. C. Ramalho, F. M. Bickelhaupt, *Phys. Chem. Chem. Phys.* **2021**, *23*, 13842.

[106] A. Bauzá, T. J. Mooibroek, A. Frontera, *ChemPhysChem.* **2015**, *16*, 2496.

[107] A. Grabarz, M. Michalczyk, W. Zierkiewicz, S. Scheiner, *ChemPhysChem.* **2020**, *21*, 1934.

[108] a) J. S. Murray, P. Lane, T. Clark, P. Politzer, *J. Mol. Model.* **2007**, *13*, 1033; b) P. Politzer, P. Lane, M. C. Concha, Y. Ma, J. S. Murray, *J. Mol. Model.* **2007**, *13*, 305.

[109] a) M. Tamm, L. P. Ho, A. Nasr, P. G. Jones, A. Altun, F. Neese, G. Bistoni, *Chem. Eur. J.* **2018**, *24*, 18922; b) W. Zierkiewicz, D. Michalska, T. Zeegers-Huyskens, *Phys. Chem. Chem. Phys.* **2010**, *12*, 13681.

[110] P. Hobza, K. Müller-Dethlefs, *Non-covalent interactions*. *Theory and experiment*, Royal Society of Chemistry, Cambridge, **2010**.

[111] S. Zahn, R. Frank, E. Hey-Hawkins, B. Kirchner, *Chem. Eur. J.* **2011**, *17*, 6034.

[112] R. Pietschnig, *J. Organomet. Chem.* **2007**, *692*, 3363.

[113] W. Smith, G. W. Davis, *J. Chem. Soc., Trans.* **1882**, *41*, 411.

[114] R. Hulme, J. T. Szymanski, *Acta Cryst. B* **1969**, *25*, 753.

[115] D. Mootz, V. Händler, *Z. Anorg. Allg. Chem.* **1986**, *533*, 23.

[116] a) B. N. Menshutkin, *Chem. Zentr.* **1910**, *2*, 378; b) B. N. Menshutkin, *Chem. Zentr.* **1910**, *2*, 379; c) B. N. Menshutkin, *Chem. Zentr.* **1910**, *2*, 381; d) B. N. Menshutkin, *Chem. Zentr.* **1912**, *2*, 1437; e) B. N. Menshutkin, *Chem. Zentr.* **1912**, *2*, 1436; f) B. N. Menshutkin, *Chem. Zentr.* **1912**, *2*, 1437; g) B. N. Menshutkin, *Chem. Zentr.* **1912**, *2*, 1437; h) B. N. Menshutkin, *Chem. Zentr.* **1912**, *2*, 1438; i) B. N. Menshutkin, *Chem. Zentr.* **1912**, *2*, 1439.

[117] R. Hulme, D. J. E. Mullen, *J. Chem. Soc., Dalton Trans.* **1976**, 802.

[118] a) H.-H. Perkampus, E. Schönberger, *Z. Naturforsch. B* **1976**, *31*, 73; b) A. Lipka, D. Mootz, *Z. Naturforsch. B* **1982**, *37*, 695; c) H. Schmidbaur, J. M. Wallis, R. Nowak, B. Huber, G. Müller, *Chem. Ber.* **1987**, *120*, 1837; d) H. Schmidbaur, R. Nowak, B. Huber, G. Mueller, *Organometallics* **1987**, *6*, 2266; e) H. Schmidbaur, R. Nowak, O. Steigelmann, G. Müller, *Chem. Ber.* **1990**, *123*, 19; f) A. Demaldé, A. Mangia, M. Nardelli, G. Pelizzi, M. E. V. Tani, *Acta Cryst. B* **1972**, *28*, 147; g) D. Mootz, V. Hndler, *Z. Anorg. Allg. Chem.* **1985**, *521*, 122; h) H. Schmidbaur, R. Nowak, O. Steigelmann, G. Müller, *Chem. Ber.* **1990**, *123*, 1221; i) T. Probst, O. Steigelmann, J. Riede, H. Schmidbaur, *Chem. Ber.* **1991**, *124*, 1089; j) N. Burford, J. A. C. Clyburne, J. A. Wiles, T. S. Cameron, K. N. Robertson, *Organometallics* **1996**, *15*, 361; k) M. B. Ferrari, M. R. Cramarossa, D. Iarossi, G. Pelosi, *Inorg. Chem.* **1998**, *37*, 5681; l) J. Beckmann, T. Heek, M. Takahashi, *Organometallics* **2007**, *26*, 3633; m) W. Frank, J. Weber, E. Fuchs, *Angew. Chem.* **1987**, *99*, 68; *Angew. Chem. Int. Ed.* **1987**, *26*, 74; n) L. P. Battaglia, A. B. Corradi, I. M. Vezzosi, F. A. Zanoli, *J. Chem. Soc., Dalton Trans.* **1990**, 1675; o) I. M. Vezzosi, A. F. Zanoli, L. P. Battaglia, A. B. Corradi, *J. Chem. Soc., Dalton Trans.* **1988**, 191; p) H. J. Breunig, E. Lork, C. Raţ, *Z. Naturforsch. B* **2007**, *62*, 1224; q) L. P. Battaglia, M. R. Cramarossa, I. M. Vezzosi, *Inorg. Chim. Acta* **1995**, *237*, 169; r) A. Schier, J. M. Wallis, G. Müller, H. Schmidbaur, *Angew. Chem.* **1986**, *98*, 742; *Angew. Chem. Int. Ed.* **1986**, *25*, 757.

[119] R. Lo, P. Švec, Z. Růžičková, A. Růžička, P. Hobza, *Chem. Commun.* **2016**, *52*, 3500.

[120] A. Lipka, *Z. Anorg. Allg. Chem.* **1980**, *466*, 195.

[121] a) A. Lipka, *Z. Anorg. Allg. Chem.* **1978**, *440*, 224; b) A. Lipka, D. Mootz, *Z. Anorg. Allg. Chem.* **1978**, *440*, 217.

[122] a) C. Silvestru, H. J. Breunig, H. Althaus, *Chem. Rev.* **1999**, *99*, 3277; b) A.-M. Fritzsche, S. Scholz, M. Krasowska, K. Bhattacharyya, A. M. Toma, C. Silvestru, M. Korb, T. Rüffer, H. Lang, A. A. Auer, M. Mehring, *Phys. Chem. Chem. Phys.* **2020**, *22*, 10189; c) L. E. Turner, M. G. Davidson, M. D. Jones, H. Ott, V. S. Schulz, P. J. Wilson, *Inorg. Chem.* **2006**, *45*, 6123; d) G. Becker, J. Egner, M. Meiser, O. Mundt, J. Weidlein, *Z. Anorg. Allg. Chem.* **1997**, *623*, 941; e) J. Bresien, A. Schulz, M. Thomas, A. Villinger, *Chem. Ber.* **2019**, *2019*, 1279; f) I. Caracelli, I. Haiduc, J. Zukerman-Schpector, E. R. Tiekink, *Coord. Chem. Rev.* **2013**, *257*, 2863; g) J. Zukerman-Schpector, A. Otero-de-la-Roza, V. Luaña, E. R. T. Tiekink, *Chem. Commun.* **2011**, *47*, 7608; h) V. M. Cangelosi, M. A. Pitt, W. J. Vickaryous, C. A. Allen, L. N. Zakharov, D. W. Johnson, *Cryst. Growth Des.* **2010**, *10*, 3531.

[123] A. A. Auer, D. Mansfeld, C. Nolde, W. Schneider, M. Schürmann, M. Mehring, *Organometallics* **2009**, *28*, 5405.

[124] H. Schmidbaur, A. Schier, *Organometallics* **2008**, *27*, 2361.

[125] A. A. Auer, M. Mehring, K. Bhattacharyya, E. Schiavo, *Chem. Eur. J.* **2021**, *27*, 14520.

[126] S. Grimme, *Angew. Chem.* **2008**, *120*, 3478; *Angew. Chem. Int. Ed.* **2008**, *47*, 3430.

[127] a) M. Krasowska, W. B. Schneider, M. Mehring, A. A. Auer, *Chem. Eur. J.* **2018**, *24*, 10238; b) M. Krasowska, A.-M. Fritzsche, M. Mehring, A. A. Auer, *ChemPhysChem.* **2019**, *20*, 2539.

[128] J. Oddershede, S. Larsen, *J. Phys. Chem. A* **2004**, *108*, 1057.

[129] a) H. W. W. Ehrlich, *Acta Cryst.* **1957**, *10*, 699; b) M. Lusi, I. J. Vitorica-Yrezabal, M. J. Zaworotko, *Cryst. Growth Des.* **2015**, *15*, 4098; c) M. Woińska, S. Grabowsky, P. M. Dominiak, K. Woźniak, D. Jayatilaka, *Sci. Adv.* **2016**, *2*, e1600192.

[130] P. Kilian, F. R. Knight, J. D. Woollins, *Chem. Eur. J.* **2011**, *17*, 2302.

[131] D. Seyferth, S. C. Vick, *J. Organomet. Chem.* **1977**, *141*, 173.

[132] M. A. Tinga, G. J. Buisman, G. Schat, O. S. Akkerman, F. Bickelhaupt, W. J. Smeets, A. L. Spek, *J. Organomet. Chem.* **1994**, *484*, 137.

[133] B. A. Chalmers, K. S. Athukorala Arachchige, J. K. D. Prentis, F. R. Knight, P. Kilian, A. M. Z. Slawin, J. D. Woollins, *Inorg. Chem.* **2014**, *53*, 8795.

[134] V. Balasubramaniyan, *Chem. Rev.* **1966**, *66*, 567.

[135] R. W. Alder, P. S. Bowman, W. R. S. Steele, D. R. Winterman, *Chem. Commun.* **1968**, 723.

[136] A. F. Pozharskii, V. A. Ozeryanskii, *Mendeleev Commun.* **2012**, *22*, 117.

[137] R. W. Alder, *Chem. Rev.* **1989**, *89*, 1215.

[138] a) H. E. Katz, *J. Am. Chem. Soc.* **1985**, *107*, 1420; b) C. Becker, J. Schwabedissen, B. Neumann, H.-G. Stammler, N. W. Mitzel, *Dalton Trans.* **2022**, *51*, 6547.

[139] D. Nori-Shargh, M. M. Amini, S. Jameh-Bozorghi, *Phosphorous Sulfur Silicon Relat. Elem.* **2003**, *178*, 2529.

[140] a) M. W. Stanford, F. R. Knight, K. S. Athukorala Arachchige, P. Sanz Camacho, S. E. Ashbrook, M. Bühl, A. M. Z. Slawin, J. D. Woollins, *Dalton Trans.* **2014**, *43*, 6548; b) F. R. Knight, L. M. Diamond, K. S. Athukorala Arachchige, P. Sanz Camacho, R. A. M. Randall, S. E. Ashbrook, M. Bühl, A. M. Z. Slawin, J. D. Woollins, *Chem. Eur. J.* **2015**, *21*, 3613; c) A. Nordheider, E. Hupf, B. A. Chalmers, F. R. Knight, M. Bühl, S. Mebs, L. Chęcińska, E. Lork, P. S. Camacho, S. E. Ashbrook, K. S. Athukorala Arachchige, D. B. Cordes, A. M. Z. Slawin, J. Beckmann, J. D. Woollins, *Inorg. Chem.* **2015**, *54*, 2435.

[141] J. Henning, K. Eichele, R. F. Fink, L. Wesemann, *Organometallics* **2014**, *33*, 3904.

[142] J. Schneider, J. Henning, J. Edrich, H. Schubert, L. Wesemann, *Inorg. Chem.* **2015**, *54*, 6020.

[143] a) C. R. Wade, A. A. Yakovenko, F. P. Gabbaï, *New J. Chem.* **2010**, *34*, 1646; b) N. Meyer, C. W. Lehmann, T. K.-M. Lee, J. Rust, V. W.-W. Yam, F. Mohr, *Organometallics* **2009**, *28*, 2931.

[144] J. d. Hoefelmeyer, F. P. Gabbaï, *J. Am. Chem. Soc.* **2000**, *122*, 9054.

[145] a) W. Yang, L. Zhang, D. Xiao, R. Feng, W. Wang, S. Pan, Y. Zhao, L. Zhao, G. Frenking, X. Wang, *Nat. Commun.* **2020**, *11*, 3441; b) S. Zhang, X. Wang, Y. Sui, X. Wang, *J. Am. Chem. Soc.* **2014**, *136*, 14666; c) S. Zhang, X. Wang, Y. Su, Y. Qiu, Z. Zhang, X. Wang, *Nat. Commun.* **2014**, *5*, 4127; d) W. Yang, W. Wang, L. Zhang, L. Zhang, H. Ruan, Z. Feng, Y. Fang, X. Wang, *Chem. Commun.* **2021**, 5067.

[146] R. D. Jackson, S. James, A. Orpen, P. G. Pringle, *J. Organomet. Chem.* **1993**, *458*, C3-C4.

[147] A. Karaar, H. Thönnessen, P. G. Jones, R. Bartsch, R. Schmutzler, *Heteroatom Chem.* **1997**, *8*, 539.

[148] A. Karaçar, H. Thönnessen, P. G. Jones, R. Bartsch, R. Schmutzler, *Chem. Ber.* **1997**, *130*, 1485.

[149] S. A. Reiter, S. D. Nogai, K. Karaghiosoff, H. Schmidbaur, *J. Am. Chem. Soc.* **2004**, *126*, 15833.

[150] a) A. Karaçar, M. Freytag, H. Thönnessen, P. G. Jones, R. Bartsch, R. Schmutzler, *J. Organomet. Chem.* **2002**, *643-644*, 68; b) P. G. Jones, H. Thönnessen, A. Karaçar, R. Schmutzler, *Acta Cryst. C* **1997**, *53*, 1119; c) P. Kilian, A. M. Z. Slawin, J. D. Woollins, *Dalton Trans.* **2003**, 3876.

[151] A. Karaçar, M. Freytag, P. G. Jones, R. Bartsch, R. Schmutzler, *Z. Anorg. Allg. Chem.* **2002**, *628*, 533.

[152] P. Kilian, A. M. Z. Slawin, J. D. Woollins, *Chem. Eur. J.* **2003**, *9*, 215.

[153] L. J. Taylor, B. A. Surgenor, P. Wawrzyniak, M. J. Ray, D. B. Cordes, A. M. Z. Slawin, P. Kilian, *Dalton Trans.* **2016**, *45*, 1976.

[154] L. J. Taylor, M. Bühl, B. A. Chalmers, M. J. Ray, P. Wawrzyniak, J. C. Walton, D. B. Cordes, A. M. Z. Slawin, J. D. Woollins, P. Kilian, *J. Am. Chem. Soc.* **2017**, *139*, 18545.

[155] T. Mizuta, T. Nakazono, K. Miyoshi, *Angew. Chem.* **2002**, *114*, 4053; *Angew. Chem. Int. Ed.* **2002**, *41*, 3897.

[156] P. Wawrzyniak, A. M. Z. Slawin, A. L. Fuller, J. D. Woollins, P. Kilian, *Dalton Trans.* **2009**, 7883.

[157] T. Costa, H. Schmidbaur, *Chem. Ber.* **1982**, *115*, 1374.

[158] B. A. Chalmers, M. Bühl, K. S. Athukorala Arachchige, A. M. Z. Slawin, P. Kilian, *J. Am. Chem. Soc.* **2014**, *136*, 6247.

[159] B. A. Chalmers, M. Bühl, K. S. Athukorala Arachchige, A. M. Z. Slawin, P. Kilian, *Chem. Eur. J.* **2015**, *21*, 7520.

[160] a) B. A. Chalmers, D. M. U. K. Somisara, B. A. Surgenor, K. S. Athukorala Arachchige, J. D. Woollins, M. Bühl, A. M. Z. Slawin, P. Kilian, *Molecules* **2021**, *26*, 7222; b) P. Wawrzyniak, A. L. Fuller, A. M. Z. Slawin, P. Kilian, *Inorg. Chem.* **2009**, *48*, 2500.

[161] E. Hupf, E. Lork, S. Mebs, L. Chęcińska, J. Beckmann, *Organometallics* **2014**, *33*, 7247.

[162] M. Jura, W. Levason, G. Reid, M. Webster, *Dalton Trans.* **2008**, 5774.

[163] J. Meinwald, S. Knapp, T. Tatsuoka, J. Finer, J. Clardy, *Tetrahedron Letters* **1977**, *18*, 2247.

[164] J. d. Hoefelmeyer, M. Schulte, F. P. Gabbaï, *Inorg. Chem.* **2001**, *40*, 3833.

[165] J. d. Hoefelmeyer, D. L. Brode, F. P. Gabbaï, *Organometallics* **2001**, *20*, 5653.

[166] F. P. Gabbaï, A. Schier, J. Riede, A. Sladek, H. W. Görlitzer, *Inorg. Chem.* **1997**, *36*, 5694.

[167] J. d. Hoefelmeyer, F. P. Gabbaï, *Chem. Commun.* **2003**, 712.

[168] M. Tschinkl, J. d. Hoefelmeyer, T. M. Cocker, R. E. Bachman, F. P. Gabbaï, *Organometallics* **2000**, *19*, 1826.

[169] C. R. Wade, T.-P. Lin, R. C. Nelson, E. A. Mader, J. T. Miller, F. P. Gabbaï, *J. Am. Chem. Soc.* **2011**, *133*, 8948.

[170] T.-P. Lin, C. R. Wade, L. M. Pérez, F. P. Gabbaï, *Angew. Chem.* **2010**, *122*, 6501; *Angew. Chem. Int. Ed.*, **2010**, *49*, 6357–6360.

[171] B. Cordero, V. Gómez, A. E. Platero-Prats, M. Revés, J. Echeverría, E. Cremades, F. Barragán, S. Alvarez, *Dalton Trans.* **2008**, 2832.

[172] T.-P. Lin, R. C. Nelson, T. Wu, J. T. Miller, F. P. Gabbaï, *Chem. Sci.* **2012**, *3*, 1128.

[173] M. Baba, T. Mizuta, *Polyhedron* **2015**, *92*, 30.

[174] C. Ganesamoorthy, S. Heimann, S. Hölscher, R. Haack, C. Wölper, G. Jansen, S. Schulz, *Dalton Trans.* **2017**, *46*, 9227.

[175] K. Dzialkowski, A. Gehlhaar, C. Wölper, A. A. Auer, S. Schulz, *Organometallics* **2019**, *38*, 2927.

[176] A. Gehlhaar, E. Schiavo, C. Wölper, Y. Schulte, A. A. Auer, S. Schulz, *Dalton Trans.* **2022**, *51*, 5016.

[177] F. Neese, *Wiley Interdiscip. Rev. Comput. Mol. Sci* **2022**, e1606.

[178] F. Neese, F. Wennmohs, U. Becker, C. Riplinger, *J. Chem. Phys.* **2020**, *152*, 224108.

[179] F. Neese, *Wiley Interdiscip. Rev. Comput. Mol. Sci* **2012**, *2*, 73.

[180] F. Neese, *Wiley Interdiscip. Rev. Comput. Mol. Sci* **2018**, *8*, e1327.

[181] a) C. Riplinger, P. Pinski, U. Becker, E. F. Valeev, F. Neese, *J. Chem. Phys.* **2016**, *144*, 24109; b) D. G. Liakos, A. Hansen, F. Neese, *J. Chem. Theory Comput.* **2011**, *7*, 76; c) F. Neese, A. Hansen, F. Wennmohs, S. Grimme, *Acc. Chem. Res.* **2009**, *42*, 641.

[182] C. Riplinger, F. Neese, *J. Chem. Phys.* **2013**, *138*, 34106.

[183] F. Neese, A. Hansen, D. G. Liakos, *J. Chem. Phys.* **2009**, *131*, 64103.

[184] C. Adamo, V. Barone, *J. Chem. Phys.* **1999**, *110*, 6158.

[185] F. Weigend, R. Ahlrichs, *Phys. Chem. Chem. Phys* **2005**, *7*, 3297.

[186] A. Gehlhaar, C. Wölper, F. van der Vight, G. Jansen, S. Schulz, *Eur. J. Inorg. Chem.* **2021**, *2022*.

[187] J. D. Kennedy, W. McFarlane, G. S. Pyne, P. L. Clarke, J. L. Wardell, *J. Chem. Soc., Perkin Trans. 2* **1975**, 1234.

[188] H. Fujihara, H. Ishitani, Y. Takaguchi, N. Furukawa, *Chem. Lett.* **1995**, *24*, 571.

[189] J. F. Blount, F. Cozzi, J. R. Damewood, L. D. Iroff, U. Sjostrand, K. Mislow, *J. Am. Chem. Soc.* **1980**, *102*, 99.

[190] M. Tosolini, J. Avó, A. J. Parola, G. Balducci, P. Tecilla, *Chem. Ber.* **2020**, *2020*, 3859.

[191] E. D. Glendening, J. K. Badenhoop, A. E. Reed, J. E. Carpenter, J. A. Bohmann, C. M. Morales, P. Karafiloglou, C. R. Landis, and F. Weinhold, *NBO 7.0*, Theoretical Chemistry Institute, University of Wisconsin, Madison, **2018**.

[192] T. Lu, F. Chen, *J. Comput. Chem.* **2012**, *33*, 580.

[193] W. Humphrey, A. Dalke, K. Schulten, *Journal of Molecular Graphics* **1996**, *14*, 33.

[194] F. Weigend, *Phys. Chem. Chem. Phys* **2006**, *8*, 1057.

[195] Becke, *Phys. Rev. A Gen. Phys.* **1988**, *38*, 3098.

[196] Perdew, *Phys. Rev. B: Condens. Matter* **1986**, *33*, 8822.

[197] Perdew, Burke, Ernzerhof, *Phys. Rev. Lett.* **1996**, *77*, 3865.

[198] J. P. Perdew, M. Ernzerhof, K. Burke, *J. Chem. Phys.* **1996**, *105*, 9982.

[199] a) C. F. Matta, *The Quantum Theory of Atoms in Molecules*. *From Solid State to DNA and Drug Design,* 1. Aufl., John Wiley & Sons Incorporated, Hoboken, **2007**; b) S. Emamian, T. Lu, H. Kruse, H. Emamian, *J. Comput. Chem.* **2019**, *40*, 2868.

[200] a) H.-J. Werner, P. J. Knowles, G. Knizia, F. R. Manby, M. Schütz, *Wiley Interdiscip. Rev. Comput. Mol. Sci* **2012**, *2*, 242; b) H.-J. Werner, P. J. Knowles, F. R. Manby, J. A. Black, K.

Doll, A. Heßelmann, D. Kats, A. Köhn, T. Korona, D. A. Kreplin, Q. Ma, T. F. Miller, A. Mitrushchenkov, K. A. Peterson, I. Polyak, G. Rauhut, M. Sibaev, *J. Chem. Phys.* **2020**, *152*, 144107.

[201] a) C. Riplinger, B. Sandhoefer, A. Hansen, F. Neese, *J. Chem. Phys.* **2013**, *139*, 134101; b) F. Neese, F. Wennmohs, A. Hansen, *J. Chem. Phys.* **2009**, *130*, 114108.

[202] a) A. Hesselmann, G. Jansen, M. Schütz, *J. Chem. Phys.* **2005**, *122*, 14103; b) G. Jansen, *Wiley Interdiscip. Rev. Comput. Mol. Sci* **2014**, *4*, 127.

[203] A. Heßelmann, G. Jansen, *Chem. Phys. Lett.* **2002**, *357*, 464.

[204] A. Hellweg, C. Hättig, S. Höfener, W. Klopper, *Theoret. Chim. Acta* **2007**, *117*, 587.

[205] S. F. Boys, F. Bernardi, *Molecular Physics* **1970**, *19*, 553.

[206] N. G. Connelly, W. E. Geiger, *Chem. Rev.* **1996**, *96*, 877.

[207] A. Bondi, *J. Phys. Chem.* **1964**, *68*, 441.

[208] S. Sasaki, K. Sutoh, F. Murakami, M. Yoshifuji, *J. Am. Chem. Soc.* **2002**, *124*, 14830.

[209] A. Gehlhaar, H. M. Weinert, C. Wölper, N. Semleit, G. Haberhauer, S. Schulz, *Chem. Commun.* **2022**, *58*, 6682.

[210] D. Kost, E. H. Carlson, M. Raban, *J. Chem. Soc. D* **1971**, 656.

[211] H. J. Breunig, E. Lork, O. Moldovan, C. I. Raţ, *Z. Naturforsch. B* **2013**, *68*, 87.

[212] M. J. Frisch, G. W. Trucks, H. B. Schlegel, G. E. Scuseria, M. A. Robb, J. R. Cheeseman, G. Scalmani, V. Barone, G. A. Petersson, H. Nakatsuji, X. Li, M. Caricato, A. V. Marenich, J. Bloino, B. G. Janesko, R. Gomperts, B. Mennucci, H. P. Hratchian, J. V. Ortiz, A. F. Izmaylov, J. L. Sonnenberg, Williams, F. Ding, F. Lipparini, F. Egidi, J. Goings, B. Peng, A. Petrone, T. Henderson, D. Ranasinghe, V. G. Zakrzewski, J. Gao, N. Rega, G. Zheng, W. Liang, M. Hada, M. Ehara, K. Toyota, R. Fukuda, J. Hasegawa, M. Ishida, T. Nakajima, Y. Honda, O. Kitao, H. Nakai, T. Vreven, K. Throssell, J. A. Montgomery Jr., J. E. Peralta, F. Ogliaro, M. J. Bearpark, J. J. Heyd, E. N. Brothers, K. N. Kudin, V. N. Staroverov, T. A. Keith, R. Kobayashi, J. Normand, K. Raghavachari, A. P. Rendell, J. C. Burant, S. S. Iyengar, J. Tomasi, M. Cossi, J. M. Millam, M. Klene, C. Adamo, R. Cammi, J. W. Ochterski, R. L. Martin, K. Morokuma, O. Farkas, J. B. Foresman, D. J. Fox, *Gaussian 16 Rev. C.01*, Wallingford, CT, **2016**.

[213] a) G. te Velde, F. M. Bickelhaupt, E. J. Baerends, C. Fonseca Guerra, S. J. A. van Gisbergen, J. G. Snijders, T. Ziegler, *J. Comput. Chem.* **2001**, *22*, 931; b) E. J. Baerends, T. Ziegler, A. J. Atkins, J. Autschbach, O. Baseggio, D. Bashford, A. Bérces, F. M. Bickelhaupt, C. Bo, P. M. Boerrigter, C. Cappelli, L. Cavallo, C. Daul, D. P. Chong, D. V. Chulhai, L. Deng, R. M. Dickson, J. M. Dieterich, F. Egidi, D. E. Ellis, M. van Faassen, L. Fan, T. H. Fischer, A. Förster, C. Fonseca Guerra, M. Franchini, A. Ghysels, A. Giammona, S. J. A. van Gisbergen, A. Goez, A. W. Götz, J. A. Groeneveld, O. V. Gritsenko, M. Grüning, S. Gusarov, F. E. Harris, P. van den Hoek, Z. Hu, C. R. Jacob, H. Jacobsen, L. Jensen, L. Joubert, J. W. Kaminski, G. van Kessel, C. König, F. Kootstra, A. Kovalenko, M. V. Krykunov, P. Lafiosca, E. van Lenthe, D. A. McCormack, M. Medves, A. Michalak, M. Mitoraj, S. M. Morton, J. Neugebauer, V. P. Nicu, L. Noodleman, V. P. Osinga, S. Patchkovskii, M. Pavanello, C. A. Peeples, P. H. T. Philipsen, D. Post, C. C. Pye, H. Ramanantoanina, P. Ramos, W. Ravenek, M. Reimann, J. I. Rodríguez, P. Ros, R. Rüger, P. R. T. Schipper, D. Schlüns, H. van Schoot, G. Schreckenbach, J. S. Seldenthuis, M. Seth, J. G. Snijders, M. Solà, M. Stener, M . Swart, D. Swerhone, V.

Tognetti, G. te Velde, P. Vernoojis, L. Versluis, L. Visscher, O. Visser, F. Wang, T. A. Wesolowski, E. M. van Wezenbeeck, G. Wiesenekker, S. K. Wolff, T. K. Woo, A. L. Yakovlev, *ADF 2020.1*, SCM, Theoretical Chemistry, Vrije Uniserteit, Amserdam, The Netherlands, http://www.scm.com.

[214] Todd A. Keith, TK Gristmill Software, Overland Park KS, USA, 2019 (aim.tkgristmill.com), *AIMAll (Version 19.10.12)*, **2019**.

[215] a) Lee, Yang, Parr, *Phys. Rev. B: Condens. Matter* **1988**, *37*, 785; b) B. Miehlich, A. Savin, H. Stoll, H. Preuss, *Chem. Phys. Lett.* **1989**, *157*, 200.

[216] A. E. Reed, L. A. Curtiss, F. WEINHOLD, *Chem. Rev.* **1988**, *88*, 899.

[217] F. M. Bickelhaupt, E. J. Baerends in *Reviews in Computational Chemistry*, *Vol. 15* (Hrsg.: D. B. Boyd, K. B. Lipkowitz), Wiley-VCH, New York, **2000**, S. 1–86.

[218] R. F. W. Bader, *Atoms in molecules*. *A quantum theory*, Clarendon Press, Oxford, **2003**.

[219] M. A. Blanco, A. Martín Pendás, E. Francisco, *J. Chem. Theory Comput.* **2005**, *1*, 1096.

[220] B. Twamley, C. D. Sofield, M. M. Olmstead, P. P. Power, *J. Am. Chem. Soc.* **1999**, *121*, 3357.

[221] J. d. Hoefelmeyer, F. P. Gabbaï, *Organometallics* **2002**, *21*, 982.

[222] a) R. J. Bailey, P. Card, H. Shechter, *J. Am. Chem. Soc.* **1983**, *105*, 6096; b) M. Gessner, P. Card, H. Shechter, G. G. Christoph, *J. Am. Chem. Soc.* **1977**, *99*, 2371.

[223] J. Ohshita, K. Matsushige, A. Kunai, A. Adachi, K. Sakamaki, K. Okita, *Organometallics* **2000**, *19*, 5582.

[224] T. Mizuta, Y. Iwakuni, T. Nakazono, K. Kubo, K. Miyoshi, *J. Organomet. Chem.* **2007**, *692*, 184.

[225] J. Meinwald, S. Knapp, S. K. Obendorf, R. E. Hughes, *J. Am. Chem. Soc.* **1976**, *98*, 6643.

[226] M. A. G. M. Tinga, G. Schat, O. S. Akkerman, F. Bickelhaupt, W. J. J. Smeets, A. L. Spek, *Chem. Ber.* **1994**, *127*, 1851.

[227] A. Hergel, H. Pritzkow, W. Siebert, *Angew. Chem.* **1994**, *106*, 1342; *Angew. Chem. Int. Ed.* **1994**, *33*, 1247.

[228] J. R. Aranzaes, M.-C. Daniel, D. Astruc, *Can. J. Chem.* **2006**, *84*, 288.

[229] G. M. Sheldrick, *Acta Cryst.* **1990**, *46*, 467.

[230] a) G. M. Sheldrick, *Acta Cryst.* **2015**, *71*, 3; b) C. B. Hübschle, G. M. Sheldrick, B. Dittrich, *J. Appl. Crystallogr.* **2011**, *44*, 1281.

[231] W. Uhlig, *Z. Naturforsch. B* **1995**, *50*, 1674.

[232] B. Schiemenz, P. P. Power, *Organometallics* **1996**, *15*, 958.

[233] R. L. Letsinger, J. A. Gilpin, W. J. Vullo, *J. Org. Chem.* **1962**, *27*, 672.

[234] J. P. Nietfeld, R. L. Schwiderski, T. P. Gonnella, S. C. Rasmussen, *J. Org. Chem.* **2011**, *76*, 6383.

[235] D. H. Barton, N. Y. Bhatnagar, J.-P. Finet, W. B. Motherwell, *Tetrahedron* **1986**, *42*, 3111.

[236] F. Challenger, C. F. Allpress, *J. Chem. Soc., Trans.* **1915**, *107*, 16.

[237] H. Bhattacharjee, J. Zhu, J. Müller, *Angew. Chem.* **2019**, *131*, 16728; *Angew. Chem. Int. Ed.* **2019**, *58*, 16575.

List of Figures

List of Schemes

List of Tables

Crystallographic Details

Table 15. Crystallographic details for published compounds **60** and **57b** in chapter 5.1.[176]

Compound	**60**	**57b**
Empirical formula	$C_{20}H_{12}Bi_2$	$C_{20}H_{12}As_2$
M	670.26	402.14
Crystal size [mm]	0.124 × 0.045 × 0.031	0.177 × 0.069 × 0.067
T [K]	100(2)	100(2)
Crystal system	monoclinic	triclinic
Space group	$C2/c$	$P\bar{1}$

a [Å]	19.3995(17)	8.3154(8)
b [Å]	5.1523(4)	9.7984(10)
c [Å]	31.532(3)	10.2317(7)
α [°]	90	75.105(6)
β [°]	98.603(4)	69.115(6)
γ [°]	90	78.997(8)
V [Å^3]	3116.2(5)	748.15(12)
Z	8	2
D_{calc} [g·cm^{-3}]	2.857	1.785
μ(MoK_α [mm^{-1}])	22.550	5.450
Transmissions	0.02/0.01	0.75/0.57
F(000)	2384	396
Index ranges	$-25 \le h \le 25$	$-10 \le h \le 9$
	$-6 \le k \le 6$	$-12 \le k \le 12$
	$-41 \le l \le 41$	$-13 \le l \le 13$
θ_{max} [°]	28.329	80.944
Reflections collected	17944	65245
Independent reflections	3860	3269
R_{int}	0.1025	0.0385
Refined parameters	199	199
R_1 [$I > 2\sigma(I)$]	0.0550	0.0260
wR_2 [all data]	0.1109	0.0690
GooF	1.006	1.061
$\Delta\rho_{final}$ (max/min) [e·Å^{-3}]	1.812/–1.382	1.685/–0.847

Table 16. Crystallographic details for published compounds **41**, **61**, and **63**-**65** in chapter 5.2.[186]

Compound	**41**	**61**	**63**	**64**	**65**
Empirical formula	$C_{34}H_{26}Sb_2$	$C_{36}H_{28}Sb_2$	$C_{34}H_{26}Bi_2$	$C_{25}H_{25}BiSn$	$C_{32}H_{22}Bi_2$
M [g/mol]	678.05	704.08	825.51	653.12	824.45
Crystal size [mm]	0.702 × 0.348 × 0.224	0.219 × 0.071 × 0.028	0.206 × 0.061 × 0.043	0.226 × 0.128 × 0.100	0.208 × 0.122 × 0.085
T [K]	100(2)	100(2)	100(2)	100(2)	100(2)
Crystal system	orthorhombic	orthorombic	monoclinic	monoclinic	triclinic
Space group	$P2_12_12_1$	$P2_12_12_1$	$P2_1$	$P2_1/n$	$P\bar{1}$
a [Å]	12.473(2)	12.515(2)	6.0465(3)	9.9246(18)	9.5198(10)
b [Å]	13.572(3)	13.494(3)	17.5165(8)	15.138(3)	10.9245(13)
c [Å]	16.481(3)	17.453(3)	12.6945(6)	15.629(3)	12.7396(13)
α [°]	90	90	90	90	94.626(6)
β [°]	90	90	99.066(2)	108.214(4)	107.494(5)

γ [°]	90	90	90	90	104.699(6)
V [Å^3]	2790.0(9)	2947.4(9)	1327.72(11)	2230.5(7)	1204.5(2)
Z	4	4	2	4	2
D_{calc} [g·cm^{-3}]	1.614	1.587	2.132	1.945	2.273
μ(MoK_α [mm^{-1}])	1.957	1.855	13.257	9.005	14.609
Transmissions	0.75/0.61	0.75/0.64	0.11/0.02	0.50/0.33	0.03/0.01
F(000)	1328	1384	792	1232	760
Index ranges	$-18 \le h \le 18$	$-19 \le h \le 19$	$-9 \le h \le 9$	$-15 \le h \le 15$	$-14 \le h \le 14$
	$-20 \le k \le 19$	$-20 \le k \le 20$	$-26 \le k \le 26$	$-23 \le k \le 23$	$-16 \le k \le 16$
	$-25 \le l \le 25$	$-26 \le l \le 26$	$-19 \le l \le 19$	$-24 \le l \le 24$	$-19 \le l \le 19$
θ_{max} [°]	33.342	33.388	33.227	33.329	33.269
Reflections collected	33623	155429	44394	93260	91891
Independent reflections	10520	11435	10180	8619	9244
R_{int}	0.0308	0.0742	0.0718	0.0359	0.0340
Refined parameters	325	343	325	247	307
R_1 [$I > 2\sigma(I)$]	0.0205	0.0311	0.0341	0.0344	0.0209
wR_2 [all data]	0.0510	0.0662	0.0584	0.0845	0.0439
X(Flack)	-0.010(6)	-0.008(10)	-0.015(7)	-	-
GooF	1.081	1.058	0.989	1.072	1.073
$\Delta\rho_{final}$ (max/min) [e·Å^{-3}]	0.747/–0.414	0.739/–0.549	1.582/–0.963	4.075/–4.791	2.762/–1.948

Table 17. Crystallographic details for compounds **66-68** in chapter 5.3.

Compound	**66**	**67**	**68**
Empirical formula	$C_{70}H_{98}Sb_2$	$C_{70}H_{98}Bi_2$	$C_{79}H_{75}BF_{20}Sb_2$
M [g/mol]	1182.98	1357.44	1658.70
Crystal size [mm]	0.422 x 0.356 x 0.184	0.416 × 0.155 × 0.118	0.428 × 0.417 × 0.250
T [K]	100(2)	100(2)	100(2)
Crystal system	orthorhombic	monoclinic	triclinic
Space group	$P2_12_12$	$C2/c$	$P\bar{1}$
a [Å]	15.8867(7)	34.169(3)	14.118(3)
b [Å]	14.0109(7)	10.4618(8)	15.623(3)
c [Å]	14.5536(7)	18.2971(14)	17.104(3)
α [°]	90	90	82.723(8)
β [°]	90	110.0432(19)	80.545(8)
γ [°]	90	90	78.391(8)
V [Å^3]	3239.4(3)	6144.4(8)	3627.9(12)
Z	2	4	2
D_{calc} [g·cm^{-3}]	1.213	1.467	1.518

μ(MoK_α [mm^{-1}])	0.871	11.390 (CuK_α)	0.840
Transmissions	0.75/0.66	0.75/0.44	0.75/0.62
F(000)	1240	2736	1672
Index ranges	$-26 \le h \le 26$	$-42 \le h \le 42$	$-21 \le h \le 21$
	$-23 \le k \le 23$	$-13 \le k \le 13$	$-24 \le k \le 24$
	$-24 \le l \le 24$	$-20 \le l \le 22$	$-26 \le l \le 26$
Θ_{max} [°]	36.632	80.540	33.920
Reflections collected	172477	70130	230758
Independent reflections	16019	6421	28346
R_{int}	0.0225	0.0607	0.0494
Refined parameters	338	338	958
R_1 [$I > 2\sigma(I)$]	0.0162	0.0491	0.0324
wR_2 [all data]	0.0422	0.1341	0.0769
X(Flack)	–0.0183(19)	-	-
GooF	1.087	1.102	1.125
$\Delta\rho_{final}$ (max/min) [e·Å^{-3}]	0.980/–0.558	6.445/–2.252	2.988/–1.085

Table 18. Crystallographic details for published compounds **69-72** in chapter 5.3.[209]

Compound	**69**	**70**	**71**	**72**
Empirical formula	$C_{70}H_{98}Sb_2$	$C_{70}H_{98}Bi_2$	$C_{79}H_{75}BF_{20}Sb_2$	$C_{40}H_{52}Sb_2$
M [g/mol]	1182.98	1357.44	1658.70	776.31
Crystal size [mm]	0.422 x 0.356 x 0.184	0.416 × 0.155 × 0.118	0.428 × 0.417 × 0.250	0.312 × 0.230 × 0.104
T [K]	100(2)	100(2)	100(2)	100(2)
Crystal system	orthorhombic	monoclinic	triclinic	orthorhombic
Space group	$P2_12_12$	$C2/c$	$P\bar{1}$	$Pbca$
a [Å]	15.8867(7)	34.169(3)	14.118(3)	15.8584(15)
b [Å]	14.0109(7)	10.4618(8)	15.623(3)	17.1790(15)
c [Å]	14.5536(7)	18.2971(14)	17.104(3)	26.761(2)
α [°]	90	90	82.723(8)	90
β [°]	90	110.0432(19)	80.545(8)	90
γ [°]	90	90	78.391(8)	90
V [Å^3]	3239.4(3)	6144.4(8)	3627.9(12)	7290.6(11)
Z	2	4	2	8
D_{calc} [g·cm^{-3}]	1.213	1.467	1.518	1.415
μ(MoK_α [mm^{-1}])	0.871	11.390 (CuK_α)	0.840	11.920
Transmissions	0.75/0.66	0.75/0.44	0.75/0.62	0.75/0.35
F(000)	1240	2736	1672	3152
Index ranges	$-26 \le h \le 26$	$-42 \le h \le 42$	$-21 \le h \le 21$	$-16 \le h \le 19$
	$-23 \le k \le 23$	$-13 \le k \le 13$	$-24 \le k \le 24$	$-21 \le k \le 21$
	$-24 \le l \le 24$	$-20 \le l \le 22$	$-26 \le l \le 26$	$-34 \le l \le 33$
Θ_{max} [°]	36.632	80.540	33.920	80.951
Reflections collected	172477	70130	230758	100079
Independent reflections	16019	6421	28346	7676
R_{int}	0.0225	0.0607	0.0494	0.0652
Refined parameters	338	338	958	401

R_1 [$I > 2\sigma(I)$]	0.0162	0.0491	0.0324	0.0610
wR_2 [all data]	0.0422	0.1341	0.0769	0.1613
X(Flack)	–0.0183(19)	-	-	-
GooF	1.087	1.102	1.125	1.135
$\Delta\rho_{final}$ (max/min) [e·Å^{-3}]	0.980/–0.558	6.445/–2.252	2.988/–1.085	3.216/–1.648

Table 19. Crystallographic details for compounds **73-75** in chapter 5.4.

Compound	**74**	**73**	**75**
Empirical formula	$C_{46}H_{55}As$	$C_{50}H_{63}OSb$	$C_{46}H_{55}Bi$
M [g/mol]	682.82	801.75	816.88
Crystal size [mm]	0.354 × 0.317 × 0.156	0.325 × 0.192 × 0.102	0.298 × 0.263 × 0.185
T [K]	100(2)	100(2)	100(2)
Crystal system	triclinic	monoclinic	monoclinic
Space group	$P\bar{1}$	$P2_1/n$	$P2_1/n$
a [Å]	11.3984(6)	18.1096(8)	12.6323(7)
b [Å]	12.6665(7)	14.9047(7)	22.5945(13)
c [Å]	14.3095(8)	33.0390(15)	14.0664(9)
α [°]	72.164(2)	90	90
β [°]	81.169(2)	104.788(2)	103.384(3)
γ [°]	78.868(2)	90	90
V [Å^3]	1919.80(18)	8622.4(7)	3905.8(4)
Z	2	8	4
D_{calc} [g·cm^{-3}]	1.181	1.235	1.389
μ(MoK_α [mm^{-1}])	0.915	0.674	4.543
Transmissions	0.75/0.66	0.75/0.67	0.15/0.05
F(000)	728	3376	1656
Index ranges	$-17 \le h \le 17$	$-28 \le h \le 27$	$-19 \le h \le 19$
	$-19 \le k \le 19$	$-23 \le k \le 23$	$-34 \le k \le 34$
	$-22 \le l \le 22$	$-51 \le l \le 51$	$-21 \le l \le 21$
Θ_{max} [°]	33.392	33.446	33.658
Reflections collected	165863	391847	168180
Independent reflections	14880	33522	15417
R_{int}	0.0294	0.0607	0.0367
Refined parameters	436	338	436
R_1 [$I > 2\sigma(I)$]	0.0298	0.0618	0.0333
wR_2 [all data]	0.0834	0.1222	0.0805
X(Flack)	–	–	–
GooF	1.071	1.136	1.122
$\Delta\rho_{final}$ (max/min) [e·Å^{-3}]	1.501/–0.416	2.429/–1.531	3.150/–1.034

Curriculum Vitae

Der Lebenslauf ist in der Online-Version aus Gründen des Datenschutzes nicht enthalten.

The Curriculum Vitae is not included in the online version for data protection reasons.

Publications and Conference Contributions

A. Gehlhaar, H. M. Weinert, C. Wölper, N. Semleit, G. Haberhauer, S. Schulz. Bisstibane−Distibane conversion via consecutive single-electron oxidation and reduction reaction. *Chem. Comm.* **2022**, *47*, 6682.

A. Gehlhaar, E. Schiavo, C. Wölper, A. A. Auer, S. Schulz. Comparing London Dispersion Pnictogen–π Interactions in Naphthyl-substituted Dipnictanes. *Dalton Trans.* **2022**, *51*, 5016.

A. Gehlhaar, C. Wölper, F. van der Vight, G. Jansen, S. Schulz. Noncovalent intra- and intermolecular interactions in *peri*-substituted pnicta naphthalene and acenaphthalene complexes. *Eur. J. Inorg. Chem.* **2021**, DOI: 10.1002/ejic.202100883.

Cover Feature:

J. Schoening, A. Gehlhaar, C. Wölper, S. Schulz. Selective [2+1+1] Fragmentation of P4 by heteroleptic Metallasilylenes. *Chem. Eur. J.* **2022**, DOI: 10.1002/chem.202201982.

A. Gehlhaar, H. M. Weinert, C. Wölper, N. Semleit, G. Haberhauer, S. Schulz. Bisstibane−Distibane conversion via consecutive single-electron oxidation and reduction reaction. *Chem. Comm.* **2022**, *47*, 6673.

A. Gehlhaar, E. Schiavo, C. Wölper, A. A. Auer, S. Schulz. Comparing London Dispersion Pnictogen–π Interactions in Naphthyl-substituted Dipnictanes. *Dalton Trans.* **2022***, 51,* 4931.

Publications beyond the scope of this dissertation

J. Schoening, A. Gehlhaar, C. Wölper, S. Schulz. Selective [2+1+1] Fragmentation of P4 by heteroleptic Metallasilylenes. *Chem. Eur. J.* **2022**, DOI: 10.1002/chem.202201031.

K. Dzialkowski, A. Gehlhaar, C. Wölper, A. A. Auer, S. Schulz. Structure and Reactivity of 1,8-Bis(naphthalenediyl)dipnictanes. *Organometallics* **2019**, *38*, 2927.

C. Stienen, S. Gondzik, A. Gehlhaar, R. Haack, C. Wölper, G. Jansen, S. Schulz. $(MeZn)_2(\mu\text{-}\eta^2\text{:}\eta^2\text{-}N_6Ph_2)$: A Powerful Starting Reagent for the Synthesis of Metal Hexazene Complexes. *Organometallics* **2016**, *35*, 1022.

Conference Contributions

A. Gehlhaar, S. Schulz. Non-Covalent Interactions in Naphthalenediyl-Substituted Heavy Group 15 Elements. *6th Winter School of the SPP 1807*, 15th to 16th March **2022**, Online.

A. Gehlhaar, S. Schulz. Heavy Metals in Close Combat – Non-Covalent Interactions in *peri*-Substituted Naphthalenediyl Pnictogen Compounds. *GDCh-*

Wissenschaftsforum Chemie – Chemists create solutions. 29th August to 1st September **2021**, Online.

A. Gehlhaar. Inter- and Intramolecular Interactions in homoleptic Naphthylpnictanes. 15 minutes conference talk. *5th Winter School of the SPP 1807*, 4th to 5th March **2021**, Online.

A. Gehlhaar, S. Schulz, Dispersion Interactions in Bridged bimetallic Complexes of the Heavy Group 15 Elements. Poster presentation. *Online-Vortragstagung für Anorganische Chemie der Fachgruppen Wöhlervereinigung und Festkörperchemie & Materialforschung*, 29th to 30th September **2020**, Online.

A. Gehlhaar, K. Dzialkowski, C. Wölper, A. A. Auer, S. Schulz. Dispersion Interactions in Bridged bimetallic Complexes of the Heavy Group 15 Elements. Poster presentation. *10th Young Chemists' Symposium Ruhr*, 19th September **2019**, Essen, Germany.

A. Gehlhaar. Dispersion Interactions in Bridged bimetallic Complexes of the Heavy Group 15 Elements. 15 minutes conference talk. *4th Summer School of the SPP 1807*, 16th to 19th July **2019**, Paderborn, Germany.

A. Gehlhaar, Kevin Dzialkowski, Stephan Schulz. A Combined Quantum Chemical and Experimental Study on Metal-Metal Interactions in Heavy Group 15 and Group 16 Compounds. Poster presentation. *SPP 1807 Workshop,* 25th to 26th February **2019***,* Erlangen, Germany.

Versicherung an Eides Statt

Ich versichere an Eides statt durch meine untenstehende Unterschrift, dass ich die vorliegende Arbeit mit Ausnahme der Anleitung durch die Betreuer

- selbstständig und ohne fremde Hilfe angefertigt habe und
- dass ich alle Stellen, die wörtlich oder annähernd wörtlich aus fremden Quellen entnommen sind, entsprechend als Zitate gekennzeichnet habe und
- dass ich ausschließlich die angegebenen Quellen (Literatur, Internetseiten, sonstige Hilfsmittel) verwendet habe und
- dass ich alle entsprechenden Angaben nach bestem Wissen und Gewissen vorgenommen habe, dass sie der Wahrheit entsprechen und dass ich nichts verschwiegen habe.

Mir ist bekannt, dass eine falsche Versicherung an Eides Statt nach § 156 und nach § 163 Abs. 1 des Strafgesetzbuches mit Freiheitsstrafe oder Geldstrafe bestraft wird.

Ort, Datum	Unterschrift Alexander Gehlhaar